



HAL
open science

Analysis of the cyclic behavior of an adhesive in an assembly for offshore windmills applications

Pierre Bidaud

► **To cite this version:**

Pierre Bidaud. Analysis of the cyclic behavior of an adhesive in an assembly for offshore windmills applications. Materials. Université Bretagne Occidentale, 2014. English. NNT: . tel-01127793v2

HAL Id: tel-01127793

<https://hal.science/tel-01127793v2>

Submitted on 29 Mar 2015 (v2), last revised 22 Nov 2018 (v3)

HAL is a multi-disciplinary open access archive for the deposit and dissemination of scientific research documents, whether they are published or not. The documents may come from teaching and research institutions in France or abroad, or from public or private research centers.

L'archive ouverte pluridisciplinaire **HAL**, est destinée au dépôt et à la diffusion de documents scientifiques de niveau recherche, publiés ou non, émanant des établissements d'enseignement et de recherche français ou étrangers, des laboratoires publics ou privés.



université de bretagne
occidentale



THÈSE / UNIVERSITÉ DE BRETAGNE OCCIDENTALE

sous le sceau de l'Université européenne de Bretagne

pour obtenir le titre de

DOCTEUR DE L'UNIVERSITÉ DE BRETAGNE OCCIDENTALE

Mention : Sciences de l'ingénieur

École Doctorale des Sciences de la Mer

présentée par

Pierre Bidaud

Préparée au **Laboratoire Brestois de**

Mécanique et des Systèmes (EA4325)

Analysis of the cyclic behavior of an adhesive in an assembly for offshore windmills applications

Soutenu le vendredi 12 décembre 2014

devant le jury composé de :

Pascal Casari,

Professeur des Universités, GeM, Saint-Nazaire / *Rapporteur.*

Yves Nadot,

Professeur des Universités, Institut P' / *Rapporteur.*

Rafael Estevez,

Professeur des Universités, Simap, Saint Martin d'Hérés / *Examineur.*

Christian Hochard,

Professeur des Universités, LMA, Marseille / *Examineur.*

Pierre Jousset,

Leader Dynamic Testing - CAE, Dr. Sika Technology AG, Zürich / *Examineur.*

Laurent Sohier,

Maître de Conférences, LBMS, Brest / *Examineur.*

Romain Créac'hcadec,

Maître de Conférences, LBMS, Brest / *Co-encadrant.*

David Thévenet,

Enseignant chercheur HDR, LBMS, Brest / *Directeur de thèse.*

Avant-propos

Une page vient de se tourner, avec l'obtention de mon doctorat et je profite de la rédaction de ces quelques lignes pour remercier ceux qui ont participé à l'accomplissement de ce projet et qui m'ont soutenus tout au long de ma thèse.

Trois heures, c'est environ le temps qu'il m'a été accordé pour présenter mes travaux. Pour avoir évalué mon travail durant cette présentation, je tiens à remercier Christian Hochard, qui m'a fait l'honneur de présider mon jury, Rafael Estevez, Pierre Jousset et Laurent Sohier, pour avoir été des examinateurs pertinents et des interlocuteurs intéressants (je pense et j'espère tout aussi intéressés), ainsi que messieurs Yves Nadot et Pascal Casari pour leurs travaux scrupuleux de rapporteurs ainsi que leurs remarques pointues.

Trois ans, c'est le temps qu'il a fallu pour aboutir au document qui m'a ouvert les portes de cette présentation. Pour m'avoir fourni un cadre de travail chaleureux et on ne peut plus propice à la réalisation de mes recherches je tiens à remercier un grand nombre de personnes de l'équipe Mécanique des Matériaux et Assemblage du Laboratoire Brestois des Mécanique et des Systèmes:

- En commençant par Jean-Yves Cognard qui a posé les bases du projet et qui a su me faire grimper les premières marches. Ne pas avoir pu travailler plus longtemps avec toi Jean-Yves fait partie des grandes déceptions de ce projet. Même si quelques « n'importe comment, il faut vérifier » manquent certainement au résultat final j'espère que le travail te plaît sous cette forme. Je te souhaite un bon rétablissement.
- David Thévenet et Romain Créac'hcadec, je vous dis un grands merci pour avoir su me donner des directions à suivre sans me perdre en cours de route. Grâce à vous les « burnouts » ont été évités. Sans jamais imposer les choses, vous avez su m'ouvrir les yeux, pour m'aider à cerner concrètement les problématiques et construire chacune de mes démarches scientifiques.
- Pour sa grande aide sur les aspects numériques/modélisation, je tiens à remercier grandement Nicolas Carrère qui sait souvent mettre des choses concrètes (et « physiquement admissibles ») sur des logiques que l'on ne s'explique souvent « qu'avec les mains » et ce, sans avoir à se mettre « la rate au court bouillon ». Grâce à son expertise sur les méthodes éléments-finis et son esprit didactique je tiens, par là même, à remercier Sylvain Moyne qui a su transformer certains de mes grands problèmes en de simples questionnements caducs. Merci aussi à Jean-Yves Leroux qui de mes simples questionnements en a fait de grands problèmes ... néanmoins, eux-aussi aujourd'hui caducs.
- Pour leurs soutiens techniques et logistiques (« tu ne sais pas où je peux trouver un pied à coulisse ? »), je tiens à remercier chacun des techniciens du laboratoire et en particulier Laurent Kernéis qui m'a grandement aidé à mettre en place un bon nombre de mes essais.

Trois ans, c'est la période que j'ai passé dans mon bureau, trois secondes c'est environ le temps qu'il a fallu pour m'y sentir bien. J'y ai vu voler quelques objets (tasses, porte-avions, sous marin...) mais aussi et surtout passer de chaleureux collègues : Vincent Legrand (le dernier des mohicans version princesse Disney), Nicolas Arnaud (grand auditeur à chacune de mes présentations, pourvoyeur de jolies questions et animateur de grands débats), Sarah Plessis (la princesse au grand cœur et fort caractère) et Pierrick Florin (le Kevin Langerec breton, quelques centimètres en moins mais un cabriolet Peugeot en plus). A tous, je vous dis un grand merci pour avoir rendu mon atmosphère de travail si agréable.

Trois ans, c'est aussi et surtout le temps qu'il m'a fallu pour écrire la première demi-page dans mon dictionnaire de Brestois. Pour m'avoir accepté dans votre communauté si distinguée, pour avoir su me faire découvrir les us et coutumes séculaires de votre si belle région, ô vous qui êtes si fiers de vos valeurs, ô vous fiers étendards de la pointe nord qui faites si élégamment flotter les blasons finistériens merci à vous de m'avoir l'espace d'un instant trouvé une place dans vos rangs ... merci à vous Sarah Thomas et Matthieu Corfa. Mais sans toi Estelle Bellanger, ces étendards flotteraient-ils si haut ? Je ne le crois pas. C'est toi qui es le mât de ces drapeaux, la poutre de ces édifices, l'Atlas de ce petit monde. De tout mon cœur, merci à vous trois pour avoir su m'aider sur les petits tracés de tous les jours et d'avoir su apporter de joyeux moments de pause.

Trois ans, néanmoins c'est court, et vingt-six ans ça l'est beaucoup moins. Vous, mes parents et toi mon frère, pour m'avoir accompagné à chaque étape de ma scolarité, tous les merci que j'ai pu écrire en ces quelques lignes, en quelques sortes, vous les méritez multipliés par 8,667.

Table of contents

Introduction

Chapter I: State-of-art in characterization of bonded joints under cyclic loadings.

<u>I.1. Introduction to structural adhesive bonding.....</u>	<u>13</u>
I.1.1. Formulations	13
I.1.2. Adhesion mechanisms	15
I.1.3. Surface treatments	16
<u>I.2. Designing bonded structures under cyclic loading.....</u>	<u>17</u>
I.2.1. Definition of the cyclic loading	17
I.2.2. Initiation vs. Propagation	18
I.2.3. Total life method	19
I.2.4. Prediction using fracture mechanics approach	20
I.2.5. Prediction using damage mechanics approach.....	21
I.2.6. Prediction considering the viscous behavior	22
<u>I.3. Characterization of structural adhesive</u>	<u>27</u>
I.3.1. Bulk samples.....	27
I.3.2. Bonded specimens.....	28
I.3.3. Advanced tests	32
<u>I.4. Modeling of structural adhesives.....</u>	<u>35</u>
I.4.1. Phenomenological approach.....	35
I.4.2. Theories for viscous behavior	37
I.4.3. 3D model formulations for plasticity	40
<u>I.5. Conclusion & main issues</u>	<u>43</u>
I.5.1. Which model to describe the mechanical behavior under cyclic loading?	43
I.5.2. Which characterization test?	43
I.5.3. How to analyze the mechanical behavior of a bonded structure?	44
I.5.4. Presentation of the approach adopted	45

Chapter II: Experimental approach for the characterization of the viscous adhesive joint mechanical behavior.

II.1. Bonded specimens	49
II.1.1. Polyurethane bi-component adhesive	49
II.1.2. Substrates	50
II.2. Experimental method	53
II.2.1. Bonding procedure	53
II.2.2. Modified Arcan device and experimental tests	54
II.2.3. Measurement of the adhesive deformation	55
II.3. Characterization strategy	56
II.3.1. Monotonic behavior	56
II.3.2. Creep behavior	58
II.3.3. Cyclic behavior	60
II.4. Experimental campaign overview	64
II.4.1. Ageing as a factor of influence in the mechanical behavior	64
II.4.2. Reproducibility	64
II.4.3. Information on failure	65
II.5. Conclusion	66

Chapter III: Modeling and identification of the mechanical cyclic behavior.

III.1. Shear behavior: numerical approach	69
III.1.1. Viscous behavior definition	69
III.1.2. Inverse identification	70
III.1.3. Stress distribution under creep/recovery conditions	75
III.1.4. Numerical and experimental comparison	76
III.2. 3D constitutive behavior	79
III.2.1. Constitutive equations	80
III.2.2. Computational algorithm	81
III.2.3. Inverse identification	86
III.3. Conclusion	92

Chapter IV: Cyclic behavior of a bonded specimen with low edge effects.

IV.1. Experimental results under shear loading	97
---	-----------

IV.1.1.	Reproducibility	98
IV.1.2.	Mean load influence.....	98
IV.1.3.	Influence of the load amplitude.....	99
IV.1.4.	Influence of the loading rate	100
IV.1.5.	Joint stiffness	101
IV.1.6.	Failure scenarii.....	102
IV.2.	<u>Numerical prediction.....</u>	103
IV.2.1.	Failure criterion	103
IV.2.2.	Prediction of the cumulative displacement	106
IV.2.3.	Influence of the mean load on the ratcheting effect.....	107
IV.2.4.	Influence of the load amplitude on the ratcheting effect.....	108
IV.2.5.	Influence of the loading rate on the ratcheting effect	108
IV.2.6.	Fatigue life prediction.....	109
IV.3.	<u>Results under tensile-shear loading.....</u>	110
IV.3.1.	Reproducibility	110
IV.3.2.	Mean load influence.....	110
IV.3.3.	Load amplitude influence	111
IV.3.4.	Joint stiffness	112
IV.3.5.	Fatigue life.....	112
IV.3.6.	Numerical prediction.....	113
IV.4.	<u>Results under tensile loading.....</u>	116
IV.4.1.	Ratcheting effect	116
IV.4.2.	Joint stiffness	116
IV.4.3.	Fatigue lifetime	116
IV.5.	<u>Conclusion.....</u>	118

Chapter V: Toward cyclic behavior of windmill structures: case studies.

V.1.	<u>Arcan specimen with thick adhesive joint.....</u>	121
V.1.1.	Bonded specimen.....	121
V.1.2.	Monotonic results	121
V.1.1.	Identification of parameters for thick adhesive.....	126
V.1.2.	Stress distribution under creep conditions	129
V.1.3.	Cyclic results	131
V.1.4.	Numerical simulation of cyclic tests.....	135

<u>V.2. Arcan specimen with composite blade</u>	<u>136</u>
V.2.1. Composite material.....	136
V.2.2. Bonded specimen.....	138
V.2.3. Monotonic results	139
V.2.4. Cyclic results	141
<u>V.3. Case study</u>	<u>144</u>
V.3.1. Wind blade structure	144
V.3.2. Testing wind blade structures.....	145
V.3.3. Development of a coupon-size experimental method	147
V.3.4. Experimental results	152
V.3.5. Toward a fatigue lifetime prediction: numerical investigations.....	157
<u>V.4. Conclusion</u>	<u>160</u>

Conclusions & prospects

References

Introduction

The Wind energy was used by civilizations since early recorded history. Indeed, wind propelled boats along the Nile River as early as 5000 B.C. (Figure 1a), and helped Persians pump water and grind grain between 500 and 900 B.C. As cultures understood the power that wind offered, the use of windmills spread from Persia to the surrounding areas in the Middle East. Around 1000 A.D., the wind power technology spread to European countries such as Netherlands, where windmills were used extensively in food production (Figure 1b). In the late 1800s, Daniel Halladay and John Burnham build the “Halladay” windmill (Figure 1c). Especially designed for the landscape of the American West, this design helped farmers and ranchers pump water for irrigation.

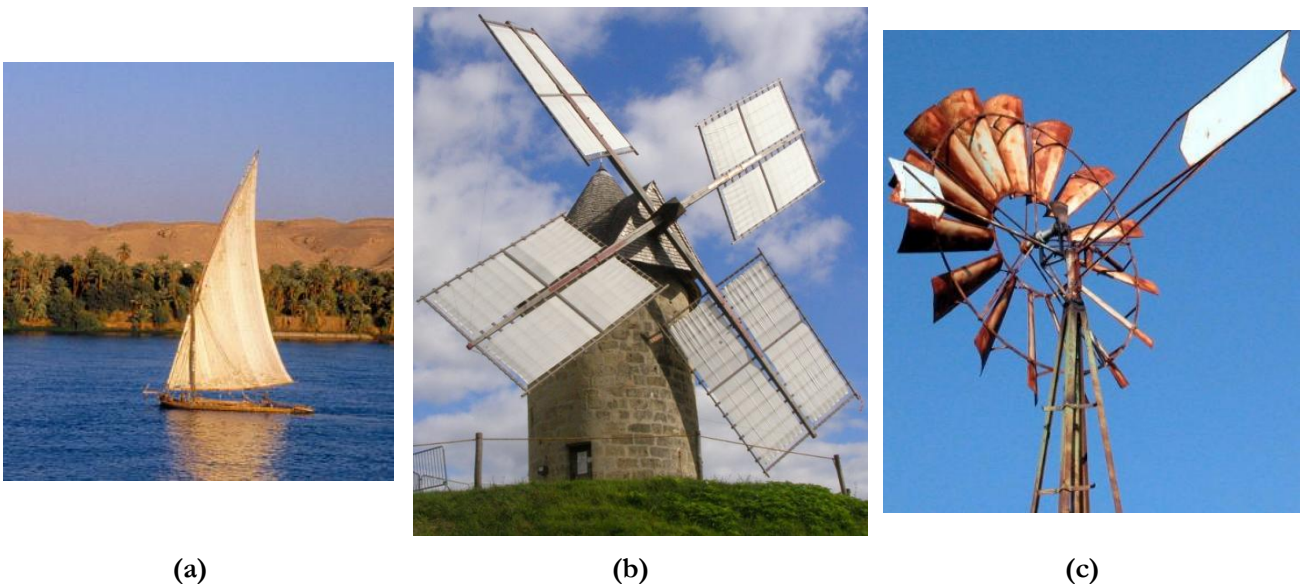


Figure 1: History of wind power: boat on the Nil river (a), windmill in Holland (b) and Halladay windmill (c).

As the 21st century began, fossil fuel was still relatively cheap, but rising concerns over energy security, global warming and eventual fossil fuel depletion led to an expansion of interest in wind energy. Therefore, renewable energy directives imply an important growth of wind energy in Europe. For example, the Upwind project (Fichaux, et al., 2011) is the largest public/private partnership ever designed for the wind energy sector and relies on clear objective: the acceleration of the innovation rate with project supported by the European Commission as the “Wind Energy Thematic Network” (WEN). As shown in Figure 2, up-scaling in wind turbine designs is an objective of this project and the typical parameter for this growth is the diameter of the rotor and the wind blades. For these modern designs such as offshore wind-turbines (Figure 3a), blades are made from integral manufactured parts that are bonded together.

In these modern lightweight designs, Fiber-Reinforced Plastics (FRP) are increasingly used for three principle reasons: weight saving, good fatigue resistance and good corrosion resistance to provide long-term solutions. In all mechanical components the introduction of holes gives stresses concentration factors. For composite pieces holes imply cut fibers and induce weakening of the fracture resistance. Therefore, considering the lost of mechanical performance due to riveting and bolting FRP, adhesive bonding solutions for FRP imply an important advantage.

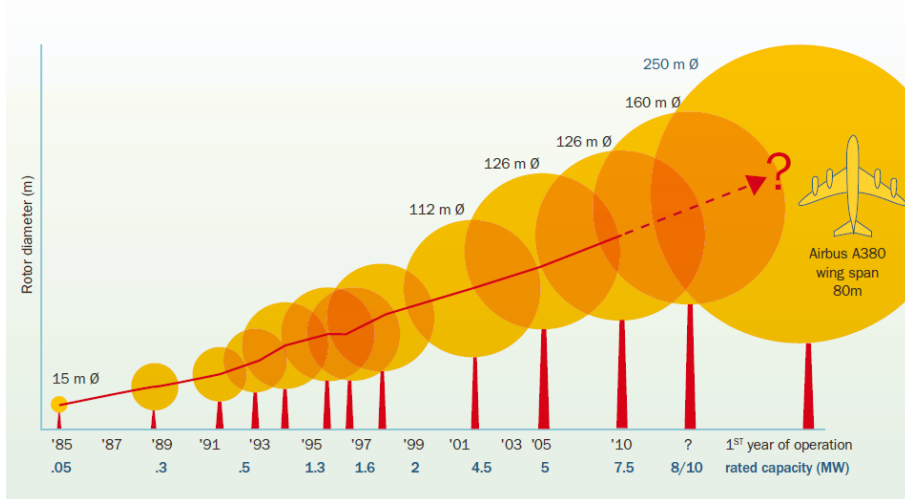


Figure 2: Up-scaling history and objectives for wind turbine rotor diameters (WEN) (Fichaux, et al., 2011).



(a)



(b)

Figure 3: Example of an offshore windmill (a) and adhesive bond-line in a wind turbine blade (b).

Hence, in a wind turbine blade with a length of 60 meters approximately 500kg of bonding paste are used (Figure 3b) and adhesives contributes strongly to the structural integrity. An example for a structural bond line is the joining of the spar caps and webs of a blade: Figure 4 shows the bond lines of structural adhesives. The bond lines in modern wind turbines present a particular design challenge because both the thickness and length of the adhesive bond are much larger than in other applications.

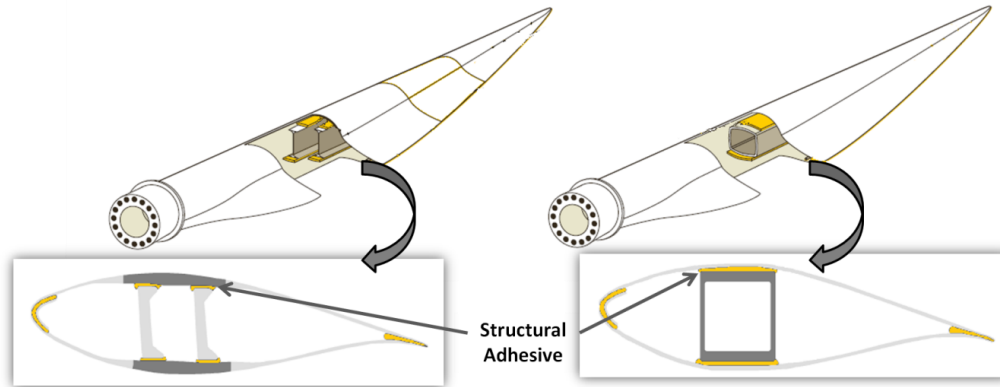


Figure 4: Example of structural bond lines on two wind blade designs.

Therefore, in the application of wind turbine-blade structural adhesives must meet special requirements:

- Resistance to complex stress states due to bond line thickness,
- Resistance to extreme environmental conditions, particularly for offshore applications,
- Easy processing to enable very long adhesive joints to be manufactured at one time,
- High resistance to manufacturing defects.

The range of uses for structural bonding technology covers a large field of applications. As a result, many adhesive formulations were set up to cover all areas. In this study the application case of the SikaForce®-7817 L60MR (Sika, 2011) is considered. The chemical and mechanical properties of the adhesive considered were accurately selected in order to bond the wind-blades mechanical components such as the spar caps Figure 4.

Wind turbine blades are subjected to flap-wise and edgewise bending loads, inertia forces, loads due to pitch acceleration, as well as torsional loading. Most of these cyclic loadings are thus transferred to the assembly by the adhesive bond-lines. Therefore, an accurate characterization and modeling of structural adhesives is a key objective for the wind-blade designers in order to avoid blade failures (Figure 5).



Figure 5: Examples of wind turbine accidents due to blade failures.

In this work, in a first step, the characterization of the adhesive material in its bonded form needed to be conducted. The mechanical behavior of adhesives strongly depends on the type of load applied.

Indeed the behavior in tension cannot be extrapolated from a single shear test (Créac'hcadec, 2008). Furthermore as a polymeric material, adhesive joints behaviors are strongly linked to viscous phenomena. Assuming these two important aspects, the characterization of the bonded joints needs an experimental method able to satisfy the several following conditions:

- A range of loading combinations with different ratios of tension and shear using the same design of bonded specimen;
- The possibility of different loading cases involving the long term mechanical behavior of the sample;
- Limitation of edge effects in the bond-line, in order to obtain an accurate characterization of the adhesive material.

Unfortunately, most of the tests proposed by standards for the characterization of adhesive joints suffer from edge-effects. Nevertheless, in recent studies Thevenet et al. (Thevenet, et al., 2013), demonstrated the interest of the modified Arcan device on structural adhesives since they were able to produce a large data base for a bonded structure under cyclic loadings.

In this study, the first aim was to extend the use of such a device to the characterization of the cyclic and fatigue behavior. Therefore, with the approach chosen, importances of the viscous phenomena occurring in the bonded specimen were highlighted. The experimental campaign should thus need specific long-term tests (for example creep tests) to be performed on bonded specimens. Then, the objective was to propose a 3D numerical model able to describe viscous phenomena and to retrieve the cyclic mechanical response with an adhesive layer showing low edge effects. These two first steps of the approach were thus based on bonded specimen using aluminum substrates with typical specimen geometries (Créac'hcadec, 2008) (Maurice, 2012) (Thevenet, et al., 2013) using thin adhesive bond-line.

From there, different validations of the approach were proposed progressing to sample getting closer to the industrial application case: composite bonded structures with thick adhesive layers. Therefore, the objective was in a second time to investigate the application of the approach to structures with adhesive/composite interfaces and thick bond-lines.

This document presents results for all of these steps presented in five chapters. The first chapter proposes a literature review of structural bonding under cyclic loadings, focusing on the effects of viscosity on the mechanical behavior of bonded structures. In a second chapter, an experimental characterization of the 3D viscous behavior of the SikaForce®-7817 L60MR structural adhesive is performed mainly using the creep behavior. Thanks to the experimental database established with a modified Arcan device using samples with low edge effects, a 3D visco-elastic visco-plastic model is proposed in the third chapter. In this chapter, an identification strategy is then presented using creep results obtained in shear and tension-shear. The numerical results are then confronted to the cyclic experimental responses using the same bonded specimen and the same testing method. Finally, in chapter five, the application of the approach is investigated. This aim is reached using two intermediate steps: influence of the bond-line thickness and influence of the composite/adhesive interfaces. A final case study is then proposed using a representative FRP bonded sample under a four point bending loading case.

This three years work has been conducted in the LBMS (Laboratoire Brestois de Mécanique et des Systèmes) and he was financially supported by Sika Technology and the Brittany region.

Chapter I:

State-of-art in characterization of bonded joints under cyclic loadings

Introduction

This chapter aims to give an overview of the fatigue behavior characterization, concerning bonded structures. Different aspects concerning structural adhesives under cyclic loading are reviewed trying to size the field of the scientific domains concerned in bonded joints design. As a first step, the chemical principles and the key definitions useful for the adhesive bonding definition are given. Then, results from the literature, and the approach adopted concerning the fatigue design and characterization of bonded structures are detailed. In a second part, the advances in structural bonding testing and numerical modeling applied to cyclic characterization are presented. Finally, in view of the contents of the bibliography, a conclusion is given and the approach adopted is detailed.

Contents:

<u>I.1. Introduction to structural adhesive bonding.....</u>	<u>13</u>
I.1.1. Formulations	13
I.1.2. Adhesion mechanisms	15
I.1.3. Surface treatments	16
<u>I.2. Designing bonded structures under cyclic loading.....</u>	<u>17</u>
I.2.1. Definition of the cyclic loading	17
I.2.2. Initiation vs. Propagation	18
I.2.3. Total life method	19
I.2.4. Prediction using fracture mechanics approach	20
I.2.5. Prediction using damage mechanics approach.....	21
I.2.6. Prediction considering the viscous behavior	22
<u>I.3. Characterization of structural adhesive</u>	<u>27</u>
I.3.1. Bulk samples.....	27
I.3.2. Bonded specimens.....	28
I.3.3. Advanced tests	32
<u>I.4. Modeling of structural adhesives.....</u>	<u>35</u>
I.4.1. Phenomenological approach.....	35
I.4.2. Theories for viscous behavior	37
I.4.3. 3D model formulations for plasticity	40
<u>I.5. Conclusion & main issues</u>	<u>43</u>
I.5.1. Which model to describe the mechanical behavior under cyclic loading?	43
I.5.2. Which characterization test?	43
I.5.3. How to analyze the mechanical behavior of a bonded structure?	44
I.5.4. Presentation of the approach adopted	45

I.1. Introduction to structural adhesive bonding

In the year 2000, adhesive bonding is a global market of 8.8 million of tones and a 21.6 million Euros of standard turnovers. In this market, structural adhesives represent 5%. The “Structural” definition of the adhesive is a normalized engineering term meaning that the adhesive joint is an integrated part of the structure playing a role in its mechanical behavior. With this precision structural bonding is distinguished from function as water-tightness adhesives or positioning adhesives. Knowledge on the structural adhesives, the mechanisms of adhesion and the joint mechanical behavior stay limited but the combined study of chemistry and mechanical engineering principles provides basic skills for the structural bonding. According to Burchardt (Burchardt, 2010), the structural bonding goals are to build complex structures made of different materials from different parts that fulfils a required function and predicted lifetime. As a basic principle, in order to develop better mechanical performances, it is clear that the bonding surface areas need to be sufficient to transfer the expected loading. Under many conditions, it is better to use an adhesive with higher elongation and lower strength combined with a larger area. This principle allows more even stress distribution which results in bonding less sensitive to overload and defects. For example, in bonding fiber reinforced composites structures an adhesive that is too strong can lead to a failure between the matrix and the fibers. In this case, the reason is too high local stresses and failure can be avoided by using an adhesive with a lower strength but a higher elongation. Furthermore, the design of adhesive joints is highly dependent on the adherent properties. Various materials for the substrates and various applications suggest particular design. Therefore, the key to design structural bonding successfully is to design adhesives for a particular function or to define the best one for that application from existing and known adhesive systems used in the industry. As suggested in Figure I.1-1, the necessary skills for structural bonding need both the accurate understanding of the “engineering principles” and “chemical mechanisms”.

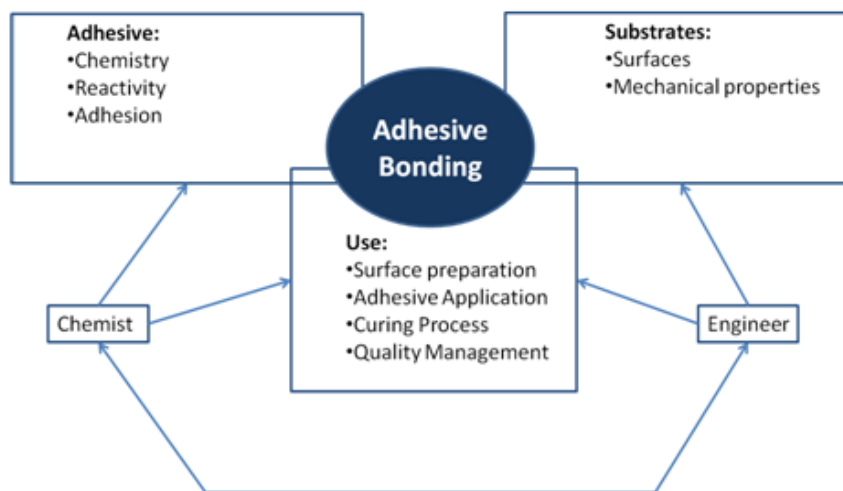


Figure I.1-1: Skills necessary for structural bonding (adapted from (Burchardt, 2010)).

I.1.1. Formulations

Structural adhesives are based on a list of different chemical compositions. Each of these chemical compositions offers a range of mechanical properties and has specific abilities helping engineers to make a choice for the application considered. In fact the general adhesive mechanical properties are still defined by the base chemistry. Even if many other systems exist, only the main structural adhesives chemical compositions will be described:

- **Epoxy:** the main workhorse of structural adhesive formulation. Epoxides exhibit capacities to form extremely strong and durable bonds. They are available in a wide variety of forms from low viscosity liquids to solid pastes or films. Nevertheless the mechanism of curing (termed addition) stay the same, requiring precise quantity of resins and hardener and the reaction is strongly influenced by temperature (Moussa, et al., 2012): the higher the temperature, the faster the reaction becomes. For a two-part system epoxide adhesive complete cure times at room temperature range from hours to several days, while with high temperatures a time of 10 minutes can be obtained.
- **Reactive acrylic:** these adhesive formulations have preferences toward bonding plastic systems, such as polycarbonates, PolyMethyl MethAcrylate (PMMA), or Acrylonitrile Butadiene Styrene (ABS). Reactive acrylics are two-part systems comprising a viscous resin and an activator carried in a low volume of solvent. These formulations have the benefits to rapidly cure (normally a few minutes).
- **Toughened acrylic:** these adhesive tolerate a minimal surface preparation to bond well to a very wide range of materials. The cure mechanism of this two-part system is such that acrylics are tolerant of imperfect mixing ratios.
- **Anaerobic acrylic:** known as thread-locking fluid applications, this formulation is used to secure, seal and retain turned screws or closely fitting metal parts to prevent loosening, leakage or corrosion. As a member of the acrylic family of adhesives they are often in the form of low viscosity liquids. These single part adhesives cure when oxygen is excluded (anaerobic conditions) and in presence of metal the cure rate is much faster. The close fit excludes air and the metal surface speeds the rate of cure, hence it specific range of use.
- **Cyanoacrylate:** these adhesives known as “superglues” need close fitting joints as well and usually solidify in seconds. Primarily curing requires a thin film of moisture on the surface to be bonded. Therefore preferred bonded surfaces are non-porous materials. Compared to the previous systems, cyanoacrylate is a thermoplastic system hence this formulation is more susceptible to creep, especially at elevated temperatures.
- **Silicone:** owing to their low modulus of elasticity, silicone has gained popularity in structural and semi-structural applications requiring flexible bonding and resistance to environmental extremes. Therefore, main application for silicone adhesives is for glass bonding either as structural glazing or for tank fabrication, where both specific properties are needed. Silicone systems are available in single or two-part forms. Most of these products are applied and cured under ambient conditions and they are termed room-temperature vulcanizing (RTV) products.
- **Polyurethane (PU or PUR):** PU adhesives are chemically reactive formulations that may exist in single part or two part systems. For the single part systems cure is initiated by moisture in the atmosphere. Such as acrylic or epoxide formulations, for two part systems cure can be controlled via catalysts or heating. PU find major uses in bonding composite structures especially glass fiber reinforced plastics (GRP). A wide variety of PU adhesives exist and Figure I.1-2 shows the three most commonly used structural adhesives in terms of their shear modulus and elongation. PU adhesives encompass a large area in this figure and are therefore the most versatile adhesive technology: from very soft and elastic, to very rigid. The key to use this kind of formulation is to control variables as cross link density, chain length or molecular building blocks properties in order to achieve interesting mechanical properties.

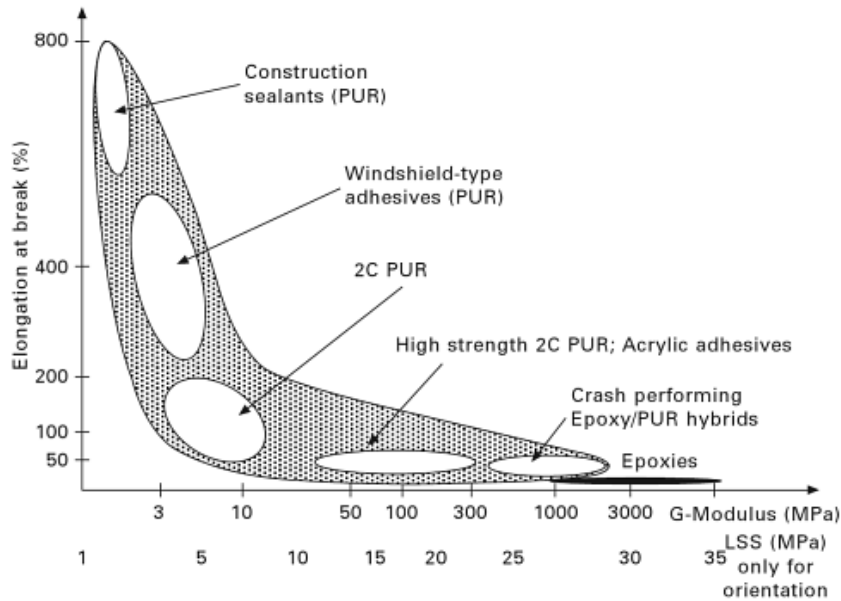


Figure I.1-2: Landscape of PUR (Burchardt, 2010).

I.1.2. Adhesion mechanisms

For each formulation, quality of an adhesive is grounded on two essential properties:

- “**Cohesion**” according to NF-EN-923 (AFNOR, 2008): mechanical properties within the adhesive joint itself;
- “**Adhesion**” according to NF-EN-923 (AFNOR, 2008): property related to the adherend used and interfacial mechanisms implemented.

“Cohesion” properties, based on molecular interactions, concern every material from metallic to polymeric materials. “Adhesion” properties are specific to the adhesives and the bonding mechanisms. Theories developed to understand adhesion are complex and are based on different aspects involving chemistry, solid and surface mechanisms ... From a chemist point of view, adhesion lays on molecular interaction between the adhesive and the adherend. For physicists, the adhesion phenomena are based on energy dissipation mechanisms. Therefore, these different aspects have to be understood in order to apprehend the numerous parameters of a bonding process. In his thesis (Joannes, 2007) through the study of (Kinloch, 1987) and (Shanahan, et al., 1991) proposed the “Adhesion” phenomena under different aspects presented on Figure I.1-3:

- **Mechanical adhesion:** the basic idea, related by (Mc Bain, et al., 1925), defines mechanical theories to describe adhesion and provides useful models. In these models, surface roughness of the adherend plays an essential role in adhesion: the theory is based on penetration of the adhesive joint in both micro and macro cavities during the bonding process.
- **Physicochemical adhesion:** this theory is grounded on different models:
 - Adsorption theory: this model is based on the observation that the adhesive and substrate must come into contact for the possibility of the formation of an adhesive bond. Thermodynamic theories relate surface energies and surface tension to wetting and spreading in order to describe the adhesion;

- Electrostatic theory: this theory was put forward by (Deryagin, et al., 1957). The models developed rely on both electrostatic and van der Waals forces to explain adhesion forces;
- Diffusion theory: the first model provided by (Voyutskii, et al., 1957) associates the adhesion to inter-diffusion of polymer chains: molecules of the two parts of the specimen inter-diffuse. For this model developed for polymer adhesion, an important question is the mutual solubility-compatibility of the adherend and the adhesive.

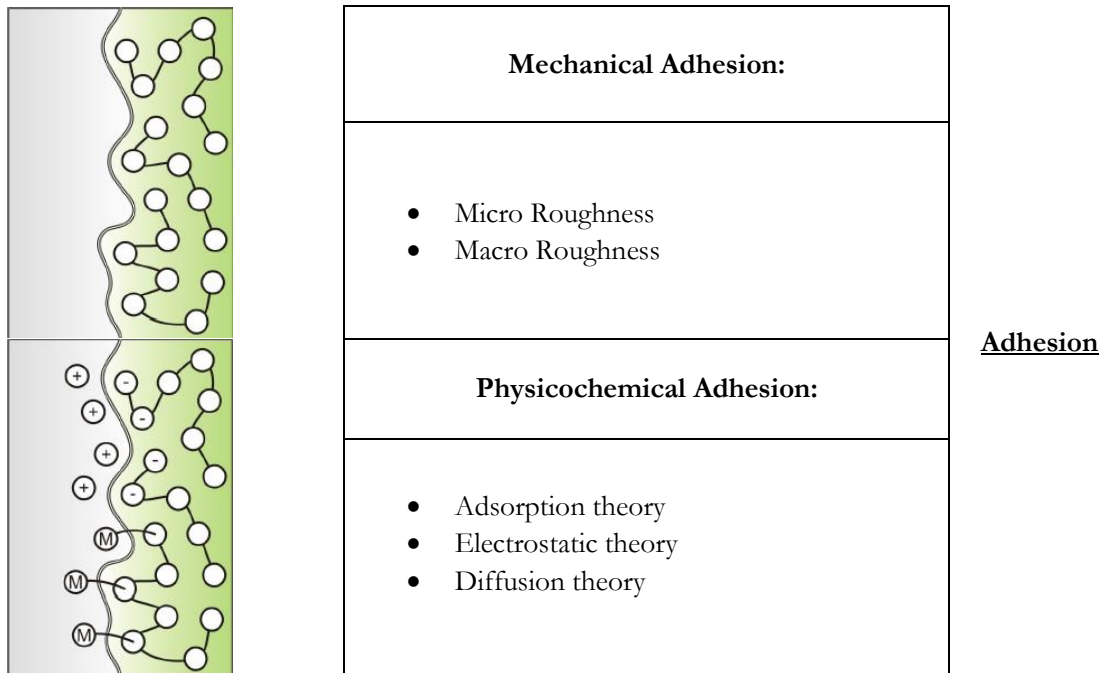


Figure I.1-3: Adhesion mechanisms: different theories.

I.1.3. Surface treatments

“Adhesion” theories have shown complex phenomena involving many parameters to consider for adhesive bonding. Before bonding, a surface pretreatment permits to optimize the adhesion mechanisms. The pretreatment depends on the adherend, the adhesive formulation and the mechanical performances needed. The first step of a pretreatment is an extensive cleaning to remove environmental contaminations and to maintain a molecularly “clean” surface: good adhesion is aided by high surface energy, partly to aid wetting. The process of cleaning may be:

- **Mechanical treatments:** these treatments (abrasion, sanding, ultrasounds...) generally remove friable surface layers and generate macro rough surface on metallic surfaces. They are generally combined with a degrease process;
- **Chemical treatments:** such as the mechanical treatments, a purpose of such treatments is to remove friable organic or inorganic layers including oxides or corrosion products and to leave an enhanced surface topography. Chemical treatments can also be considered as used to produce chemical conversion coatings. Examples of these coatings are chromate-phosphate, titanium-zirconium or molybdenum based solutions. In order to reduce the environmental impact of chemical treatments (in particular chromate containing treatments), extensive efforts are ongoing to help develop drop-in replacements;

- **Electrochemical treatments:** these treatments are complex, time consuming and costly to carry out. However, for structural metal bonding, these treatments are highly recommended as they impart all of the physicochemical properties (wettability, roughness...) required providing the best level of adhesion. As an example of this kind of treatments, the most successful treatments for aluminum and titanium include direct current anodic oxidation in chromic, phosphoric, or sulfuric acid electrolytes.

As a conclusion, adhesive bonding involves several physicochemical principles which remain difficult to experimentally highlight. Indeed, chemical reactions are involved in the polymeric material building as well as in the adhesion of the polymer with the substrate and its results are hardly linked to the reliability of the bonded structure.

In this study the application case of a structural adhesive SikaForce®-7817 L60MR (Sika, 2011) is considered. In order to ensure a certain quality in the experimental results, an accurate control was brought on the different physicochemical factors involved in the adhesive bonding. The different aspects listed in this chapter were thus considered as key steps in order to precisely define a framework in the experimental testing.

Wind-blades are the key-components of efficient wind turbines. Therefore increasing the durability and the abilities to bear cyclic loadings for these products, is an important problem for the designers. The issues for them are in one hand that blade deformations should remain very small in order to sustain the aerodynamic properties and to avoid hitting other parts of the wind turbine. And in the other hand that the effects of materials damaging due to cyclic loading from the rotation remains negligible.

Following, the physicochemical principles mentioned, the properties of the adhesive considered were accurately selected in order to bond wind-blade mechanical components. As Adhesive bond-lines play an important role in the wind blade mechanical behavior, SikaForce®-7817 L60MR mechanical properties under cyclic loadings may determine performances and lifetime of the turbine. In order to investigate these performances, the following section, will present the different approaches developed in order to characterize the cyclic and fatigue behavior of adhesively bonded structures.

I.2. Designing bonded structures under cyclic loading

Fatigue involves the failure of material under cyclic loading. In fatigue tests, the maximum load considered can be significantly lower than that required to cause failure in a monotonic test. Considering the fact that in structures, compared to other bonding methods such as bolted assembly, adhesive permits to reduce stress concentrations, adhesive joints have potentially good fatigue resistance compared to other joining methods. However, adhesive joints are susceptible to accelerate the fatigue failure due to the effect of the adhesive ageing or mostly to viscous behavior in creep.

I.2.1. Definition of the cyclic loading

In fatigue, the loading varies with time, and the load is usually characterized in terms of peaks and troughs in the varying load. A fatigue cycle is defined as the time between adjacent peaks, and the fatigue frequency is the number of cycles in a second of time. For a simple sample, the fatigue loading can be characterized in terms of an applied stress or an applied strain. Commonly, studies on fatigue

represent the loading as constant amplitude. Concerning a stress driven fatigue test, the loading is characterized by two values taken from:

- The maximum stress σ_{max} and minimum stress σ_{min} ;
- The mean stress: $\sigma_m = \frac{\sigma_{max} + \sigma_{min}}{2}$;
- The stress amplitude σ_a (or stress range $\Delta\sigma$): $\sigma_a = \frac{\sigma_{max} - \sigma_{min}}{2} = \frac{\Delta\sigma}{2}$;
- The load ratio: $R = \frac{\sigma_{min}}{\sigma_{max}}$.

Figure I.2-1 represents these values on a sinusoidal waveform loading. Once the loading is generated, it can be used in testing as well as in simulations. In order to accelerate a fatigue test program, it is common in laboratory experiments to increase the load frequency. In metals, where the material may generally be rate insensitive over a large range of stress, an easy method of accelerating the test campaign is thus to increase the frequency by accelerating the loading rate. If these acceleration methods are performed for adhesive joints tests, care must be taken that any time dependent effects, such as creep or environmental factors, do not influence the mechanical behavior.

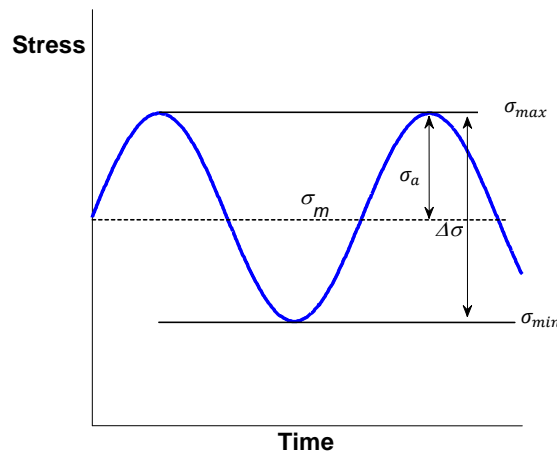


Figure I.2-1: Stress controlled cyclic loading (sinusoidal waveform).

I.2.2. Initiation vs. Propagation

The fatigue life of a bonded structure is commonly divided into two phases occurring in the mechanical behavior of the adhesive joint: initiation and propagation phases. In order to differentiate the initiation and the propagation phases, the distinction is often made between how a propagating crack is analyzed (propagation phase) and how the number of cycles before a crack has occurred can be predicted (initiation phase). As the first phase of the fatigue phenomena, initiation may be linked to important flaws registered within the adhesive material. As the end of the initiation phase, the definition of the crack appearance can be made at different scales: cracks in the material micro-structure or an observable macro-crack. Hence, the initiation in adhesives remains a really complex study and a little understood process. In the fatigue behavior, two different regions may be drawn, characterized by the crack length within the material: for a length below a certain value, only the initiation phase is considered and for a length above this value, the propagation phase dominates the fatigue behavior (Figure I.2-2).

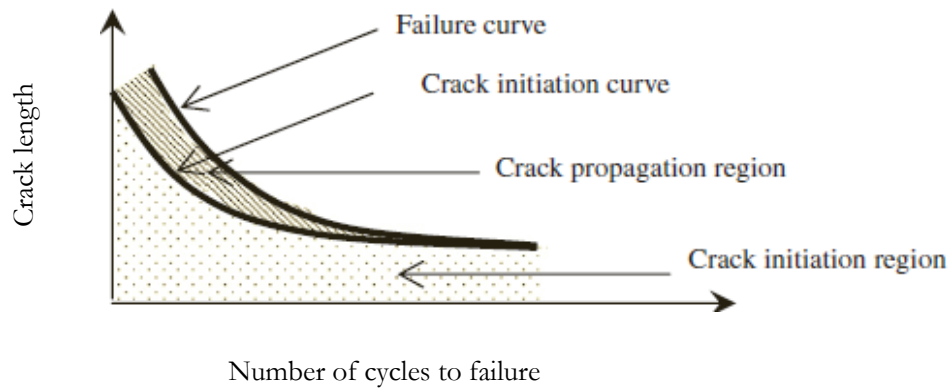


Figure I.2-2: Schematic representation of the fatigue behavior into two phases: cycles to failure (N_f) vs. crack length (L) diagram (Shenoy, et al., 2010).

For the stress analyst, a useful differentiation is to treat the fatigue as an initiation phase until a sufficient crack can be observed. However, the definition of this crack may be linked to the mean of observation used. Therefore, the lost of mechanical properties in the experimental record may be a relevant indicator that a sufficient crack has formed that further growth will be predicted using fracture mechanics.

I.2.3. Total life method

In these methods, the loading is low enough that the assumption of a linear elastic behavior is made. The number of cycles to failure (N_f) is generally plotted as a function of a load related variable, such as stress or strain amplitude. The stress variable S (for example, the stress amplitude σ_a) is usually chosen and the resultant plot is termed an $S-N$ curve, or Wöhler plot, and is known as the stress life approach. Figure I.2-3 presents typical load life experimental data for single lap joints using different load ratios R .

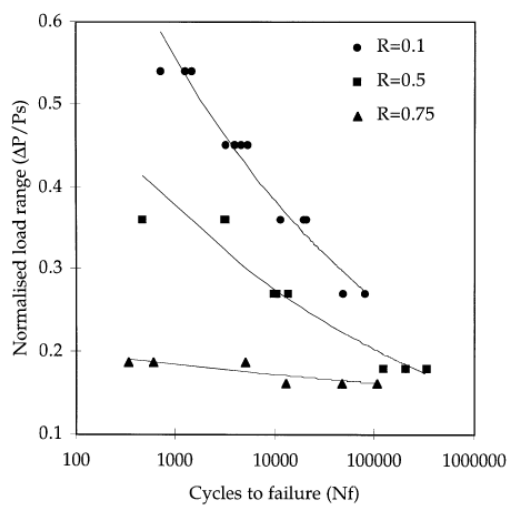


Figure I.2-3: Wöhler plot for failure in SLJ samples for different load ratios: cycles to failure vs. normalized load range (Crocombe, et al., 1999).

Fatigue behavior characterized through the use of experimentally derived stress life plot such as in metallic materials studies is considered as a classical and traditional approach. However, the standard stress life method gives no indication of the progression of damage and do not allow the initiation and propagation phases to be differentiated. This approach is useful as a design tool and in fatigue modeling as a source of validation data.

The total life method uses several standards: EN ISO 9664:1995 and ASTM D3166-99 (ASTM Int., 2012). This type of specimen and testing methods are known to introduce important stress concentrations. Therefore, in testing these samples in fatigue, the crack generally appears early at the edge of the adhesive joint, and the onset of cracking can be easily registered (Dessureault, et al., 1997) (Shenoy, et al., 2009) (Figure I.2-4).

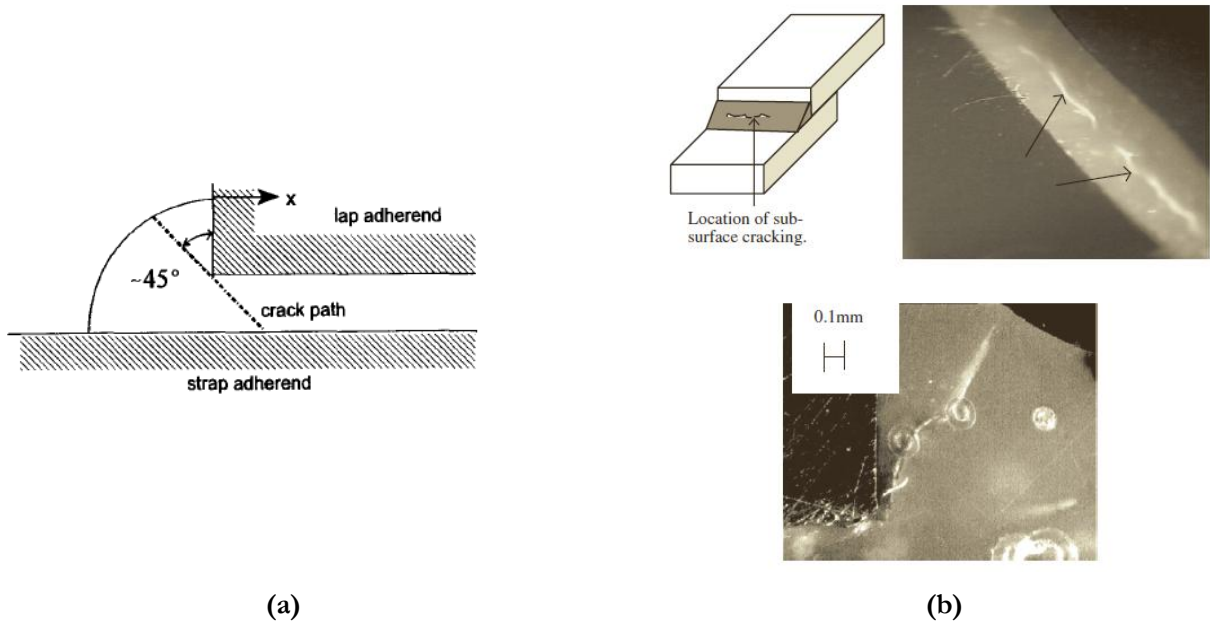


Figure I.2-4: Typical fatigue crack initiation site within the adhesive joint (Dessureault, et al., 1997)(a) and subsurface micro-crack images (b) (Shenoy, et al., 2009)

I.2.4. Prediction using fracture mechanics approach

As the main approach concerning the propagation phase, fracture mechanics assume the crack initiation as a phenomenon occurring during the early stage of the fatigue cycling or even a preexisting crack is initially considered. A rate of fatigue crack growth per cycle is thus defined by $\frac{da}{dN}$ as the principal variable and attempts are made to correlate it with appropriate fracture mechanics parameters and material constants. Therefore, in 1961, in a linear elastic framework, Paris proposed a power function of the stress intensity factor range $\Delta K = (K_{max} - K_{min})$:

$$\frac{da}{dN} = C(\Delta K)^m \quad (\text{Eq 1.1})$$

Although K is the most widely used parameter in the fracture analysis of a large range of materials (Irwin) (Paris, et al., 1961), other appropriate parameters such as the strain energy release rate G (Griffith, 1921) are also used. Instead of simple elastic assumptions, elastic-plastic fracture mechanics parameters can also be developed using new parameters such as the J-integral (Rice, 1968). For adhesive bonding, experimental tests using specific fracture tests (Double Cantilever Beam) (Ashcroft,

et al., 2002) (Kinloch, et al., 1993) showed that the measured crack growth rate plotted against the calculated maximum strain energy G_{max} (Figure I.2-5) can be divided in 3 parts:

- A first region is defined below a threshold strain energy rate G_{th} . Within this area the evolution of $\frac{da}{dN}$ is generally neglected;
- The second part of the curve can be described using a power law as developed by Paris (Eq 1.1), giving a linear prediction in a log-log diagram;
- The third region, not drawn in (Figure I.2-5), is characteristic of a fast evolution of the crack growth as the value of G get closer to the critical strain energy representative of the failure G_c .

Using this experimental results and a power law approach of the fatigue crack growth, the number of cycles to failure is thus numerically determined for bonded lap joints (Erpolat, et al., 2004).

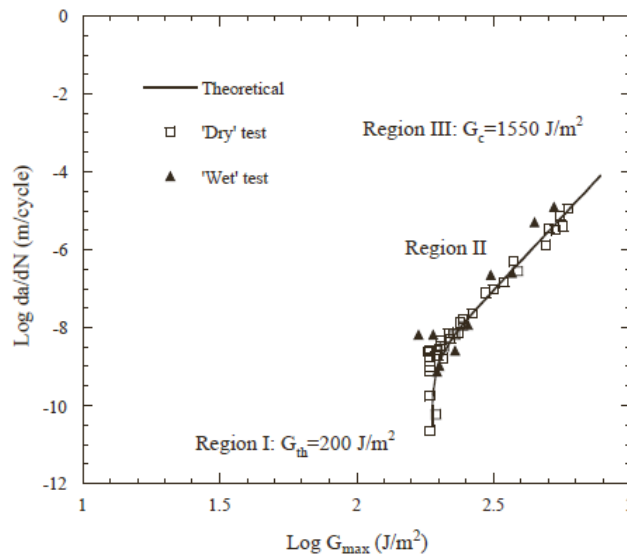


Figure I.2-5: Experimental data and numerical predictions for different bonded joints using a fracture mechanics approach: maximum strain energy (G_{max}) vs. crack growth rate ($\frac{da}{dN}$) (Hadaviana, et al., 2003).

I.2.5. Prediction using damage mechanics approach

The important limitation of the design methods based on Fracture Mechanics is the hypothesis of a pre-cracked sample. Therefore, considering a “well” bonded joint, the initiation phase is not accounted for. In the model of bonded joints, the damage mechanics approach allows the consideration of a progressive degradation and failure of the adhesive representing both initiation and propagation phases at a microscopic. Generally, the introduction of a damage variable D is required: initially equal to 0 (for an undamaged material) the variable evolved following fatigue damage equations to 1 for a fully damaged material (Lemaître, et al., 2000).

The continuum damage approach characterizes the evolutions recorded in the mechanical properties as effects of degradations within the material micro-scale. Therefore, in numerical simulations, for a damage fatigue law implementation in FE analysis, the damage variable D degrades the elements properties (Shenoy, et al., 2010) such as the Young modulus E_0 :

$$D = E_0(1 - D) \quad (\text{Eq 1.2})$$

A damage variable as $D = 1$ will represent a fully damaged element in the FE analysis and will thus be used to define the macro crack length.

In order to define the damage per cycle N , Shenoy et al. (Shenoy, et al., 2010) linked the damage rate $\frac{dD}{dN}$ to the localized equivalent plastic strain range $\Delta\varepsilon_p$, with a power law:

$$\frac{dD}{dN} = C_D(\Delta\varepsilon_p)^{m_D} \quad (\text{Eq 1.3})$$

where C_D and m_D are experimentally defined material constants. As a similar approach and with two material constants as well (C_{th}, m_{th}) , Khoramishad, et al (Khoramishad, et al., 2010) define a behavior with a threshold and relates the damage rate to a yielding strain ε_{th} below which, fatigue damage does not occur:

$$\frac{dD}{dN} = \begin{cases} C_D(\varepsilon_{max} - \varepsilon_{th})^{m_D}, & \varepsilon_{max} \geq \varepsilon_{th} \\ 0, & \varepsilon_{max} \leq \varepsilon_{th} \end{cases} \quad (\text{Eq 1.4})$$

The damage mechanics approaches are particularly suitable to Finite Element (FE) applications to degrade the properties of the elements (Moroni, et al., 2009).

I.2.6. Prediction considering the viscous behavior

Creep deformations are time-dependent deformations which can occur in materials which are considered visco-elastic or visco-plastic. Creep tests are defined by the application of a constant stress (Figure I.2-6). In experimental characterization tests, creep may be followed by a return of the loading to a zero-value. Then, during a second part of the test, measurement of a “recovery” in the creep deformation is thus possible: these tests are so called creep-recovery tests.

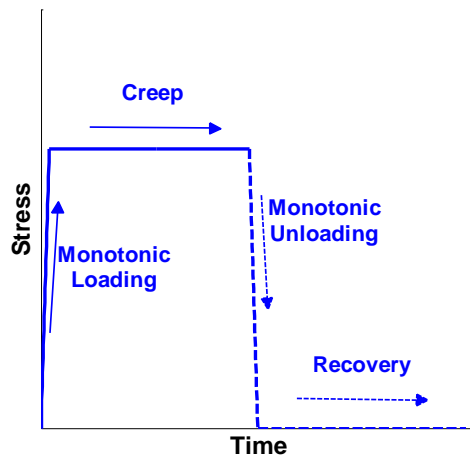


Figure I.2-6: Creep-recovery loading.

a. *Creep in fracture mechanics*

Polymeric adhesives may exhibit some degrees of viscous behavior over a part of their operating range. Evidences of creep in fatigue testing can be observed and application of a standard fracture mechanics can significantly over predict the fatigue life if there is significant accumulated creep. Hence, assuming viscous effects to be influent in the fatigue crack growth, the fracture mechanics approaches have been represented with a frequency dependency (Figure I.2-7). In 1976, (Landes, et al., 1976) proposed a fatigue crack growth $\frac{da}{dN}$ definition adapted from (Eq 1.1) with the introduction of a time-dependant expression C^* in place of the material constant C :

$$C^* = \int_{\Gamma} W^* dy - T_i \left\{ \frac{\partial \dot{u}}{\partial x} \right\} ds \quad (\text{Eq 1.5})$$

with,

$$W^* = \int_0^{\dot{\epsilon}_{ij}} \sigma_{ij} d\dot{\epsilon}_{ij} \quad (\text{Eq 1.6})$$

where W^* is the strain energy rate density and σ_{ij} is the component of the stress tensor considered and $\dot{\epsilon}_{ij}$ is the associated strain rate. T_i is the traction vector defined by the outward normal along the line contour taken from the lower crack surface to the upper crack surface, Γ . \dot{u} is the displacement rate vector, x is the overlap length coordinate and s is the arc length along the contour.

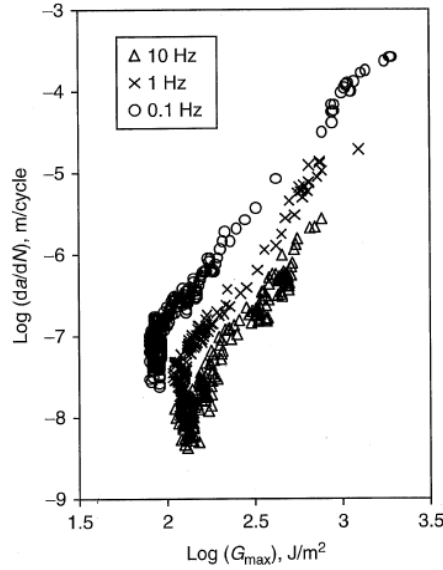


Figure I.2-7: Influence in the frequency in the fatigue crack growth: maximum strain energy (G_{max}) vs. crack growth ($\frac{da}{dN}$) (Al-Ghamdi, et al., 2003).

This approach has been used by (Al-Ghamdi, et al., 2003) to partition the crack growth into separate fatigue-dependent and creep-dependent components:

$$\frac{da}{dN} = \left(\frac{da}{dN} \right)_{fatigue} + \left(\frac{da}{dN} \right)_{creep} \quad (\text{Eq 1.7})$$

where the fatigue part is determined using high-frequency tests (to limit time dependent phenomena) and the creep part, using a low rate constant load crack growth.

b. *Failure in creep tests*

Generally, the failure in long-term behavior may often not be linked to the failure of a same specimen under a static load which usually involves random fracture mechanisms and causes a wide scattering of the results in terms of displacement to failure. Since creep is considered as a key weakness for polymeric materials such as adhesive joints, studies have been performed to evaluate the creep resistance of bonded joints (Geiss, 1998). Figure I.2-8a represents a typical response of a structural adhesive bonded specimen for a creep test. The evolution of the displacement measured along the creep time can be divided into three parts:

- In the phase one of the creep, the instantaneous elastic strain and the short term viscous strains occurs and complete quickly;
- The second seems dominated by a secondary slower phenomenon represented by the long term viscous behavior generally termed the steady-state creep;
- At the end of second phase creep accelerates in an hyperbolic shaped curve leading to failure of the specimen at the end.

The shape of the creep curve for a same specimen varied with the creep load level applied giving a different weight on each part in the creep strength behavior (Figure I.2-8b). Generally, for polymeric materials (Spathis, et al., 2012), the third part of the creep curve does not significantly contributes in the long term strength (Geiss, 1998). Hence, creep strength-time curves can be drawn joining time and load related limit points limiting the second phase for each static load conditions (Figure I.2-8b).

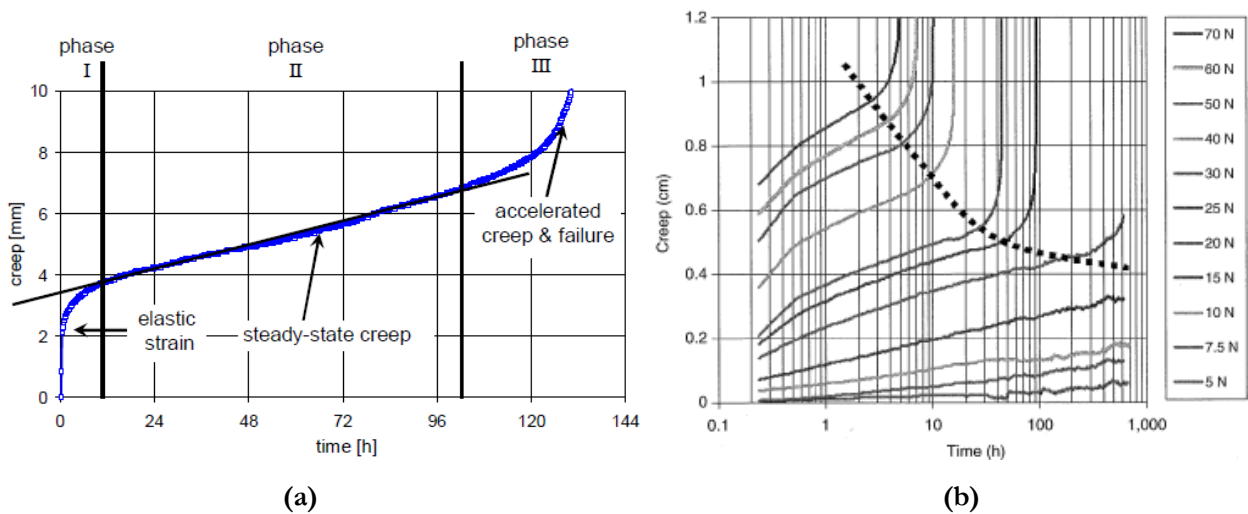


Figure I.2-8: Typical shape in creep data for SLJ specimen bonded with structural adhesives (a) and effects of different levels of static loads (b) (Geiss, et al., 2007).

c. *Ratcheting*

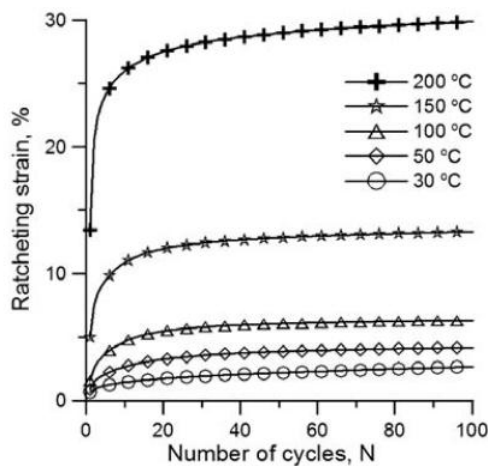
For cyclic tests with a non-zero mean stress, two phenomena can be observed depending on the material and on the loading conditions:

- A cyclic stabilization of the loops: the shape of the loops does not vary and the strain describes a stabilized hysteretic loop in stress-strain plane;
- A progressive cumulative strain growth after each cycle during the test.

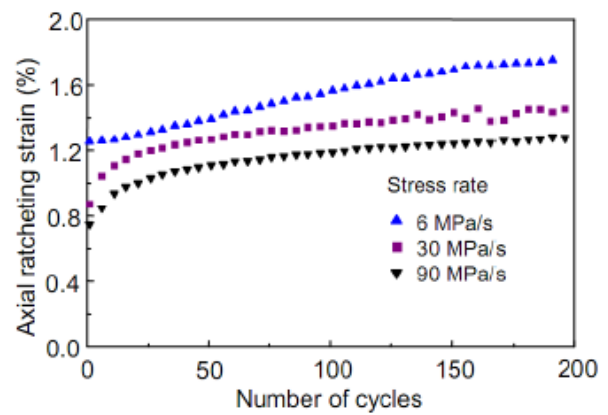
Therefore, the ratcheting effect is considered as this second phenomenon, experimentally recorded in materials for stress imposed cyclic loadings. The ratcheting strain ε_r is classically defined as the mean value along a cycle:

$$\varepsilon_r = \frac{\varepsilon_{max} + \varepsilon_{min}}{2} \quad (\text{Eq 1.8})$$

As presented in Figure I.2-9 and Figure I.2-10, for a large range of polymeric thermoplastic materials, different parameters of the cyclic loading have been identified to affect the ratcheting: the temperature (Zhang, et al., 2010), the loading rate or cycling frequency (Pan, et al., 2010), the mean load and the load amplitude (Bouvet, 2013). In the ratcheting curves of the polymeric materials two phases can be identified. Such as in creep curves, in the first part the material mechanical behavior leads to a high evolution rate of the strain recorded until a second part dominated by a steady state.

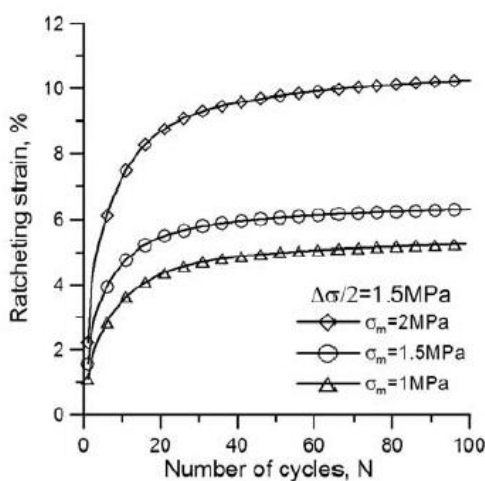


(a)

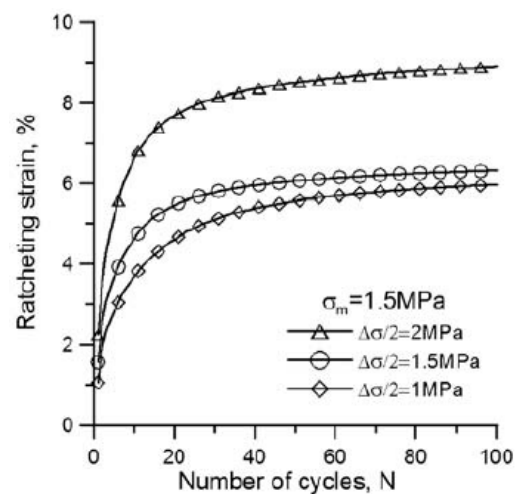


(b)

Figure I.2-9: Ratcheting strain vs. number of cycles diagrams: influence of the temperature on PTFE (a) (Zhang, et al., 2010) and influence of the loading rate on PEI(b) (Pan, et al., 2010).



(a)



(b)

Figure I.2-10: Ratcheting strain vs. number of cycles diagrams: influence of the mean stress (a) and influence of the load amplitude (b) on PTFE (Bouvet, 2013).

Increasing the temperature, Zhang et al. (Zhang, et al., 2010) have shown that the ratcheting strain of a polytetrafluoroethylene material (PTFE) is accelerated. Testing the same material and using the same method, an assessment of the effects of an increase on the mean load showed a higher ratcheting rate and a higher level of the steady-state. The influence of the load amplitude revealed a similar phenomenon with lower amplitudes. The loading rate influence investigated on polyethylenimine (PEI) (Pan, et al., 2010), has shown that for low loading rates the viscous behavior led to an increase of the cumulative strain per cycle. Even if the production remain fewer, studies have been driven on thermo-hardening materials, mainly on epoxy resins (Tao, et al., 2005) leading to a similar ratcheting behavior (Figure I.2-11) and the similar conclusions than using thermoplastics have thus been made.

As defined by (Vinogradov, et al., 2001), the mean cumulative displacement along a cyclic test can be view as a creep-fatigue interaction. The previous empirical observations on the shape of the ratcheting curves and the factors influencing are enough of evidences of the similar effects of viscosity on both fatigue and creep behavior. The creep fatigue interaction is thus based on the fact that failure of polymers due to dynamic fatigue greatly depends on their creep characteristics.

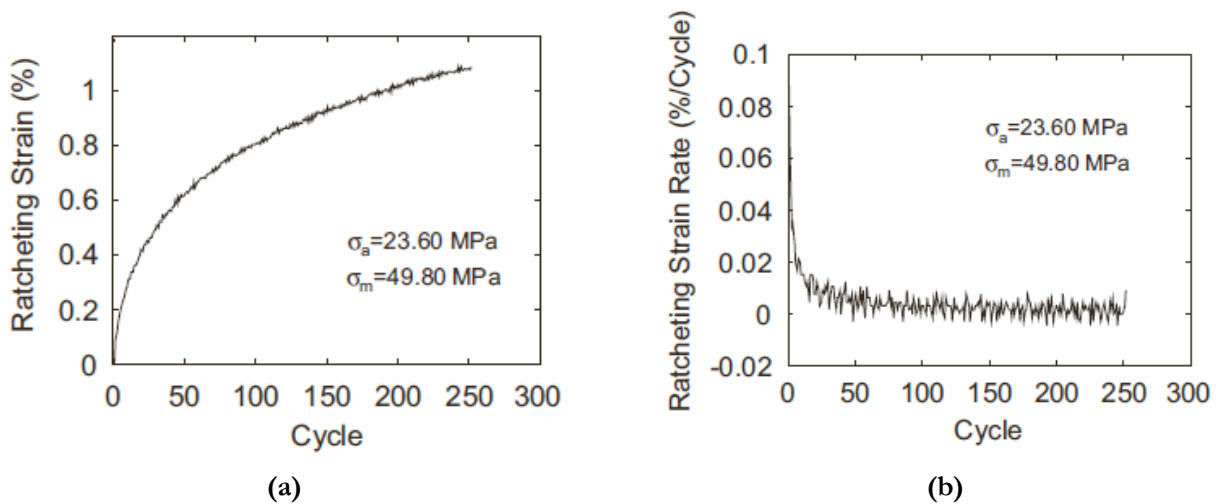


Figure I.2-11: Ratcheting strain vs. number of cycles diagrams (a) and ratcheting strain rate vs. number of cycles (b) on an epoxy polymer (Tao, et al., 2005).

Since for thermoplastic polymers, the creep rate and the ratcheting rate tend to increase at elevated temperatures, (Nguyen, 2013) (Launay, et al., 2011) a number of studies postulates that cyclic life of polymers depends mostly on the material self-heating. This approach is particularly true for higher stress levels and frequencies. However, the definition of the ratcheting and the damage accumulation processes will have an importance for thermo-hardening polymers subjected to lower stresses and lower frequencies.

All the previous studies on the ratcheting effect have been performed on bulk polymer samples. Aside tests performed on adhesive film samples (Ma, et al., 2011), the notion of ratcheting effect in adhesive bonding remains confidential. Indeed, in studies concerning adhesive bonding, since the initiation phase seems to end early with the apparition of cracks at the edges of the overlap (Dessureault, et al., 1997), fracture mechanics are considered to have the major role in the fatigue behavior. Investigations on the effects of the adhesive material mechanical behavior on the initiation of cracks are mostly just sidelined in studies. More generally, in designing bonded structures under cyclic loading, effects of the viscous mechanisms are not clearly taken into account. Hence, in a work performed on structural

adhesives, Crocombe (Crocombe, et al., 1999), concluded on a relatively unimportant effect of the frequency on the fatigue behavior.

Yet despite this early assumption, the effect of viscosity in the adhesives behavior has been clearly highlighted in studies, by performing creep tests and tests under various loading rates (Cognard, et al., 2008), (Dean, 2006). Thus creep effects can be assumed to be significant in the lifetime of bonded structures (Jeandrau, 2011) (Imanka, et al., 2003) (Al-Ghamdi, et al., 2003).

The aim of this study is to experimentally underline evidences of the viscous phenomena occurring in the adhesive bond-line, in order to apply to bonded structures, an approach based on the numerous works performed on polymers (Launay, et al., 2011) (Nguyen, 2013) and composite materials (Laurin, 2005) (Albouy, 2013). A first important step, to justify a creep-fatigue approach, is the observation of cumulative strains in bonded specimen under stress controlled cyclic loading. In order to reach this goal, an overview of the experimental methods developed in structural adhesive testing is important.

I.3. Characterization of structural adhesive

For the characterization of the bonded structure especially concerning the adhesive joint behavior itself, two approaches may be defined:

- The first one is based on a “bulk material” approach. This approach considers the adhesive as a polymeric based material to study only the mechanical behavior and the “Cohesion” problems within the adhesive joint. This kind of models gives explanations concerning the general mechanical behavior of bonded joints. Nevertheless, in these approaches, “Adhesion” issues are neglected leaving aside the role of the surfaces and the interfaces;
- The second one takes the bonded joint entirely, considering both issues concerning “Cohesion” and “Adhesion”. These tests characterized the bonded structure taking into account the adhesive itself and also the surfaces and their treatments. These models rely as much on the mechanical behavior of the adhesive joint as the role of the interfaces. However, with this approach the two parts of the structural bonding behavior are not clearly separated.

I.3.1. Bulk samples

a. Tensile tests

These tests are based on a material approach: the properties determined are intrinsic to the material, with no influence of the adherend. The tensile tests on bulk specimens remain the most common type of tests to determine strength properties of the adhesives. In order to define the adhesive characteristics, bulk specimens are usually done by pouring or injecting the adhesive into a mold. The final geometry usually used for tensile tests is the “dog-bone” shape specimen according to standard NF EN ISO 527 (AFNOR, 2012).

b. Compressive tests

Less common than the tensile test, this tests is useful if the adhesive joint behavior is assumed to depend on the hydrostatic stress component: the compressive strength differs from those obtained in tension. For compressive tests samples, a square base is recommended by the French standard NF T

51-101 (AFNOR, 1981) whereas for ASTM D695 (ASTM Int., 2010), the preferred specimen is cylinder.

c. Torsion tests

The shear adhesive properties can be obtained with solid bars or cylinders loaded in torsion. However the round shape of the specimens is hard to obtain and needs precise machining. No standard exists for these tests and the dimensions of the specimens vary from one author to another (Nadai, 1931) (Chen, et al., 2011).

d. Iosipescu and Arcan tests

Iosipescu test method, also known as the “V-notched beam shear method” and the Arcan test method (“notched plate shear method”) permit to measure the shear properties of the materials. These two methods differ in the type of loading and in the specimen geometry (Figure I.3-1). The aim of Arcan in the development of the “Notched plate shear method” is to devise a bulk specimen and a type of loading in order to produce uniform distribution of the loading. A photo-elastic analysis on a plane circular sample with a force P applied shows a stress state with 2 main advantages (Arcan, et al., 1987):

- a uniform stress distribution all along a significant section;
- a lack of stress concentration.

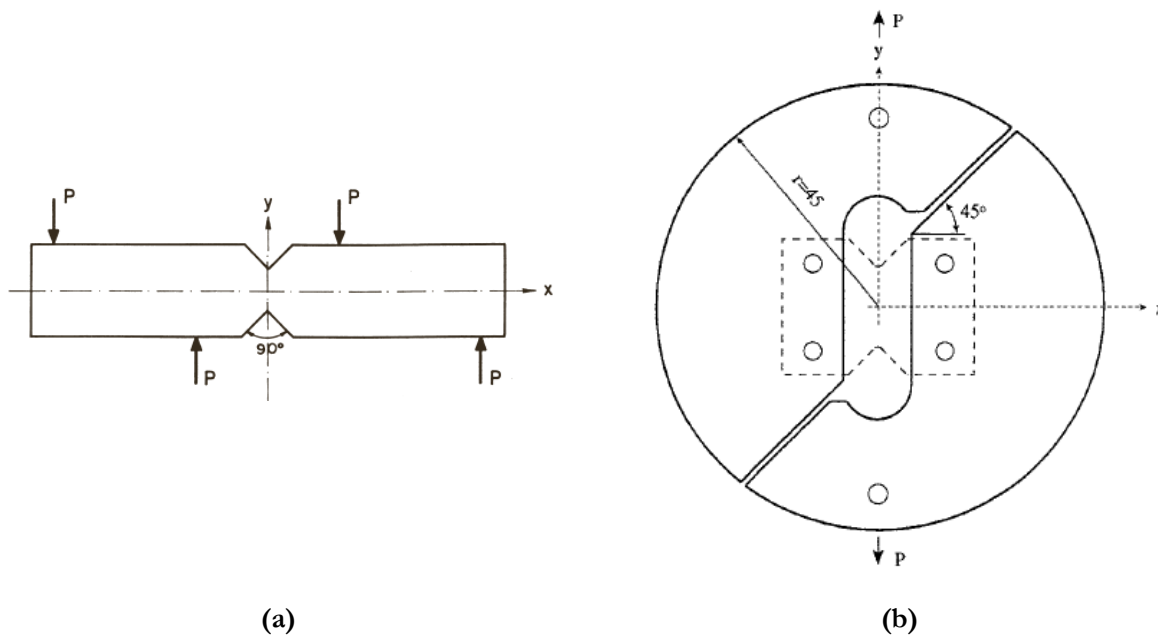


Figure I.3-1: V-notched (Iosipescu) specimen geometry and loading (a) (Almeida, et al., 1999) and notched plate shear loading device and specimen geometry (b) (Brosh, et al., 1996).

I.3.2. Bonded specimens

For the bulk tests, mechanical properties are highly dependent to the presence of defects such as voids or micro cracks introduced during the molding process of the specimen. Generally the strain at failure presents a very large dispersion unless the manufacture is very well controlled. Furthermore, the chemical reactions induced by the adherend within the adhesive may have a role in the mechanical behavior of the bond-line. Therefore, tests on bonded specimens are generally used to characterize the adhesive behavior.

a. *Modes of failure*

Considering bonded specimen, the two aspects defining the quality of an adhesive, “Adhesion” and “Cohesion”, will lead to different modes of failure, determining the strength of the bonded assembly:

- Presented in Figure I.3-2a and indicated by (1), a failure corresponding to a crack path growing through the interface between the adherend and the adhesive joint characterize a weak “Adhesion”. This kind of failure leading to an adherend completely free of adhesive material is considered as an **adhesive failure**;
- A failure within one of the bonded materials is called **cohesive failure**. A cohesive failure, as shown in Figure I.3-2a indicated by (2), is characterized by adherends both sides of the adhesive joints covered by adhesive material after failure.

In a same loading, the failure of a bonded assembly can initiate adhesively or cohesively in the adhesive and in the substrate (Figure I.3-2a). This type of initiation can lead to complex crack propagation within the bonded joint.

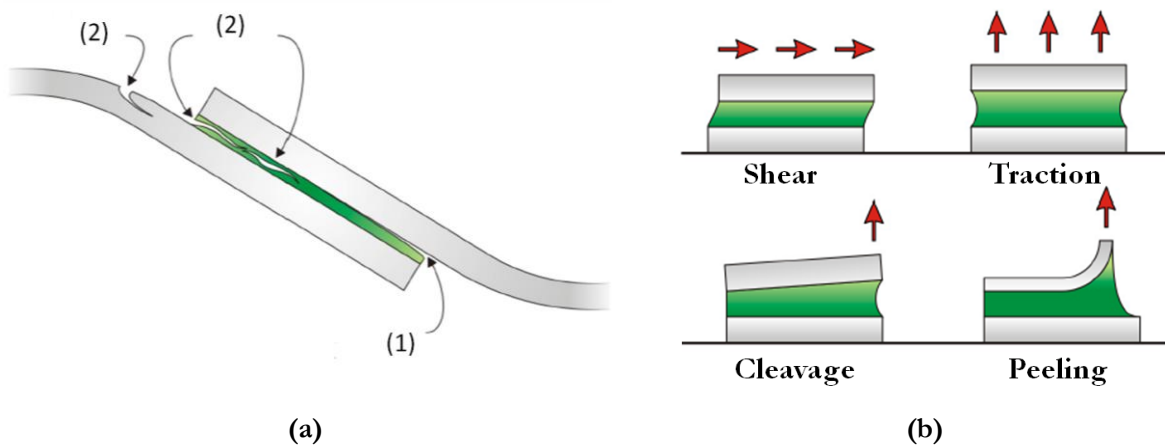


Figure I.3-2: Characteristic mode of failure associated to Single Lap Joint (a) and modes of loading for a bonded specimen (b) (Joannes, 2007).

b. *Modes of loading*

In order to define the structural bonding characteristics, from the perspective to design a bonded structure, four different modes of loading have to be considered. The nature of the solicitation greatly influences the stress distribution in the adhesive joint. Figure I.3-2b presents each mode of loading. As a general rule of bonding design, cleavage and peel are the most critical, from the fact that these modes imply critical stress distribution at the edge of the joint.

c. *Single Lap Joint (SLJ)*

Single lap joint (SLJ) uses bonded specimens with thin sheet of adherends and are very common tests in industry: this test reproduces joints encountered in many industries from aeronautical (pioneers of adhesive bonding technologies) to automotive. Standards exist to define this test, such as ASTM D 1002 (ASTM Int., 2006a) (Figure I.3-3a). During the loading, SLJ samples are in a complex state of stress. This non-uniform stress distribution of sheer and peel, highlighted by Volkersen (Volkersen, 1938) is due to the differential straining effects during the loading of the specimen. Numerical simulations performed by Harris (Harris, et al., 1984) showed for Finite Element (FE) results and closed-form solutions distributions with important stress concentrations at the edge of the adhesive

bond-line. Figure I.3-3b and Figure I.3-3c show these results concerning the left edge of a SLJ bond-line under a 15kN loading. Normalized values of the shear stress τ_{xy}/τ_{ave} and tensile stress σ_{yy}/τ_{ave} are plotted in function of the half overlap length, c . In testing bonded specimen and particularly for the SLJ testing method, every case of failure described in Figure I.3-2a can be observed. In fact, for this type of test, if importance is not given to the choice of the adherend, failure occurs in the substrate and do not yield prior to joint failure.

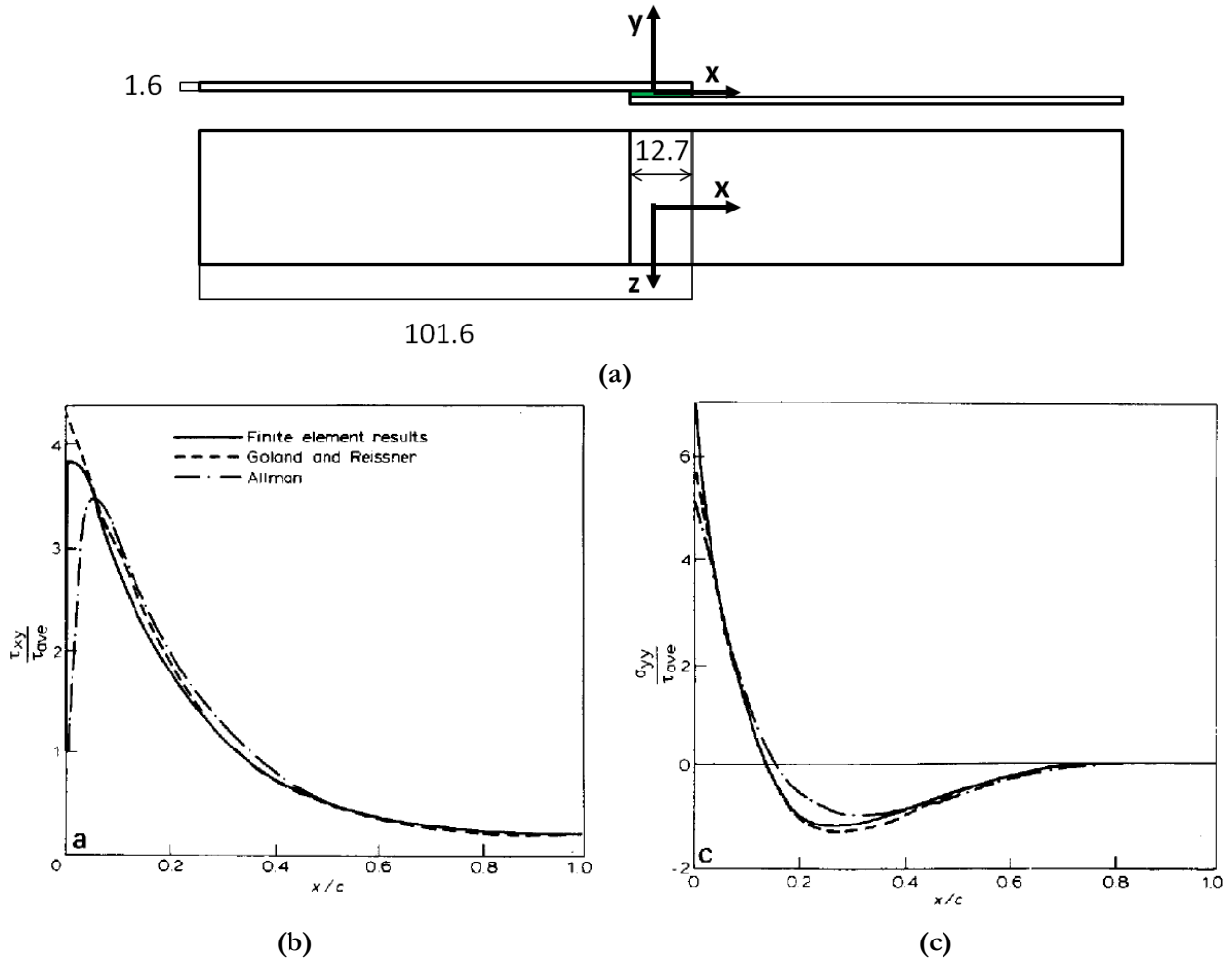


Figure I.3-3: Single Lap Joint specimen according to ASTM D 1002 standard (a) and numerical simulations for adhesive stress distributions along half of the overlap length (for the left edge): shear stress (b) and peel stress (c).

d. Thick Adherend Shear Test (TAST)

ASTM D3983 (ASTM Int., 2006b) standard makes the Thick Adherend Shear Test (TAST) one of the most popular types of failure strength test. This test, developed by Krieger (Krieger, 1988), seeks to correct the complicated state of stress that makes SLJ not suitable to the characterization of the adhesive true properties with an increase of the thickness of the substrates. Indeed TAST samples are associated to a more uniform stress distribution, permitting to move closer to a bulk material characterization. Nevertheless, FE simulations performed by Créac'hcadec (Créac'hcadec, 2008) showed that the TAST method, despite the almost uniform stress distribution in the adhesive joint in shear stress (Figure I.3-4a) and peel stress (Figure I.3-4b), stress concentrations still exist caused by side effects in the adhesive layer.

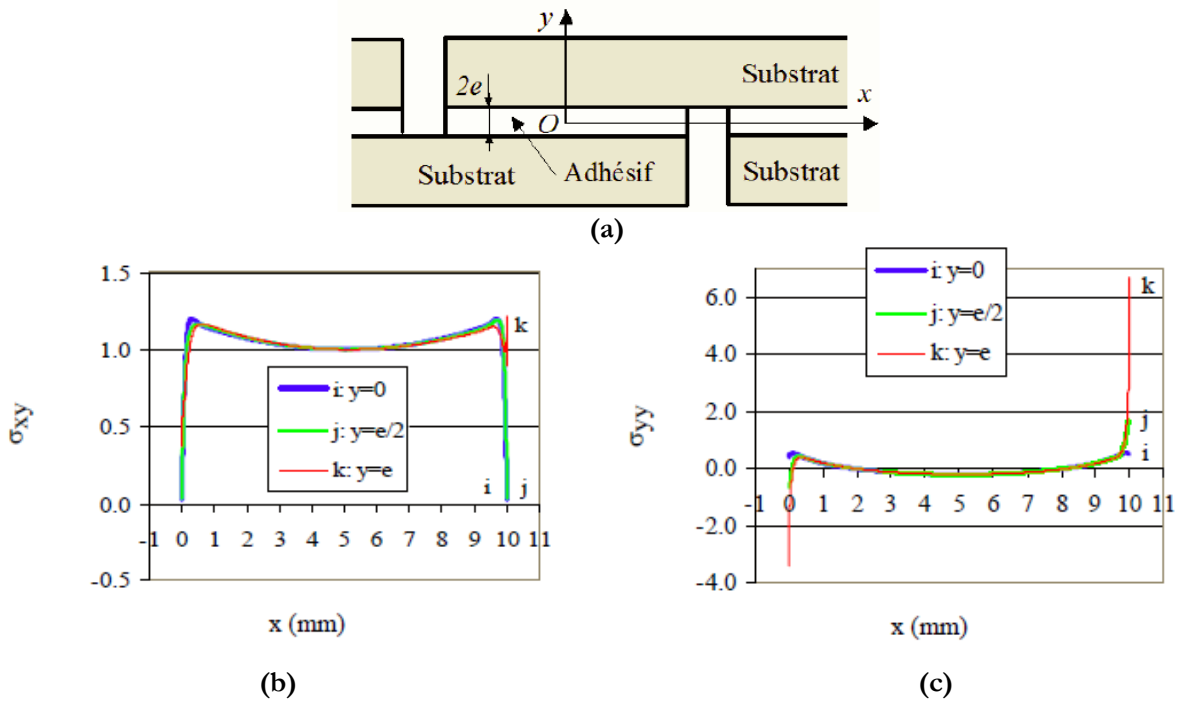


Figure I.3-4: TAST specimen geometry (a) and numerical FE simulations for adhesive stress distributions along the overlap length: shear stress (b) and peel stress (c).

e. *Tensile tests*

The purpose of this test is to characterize a thin layer of adhesive between two thick steel substrates. For these tests, as the butt joint (Figure I.3-5), there are two types of geometry defined by the ASTM standards. ASTM D897 (ASTM Int., 2006c) uses short circular specimens and ASTM D2095 (ASTM Int., 2008) includes round and square geometries. The stress state considered by the standards is of uniform tension. Nevertheless, studies (Adams, et al., 1977) have shown that the stress distribution is non-uniform, due to the constraining effects of the substrates during loading and circumferential stresses introduced at the edges of the joint by the lateral contraction of the adhesive. Adhesive displacement is usually measured by extensometers fixed on the adherends both side of the adhesive bond-line. Usually, extensometer measurements are considered to be driven by the adhesive behavior. However, Adams (Adams, et al., 1997) pointed the fact that a slight correction is necessary, considering elastic strains within the substrates during the loading. This kind of correction can be generalized to each bonded structure characterization tests.

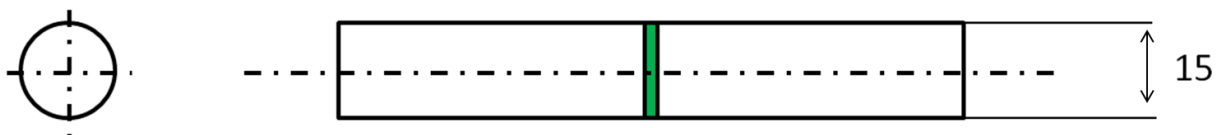


Figure I.3-5: Butt joint specimen with solid adherends according to ASTM D897 standard (ASTM Int., 2006).

f. *Shear tests*

The butt-joint specimen, with solid substrates or tube, is also used for shear test. For solid substrates, the specimen geometry is the same as the butt-joint for tensile test. As in bulk torsion method the specimen loaded in torsion is free of stress concentrations (Adams, et al., 1977). For tubular substrates

bonded with a thin layer of adhesive the test is called “napkin-ring” and is described by ASTM E229 (ASTM Int., 2003).

As described above, a wide range of tests has been developed for the characterization of a structural adhesive. Even if advantages and drawbacks of each method were brought forward, it may remain difficult to make the right choice. However, for a given adhesive joint, the properties obtained in compression, tension and shear can be related. In fact one of the objectives of an accurate adhesive characterization tests is the development of constitutive modeling of the mechanical behavior. If a von Mises criterion is used for the model the characterization of the adhesive only needs experimental data from one loading mode. Then in this particular case, only one testing method is enough.

Nevertheless, more refined yielding model (section I.4.3.b) can also be used, and then properties in at least two loading modes are necessary to complete the adhesive joint characterization. In order to validate the approach made for the adhesive mechanical behavior, agreement on the adhesive joint for a third loading mode has to be verified. The results of these predictions are strongly linked by the fact that the adhesive has a different behavior when loaded in shear and in tension, especially concerning the failure strain. In the area of the failure strain prediction, the use of a same type of specimen for all the loadings with a precise machining leads to good results.

I.3.3. Advanced tests

Except for Single Lap Joint with thin substrates, for all bonded specimens and tests methods considered in the previous section, the adhesive layer were considered to be loaded under shear or tensile stress. Nevertheless, in bonded structures, the adhesive layer experiences a composition of modes of loading (compression/tension/shear). In order to provide a same type of bonded specimen, different loading modes and to produce in the adhesive multi-axial stress states, different devices have been developed.

a. Butt-joint under multi-axial loading

The butt-joint specimen presented in section I.3.2.e for both tensile test and shear test can be loaded under a bi-axial loading, using a combined traction-torsion testing machine. Traction and torsion can be driven to develop different tensile-compression / shear ratio. Therefore, this method offers a large number of loading combinations making it a very interesting solution for both characterization and prediction of adhesive joint mechanical behavior. For the development of refined constitutive models, traction-torsion tests on napkin ring specimens have thus been widely used in recent studies (Mahnken, et al., 2005) (Vernet, et al., 2005)(Jousset, 2008).

The main disadvantage of this type of test is the difficulty of manufacturing. Furthermore, a misalignment occurring during the fabrication or testing will introduce a bending moment in the adhesive joint. Therefore, the accuracy in the alignment of the substrates and the precision of the load application needed make this method difficult to implement. However, Mahnken, et al (Mahnken, et al., 2005) and in more recent studies Arnaud (Arnaud, et al., 2014) provides precise solutions for the specimen fabrication and the load application (Figure I.3-6) in order to obtain reliable results.

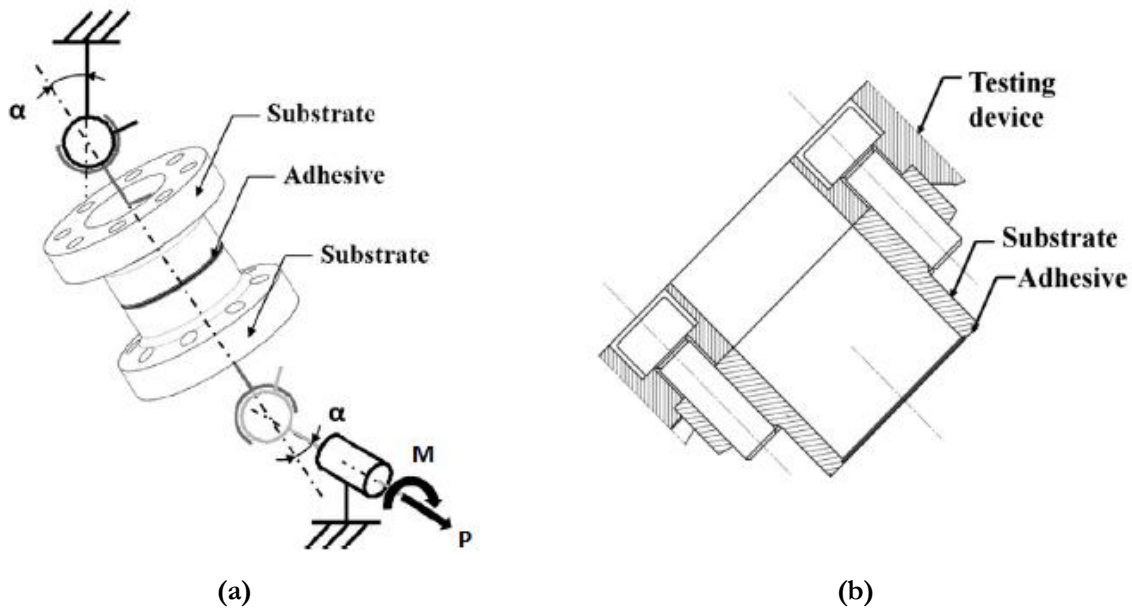


Figure I.3-6: Mechanical scheme of the boundary conditions during the tests for a tensile-torsion device (a) and specimen geometry with clamping to the device (Arnaud, et al., 2014).

b. *Modified Arcan test*

The Arcan method was initially developed in order to test bonded specimens under proportional composed tensile-shear loading using a conventional tensile testing machine. Cognard et al. (Cognard, et al., 2005), based on the work of Gineste (Gineste, 1993), proposed modifications of this method with a development of the testing device. The improvements, presented on Figure I.3-7, were first tested on composite specimens and led to an extension of the loading area to compression/shear.

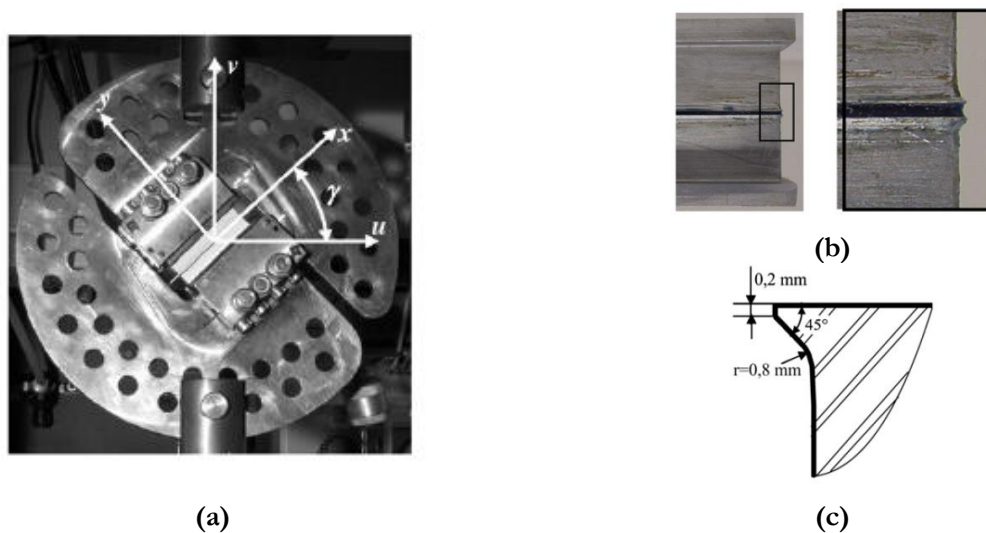


Figure I.3-7: Modified Arcan fixture for tensile-shear loading (a), shape of the bonded specimen (b) focusing on the beak geometry (c) (Cognard, 2008).

This method can offer an alternative to the traction-torsion test on butt-joint for proportional loadings. Nevertheless for the combination of non-proportional compression-tension/shear tests the use of butt-joints with a combined traction-torsion testing machine remains the only solution.

a. Reduction of edge effects

Concerning the TAST method (part), despite the almost uniform stress distribution in the adhesive joint, stress concentration still exists caused by side effects in the adhesive layer. Therefore, several studies (Lilleheden, 1994) (Cognard, et al., 2008) (Créac'hcadec, 2008) have proposed modifications of the TAST specimen geometry in order to reduce these stress concentrations located at the edges of the overlap. In the alternative proposed by Cognard et al., represented in Figure I.3-7b, the modified specimen including beaks, leads to an adhesive layer mainly loaded in shear. These modifications enable the adhesive layer to plastically deform up to higher plastic strain than specimens including stress concentration at the end of the adhesive layer.

The geometry improved on TAST method were brought to the modified Arcan Test, with the machining of a beaks on the substrates all around the bonded surface. The substrates are milled with high precision, then, after bonding the specimen is clamped in the modified Arcan fixture ensuring loading with different modes, Figure I.3-7 representing the orientation for tensile-shear loadings. Studies showed (Cognard, et al., 2008) (Créac'hcadec, 2008) that design of beaks in the substrates with angles from 30° to 45° induce stresses values close to zero at the edges of the bonded joint.

However, in later studies (Davies, et al., 2009) (Cognard, et al., 2010a), FE simulations performed under elastic assumptions in the case of shear and tensile tests showed that increasing the bond-line thickness changed the stress distribution: the stress gradients close to the free edges of the adhesive increase significantly with the joint thickness (Figure I.3-8). These observations were then put forward in order to explain the experimental reduction in the transmitted load with the increase of the joint thickness.

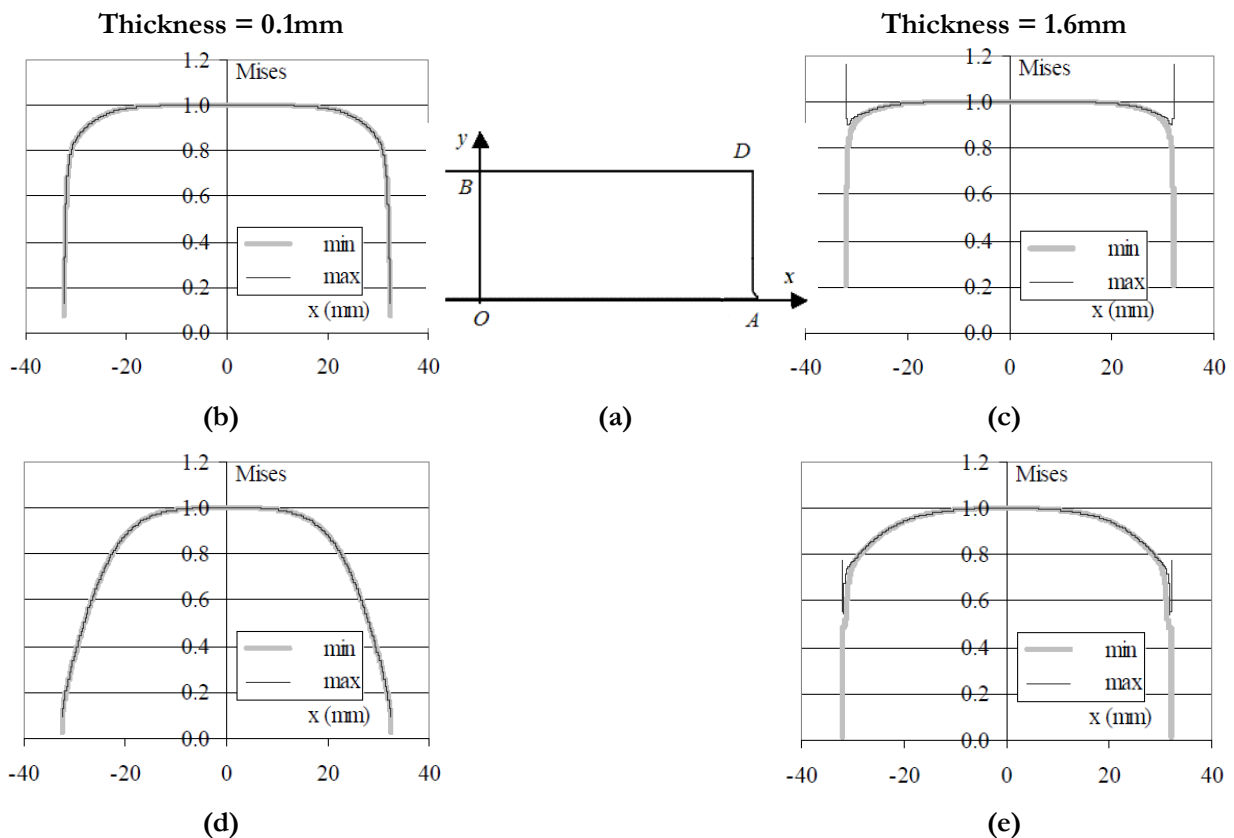


Figure I.3-8: Modified Arcan specimen geometry (a) and calculated von Mises stress distributions for thin and thick bonded joints: tensile test, thick.= 0.1 mm (b), thick.= 1.6 mm (c) and shear test, thick. = 0.1 mm (d), thick. = 1.6 mm (e).

The advanced testing methods recently developed provides interesting advantages such as the absence of stress concentrations (for thin adhesive joints and in a linear framework), or the application of mixed loading for a same type of specimen. But the necessity of a precise machining for the loading device and the bonded specimen including beaks in addition to the advanced handling constitutes a technological barrier for their standardization. Moreover, for these specimens, the decrease of the edge effects using beaks leads to a 3D non-uniform stress state within the adhesive layer.

I.4. Modeling of structural adhesives

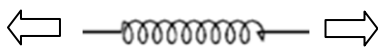
Knowledge of the material mechanical behavior permits to use the right adhesive for the application considered. In fact, designing bonded structures implies an accurate description of the mechanical abilities of the adhesive joints. Characterization tests serve as a representation of these abilities and modeling is the basis of their understanding. In this section, are proposed an overview of the theoretical approaches mostly used concerning the description of the structural adhesives mechanical behavior.

I.4.1. Phenomenological approach

a. *Rheological basic elements*

The shape of the material response to classic bulk tests allows us to make a classification of the mechanical behaviors. The main behaviors can indeed be described by a rheological analogy with some basic mechanical systems. Figure I.4-1 shows the rheological formulation and representation for elasticity, viscosity and plasticity, where σ is the stress in the system and ϵ is the strain. The elasticity is commonly associated to the mechanical behavior of a spring where E defines its stiffness. In the expression of the viscosity, the dashpot refers to a linear fluid friction where η is the viscous coefficient. As a Coulomb friction element, plasticity involves a yielding value σ_y defining a domain in which friction loss appears. Usually these three basic elements are combined in order to create rheological models. Therefore, following the deformation theory (Hencky, 1924) strains occurring in a material can be divided in three parts corresponding to the elastic strain ϵ_{el} , the viscous strain ϵ_v and the plastic strain ϵ_p :

$$\epsilon = \epsilon_{el} + \epsilon_v + \epsilon_p \quad (\text{Eq 1.9})$$



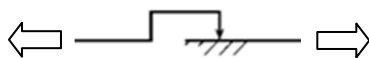
Elasticity: Spring

$$\sigma = E\epsilon$$



Viscosity: Dashpot

$$\sigma = \eta \dot{\epsilon}$$



Plasticity: Frictional device

$$|\sigma| \leq \sigma_y$$

Figure I.4-1: Representation of the mechanical behavior with basic mechanical systems.

a. Linear visco-elasticity

The Maxwell model is a serial combination of a spring (a basic mechanical component for elasticity) and a dashpot (a basic mechanical component for viscosity) and the Kelvin model is a parallel combination of both (Besson, et al., 2001). Figure I.4-2 presents their mechanical representations, their associated equations and their associated response to a creep-recovery test. In the Kelvin model, contrary to the Maxwell model, the behavior of the dashpot is restricted by a spring. Therefore, the Kelvin model exhibits a solid-like behavior with a “delayed elasticity” with the creep strain approaching the final value gradually. The Maxwell model exhibits fluid-like behavior describing unbounded creep, allowing unlimited deformation under finite stress.

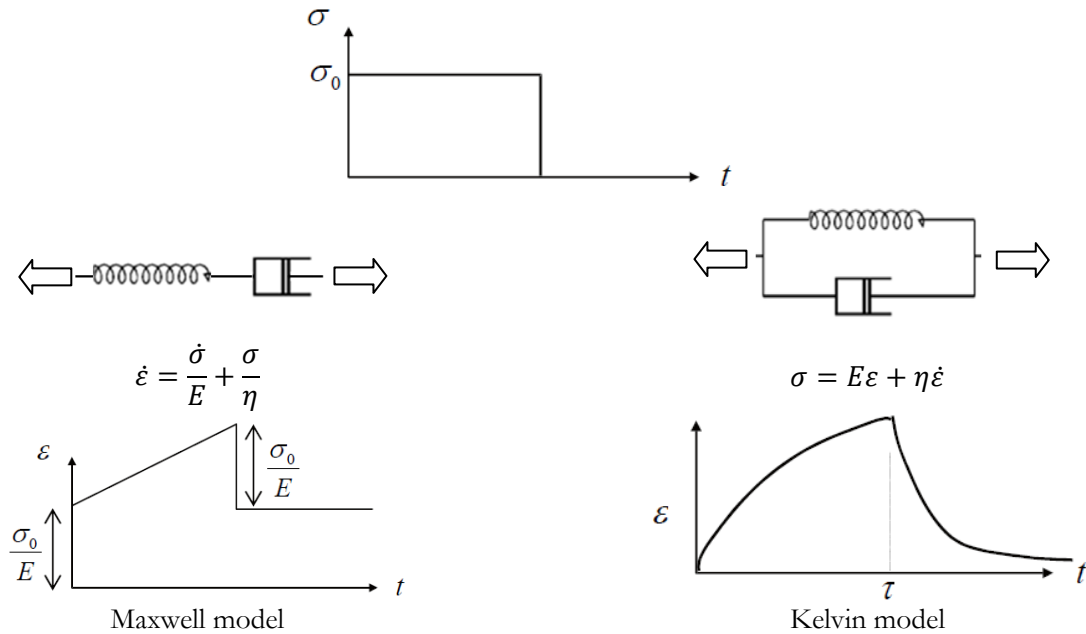


Figure I.4-2: Rheological models for visco-elasticity.

b. Linear plasticity

The serial combination of a spring and a frictional device presented in Figure I.4-3 leads to an elastic-plastic behavior. The stress in the frictional element cannot be greater in absolute than a limit value σ_y , hence the system behavior can be defined in three parts depending on the yield function f :

$$f(\sigma) = |\sigma| - \sigma_y \quad (\text{Eq 1.10})$$

- *Elastic area defined by: $f < 0$
- Elastic unloading for: $f = 0 \ \& \ \dot{f} < 0$
- Plastic flow for: $f = 0 \ \& \ \dot{f} = 0$

In the elastic area, no plastic flow exists; therefore the value of the plastic strain is zero. Outside this field the stress value does not vary. Thus, in this model, no hardening exists allowing an unlimited strain value for a constant stress level.

The Prager model (Besson, et al., 2001) is the parallel combination of these two same components. The stress X in the frictional element depends here on the plastic strain:

$$X = H\epsilon_p \quad (\text{Eq 1.11})$$

where H is a parameter defining the isotropic linear hardening. Hence, in this case, the stress is linked to the plastic flow and the yield function has the following expression depending now on the applied stress and on the stress in the frictional element:

$$f(\sigma, X) = |\sigma - X| - \sigma_y \quad (\text{Eq 1.12})$$

Figure I.4-3 presents the mechanical behavior associated to the Prager and elastic-plastic model. On the basis of observations made on polymers and composites, more advanced combinations of these mechanical elements have been tested on polymers mechanical behaviors along many studies (Hiel, et al., 1983) (Rocheferf, et al., 1983) (Launay, et al., 2011). These models present combinations leading to a viscous behavior with a reversible flow as developments of the Kelvin model (visco-elasticity) and irreversible viscous phenomenon with insertion of a friction element (visco-plasticity). Furthermore, spectral formulations exist for visco-elasticity in generalizing the sets of elementary rheological models directly by using a spectrum of variables. In order to reduce the number of free parameters in the model, a Gaussian distribution can be used for their definition (Maire, 1992) (Petipas, 2000) (Laurin, 2005).

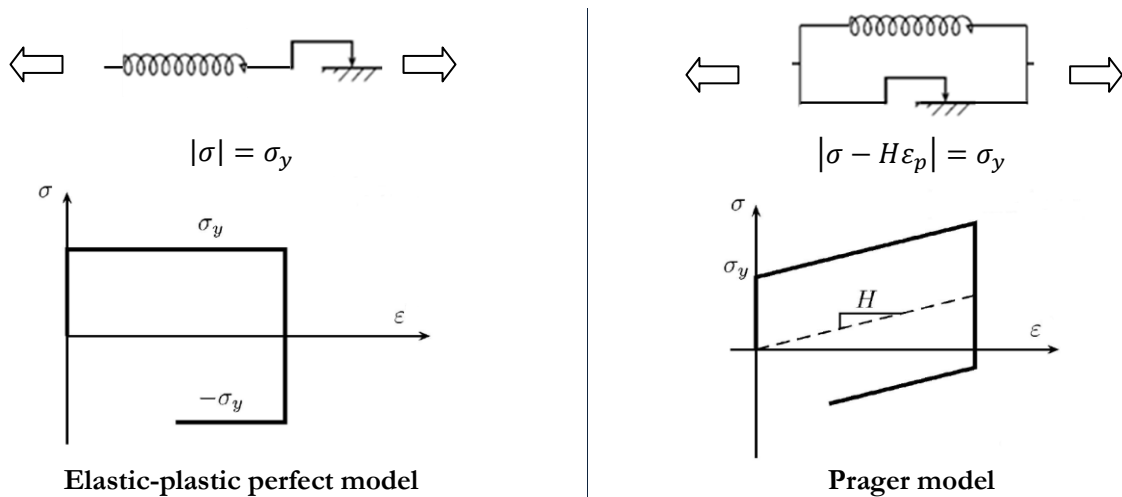


Figure I.4-3: Rheological models for plasticity.

I.4.2. Theories for viscous behavior

a. *Creep behavior*

Concerning the description of the mechanical behavior under creep loading, a variety of mathematical forms have been proposed in an empirical fashion. The simplest assumption results in a creep relation which is a linear function of stress but a non-linear function (logarithmic for example) of time. The most commonly used creep relation is the “power-law” compliance (Weitsman, 1981) (Ravi-Chandar, et al., 1984):

$$\mathcal{C}(t) = \mathcal{C}_0 + \mathcal{C}_1 t^n \quad (\text{Eq 1.13})$$

where the compliance \mathcal{C} is a function of time and $(\mathcal{C}_0, \mathcal{C}_1, n)$ are material constants. For the identification of these parameters, various methods have been proposed, listed by Dillard et al. (Dillard, et al., 1985). Other alternative non-linear creep functions, with an extension to creep under multi-axial stress, have also been evaluated on adhesive materials (Dean, 2006). Nonlinear visco-elastic theories have also been studied by (Green, et al., 1960) for polymeric materials applications.

b. Reduction in stress concentration due to viscous behavior

(Weitsman, 1981) utilized the non-linear visco-elastic power law response to describe a stress-enhanced creep process to illustrate time-dependent reduction in shear stress peaks along the adhesive layers in the example of double lap joint. Later Sancaktar (Sancaktar, 2011) applied a correspondent principle with the use of a generalized Maxwell model.

c. Rate-dependent visco-elastic behavior

Another aspect of the viscosity is the rate-dependency on the mechanical behavior. In order to describe the loading-rate dependency of elastic yield strain (γ_{el}), Renieri proposed a semi empirical approach which was tested on various studies on polymeric materials (Renieri, et al., 1976):

$$\gamma_{el} = \phi_0 + \phi_1 \log \left[\frac{\left(\frac{d\gamma}{dt}\right)}{\left(\frac{d\gamma'}{dt}\right)} \right] \quad (\text{Eq 1.14})$$

where (ϕ_0, ϕ_1) are material constants, $\left(\frac{d\gamma}{dt}\right)$ is the initial elastic strain rate and $\left[\frac{\left(\frac{d\gamma}{dt}\right)}{\left(\frac{d\gamma'}{dt}\right)}\right]$ characterize the strain rate variation.

d. Unified theory models

Comparisons have been conducted between rate-dependent models and the “power-law” creep models (Yu, et al., 2001). In these studies, the fit of the different models is evaluated on bulk specimens under tensile loading with constant strain rate and creep tests. The three models considered (Eq 1.15, Eq 1.16 Eq 1.17) are based on the unified theory which divides the total strain in an elastic part and an inelastic part. The inelastic part generates strains at all time without using a yield function. For these models, inelastic behavior, described by the evolution of the inelastic strain $\dot{\epsilon}_{in}$, is defined by the flow functions:

$$\dot{\epsilon}_{in} = \frac{\sigma - g}{Rk(\sigma - g)} \quad (\text{Eq 1.15})$$

$$\dot{\epsilon}_{in} = K \exp \left[-\frac{A}{2} \left(\frac{Z^2}{1.5(\sigma - g)^2} \right)^n \right] \text{sign}[\sigma - g] \quad (\text{Eq 1.16})$$

$$\dot{\epsilon}_{in} = a_0 \exp \left[-\left(\frac{F(W_p)}{|\sigma|} \right)^n \right] \text{sign}[\sigma] \quad (\text{Eq 1.17})$$

The first model (Eq 1.15) proposed by (Cernocky, 1982) is based on the overstress concept. The overstress ($\sigma - g$) is represented by the difference between the stress applied and the backstress g . In this model the viscous function is linear and represented by the material constants R and k . The second model (Eq 1.16) (Chiu, et al., 1995) also based on the overstress concept. For the flow law definition, where A , K and n are material constants, this model take into account the plastic work in the material through the function $Z(W_p)$. In the last model, proposed by Bodner et al. (Eq 1.17) (Bodner, et al., 2010), the plastic work function F does not consider the overstress ($\sigma - g$).

The numerical responses of the Chiu, et al. model (Eq 1.16) and a model based on the “power-law” creep (Eq 1.13) are presented in Figure I.4-4. The responses are compared to bulk specimen uni-axial experimental results under creep loading with different load levels. Both models presents a good fit for the low load levels (35MPa and 40MPa). Nevertheless, for load levels above a 45MPa value, whereas

the unified theory model studied keep a low discrepancy (Figure I.4-4b) with the experimental data, the power-law underestimates the experimental creep strains (Figure I.4-4a). Regarding the comparison with the monotonic results (Figure I.4-4c), abilities of this second model may be called into question as the short-term numerical response tends to an important underestimation of the experimental strains.

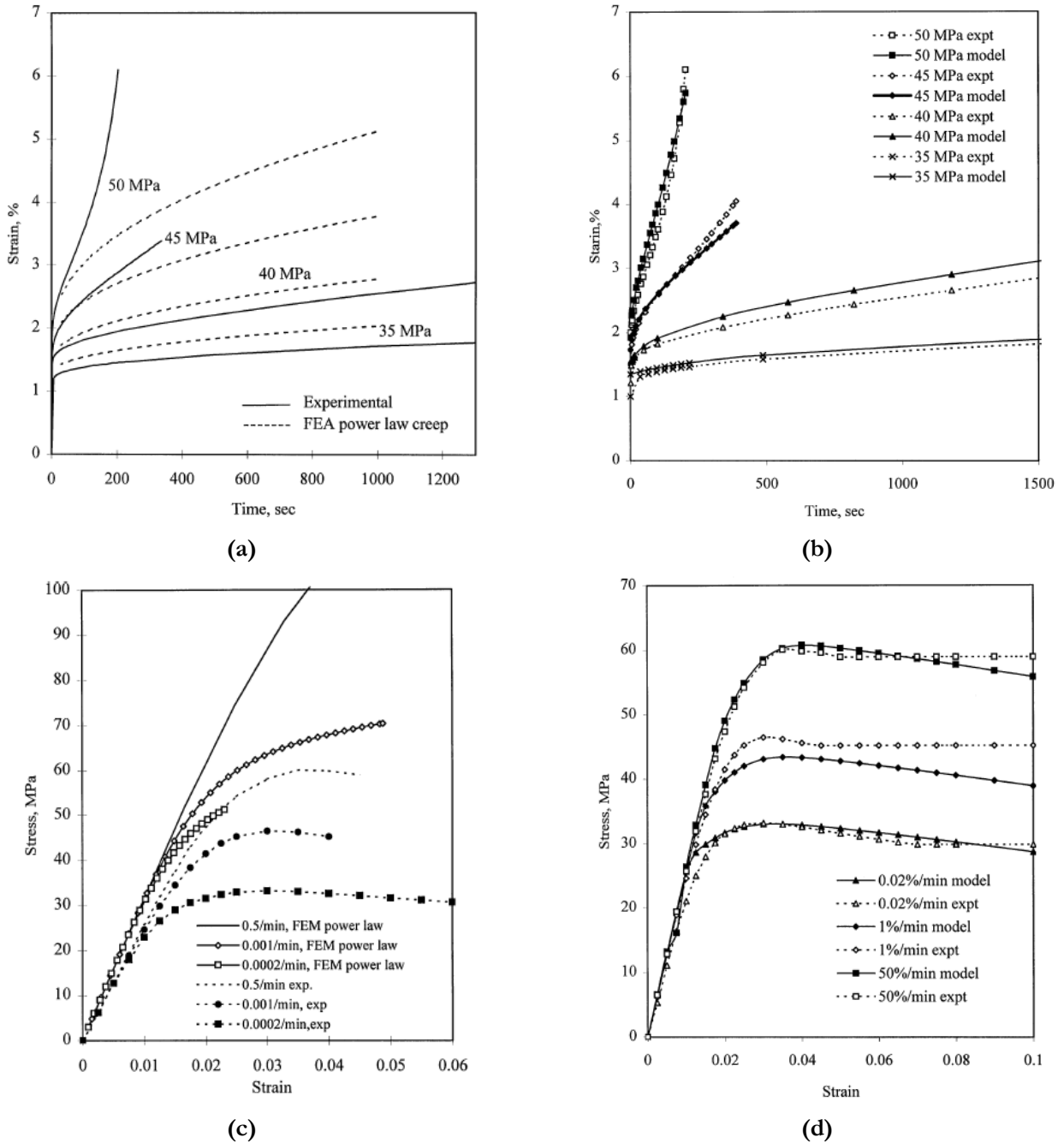


Figure I.4-4: Unified theory model fits to the creep compliance data (b) and to constant strain rate data (d) using model from Chiu, et al (Chiu, et al., 1995). Power-law creep model fits to the creep compliance data (a) and to constant strain rate data (c) (Yu, et al., 2001).

However, the fit of the monotonic experimental data, is significantly better with a model based on the unified theory. Indeed the description of the non-linear behavior with the model from Chiu, et al permit to have a high-quality description of the viscous phenomena involved in monotonic test and the increase of the loading-rate. Therefore, using a theory dividing the total strain in an elastic part and an

inelastic part (function of the overstress $(\sigma - g)$ with a non-linear definition), seems to develop an interesting description of the time-dependant effects occurring in an adhesive under uni-axial loadings.

Nevertheless, the important problem in the formulation of the models developed in this study (Chiu, et al) is the lack of multi-axial loading considerations in their definitions. Furthermore the unloading behavior was not observed in this study and reversibility of the measured strains was not investigated.

I.4.3. 3D model formulations for plasticity

Until this section, all the models considered were described only in one dimension (1D). In order to describe material behavior in a general thermodynamic framework, (Lemaître, et al., 2000) proposed a theoretical approach by the definition of thermodynamic variables. In this approach, any evolution occurring in the material is considered to be the succession of equilibrium states respecting the equations defining the model. In an elastic-plastic model definition, the strain tensor can be considered with the following decomposition:

$$\underline{\underline{\varepsilon}} = \underline{\underline{\varepsilon}}_e + \underline{\underline{\varepsilon}}_p \quad (\text{Eq 1.18})$$

where $\underline{\underline{\varepsilon}}_e$ defines the instantaneous reversible strain and $\underline{\underline{\varepsilon}}_p$ describes the irreversible strain in tensors.

a. *Yield criterion*

In order to model the plastic mechanical behavior of a material loaded in a multi-axial stress state it is necessary to characterize the different yielding values in 3D. In this section, a review of the different common tools used will be done, leading to a classification of the different criterion. As in the previous 1D definition (I.4.1.b), the limits of the elastic domain are given by the yield function:

$$f(\underline{\underline{\sigma}}) = g(\underline{\underline{\sigma}}) - \sigma_y \leq 0 \quad (\text{Eq 1.19})$$

where g is a function characterizing the yield criterion with a relation between the stress tensor components. This function needs to be independent from the mapping of the stress tensor. The function g is thus usually written according to the three stress invariants I_1, I_2 and I_3 :

$$I_1 = Tr(\underline{\underline{\sigma}}) \quad (\text{Eq 1.20})$$

$$I_2 = (1/2)Tr(\underline{\underline{\sigma}}^2) \quad (\text{Eq 1.21})$$

$$I_3 = (1/3)Tr(\underline{\underline{\sigma}}^3) = Det(\underline{\underline{\sigma}}) \quad (\text{Eq 1.22})$$

Two types of formalisms exist, depending on the use or not of the hydrostatic pressure for the definition of the yield function. In the case of non hydrostatic pressure dependant models, the invariants (J_1, J_2 and J_3) used are only deviatoric stresses $\underline{\underline{S}}$ dependent:

$$\underline{\underline{S}} = \underline{\underline{\sigma}} - (1/3)Tr(\underline{\underline{\sigma}})Id \quad (\text{Eq 1.23})$$

$$J_1 = Tr(\underline{\underline{S}}) = 0 \quad (\text{Eq 1.24})$$

$$J_2 = (1/2)Tr(\underline{\underline{S}}^2) \quad (\text{Eq 1.25})$$

$$J_3 = (1/3)Tr(\underline{\underline{S}}^3) \quad (\text{Eq 1.26})$$

The two main criteria of this first class are the Tresca criterion and the von Mises criterion (Table I.4-1). In order to have a yield function expression consistent with a stress, the von Mises criterion uses an invariant J instead of the invariant J_2 . The Tresca criterion use the expression of the principal shear stresses defined by $(\sigma_i - \sigma_j)$ where σ_i (principal stresses) for $i \in [1,3]$ are the diagonal components of the diagonalized stress tensor.

von Mises criterion	$f = J - \sigma_y \leq 0 ; J = \sqrt{\left(\frac{3}{2}\right)J_2}$	(Eq 1.27)
Tresca criterion	$f = \max_{i,j} \sigma_i - \sigma_j - \sigma_y \leq 0$	(Eq 1.28)

Table I.4-1 : Basic yield criteria.

b. Hydrostatic pressure dependent yield criteria

In several studies, tests were conducted under compression as well as tension. It was shown that the hydrostatic sensitive nature was manifest in creep (Yu, et al., 2001) as well as under constant strain rate loading (Crocombe, 1995): for bulk specimen, ultimate tensile strength, under tension, is substantially lower than for a similar test under compression. The hydrostatic pressure dependent criteria permit to express the fact that a hydrostatic compression stress makes the plastic strain more difficult and leads to a dissymmetry between traction and compression. Table I.4-2 lists the main hydrostatic pressure dependent criteria.

Modified von Mises (Linear Drucker Prager)	$f = J - \sigma_0 - \mu I_1$		(Eq 1.29)
	2 parameters	μ : Sensitivity to hydrostatic stress σ_0 : Initial yield stress in shear	
Modified Tresca	$f = \max_{i,j} \sigma_i - \sigma_j - \sigma_0 - \mu I_1$		(Eq 1.30)
	2 parameters	μ : Sensitivity to hydrostatic stress σ_0 : Initial yield stress in shear	
Exponent Drucker Prager	$f = aJ^b - p_0 + I_1$		(Eq 1.31)
	3 parameters	μ : Sensitivity to hydrostatic stress (a, b) : Material constants	
Rolfes	$f = J^2 - a_0 + a_1 I_1$		(Eq 1.32)
	3 parameters	(a_0, a_1) : Material constants	
Mahnken Schlimmer (MS)	$f = J^2 - \frac{1}{3}(Y_0^2 - a_1 Y_0 I_1 - a_2 Y_0 I_1^2)$		(Eq 1.33)
	3 parameters	(a_0, a_1) : Material constants Y_0 : Shear yield stress	

Table I.4-2 : Hydrostatic pressure dependant yield criteria

The more commonly used criterion is the Drucker-Prager criterion (Wang, et al., 2000) which is an extension of the von Mises criterion with a linear combination of the deviatoric invariant J and the first invariant I_1 (LDP). An exponent form of this criterion (EDP) is also widely used (Wang, et al., 2000)(Dean, et al., 2004) (Jousset, 2008) (Malvade, et al., 2009). The criterion proposed by Rahgava

(Raghava, et al., 1973) can be seen as a quadratic expression of the linear Drucker-Prager. Rolfes and Mahnken Schlimmer criteria (Rolfes, 2008) (Mahnken, et al., 2005) (Jousset, 2008) (Maurice, 2012) are particular adaptations of the EDP. The Tresca criterion has also been modified by Wang and Chalkley (Wang, et al., 2000) to take into account the hydrostatic pressure.

c. Non-associated formulation

The yield criterion through the definition of a function defines the domain of the reversible transformations. In a general formulation, the yield function f depends on the stress tensor $\underline{\underline{\sigma}}$ and the state variables \underline{V}_i . The flow rule characterizes the strain rate for the plasticity and the hardening rule gather the transformations within the material leading to dissipations of the mechanical energy. The position and the size of the area delimited by the yield function within the 3D stress domain are defined by the hardening function.

The generalized standard formulation (Eq 1.34) associates flow and hardening phenomena to the yield function. However other formalisms exist for the description of the flow and the hardening with the implementation of other functions. Three types of models can be distinguished depending on what it is used for the description of the elastic domain, the flow and the hardening. The models defined by (Eq 1.34) involves only the slip rate $\dot{\lambda}$ and the yield function f . For the (Eq 1.35) models, called simply associated models, the yield function is used only in the flow definition. Hence, a different function, here called F is introduced in the hardening rule definition. The last case (Eq 1.36) characterizes the non associate models where the yield function is used neither in the flow rule nor in the hardening rule.

Yield-function	Flow rule	Hardening rule	
f	$\underline{\underline{\dot{\epsilon}}}_p = \dot{\lambda} \frac{\partial f}{\partial \underline{\underline{\sigma}}}$	$\underline{\underline{\dot{V}}}_i = -\dot{\lambda} \frac{\partial f}{\partial \underline{V}_i}$	(Eq 1.34)
f	$\underline{\underline{\dot{\epsilon}}}_p = \dot{\lambda} \frac{\partial f}{\partial \underline{\underline{\sigma}}}$	$\underline{\underline{\dot{V}}}_i = -\dot{\lambda} \frac{\partial F}{\partial \underline{V}_i}$	(Eq 1.35)
f	$\underline{\underline{\dot{\epsilon}}}_p = \dot{\lambda} \frac{\partial G}{\partial \underline{\underline{\sigma}}}$	$\underline{\underline{\dot{V}}}_i = -\dot{\lambda} \frac{\partial F}{\partial \underline{V}_i}$	(Eq 1.36)

d. 3D models for adhesive behavior

The effectiveness of a hydrostatic pressure dependent model with a non associated formulation has been studied through the MS model (Mahnken, et al., 2005) (Jousset, 2008) (Maurice, 2012). The key point in the implementation of the non-associate model (Eq 1.36) is the definition of the flow rule. In order to write the flow function, the dependence on the hydrostatic stress component remains and generally a similar form with different material constants is generally used. Therefore, for example in the MS model, five material constants ($a_1, a_2, a_1^*, a_2^*, Y_0$) have to be identified:

Yield function:

$$f = J^2 - \frac{1}{3}(Y_0^2 - a_1 Y_0 I_1 - a_2 Y_0 I_1^2) \quad (\text{Eq 1.37})$$

Flow function:

$$g = J^2 - \frac{1}{3}(Y_0^2 - a_1^* Y_0 I_1 - a_2^* Y_0 I_1^2) \quad (\text{Eq 1.38})$$

In order to analyze the effectiveness of the 3D formulations on the adhesive mechanical behavior, Jousset then Maurice proposed an implementation of the MS model. The material constants of the (Erpolat, et al., 2004) model are identified from uni-axial torsion and tensile tests for napkin ring

specimen (section I.3.2.f) and a validation of the constants is made on a combined tensile-torsion loading test for the same shape of specimen. For these multi-axial tests, where a constant dependency exists between the two directions of loading, results outline the differences in the fits between numerical and experimental responses, in particular for the EDP. Furthermore the studies made underlines the difficulties encounter in the implementation of these models from the choice of the tests for the identification of the material constants to the implementation in FE codes.

I.5. Conclusion & main issues

I.5.1. Which model to describe the mechanical behavior under cyclic loading?

Constitutive modeling of adhesive includes considerations for deformation theories on viscosity, considerations on the reversibility of the strains, or considerations on the influence of the hydrostatic pressure. Furthermore, for all these models the definition of a flow rule and a hardening rule, then for models including non reversible strains, the definition of the elastic domain boundaries opens a large space of possibilities for the numerical description of the mechanical behavior. Considering the large number of models available, it can be seen that there is no consensus on the choice of the most appropriate constitutive law. However, non-associated formalism is also recognized as a must since associated models rapidly show their limits (Cr  ac'hedec, 2008) (Jousset, 2008) (Maurice, 2012). A direct drawback in the choice of these advanced implementations is in an increasing number of material constants to be identified and thus, increasing the complexity in the identification strategy to be deployed. Aside from the material constants definition, characterization tests will validate all assumptions made on the adhesive mechanical behavior.

I.5.2. Which characterization test?

Therefore, modeling bonded structures is strongly linked to the characterization tests. Indeed the experimental method chosen will lead to the definition of the material constants. As described above (section I.2) a wide range of test methods is available and this list can be split in two parts: tests on bulk specimens and tests on bonded specimens. Nevertheless, the quality of an adhesive is grounded on its adhesion properties, which are hardly linked to different physical and chemical principles (section I.1.2) depending on the adherend or the adhesive joint thickness. Thus, in order to design bonded structures, test methods with bonded specimens such as SLJ or TAST are widely used as they involve joint geometries close to the industrial framework. Concerning these tests, a major conclusion is that the shear strain is highly dependent on the quality of the specimen.

Moreover, in order to model the adhesive mechanical behavior with hydrostatic pressure dependency, the response of the material for different loading modes is needed in the experimental database. Hence, devices based on Arcan geometries were developed that can apply mixed loadings to the same type of specimen. Results obtained with the modified Arcan device with bonded specimen including beaks, as they involve a free concentration stress state in the adhesive joint, showed a very low scatter and have enabled the generation of large database for monotonic tests and cyclic tests (Thevenet, et al., 2013).

The major interest of a test method leading to a loading without stress concentration is to characterize a confined adhesive material with considerations close to the study of a bulk polymer specimen. Yet the

modifications provided to specimen bring a 3D non-uniform stress state as the decrease of the edge effect is associated with an important stress gradient along the overlap. The acquisition of a stress-strain response from these tests cannot therefore be immediate and a reverse engineering is required to adjust it in-situ.

I.5.3. How to analyze the mechanical behavior of a bonded structure?

Adhesive joint stress analysis usually involves three-dimensional stresses and strains, hence bonded structures design is a 3D problem by nature. To solve these problems, numerical methods such as FE analysis as well as analytical solutions are used. These both solutions are important in terms of identifying fundamental characteristics then in determining the strength of adhesively bonded joints. The last one based on simple and closed form solutions can offer in timely fashion, simple, quick and meaningful answers.

a. Analytical approach

Considerable efforts have been devoted to the development of analytical approaches for determining stress and strength of adhesively bonded joints. The SLJ (section I.3.2.c), considered as the simplest geometric configuration, has been shown to be representative and challenging in identifying fundamental characteristics in bonded joint. For SLJ, (Volkersen, 1938) proposed a shear lag model with considering the adherend as a rod undergoing axial and longitudinal deformations (2D). Then, other models have been proposed using Euler beam theory (Goland, et al., 1944), or under 2D elasticity considerations in which both adhesives and adherends are described as elastic material (Adams, et al., 1992)(Zhao, et al., 2009) leading to applications on joints with thick adhesives. For a linear elastic and perfectly plastic model to describe the adhesive shear stress-strain relationship and linear property for the peel stress, Adams (Adams, 1989), have proposed a single design methodology for SLJ specimen. However, fully coupled non-linear analytical solutions for adhesive joints are very complicated and analytical solutions do not seem to be admissible in general. Furthermore, in the last few years, the increasing performance of numerical tools has enable the model of complex geometry and complex material behavior using a computer-based method of numerically solving a range of boundary problems: the Finite Element Method (FEM).

b. Numerical approach: FE analysis

In FE analysis, a continuous structure is considered as a number of smaller elements joined at nodes and the numerical solving for systems of non-linear equations needs incremental and iterative methods. These methods permit both thermal and mechanical analysis. A post processing of the solutions enables the user to view results in 3D graphical mode as well as in text. Due to the complex behavior of adhesive joints and effects of environmental factors on their performance, FE analysis has been proven to be one of the best tools for adhesive joint design and analysis. Since displacements are computed at nodes and stress and strains computed in the elements, FE analyses can provides solutions to problem with complex geometries in increasing the number of elements. A fundamental dilemma thus appears: the accuracy of the global response increases with the number of elements implying a growth of the computational cost too. Therefore, the definition of the mesh for the bonded joint is an important step in FE analysis and the efficient numerical definition of the stresses within the adhesive joint.

c. Inverse Identification

In order to illustrate the efficiency of FE analyses for the adhesive joint design, Gegner et al. (Gegner, et al., 2004) proposed an analysis of a bonded metal joint test method according to the ISO 11003-2 standard (section I.3.2.d). In this work they also proposed a method for the determination of the adhesive joint elastic constants using an iterative finite element computation. The idea of the “inverse identification” process proposed is to use the experimentally determined shear modulus for the FE modeling, and to iterate the second parameter of elasticity (for the tensile behavior) until the experimental displacement can be approximated numerically. This technique proposed has been extended to the identification of the material constants for complex elastic-plastic behavior, using butt joint in traction-torsion (Jousset, 2008) or modified Arcan test (Créac'hedec, 2008) (Jousset, 2008) (Maurice, 2012). In these recent studies, the minimization of the error between the numerical results vs. the experimental response enabled the definition of material constants which cannot be directly measured. The use of inverse identification also resolves the problem of taking into account the deformations of adherends underlined by (Adams, et al., 1992) (section I.3.2.e) on different test methods. However, this technique involving the use of accurate FE analysis should be done keeping in mind the factors influencing the numerical model and the optimization process: definition of the meshing and the increment size for the non linear FE analysis and choice of the algorithm, initial values and the error definition for the optimization. The definition of the adapted parameter set, as an optimized solution, is strongly linked to the abilities of the algorithm to get through the local minima in order to ensure the convergence to the global minimum.

I.5.4. Presentation of the approach adopted

The aim of this work is to develop a tool describing the mechanical behavior of a bi-component structural adhesive in an assembly under cyclic loading. The first step consists in the choice of an experimental approach leading to the accurate definition of a bonding process, the shape of the bonded specimen then the construction of an experimental method. Modified Arcan device, using bonded specimen including beaks, is associated with low edge effects and a maximum stress state in the centre of the adhesive. In the first chapter, using such a device, experimental results under monotonic and creep and cyclic loading are presented. For a two-component polyurethane SikaForce®-7817 L60 MR adhesive, the experimental results reproducibility of the monotonic and cyclic behavior are investigated.

In previous studies (Maurice, 2012) (Jousset, 2008), experimental results underlined that the evolutions of the non-linear strains strongly depend on the loading type. The model proposed for 3D finite element code implementation, allows analyzing the influence of viscosity. In order to limit the experimental test time the inverse identification of the viscous model parameters is performed from modified Arcan creep/recovery tests. The second section describes the assumptions made on the adhesive mechanical behavior, the components of the model and their implementation and the inverse identification process of the model material constants.

The finite element simulations of bonded structures using the model developed allows a description of the cyclic behavior. Then using an adequate failure criterion based on the viscous strains evolutions, a prediction on fatigue life is performed in the third section. Since this work is dedicated to the study of bonded structures in offshore windmills applications, an investigation on the fatigue behavior of composite structures based on an application test is proposed in the last section.

Chapter II:

Experimental approach for the characterization of the viscous adhesive joint mechanical behavior

Introduction:

As they permit assumptions to be made on the mechanical behavior, modeling bonded structures relies on the characterization test method. Then, experimental data will lead to the material constants definition. As described in the previous part, a wide range of test methods is available and this list can be split in two parts: tests on bulk specimen and tests on bonded specimen. Nevertheless, physical-chemical properties of an adhesive are strongly linked to its adhesion chemical reactions with the adherend. Thus, in order to design bonded structures, test methods with bonded specimens which include adherend/adhesive interfaces are preferable.

This chapter presents the set-up of the bonding process and the experimental test method used for the characterization of the mechanical behavior of polyurethane structural adhesive with the modified Arcan test developed by the Laboratoire Brestois de Mécanique et des Systèmes (LBMS). As discussed in the previous section, edge effects reduction is a key point in order to reduce the stress concentrations in the adhesive bond-line. Indeed, a structure with low edge effects permits to study accurately the adhesive bond-line mechanical behavior. In this section, dedicated to the characterization of the adhesive polymeric material, a low adhesive thickness was considered (0.2mm) in order to stay within the framework defined by Cognard et al. (Cognard, et al., 2005) for the edge effects reduction.

The first part presents the bonded specimen and focuses on the bonded substrates characteristics. In the second part, the experimental method from the bonding procedure to the data measurement is detailed. Then, in a third part, results obtained are presented and assumptions are proposed with a focus on the viscous behavior. Finally, the last part will permit to exhibit some warnings on the experimental method, and particular precautions are put forward in order to obtain good repeatability.

Contents:

<u>II.1. Bonded specimens</u>	49
II.1.1. Polyurethane bi-component adhesive	49
II.1.2. Substrates	50
<u>II.2. Experimental method</u>	53
II.2.1. Bonding procedure	53
II.2.2. Modified Arcan device and experimental tests	54
II.2.3. Measurement of the adhesive deformation	55
<u>II.3. Characterization strategy</u>	56
II.3.1. Monotonic behavior	56
II.3.2. Creep behavior	58
II.3.3. Cyclic behavior	60
<u>II.4. Experimental campaign overview</u>	64
II.4.1. Ageing as a factor of influence in the mechanical behavior	64
II.4.2. Reproducibility	64
II.4.3. Information on failure	65
<u>II.5. Conclusion</u>	66

II.1. Bonded specimens

The different results presented in the following were obtained using a two component polyurethane structural adhesive SikaForce®-7817 L60MR (Sika, 2011). This adhesive was manufactured by Sika® in accordance with ISO 9001/14001 quality assurance system, in order to give high performance moisture resistant wind turbine bonded joint. Table II.1-1 lists the main mechanical properties given by Sika®.

Properties	SikaForce®7817 L60MR
Shore D Hardness (DIN 53505)	70 (23°C/50% r.h.)
E-Modulus (ISO 527)	2,000MPa
Elongation at break (ISO 527)	2.5%
Tensile strength (ISO 527)	30MPa
Tensile lap-shear strength (ISO 4587)	20MPa
Glass transition temperature (ISO11357-2)	50°C

Table II.1-1 : Mechanical characteristics – SikaForce®-7817 L60MR (all values are approximate).

II.1.1. Polyurethane bi-component adhesive

In the civil engineering domain such as windmill construction, bonded structures are normally erected on site in outdoor conditions and adhesive joint fabrication is exposed to varying outdoor temperatures and moisture. In recent windmill constructions, due to the normal large scale of the structural components, cold-curing adhesives are used, unlike other fields where hot-curing adhesives can be used indoor. However, for a wider application of adhesive joints in this domain, an understanding of the curing behavior is important in order to reach stabilization in the chemical polymerization process. Indeed, a chemically stable adhesive is a necessary step in order to obtain repetitive responses in time and a low scatter during the characterization experimental campaign of the bonded joint.

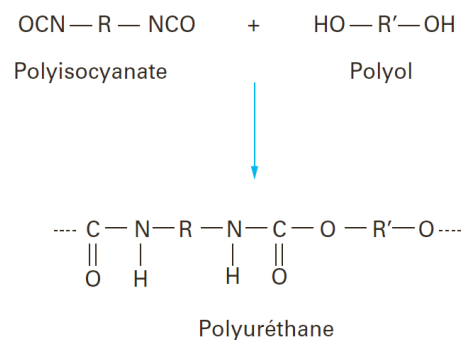


Figure II.1-1: Chemical reaction for production of polyurethane: poly-addition (Berthier, 2009).

a. *Chemical reactions*

The two components of SikaForce®-7817 L60MR are: the base part which is polyols chemically based and an isocyanate derivatives hardener. Apart from some of the one-component, moisture curing, elastic products (sealant adhesives), which usually contain free toluene diisocyanate (TDI), all the other types including SikaForce®-7817 L60MR are based on polymeric methylene diphenyl diisocyanate (MDI), the least volatile of the commonly used isocyanates. The adhesive used is a thermo hardening adhesive. Higher temperatures speed up the curing process and lower temperatures slow down the curing process. The cure starts as soon as the two components are mixed: the base and curing agent molecules react as described in Figure II.1-1. The viscosity of the mixture increases but, as the reaction proceeds, exothermic reaction heat develops. Furthermore high temperature keeps the viscosity low and facilitates chemical exchanges. A temperature increase permits to reduce the curing time. The

following part describes effects of temperature on curing mechanisms with the evaluation of some physical properties such as viscosity and heat flow measurement.

b. Physical properties

A preliminary study of the thermo-chemical properties was made using a Differential Scanning Calorimetry (DSC) device. The influence of the curing temperature on the thermal exchanges of the SikaForce®-7817 L60MR two components mixed was reported in Figure II.2-1. A maximum in the thermal exchanges is characteristic of an optimal curing temperature and for this polyurethane adhesive an exothermic curing peak was obtained at 110°C.

II.1.2. Substrates

a. Material

In these studies, the aluminum alloy used for substrates machining is an EN AW 2017 alloy. The 2000 series, alloyed with copper, and particularly the 2017 (former called Duralumin) are the most common aerospace alloys due to their machining abilities. Table II.1-2 gives the main chemical and mechanical properties of this alloy following the EN AW 2017 standard.

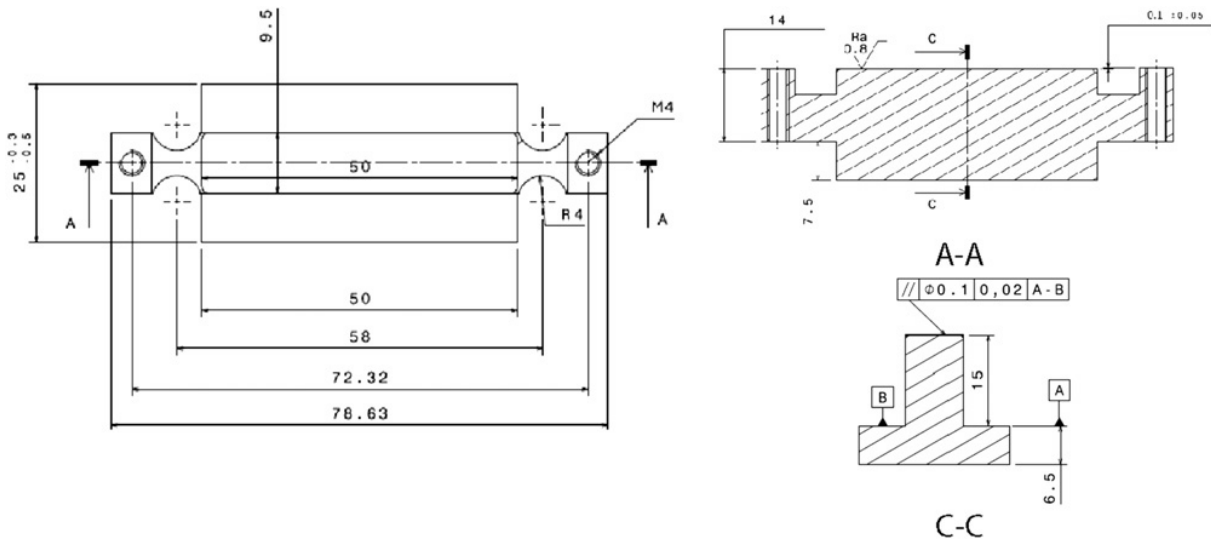
Chemical composition	
Components	Wt. (%)
Al	91.5-95.5
Cu	3.5-4.5
Mg	0.4-0.8
Si	0.2-0.8
Mn	0.4-0.1
Fe	Max 0.7
Zn	Max 0.25
Ti	Max 0.15
Cr	Max 0.1
Other components	Max 0.15
Mechanical Properties	
Modulus of elasticity	72.4GPa
Poisson's Ratio	0.33
Ultimate tensile strength	427MPa
Tensile yield strength	276MPa

Table II.1-2 : Aluminum alloy 2017 composition and main mechanical properties (mechanical values are approximate) (AFNOR, 2005).

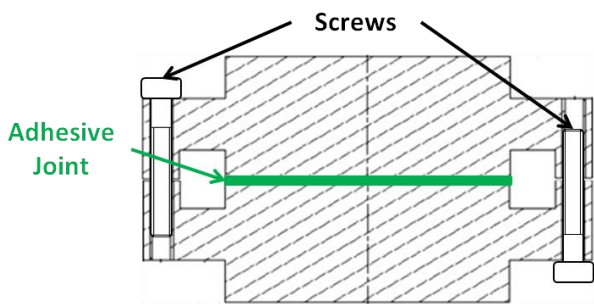
b. Geometries

Firstly, in order to obtain precise experimental results under cyclic loadings, it was necessary to ensure a precise adhesive thickness. The geometry of the typical bonded specimens used to conduct this study is reported in Figure II.1-2. The substrates made of aluminum alloy 2017 include spacers manufactured during the machining process of the substrates, and removed after the bonding process to perform the mechanical tests. The relative positioning of the two substrates is ensured by the same surfaces and using screws. Using such substrates, the bonded section is 50x9.5mm².

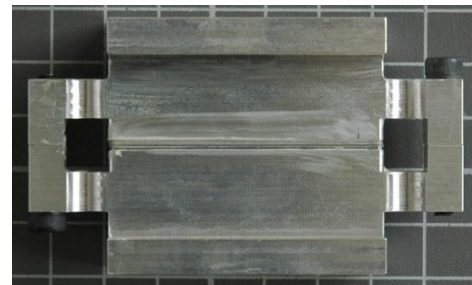
It can be noted that these bonded specimens were based on a geometry using beaks all around the substrates close to the bonded area to limit the stress concentrations. The geometry of these beaks was shown in Figure II.1-3. A precise machining process of the bonded substrates ensures a good control of each geometrical characteristics of the bonded joint and limits the scatter in the adhesive layer geometry.



(a)



(b)



(c)

Figure II.1-2: Presentation of the bonding process: Substrate main dimensions (in mm) (a), drawing (b) and image (c) of the bonding assembly.

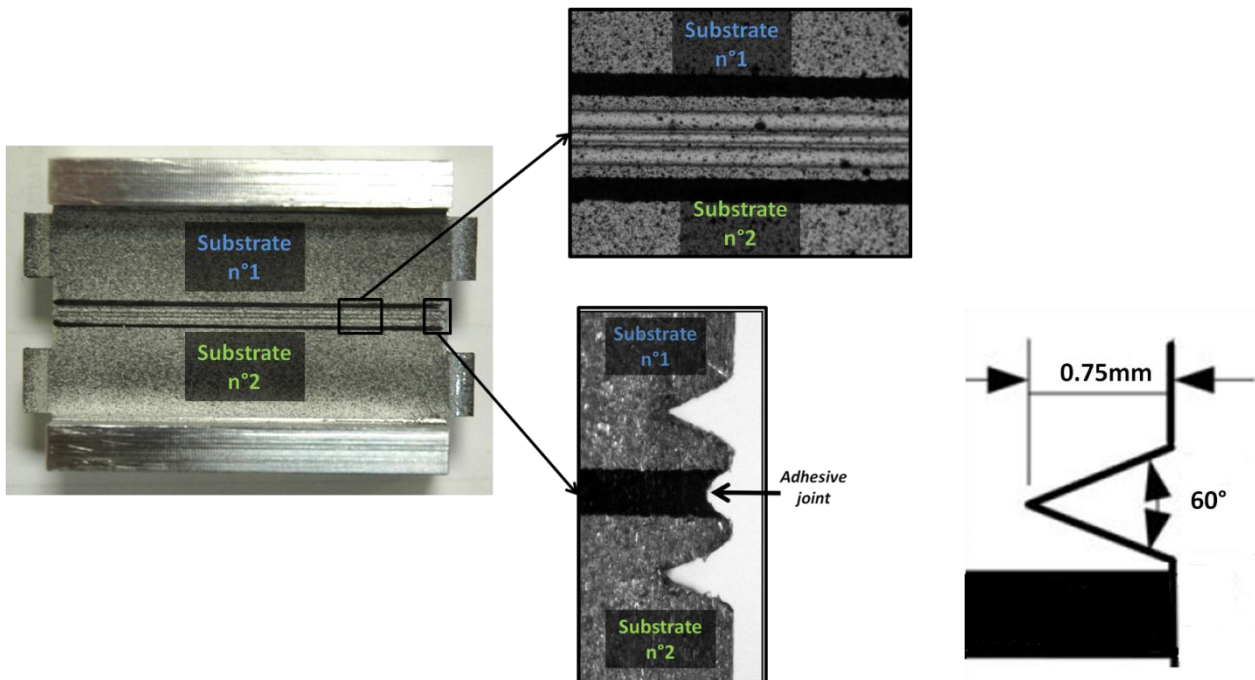


Figure II.1-3: Presentation of the bonded specimen before testing with a focus on the beaks geometry.

In testing bonded specimens, uniformity of the stress and strain is not assured and edge effects can have a significant influence on the results obtained, especially for low ductility adhesives (Cognard, 2008). Since the positive influence of the beaks on the reduction of edge effects is ensured only for thin adhesive joints (Cognard, et al., 2010) (Davies, et al., 2009), the characterization tests were performed using a low joint thickness. Considering a 0.2mm thick bonded joint, it was important in a first step to verify the effectiveness of the beaks influence on the edge effects for the adhesive considered. As the issue of the stress distribution within the adhesive bond-line for bonded specimen using beaks was already detailed in previous studies (Cognard, 2008)(Créac'hcadec, 2008) (Maurice, 2012), the case of the SikaForce®-7817 L60MR was handled with a single loading case: tensile-shear.

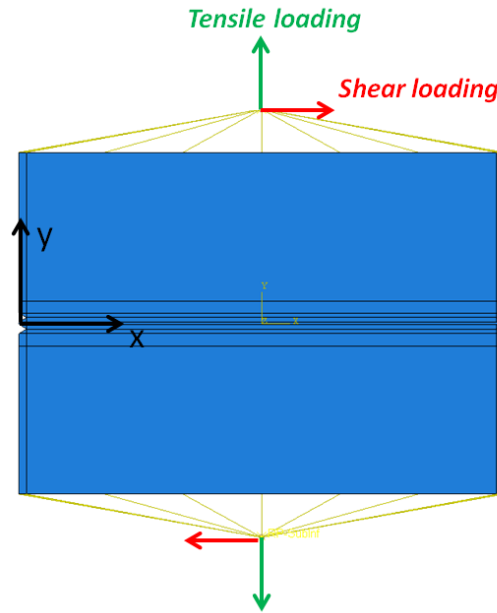


Figure II.1-4: Details of the FE model used for the stress state analysis: application of the tensile-shear loading (a) and mesh overview (b).

For the specimen geometry proposed, a 2D FE analysis was performed under elastic assumptions. The FEM was built with the Abaqus™ code using 4-node bilinear plane strain elements (CPE4) (Figure II.1-4a) under the linear elastic assumption using the mesh presented in Figure II.1-5a. Loading is applied to two driving points, which were kinematic-coupling constrained with the upper and lower surfaces of the bonded specimen. The materials data given by Table II.1-1 for the adhesive and Table II.1-2 for the substrates were used to define the adherends and adhesive bond-line mechanical properties. Figure II.1-5 presents the stresses obtained along the bonded overlap in the center and at the end of the bonded layer for a tensile-shear test at different thickness levels: $z=0$ (midplane of the joint), $z=h/4$ and $z=h/2$ (aluminum-adhesive interface). In order to obtain a good accuracy, a refined mesh was used at the ends of the overlap and within the bonded layer where 20 elements were used through the thickness. As shown in Figure II.1-5b and Figure II.1-5c, the stress non-uniformity was clearly demonstrated since, despite being almost constant in the center of the joint, all stresses components considered changed along the overlap length (x-direction). The shear stress adopts a symmetric hyperbolic-like shape with a maximum found in the midplane. The tensile stress is almost constant and the gradient is less significant at the edges. For the shear component, the value at the end of the overlap ($y=\pm l$) is lower than in the center. Concerning the tensile component, the stress state is not maximal in the middle of the overlap length but slightly greater under the beaks. Nevertheless, this

study confirms the positive influence of the beaks on thin bonded joints (0.2mm) in order to curb the edge effects. Furthermore, the stress states seems to be independent from the y-coordinate, as for the three positions (in the thickness), the shape and the value of stresses components were equivalent.

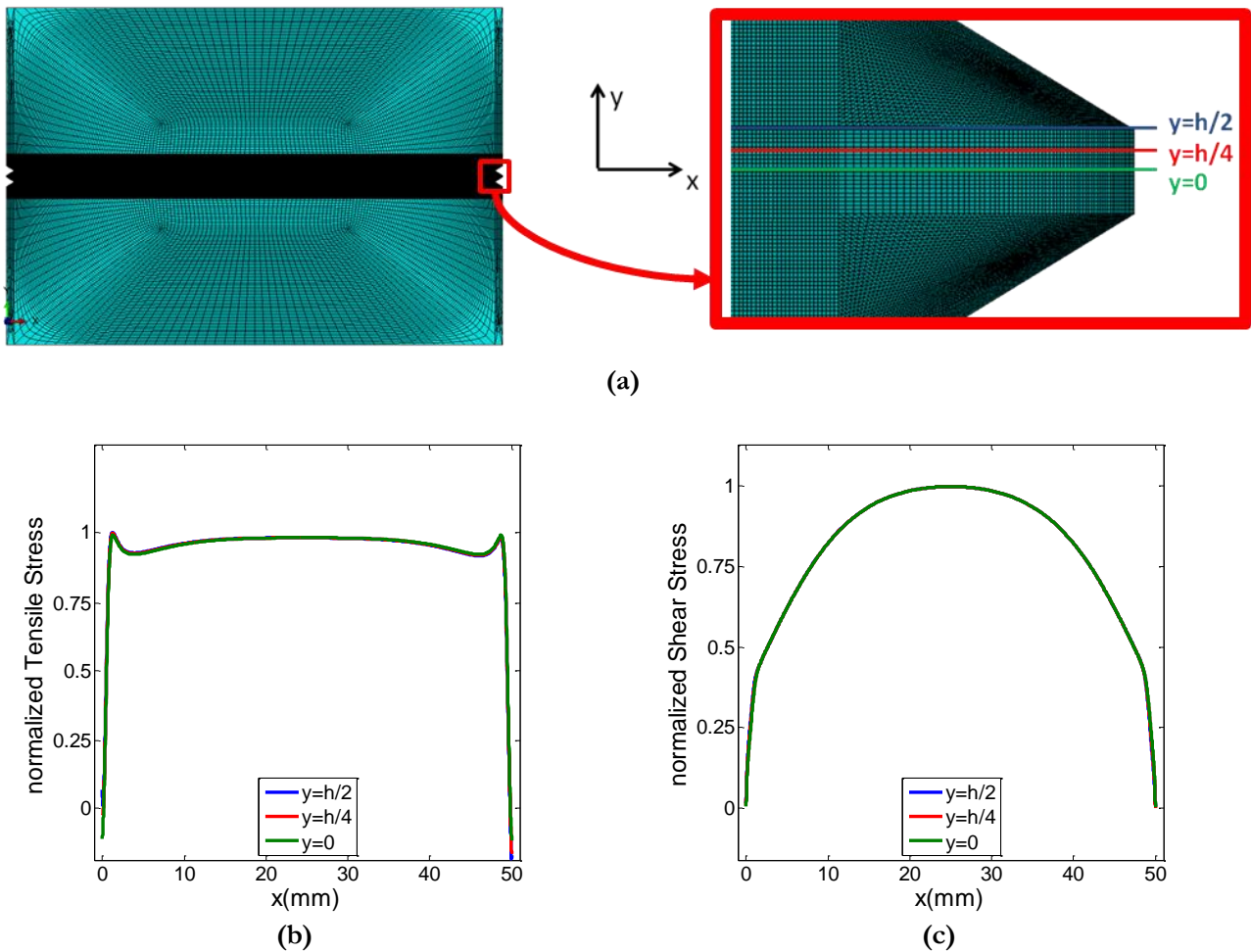


Figure II.1-5: Stress states within a 0.2mm bonded layer for a tensile-shear Arcan test: tensile stress (b) and shear stress (c) normalized values along the overlap length and the associated FEA local mesh (a).

II.2. Experimental method

The experimental part of this study is based on the approach proposed by Thevenet et al. (Thevenet, et al., 2013) for the characterization of bonded joints under cyclic loadings. In this previous work, the experimental method using a modified Arcan device was adapted from an experimental procedure proposed for monotonic tests (Créac'hcadec, et al., 2008) (Maurice, 2012).

II.2.1. Bonding procedure

a. Surface pretreatment

The 2017 alloys are susceptible to corrosion, hence in order to remove the oxides and corrosion products a mechanical treatment is performed using a sandpaper grade 120 abrasion. To remove the remaining organic and inorganic friable layers from the bonded surface, the abrasion was completed by an acetone degrease. Finally, preceded by a thermal drying of the acetone traces, a chemical treatment of the surfaces was made using a Sika® Aktivator-205 (Sika, 2010) pre-treatment (alcohol solution

containing a bond activating substance). The chemical treatment involved a precise duration to ensure the evaporation of the solvent. Therefore, during all the test campaigns, the elapsed time between the end of surface treatment and the beginning of the adhesive application was accurately controlled.

b. Thermal cure

An evolution of the polymerization leads to an evolution in the adhesive joint behavior. The Figure II.2-1 shows the effects of the curing processes applied to the bonded samples on the mechanical behavior. In order to reduce the scatter in the experimental results, it is important to reach a nearly fully polymerized material to avoid residual polymerization during the experimental campaign. A good way to obtain a nearly complete polymerization is to increase the reticulation process with a high temperature close to the exothermic curing peak (110°C). This preliminary study was made under shear loading with a modified Arcan device for a 1.0mm joint thickness and exceptionally under displacement-control (1.0mm.min⁻¹). Due to industrial issues associated to the domain of application of the adhesive (civil engineering) and because of the large bonded parts, the curing process cannot exceed a 60°C temperature (even if a higher temperature was identified to be more efficient for the curing). A cleaning of the adhesive was performed before curing in order to limit stress concentrations at the edges. In this study the bonding process include a three-day at 60°C thermal cure of the adhesive preceded by one day at room temperature. This thermal-cure process is advised by Sika® for industrial application of the SikaForce®-7817 L60MR adhesive. After the curing, samples are maintained two days at room temperature before the experimental tests.

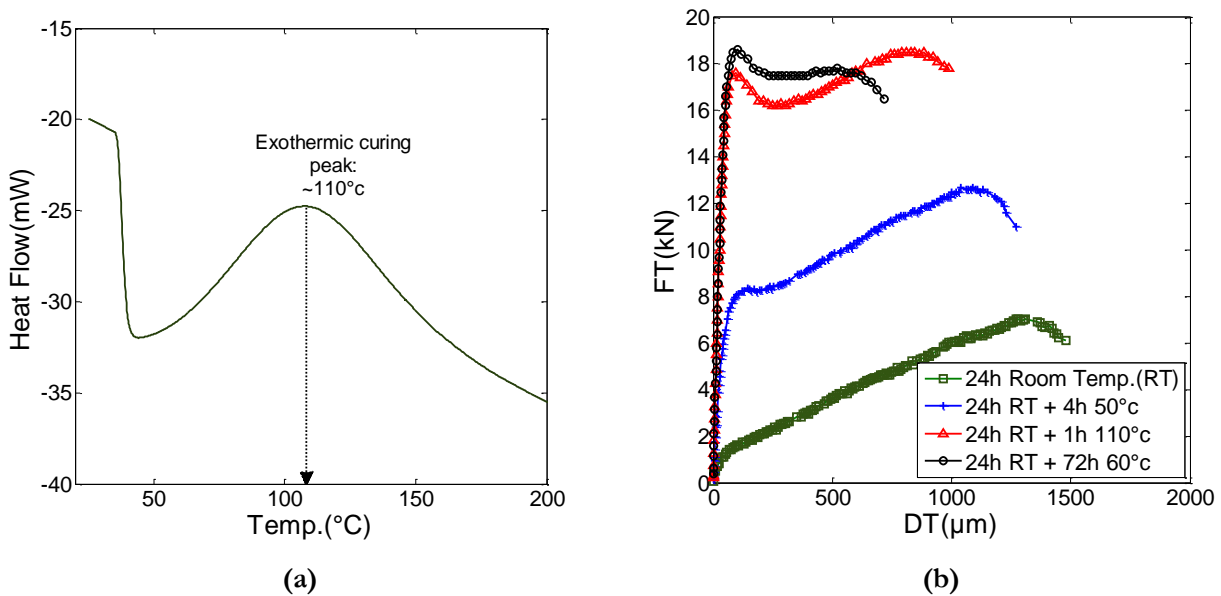


Figure II.2-1: DSC results for SikaForce®-7817 L60MR: with first heating (a), and influence of the curing process on the adhesive joint shear mechanical behavior (b).

II.2.2. Modified Arcan device and experimental tests

In order to load the bonded joint in the “normal stress-shear stress” plane a modified Arcan device allowing compression loadings is used. A clamping system was developed in previous studies (Cognard, et al., 2005) in order to fasten the specimen described in the previous section. This device enables to load a same specimen with different load ratios in a tensile machine. In order to apply these ratios, γ is defined as the angle between the loading direction imposed by the testing machine and the normal to

the bonded surface, N (Figure II.2-2). The device allows the angle γ to be varied in the range from 0° to 135° : $\gamma = 0^\circ$ corresponding to a tensile test, $\gamma = 90^\circ$ corresponding to a shear test, and mixed tensile-shear and compression-shear tests can be obtained with intermediate positions. Figure II.2-2 details the possible configurations for the Arcan device and the load ratios associated for each γ angle. For the tests performed, a traditional servo-hydraulic tensile testing machine with a 100kN capacity was used. All the experimental tests presented were performed in laboratory air and at room temperature.

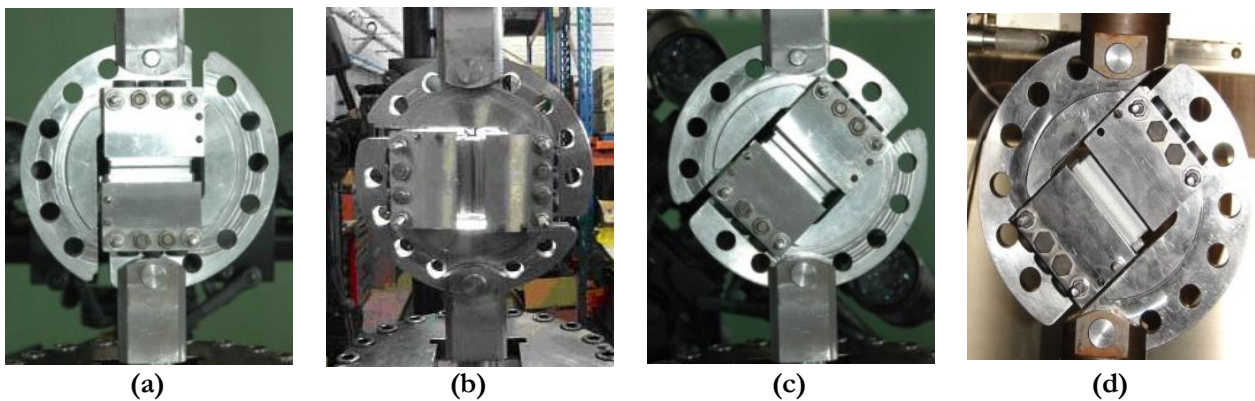
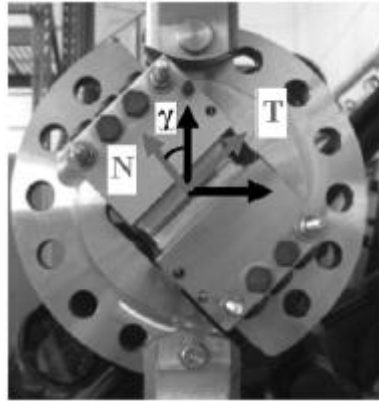


Figure II.2-2: Modified Arcan test device for different loading ratios: tensile test ($\gamma = 0^\circ$) (a), shear test ($\gamma = 90^\circ$) (b), tensile-shear test ($\gamma = 45^\circ$) (c), compression-shear test ($\gamma = 135^\circ$) (d).

II.2.3. Measurement of the adhesive deformation

In the following, FT represents the applied load in the tangential direction and FN represents the applied load in the normal direction. The load components measured during the tests are from the testing machine load cell. Following the same naming method, DT and DN are the relative displacement in the tangential and the normal direction of 2 markers placed on substrates on both part of the adhesive shown in Figure II.2-3b. This displacement is acquired using an optical non-contact extensometer by digital correlation image Figure II.2-3a. The device employed to measure local displacements in this work is an optical system using two four million pixels cameras with a 60Hz acquisition frequency. It provides results with a resolution smaller than $1\mu\text{m}$. In this measurement method, two facets (size $1 \times 1 \text{mm}^2$) are defined the markers on each substrate at a distance of 2.0mm from the edge of the bonded surface. The position of these facets is controlled by a line marked out on each substrate (Figure II.2-3a).

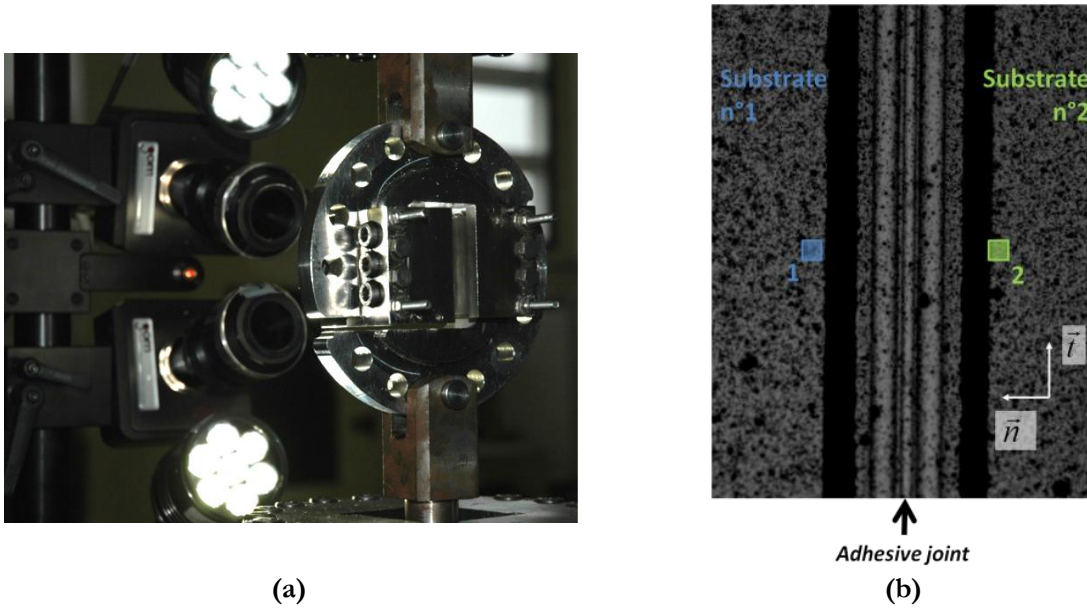


Figure II.2-3: Modified Arcan device under shear loading with 3D real time sensor GOM device (a) 3D real time sensor view of the bonded specimens using markers (1 & 2) to measure relative displacements of the substrates in the shear (\vec{t}) and the tension directions (\vec{n}) (b).

II.3. Characterization strategy

The aim of this section is to present the experimental campaign conducted on SikaForce®-7817 L60MR at room temperature. The experimental results are discussed in order to highlight the mechanical behavior of the adhesive under monotonic and cyclic loadings. Therefore, the experimental data have to be exhaustive and must include characterization tests in order to build a constitutive modeling for the adhesive behavior.

Tests were systematically conducted under load-control conditions using a same and constant loading rate in order to apply repetitive loading conditions, under both monotonic and cyclic loadings. Moreover, this choice allows avoiding the influence of the scatter in the adhesive joint thickness.

The approach proposed in this work focus on the viscous aspects of the mechanical behavior. The choice of a loading rate range is thus important. Concerning recent wind-turbine with large rotor blades, the rotation speeds of the blades are below a value of 1Hz. Therefore, in this study concerning the cyclic behavior, assuming the fact that for wind-blade the cyclic loadings are mainly due to it rotation, the experimental tests were performed on a base loading rate of 2kN/s. It will be shown in section 4.1, that a 2kN/s loading rate implies load frequencies consistent with windmills applications.

II.3.1. Monotonic behavior

a. *Arcan results*

Constant loading rate monotonic tests at 2kN/s has been performed for the SikaForce®-7817 L60MR structural adhesive. Figure II.3-1 shows the results obtained considering shear loading ($\gamma = 90^\circ$), tensile loading ($\gamma = 0^\circ$), tensile-shear loading ($\gamma = 45^\circ$), and compression-shear loading ($\gamma = 135^\circ$). The results are plotted in the tangential direction Figure II.3-1a and normal direction Figure II.3-1b. In the tangential direction, concerning test performed under shear loading, a significant non-linear

behavior was observed with a maximum displacement greater than $200\mu\text{m}$ (almost equivalent to the joint thickness).

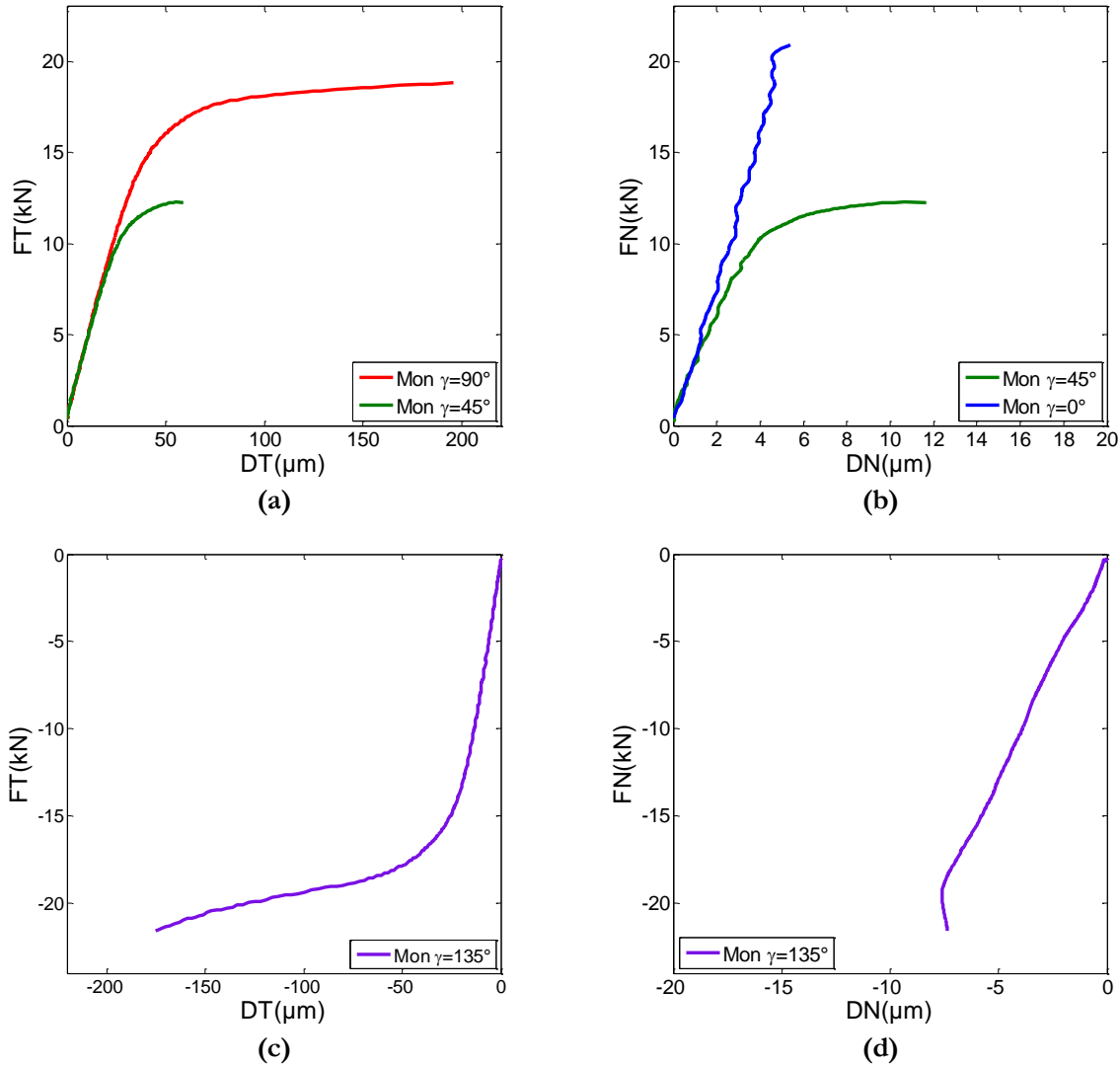


Figure II.3-1: Experimental results obtained for the SikaForce®-7817 L60MR under different load angles ($\gamma = 0^\circ$; $\gamma = 45^\circ$; $\gamma = 90^\circ$; $\gamma = 135^\circ$) in the normal direction (b and d) and in the tangential direction (a and c).

Among the different results in the normal direction, the very low magnitude of the relative displacements at failure shows a slight scatter due in the major part to noise in the acquisition. However, the quality of the results remains sufficiently good for analysis and the low level of displacement at failure (maximum $6\mu\text{m}$) with a nearly unperceivable non-linear part. For the tensile tests, the quasi linear shape of the $FN-DN$ curves makes the hypothesis of an elastic brittle behavior in the tangential direction an interesting assumption. Nevertheless, in mixed tensile-shear loading a non-linear part can be observed Figure II.3-1b.

Concerning the linear part, the identical stiffness observed for the linear part of the behavior in mixed tensile-shear and tensile loading for both shear and tensile directions confirms an isotropic behavior can be assumed for the definition of the elastic behavior. For a same specimen, the load at failure is substantially higher in compression-shear than in tensile-shear and tends to prove that the behavior of the structural adhesive considered is influenced by the hydrostatic stress.

b. Of the loading rate influence on monotonic tests

The purpose of this section is to evaluate the viscous characteristic of the adhesive through the dependency of the non-linear mechanical behavior to the loading rates. Previous studies (Renieri, et al., 1976) (Renieri, et al., 1976) (Bidaud, et al., 2012) have shown the influence of the loading rate on the mechanical response of structural adhesives. Therefore, in a first experimental campaign, under monotonic loading, three loading rates are applied to evaluate the viscous behavior of SikaForce®7817 L60MR: namely 0.2kN/s , 2kN/s and 20kN/s . In the shear direction, clear evolutions can be observed in the non-linear part of the mechanical behavior with a growth of the loading speed. A high loading rate increases the viscous stress in the material and as a consequence, the load at failure (Figure II.3-2a). The displacement at failure seems to be affected by the loading rate too: it decreases when increasing the loading rate. This second phenomenon was underlined by Deb et al. (Deb, et al., 2007) on Double Lap Shear specimen with an epoxy based adhesive joint. The influence of the loading rate on the plastic flow was a sign of time-dependent plasticity. Therefore, the irreversible flow should be called “visco-plastic” rather than “plastic”.

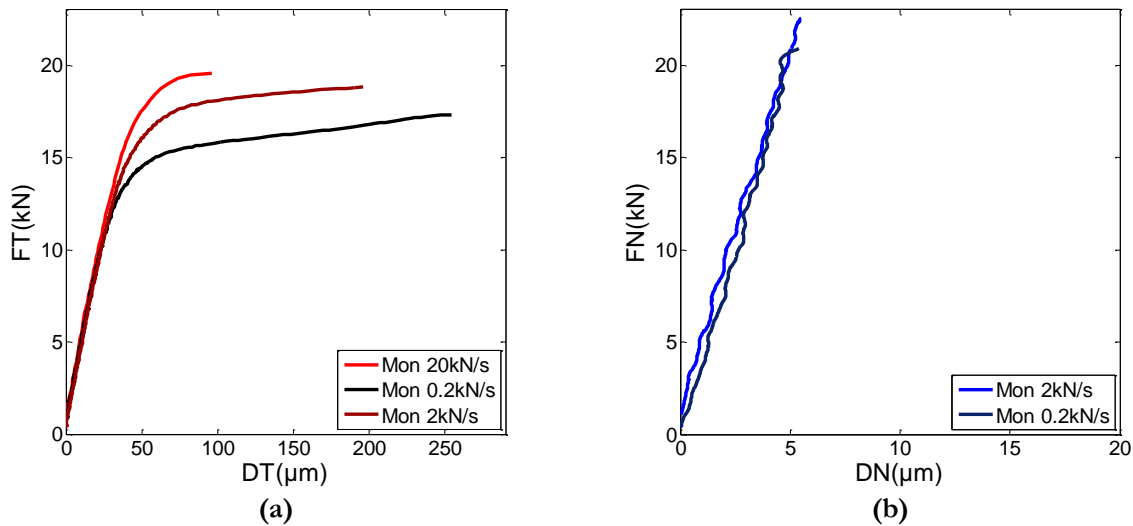


Figure II.3-2: Loading rate effect on monotonic tests: shear ($\gamma = 90^\circ$) (a) and tensile ($\gamma = 0^\circ$) (b) behaviors.

For tensile tests (Figure II.3-2b), since a non-linear behavior is not clear for the monotonic tests, the influence of the loading is not observed: a mechanical response without non-linear phenomena implies no strain rate dependency.

II.3.2. Creep behavior

a. Creep/recovery tests

In shear direction, monotonic tests using different loading rates highlighted the importance of the non-linear phenomena in the adhesive behavior and their loading rate dependency. These effects are usually considered as a consequence of the viscosity (da Silva, et al., 2008). Viscosity is a time-dependent mechanism including long-term phenomena, so monotonic tests with only three different loading rates may not be sufficient to investigate all the non-linear mechanisms. In order to evaluate the long-term viscosity effects, shear creep/recovery tests were conducted for a creep time greater than 1000s (Figure II.3-3a). During a 10kN creep, the tangential displacement shows a typical viscous response with a

non-linear growth. After a 5000s creep time, the loading was re-conducted to $0.5kN$ (necessary preload involved by the loading device) during a time equivalent recovery period. For SikaForce®-7817 L60MR the experimental response to this test shows a consistent residual displacement value (D_{res}): approximately 35% of the maximal displacement (D_{max}) for a $10kN$ load level (Figure II.3-3b).

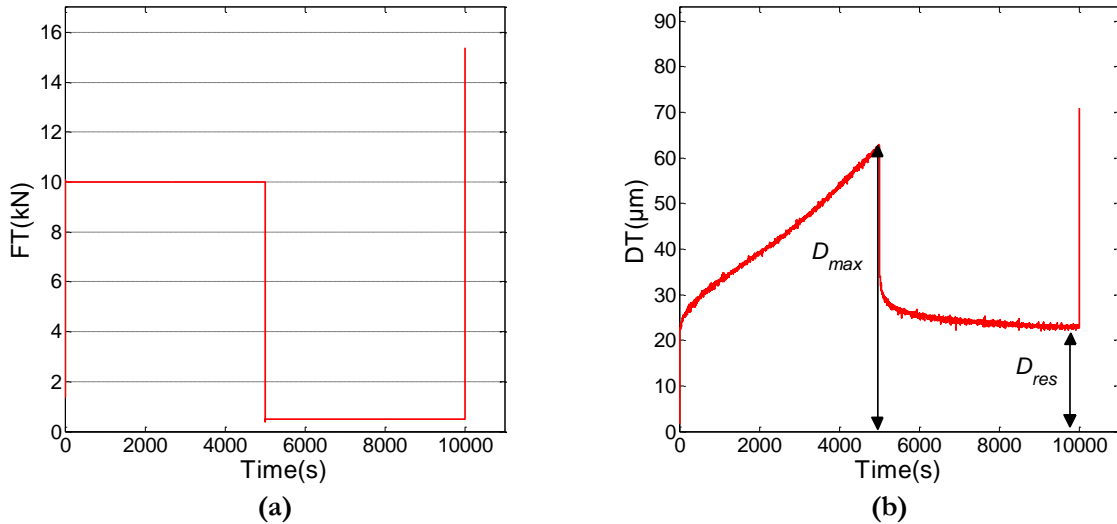


Figure II.3-3: Creep/recovery test under shear loading: load (FT) vs. $Time$ (a) and tangential displacement (DT) vs. $Time$ (b).

b. Cyclic creep/recovery tests

Cyclic creep and recovery tests are convenient for studying creep effects as for a same specimen several creep loading were played followed by a recovery part. Figure II.3-4b displays the tangential displacement (DT) during the cyclic creep/recovery test under shear. The different load values applied in this test allowed splitting viscosity in reversible and non-reversible phenomena. At low loads ($4, 6kN$), creep occurred but the tangential displacement was fully recovered after the recovery time 1800s: the time dependent effects were considered as visco-elastic. At the next higher loads ($8, 10, 12kN$), recovery was not completed and a residual tangential displacement was measured after the recovery step.

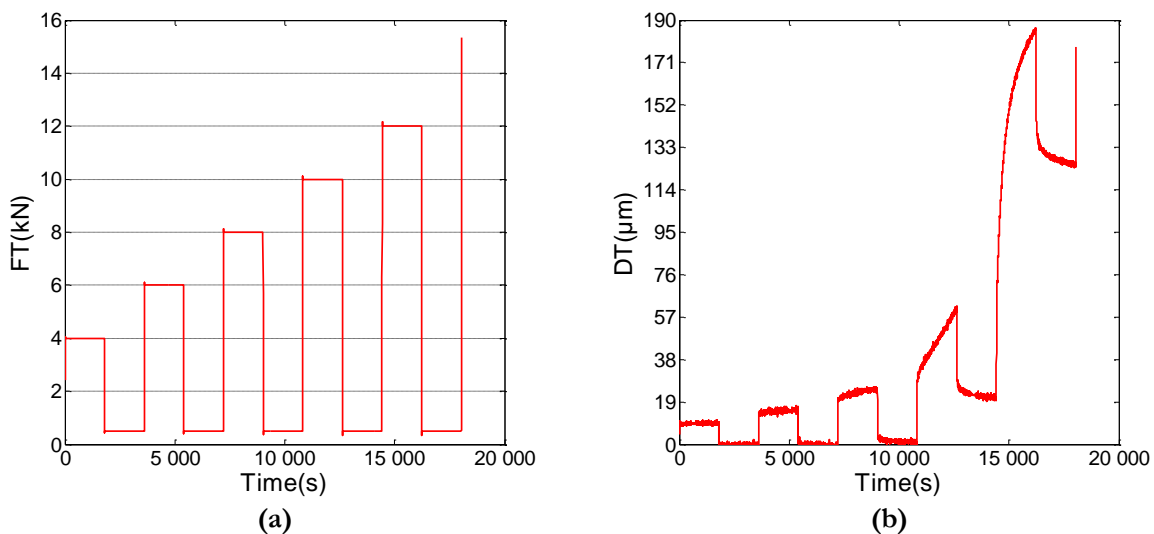


Figure II.3-4: Cyclic shear creep/recovery test: FT vs. $Time$ (a) DT vs. $Time$ and (b).

The time-dependent residual displacement may be considered as a sign of plasticity. After a recovery time of 1800s, a residual displacement still exists: therefore the residual displacement was assumed to be the evidence of a plastic flow. In the tensile direction (Figure II.3-5) even if (according to the monotonic tests) the adhesive seemed to be elastic brittle, non reversible strains was measured on the high levels of creep/recovery tests underlining by the same time dependency of the phenomenon.

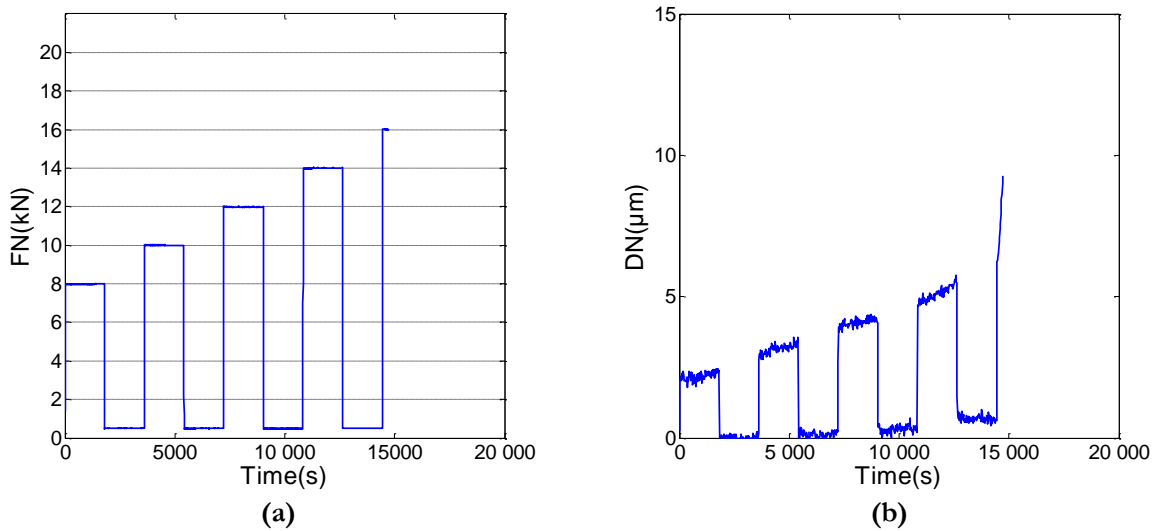


Figure II.3-5: Cyclic tensile creep/recovery test: FT vs. Time (a) DN vs. Time and (b).

II.3.3. Cyclic behavior

This part is devoted to the analysis of bonded joint behavior under cyclic loading. Particularly, the influence of the load amplitude F_a and the mean load F_m on the substrates relative displacement was investigated. In this work, all cyclic loadings were systematically performed with a load ratio $R_F = F_{min}/F_{max}$ greater than zero since an alternative compression-tensile loading was not admissible with the modified Arcan device.

Moreover, in this section the cyclic tests were conducted until failure with an increasing loading. Therefore, the cyclic tests performed here are not fatigue tests: the aim of these experimental results was to evaluate the cyclic behavior of the structure with short time tests (less than a thousand cycles). Since the shear direction gave more data with regard to the non-linear part of the mechanical behavior, the most part of the experimental results gave in this section concerns shear loadings.

As a preliminary study, an increasing cyclic loading was applied in the shear direction to a bonded specimen. Figure II.3-6 shows a mechanical behavior with hysteresis loops in the $F-D$ plane confirming the importance of the viscous phenomena observed through the results in creep and loading rate effects. A good correspondence of the cyclic behavior was retrieved with the monotonic response as the maximum displacement at each cycle followed the monotonic curve.

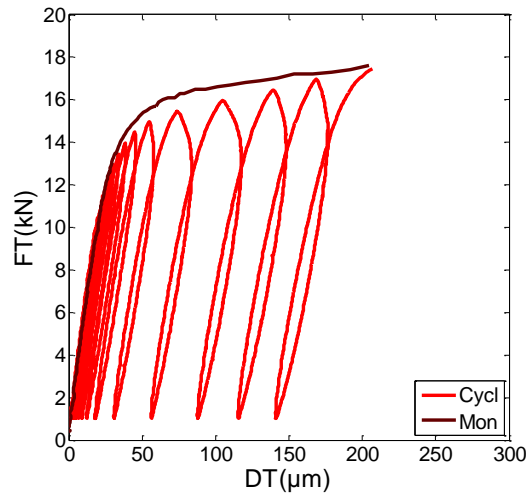


Figure II.3-6: Cyclic shear behavior of the SikaForce®-7817 L60MR using the modified Arcan test

a. Influence of the loading rate

The cyclic behavior of bonded joints using two loading rates: 0.02 kN/s and 20 kN/s were compared. The experimental results are shown for $FT_m = 7\text{ kN}$ and $FT_a = 5\text{ kN}$ in Figure II.3-7. For the same load amplitude, the area of the hysteretic loops is bigger at 0.02 kN/s than at 20 kN/s , This observation was consistent with the loading rate dependency of the visco-elastic behavior (Figure II.3-7).

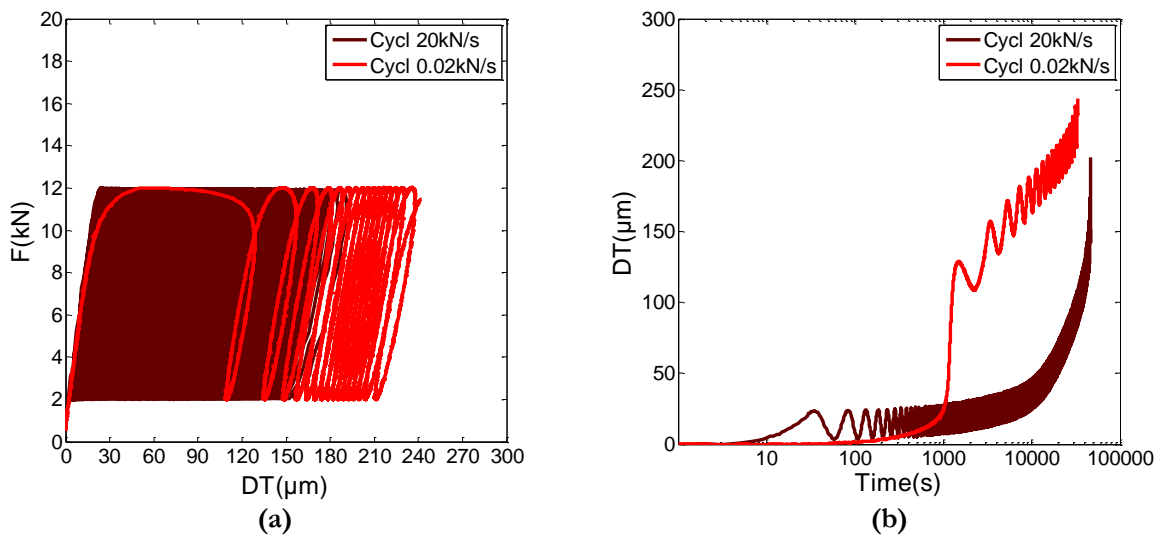


Figure II.3-7: Influence of the loading rate on the cyclic behavior under shear loading: FT vs. DT (a) and DT vs. Time (b).

The short-term visco-elasticity highlighted on the loading rate-dependent monotonic tests was held responsible of the shape of the hysteretic loops. Moreover, for a given number of cycles, the tangential cumulative displacement DT was clearly more important at 0.02 kN/s than at 20 kN/s . The loading rate dependency observed under monotonic loading was clearly highlighted under cyclic loading by examining the evolution of the cumulative tangential displacement along cycles Figure II.3-7. The residual displacement plotted in function of time in Figure II.3-7b was accelerated for the lower loading rate and the registered displacement per cycles was thus more important for 0.02 kN/s .

This dependency to the loading rate (or frequency) of the SikaForce®7817 L60 MR adhesive underlined the importance of the viscous parameters in the definition of its mechanical behavior.

b. Influence of the mean load

To characterize the mean load influence on the SikaForce®-7817 L60MR adhesive, multi load-levels cyclic tests are performed. Five shear loading cases, using blocks of 150 cycles, are applied with the same load amplitude $F_a = 2\text{kN}$ and mean load F_m varying from 2 to 12kN Figure II.3-8a. Figure II.3-8b shows the time evolution of DT during these cyclic tests. At low mean loads (for maximum loads under 8kN), the average value of DT does not evolve along the blocks. At higher mean loads, involving higher maximum loads, the average tangential displacement evolves during the 150 cycles. Such as for the previous experimental results, the visco-plastic phenomena can be observed depending on a threshold in the strength value.

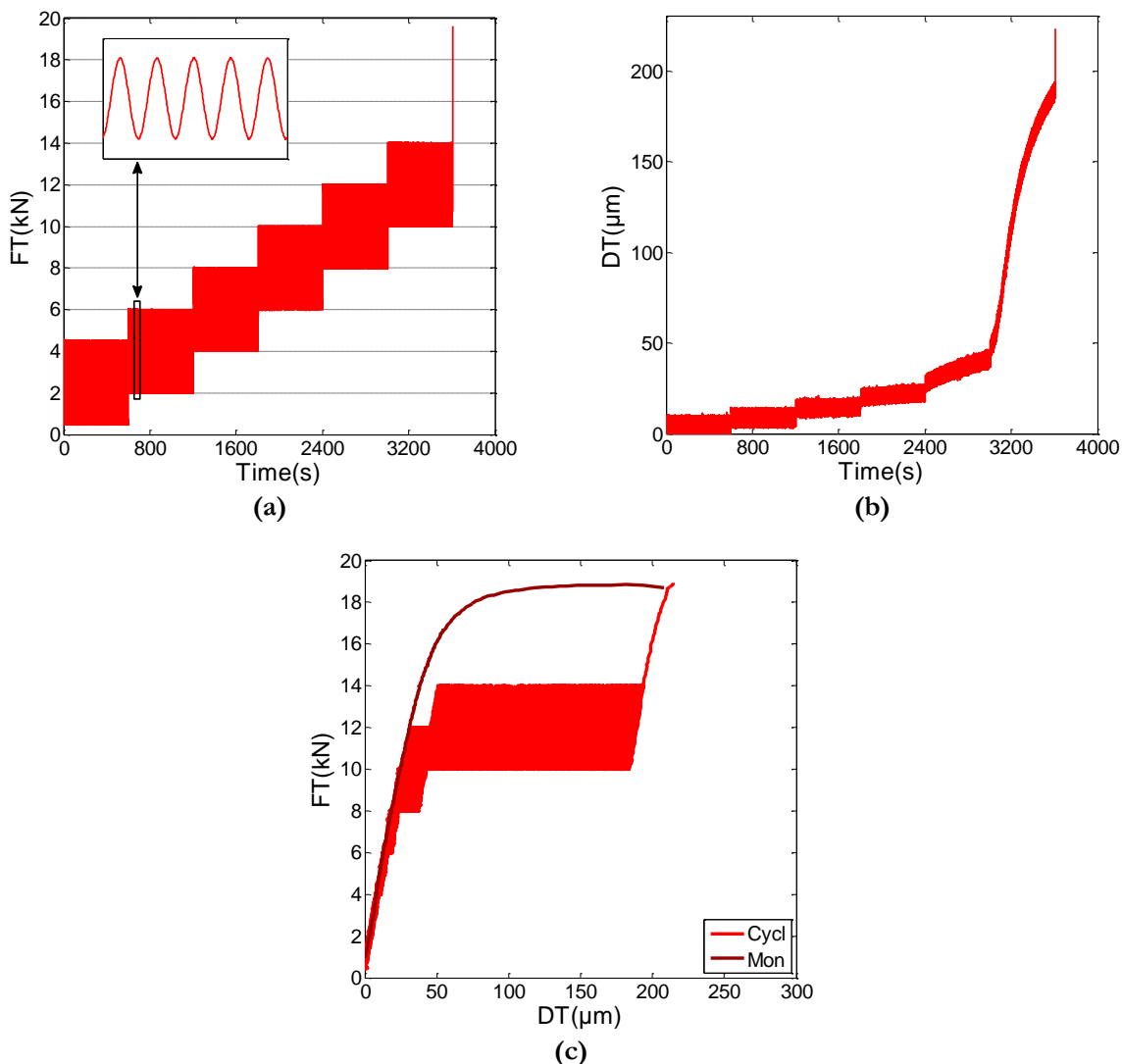


Figure II.3-8: Cyclic behavior under shear loading with influence of the mean load: applied load vs. time (a) and DT vs. time (b) and load vs. DT (c).

c. Influence of the load amplitude

Just as before, the influence of the load amplitude is investigated using blocks of 150 cycles. The same mean load $FT_m = 6.5\text{kN}$ is applied and the load amplitude FT_a is modified from 1 to 6 kN from the

first to the last block (Figure II.3-9a). The phenomena observed before in the creep tests can be compared to the cyclic loading: for high load amplitudes, time-dependent plasticity occurs. Figure II.3-9b shows the time evolution of DT during these cyclic tests. After a loading of 750 cycles (Figure II.3-9c) the correspondence between the strength and displacement at failure remains true. Furthermore, the adhesive loaded beyond the yield stress unloaded parallel to the initial elastic slope, restoring the elastic strain energy. These two observations suggested a little influence of the damaging behavior in the tangential direction.

For the loading cases tested, the maximum displacement measured after the cyclic loadings was lower than $50\mu\text{m}$ (approximately 25% of the load measured at failure). In further tests, the mean load FT_m should be increased in order to observe greater displacements, permitting a better investigation on the cyclic behavior. These multi load-levels cyclic tests, performed in order to analyze the influence of the load amplitude and mean load, are of interest in the definition of the loading cases to be studied in fatigue.

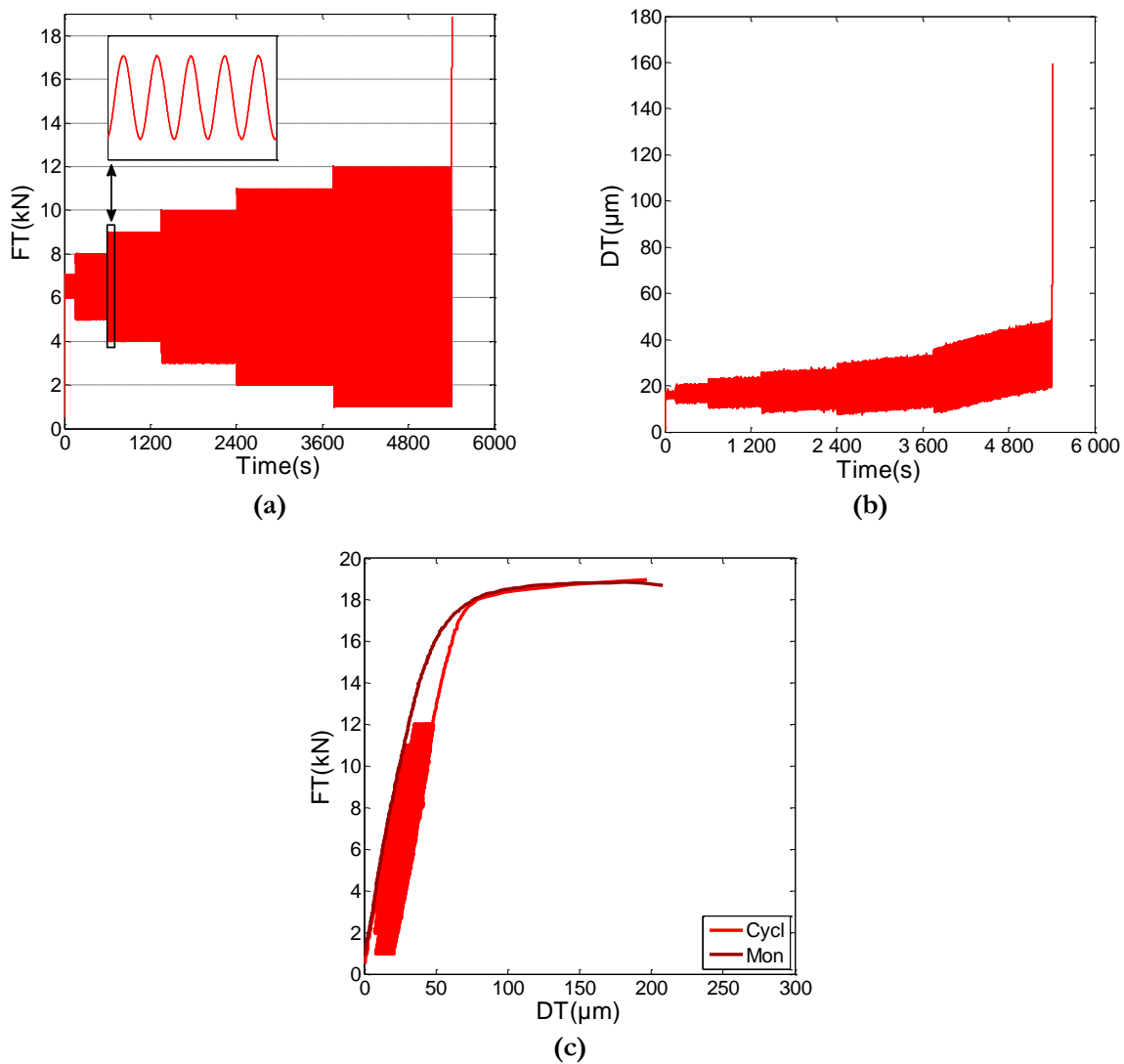


Figure II.3-9: Cyclic behavior under shear loading with influence of the load amplitude: applied load vs. time (a), DT vs. time (b) and load vs. DT (c).

II.4. Experimental campaign overview

In order to avoid the effects of ageing on the experimental results, the bonded specimens were tested in the month following the bonding process. Nevertheless, ageing of the adhesive components before mixing may have an important role.

II.4.1. Ageing as a factor of influence in the mechanical behavior

The two components of the SikaForce®-7817 L60MR adhesive were provided by Sika® in the same industrial packaging: 25kg batches. For such quantities, the recommended shelf life of the adhesive components is about one year. Following the recommendations, the adhesive was stored in a dry place at room temperature (between 10°C and 30°C).

Nevertheless, after opening the batches, the adhesive components showed have a progressive evolution. As presented in Figure II.4-1a, with a same bonding process, a 0.2mm adhesive bond-line mixed three months, and six months after the opening of the batches showed differences in its mechanical properties. In Figure II.4-1b, with the same conditions, the differences are shown for creep tests performed on adhesive joint components mixed until nine months after the opening. The differences recorded in the experimental response were important.

From a general point of view, experimental tests performed to characterize viscous effects generally lead to a more important discrepancy in the results. In fact, viscous behavior, as a time dependant phenomenon, is not characterized in the same time scale in monotonic tests and in creep or fatigue tests. Therefore, ageing of the bond-line components, which seem to affect the mechanic properties of the adhesive, can thus give completely dissimilar responses in the long-time behavior.

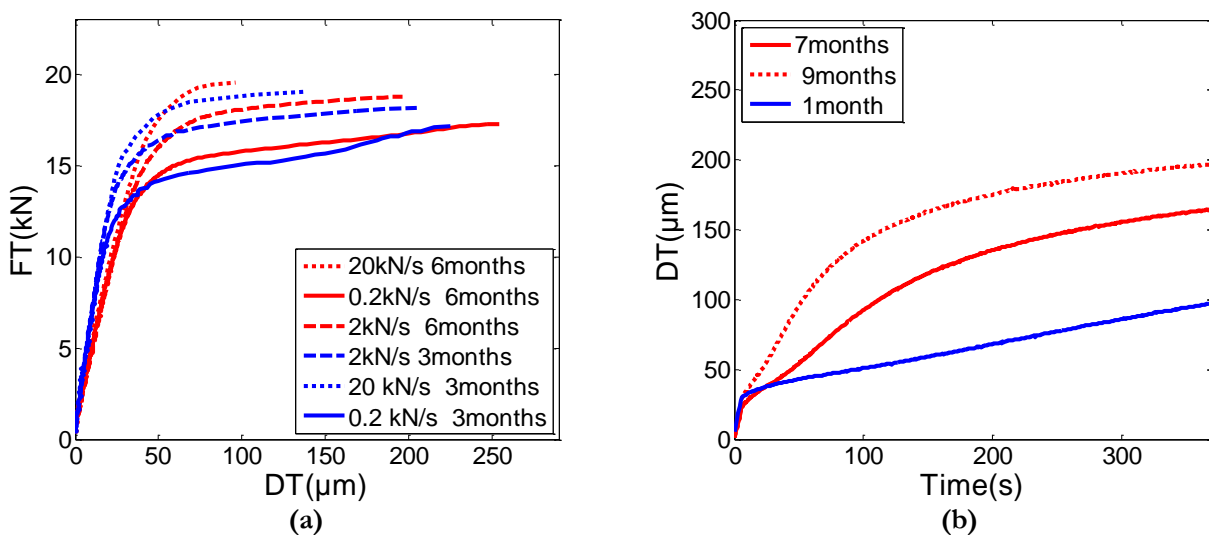


Figure II.4-1: Influence of adhesive components ageing: experimental response of different samples under monotonic shear loadings (a) and creep shear loading (b).

II.4.2. Reproducibility

An important step of this work was to ensure the reproducibility of the experimental results for experimental tests including important time scale. As influence of ageing of the adhesive may have an

important role, in order to reduce the scattering sources, the experimental results showed in this study were performed from specimen bonded in the accordance with the following criteria:

- The age of the adhesive components before mixing was controlled to be approximately the same for each characterization test;
- The bonded specimens were tested after a precise thermal cure;
- The bonded specimens were tested in the month following the bonding process avoiding room temperature post-curing.

From a general point of view, following these recommendations under monotonic loadings (Figure II.4-2a) and creep loadings (Figure II.4-2b) the behavior of bonded joints is reproducible and the experimental curves gave a really low scatter. In these two figures, the results of three different samples are plotted. Therefore, the bonding process developed for this adhesive was reliable and the Arcan device test procedure provides repetitive values of forces and displacements. To obtain these results the constraints are numerous with a lot of parameters to control during the bonding process. Hence, an experimental campaign of 60 samples was performed for the accurate characterization of the SikaForce®-7817 L60MR adhesive.

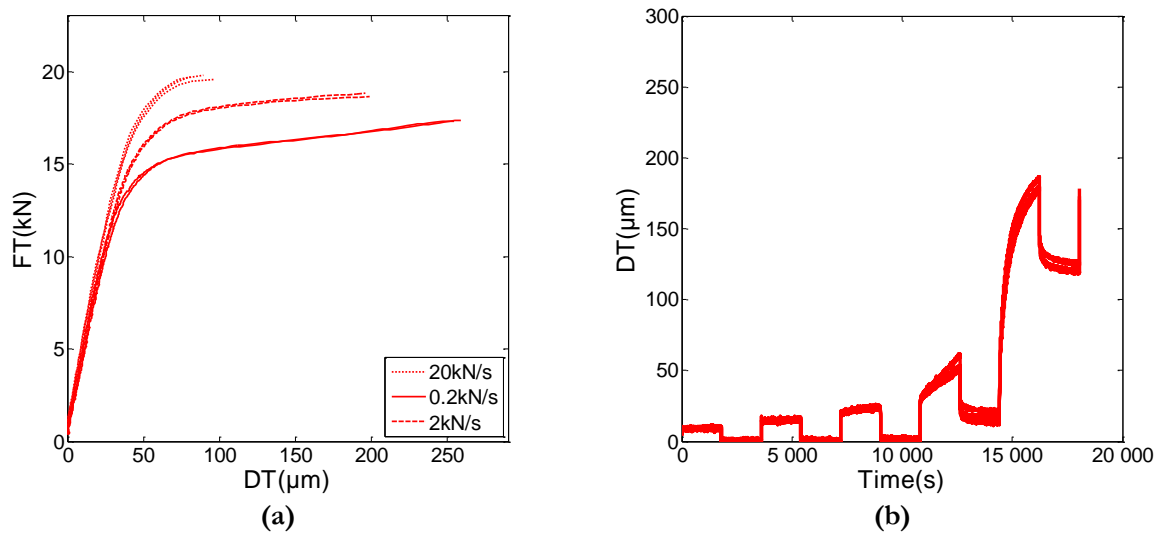


Figure II.4-2: Reproducibility (3 repetition for each loading case tested): experimental responses under monotonic shear loadings (a) and cyclic creep shear loading (b).

II.4.3. Information on failure

Furthermore, for the tested adhesive, all the specimens failed cohesively within the adhesive layer, whatever the type of load applied (configurations of the Arcan device and loading mode). Figure II.4-3 shows fracture surfaces for tensile, shear, tensile-shear and compression-shear tests. Failure occurring within the adhesive layer, testified an optimized bonding process which permit to ensure a complete characterization of the adhesive material itself as the substrate-adhesive interfaces are not the weaker part of the joints. Mechanisms leading to the failure of the bonded specimen are thus ruled by the polymeric adhesive material. Predictions on 0.2mm Arcan bonded specimen mechanical properties can be made through assumptions on the adhesive mechanical behavior performed on the adhesive bond-line.

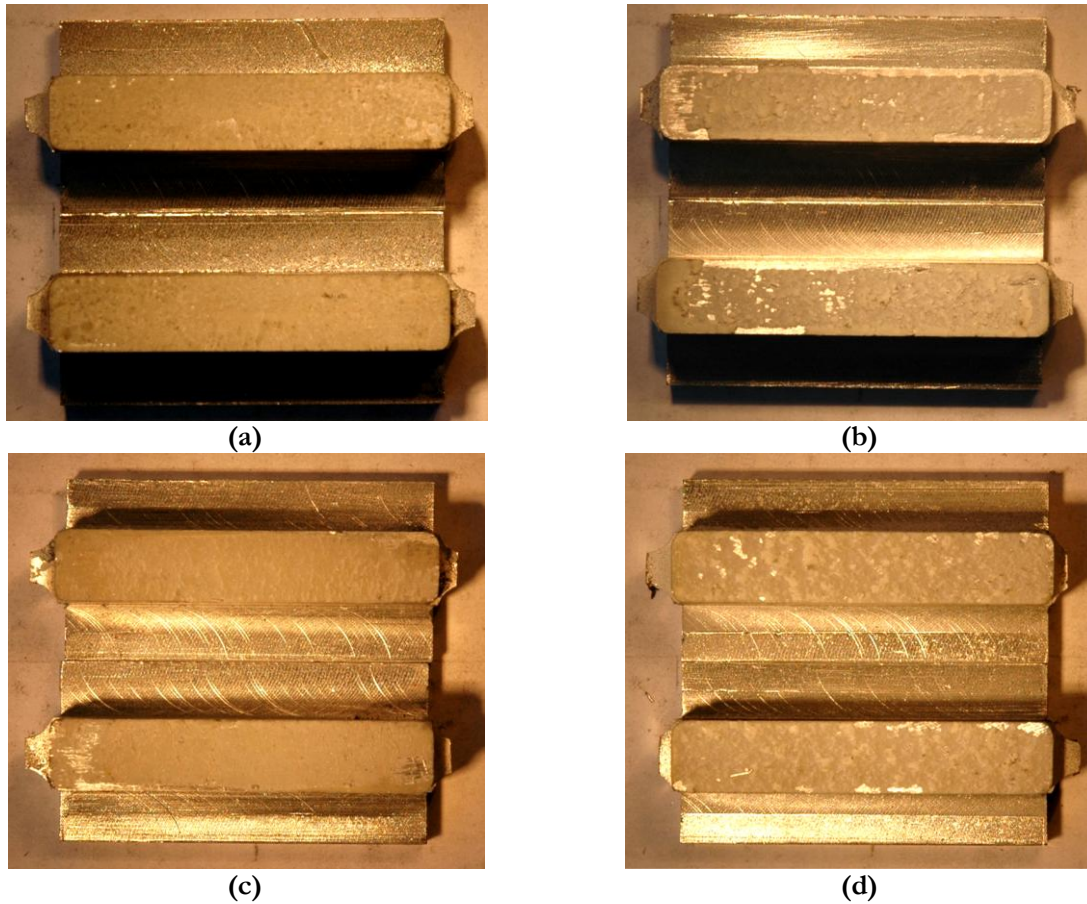


Figure II.4-3: Example of cohesive failure obtained for different loading directions: tensile test ($\gamma = 0^\circ$) (a), shear test ($\gamma = 90^\circ$) (b), tensile-shear test ($\gamma = 45^\circ$) (c), compression-shear test ($\gamma = 135^\circ$) (d).

II.5. Conclusion

Modified Arcan device using bonded specimen including beaks is associated with low edge effects and a maximum stress state in the centre of the adhesive. The major interest of a test method leading to pure loading without stress concentration is to characterize a confined adhesive material with considerations close to the study of a bulk polymer specimen. Using such a device, accurate experimental results under monotonic, creep and cyclic loadings were presented. These experimental results were associated to cohesive failures and the mechanical response could thus be associated to the adhesive material behavior and not to its adhesion properties. Furthermore, in a final part, an investigation on the repeatability of the results for different age of the adhesive components revealed an important scattering. Therefore, in this section, an accurate experimental process was proposed and developed to access to a reliable characterization test database. Therefore, as the non-linear response of the bonded specimen in shear reached high values, first assumptions were made on the mechanical behavior of the adhesive joints.

To conclude, a useful database has been created for the characterization of the viscous behavior of a SikaForce®-7817 L60MR adhesive. As the mechanical behavior was accurately defined, a model can be proposed for modeling the cyclic behavior. In the following part, the mechanical behavior recorded in shear using cyclic creep tests will serve as a basis for a numerical viscous model development. For the tensile tests, the loading rate influence and the experimental response recorded suggest a really low influence of the viscous phenomena. The model developed will have to account this effect.

Chapter III:

Modeling and identification of the mechanical cyclic behavior

Introduction:

The experimental work, managed with a modified Arcan device, exhibits for the considered structural adhesive, a non-linear and time-dependent mechanical response particularly in the shear direction. Through the loading rate and time effects, a viscous behavior was thus observed.

In order to describe the mechanical adhesive joint behavior, the numerical approach proposed in this chapter is based on the use of a non-linear visco-elastic visco-plastic model. First, to reach this purpose, an identification work, only based on the monotonic/creep experimental results under shear loading has been performed to identify the constitutive equations for the viscosity. In a second step, the influence of the hydrostatic stress with a non-associated model has been regarded, with the implementation of a 3D model.

With the approach proposed, in this chapter, the model was developed and the viscous parameters were identified in order to describe the cyclic behavior.

Contents:

<u>III.1.</u>	<u>Shear behavior: numerical approach</u>	<u>69</u>
III.1.1.	Viscous behavior definition.....	69
III.1.2.	Inverse identification.....	70
III.1.3.	Stress distribution under creep/recovery conditions.....	75
III.1.4.	Numerical and experimental comparison.....	76
<u>III.2.</u>	<u>3D constitutive behavior</u>	<u>79</u>
III.2.1.	Constitutive equations.....	80
III.2.2.	Computational algorithm.....	81
III.2.3.	Inverse identification.....	86
<u>III.3.</u>	<u>Conclusion.....</u>	<u>92</u>

III.1. Shear behavior: numerical approach

III.1.1. Viscous behavior definition

The purpose of this first section is to develop the constitutive equations in order to describe the mechanical behavior of the adhesively bonded joint under shear loading. The experimental study of the SikaForce®-7817 L60MR, analyzed in the experimental study, was undertaken to develop the model constitutive elements.

a. Phenomenological model

As part of the definition of a phenomenological model, the experimental results in shear revealed important aspects of the bonded joint behavior. The model developed for the adhesive behavior must describe several mechanical features:

- A time-dependent and non-linear behavior implying viscosity on both short and long time scales;
- At high load values, a plastic flow appears revealed by residual tangential displacements;
- The plastic flow is loading rate dependent.

Therefore, the model was divided into two parts delimited by a threshold. For load values lower than the yield stress σ_s , all strains are reversible. When load values are higher than this threshold, visco-plastic flow appears. Figure III.1-1 presents the rheological formulation of the 1D model.

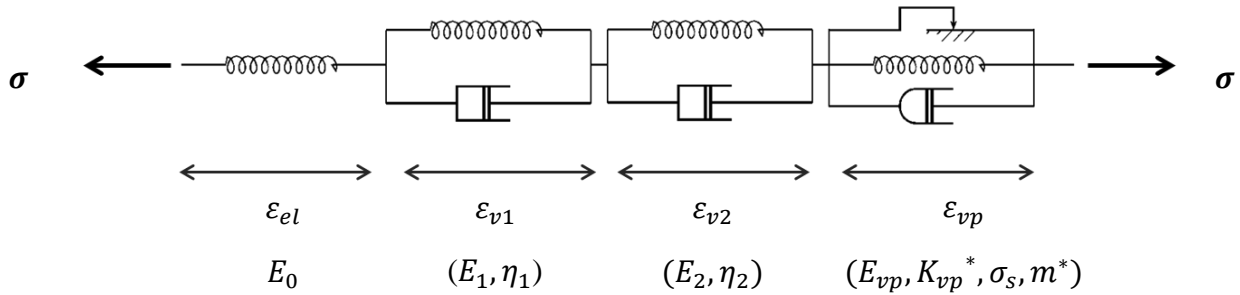


Figure III.1-1: Formulation of the phenomenological model.

b. Constitutive equations

For a good understanding, constitutive equations are detailed on the base of a simplified 1D model. The equations of the 1D model only operate on the shear components. The phenomenological model, proposed in this study, splits the total strain ε into four parts as follows.

$$\varepsilon = \varepsilon_{el} + \varepsilon_{v1} + \varepsilon_{v2} + \varepsilon_{vp} \quad (\text{Eq 1.39})$$

where the elastic strain ε_{el} is equal to:

$$\varepsilon_{el} = \frac{\sigma}{E_0} \quad (\text{Eq 1.40})$$

where σ is the Cauchy stress and E_0 is the instantaneous modulus of elasticity. ε_{v1} and ε_{v2} are the visco-elastic strains defining the short and the long creep characteristic times respectively. These

reversible viscous strains are function of the couples of parameters (E_1, η_1) and (E_2, η_2) , E_1 and E_2 the instantaneous moduli, η_1 and η_2 viscous parameters.

$$\dot{\varepsilon}_{v2} = \frac{1}{\eta_2} (\sigma - E_2 \varepsilon_{v2}) \quad (\text{Eq 1.41})$$

$$\dot{\varepsilon}_{v1} = \frac{1}{\eta_1} (\sigma - E_1 \varepsilon_{v1}) \quad (\text{Eq 1.42})$$

ε_{vp} represents the visco-plastic strain occurring above the yield stress σ_s . The rheological model corresponding to the visco-plastic law is a Chase-Goldsmith model with a non linear definition of the viscosity:

$$\dot{\varepsilon}_{vp} = \left[\frac{1}{K_{vp}^*} (|\sigma - E_{vp} \varepsilon_{vp}| - \sigma_s) \right]^{m^*} \text{sign}(\sigma - E_{vp} \varepsilon_{vp})$$

where E_{vp} is the hardening parameter and (K_{vp}^*, m^*) are material parameters defining the non-linear viscosity.

III.1.2. Inverse identification

The material constitutive equations proposed need to be implemented in a finite element code to be used in structural computations. Constitutive model developed is not available in commercial finite element software. The equations were thus implemented in a finite element model (FEM) to describe the behavior of adhesively bonded samples submitted to shear loading with the modified Arcan device. The aim of this part is to highlight the important aspects of the finite element analysis (FEA) and to present the strategy used for the inverse identification of the model parameters.

a. Finite element analysis

In order to take into account the stress distribution of the modified Arcan samples including beaks, a 2D FEM of the Arcan specimen was thus employed (Figure III.1-2). The FEM was built with the Abaqus™ code using 4-node bilinear plane strain elements with reduced integration (CPE4R). The constitutive model was implemented with a user-material (UMAT) written in FORTRAN language (details concerning the implementation of the 1D model are not given here as a complete description of the 3D model algorithms is made in the following section). In the normal direction, the mechanical behavior was considered under elastic assumptions. The following elastic parameters were used for the aluminum substrates (Young's modulus: $E_{Al} = 72\text{GPa}$, Poisson's ratio: $\nu_{Al} = 0.33$). Previous studies, based on a plastic behavior law for the adhesive mechanical behavior, showed non-linear stress distributions along the length of the adhesive joint (Cognard, 2008). Therefore in order to take into account the specific stress state, a FE model was developed.

The specific geometry involves an almost equivalent stress distribution along the adhesive thickness (for a 0.2mm thick adhesive joint), due to the use of beaks. This point justifies meshing the adhesive layer with only one element in the adhesive joint thickness to evaluate the mechanical behavior of the modified Arcan specimen: 140 elements were used in the adhesive longitudinal direction (\vec{x}). Furthermore, a mesh refinement along (\vec{x}) direction was made close to the edges and the beaks. Figure III.1-2b indicates the mesh used in this 2D FE analyses. The boundary conditions were applied on driving points with a kinematic coupling for both upper and lower substrates.

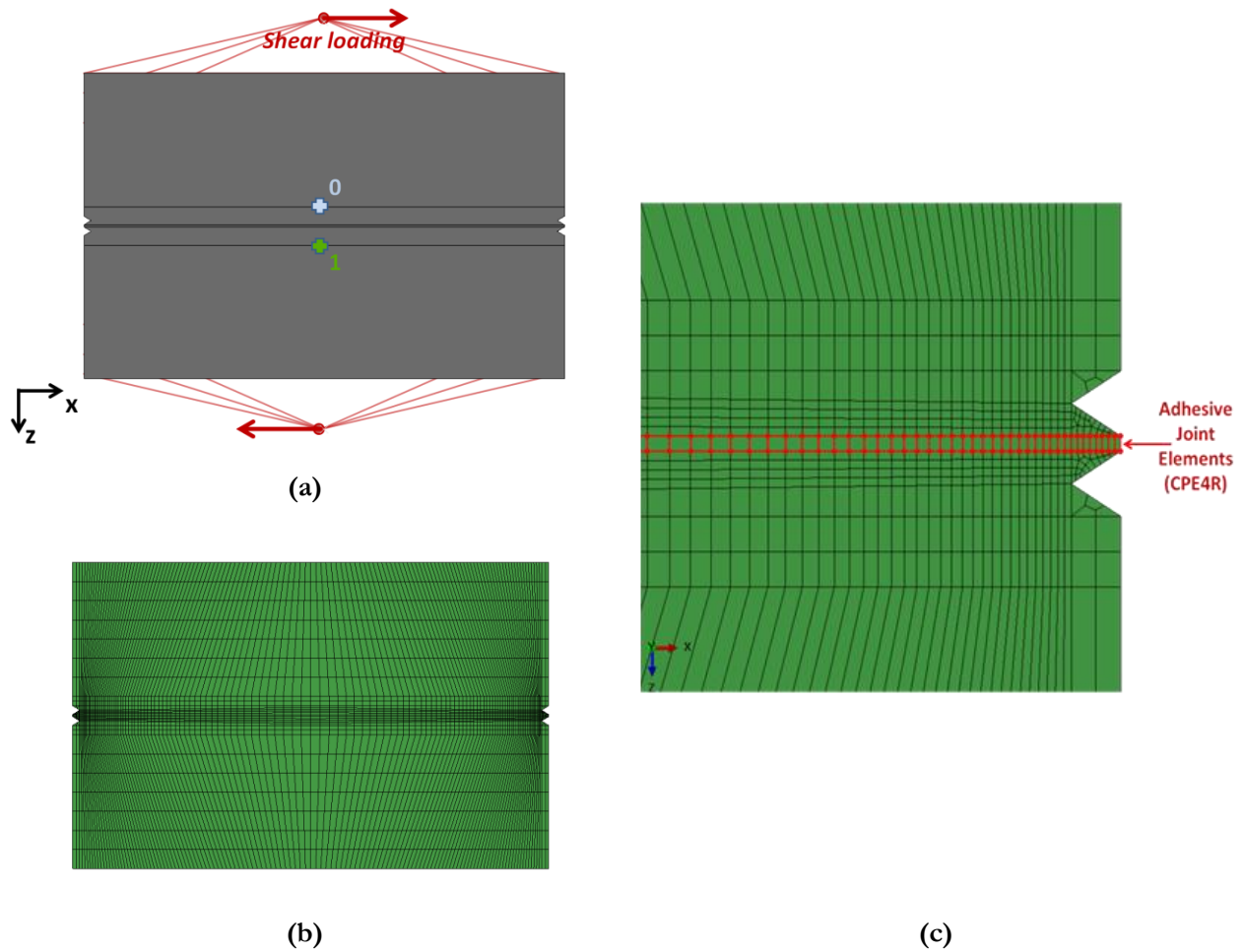


Figure III.1-2: 2D FEM of the modified Arcan sample (a), finite element mesh (b) and zoom of the adhesive with beaks (c).

Experimentally, tests were carried out under load control, so numerically the loading is applied on the upper driving point. For both driving points, rotation was free, but displacement in the normal direction of the adhesive joint was constrained. The lower driving point was controlled by equations on the free rotations and displacements: for these degrees of freedom, they were set to be the opposite of the upper driving point.

b. Identification strategy

The identification of the model using the modified Arcan test is based on an inverse process. The inverse identification method of the material parameters takes into account the non-uniform stress distribution along the adhesive overlap. This numerical method couples the FE results, given by the Abaqus™ software, and the optimization software Python™ (Python, 2014) considering the non-linear optimization library NLOPT. Concerning the optimization works performed in this thesis, the algorithm used was based on an implementation of a globally-convergent method-of-moving-asymptotes (MMA) implementation. This algorithm was developed for gradient-based local optimization, including inequality constraints. The “globally-convergent” term does not mean that the algorithm systematically converges to the global minimum. The only convergence guaranteed is to some local minimum depending on: the starting point, the constraints and the gradient definition.

Therefore, in this study, the uniqueness of the “optimized” solutions developed remains open for discussion as convergence to the global minimum was not guaranteed.

The optimization work consists in the definition of parameters giving a minimum value for the difference between experimental and numerical responses using a step-by-step approach. Here, for each increment of the optimization algorithm, a FE computation is performed, the cost function h is defined by a difference between the experimental and the numerical response in terms of displacement for a same loading imposed. The general form of this function is given by:

$$h = \sum_{i=1}^{n_{exp}} (D_{num}(i) - D_{exp}(i))^2 \quad (\text{Eq 1.43})$$

The numerical-experimental discrepancy is calculated at each experimental data point i and $D_{num}(i)$ could be an interpolated value from the numerical response.

The inverse identification procedure proposed in this work is based on the modified Arcan test campaign presented in Chapter III. The equations developed for the constitutive model implies that the identification of the shear mechanical behavior includes 9 parameters: 1 for the elastic behavior, 4 affecting the visco-elastic behavior and 4 affecting the visco-plastic behavior. The choice was made to use a step-by-step identification in order to reduce the number of parameters to vary in the optimization process. Here, three steps were defined:

- Step 1, concerns the identification of the elastic behavior: the shear modulus E_0 is defined using a linear FE analysis on the monotonic behavior;
- Step 2, concerns the identification of the visco-elastic behavior: the two couples of parameters (E_1, η_1) and (E_2, η_2) are defined using FE analysis with the constitutive law on shear creep results for low loading levels;
- Step 3, concerns the identification of the visco-plastic behavior: the material constants linked to the visco-plastic behavior $(E_{vp}, K_{vp}^*, m^*, \sigma_s)$ are defined.

In case of an identification step depending on the results of an optimization on two tests, the results of the function costs for each test are added up to have a global value. The three following sections describe the identification process for each step.

c. Definition of the linear behavior

Under monotonic shear loading, a linear behavior can be observed for the higher loading rates tested ($20kN/s$). In this part of the $FT-DT$ curve, the effects of viscosity with a time dependency are quite limited. Thus, until the plastic threshold σ_s , a good approximation of the instantaneous elastic behavior of the adhesive can be established. In the identification work of this study, the experimental data from the $20kN/s$ monotonic test, for stresses below σ_s , was actually used to identify the instantaneous modulus of elasticity E_0 of the adhesive joint. In this first step in the parameter set definition, σ_s was not already defined. Therefore, σ_s was defined in a first approximation with a low value: $\sigma_s = 15MPa$. The monotonic loading part of the creep tests can also be used for this identification.

d. Definition of the visco-elastic parameters

Classically, the visco-elasticity is defined by a characteristic time τ_i defining the saturation of the deformation vs. time and is equal to $\frac{\eta_i}{E_i}$. The influence of the viscosity on the mechanical behavior can be described in terms of loading rate effect and time effect for example in creep tests. The difference between these two effects is made by the characteristic time. The definition of the loading rate effect can be clearly described, under monotonic shear loading from $0.02kN/s$ to $20kN/s$, by a characteristic time lower than 80s, which we consider as short-time. For the short time visco-elastic behavior, the identification of the couple (E_1, η_1) can be made using the monotonic response, under the threshold $\sigma_s = 15MPa$, for different loading rates. For viscous effects with a characteristic time longer than 1000s (considered as long-time), the identification of the couple (E_2, η_2) is made using the cyclic creep/recovery tests for load values lower than the threshold $\sigma_s = 15MPa$. In order to reduce the number of experimental tests used, the identification of both short time and long-time visco-elastic parameters was made on creep/recovery test.

In order to avoid the effects of the plastic flow in the numerical response, the identification of the visco-elastic parameters needed to be performed on creep loading levels implying stress values below the threshold σ_s . Under $4kN$ and $6kN$ creep/recovery loadings, the displacement measured after the recovery part showed a close to zero value. Therefore, the first part of the cyclic creep test was associated to completely reversible mechanisms and apparently no plastic flow occurred. Therefore identification of the visco-elastic parameters was performed on this 6000s part of the test: as $4kN$ and $6kN$ loading levels seems to imply stress values in the adhesive joint below σ_s (Figure III.1-3).

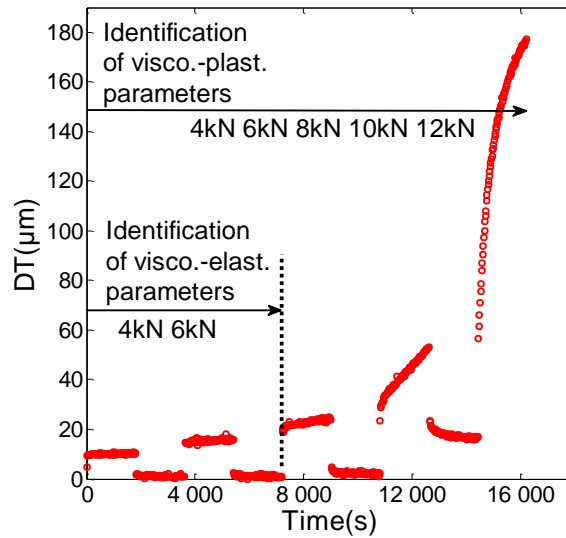


Figure III.1-3: Definition of the experimental data used in the identification strategy: Reversible and irreversible strain parts in a cyclic-creep/recovery test.

Figure III.1-4 shows the numerical/experimental responses under creep conditions. Visco-elastic phenomena are characterized on displacement values with the linear elastic part value removed. The identification was performed in two steps. First, the identification of the characteristic times $\tau_i = E_i/\eta_i$ was made on the $4kN$ creep level. In this step, comparison of the normalized value for the visco-elastic displacements (DT_{VEnorm}) given by the numerical simulations and the experimental response was

performed. In order to distinguish the values of τ_1 and τ_2 , the identification of those parameters was made with constraints: τ_1 was imposed to be lower than 80s and τ_2 bigger than this value. The second part consisted in the identification of the moduli E_1 and E_2 with a comparison of the numerical visco-elastic displacement (DT_{VE}) with the values for 4kN and 6kN creep levels. Results for this identification are shown in Figure III.1-4b.

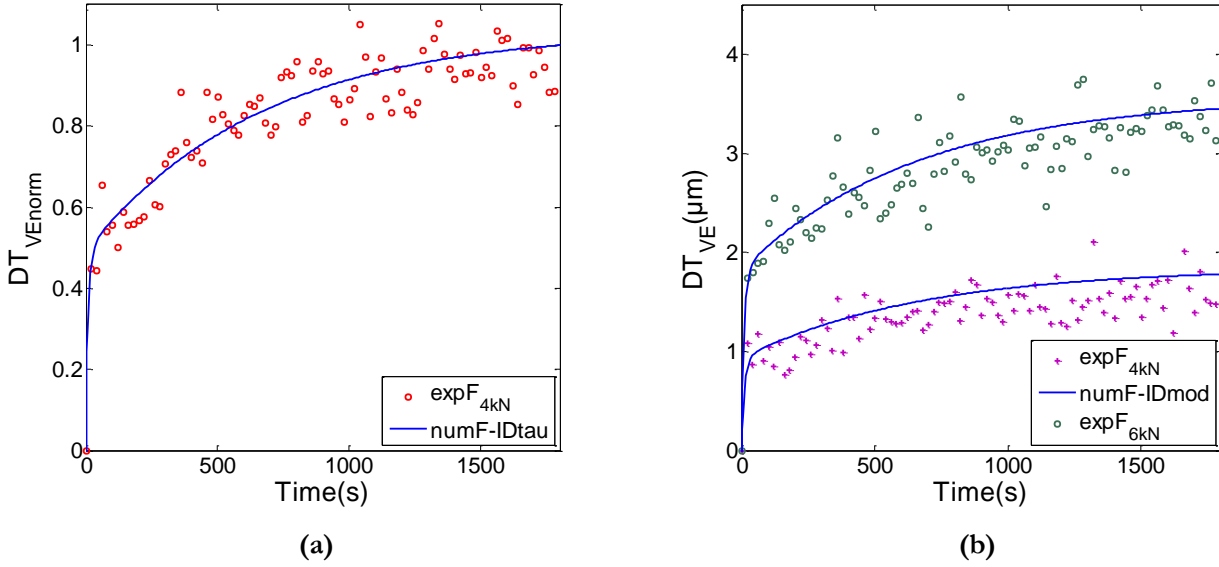


Figure III.1-4: Identification of the visco-elastic behavior. Characteristic time identified on the normalized visco-elastic tangential displacement (DT_{VE}^{norm}) for the 4kN creep level (a) and identification of the visco-elastic moduli on the visco-elastic tangential displacement (DT_{VE}) for the 4kN and 6kN creep levels (b).

e. Definition of the visco-plastic parameters

Finally, the identification of the non-linear visco-plastic parameters was performed. In this last step, a creep test with a load value higher than the threshold σ_s must be chosen. The identification of the visco-plastic parameters was performed not only on a monotonic creep test but rather on a cyclic creep/recovery test, in order to take into account the influence of several loading levels where plasticity occurs (8, 10 and 12kN). The creep/recovery test provides complete and comprehensive information in the way that all mechanisms described by the constitutive model are activated during this test.

In this last step of this identification work, $(E_{vp}, K_{vp}^*, m^*, \sigma_s)$ are determined. The plastic flow identification may be affected by a scattering in the description of the reversible phenomenon. Therefore, even if the visco-elastic parameters seem to be correctly identified, an accurate description of the experimental recovery part is important to avoid an overestimation of the plastic flow. In order to take this scattering into account in the optimization process, the definition of the visco-plastic parameters was performed considering the experimental response to the entire cyclic creep/recovery test (Figure III.1-3).

Figure III.1-5 shows the numerical/experimental responses under cyclic creep/recovery conditions. The creep/recovery of the fourth level (10kN) shows a quite underestimation of the visco-elastic phenomena through a numerical response with less important amplitude. Nevertheless, the model behavior leads to a good overall description of the “cyclic” creep behavior.

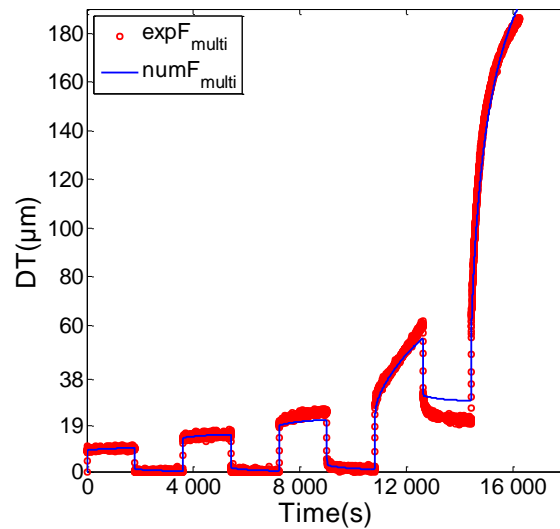


Figure III.1-5: Viscous-Plastic parameters definition on the cyclic-creep/recovery test tangential displacement response.

III.1.3. Stress distribution under creep/recovery conditions

In the identification of the material parameters, FE analyses were conducted in order to evaluate the non-uniform stress distribution along the adhesive joint under creep/recovery conditions. Figure III.1-6 and Figure III.1-7 show numerical results concerning the evolution of the shear stress distribution during the different loading steps of a creep/recovery test ($FT = 10kN$). In this figure, all the stress values are taken from the integration point of the CPE4R adhesive elements. The parameters used in this simulation are those defined by the previous identification. The monotonic loading step leads to an increase of the shear stress in the entire adhesive joint with a concave profile characteristic of the use of beaks (Figure III.1-6).

During the creep step, the stress distribution in b evolves from this concave profile (a) with a maximum stress in the middle of the adhesive joint to a nearly uniform stress field (d) after 5000s, increasing slowly the shear stress value close to the edges (b,c). The unloading part in Figure III.1-7 involves a decrease of the shear stress with a convex shape, leading to negative shear stress values in the center part of the adhesive joint at the end of the step (d). After the unloading part, the 5000s recovery time has almost no influence on this last field stress, as plastic phenomena are not called in this step. The stress distribution numerically observed at the end of the recovery relies on the plastic mechanisms which occurred during the creep step.

Stress distribution in the adhesive layer showed evolutions in its profile under creep/recovery conditions. Therefore, creep/recovery cycles seem to influence the stress state within the adhesive layer of a modified Arcan specimen and a FEM permits to take it into account. This numerical observation can be presented as a justification for the interest of an inverse-identification including FE analysis.

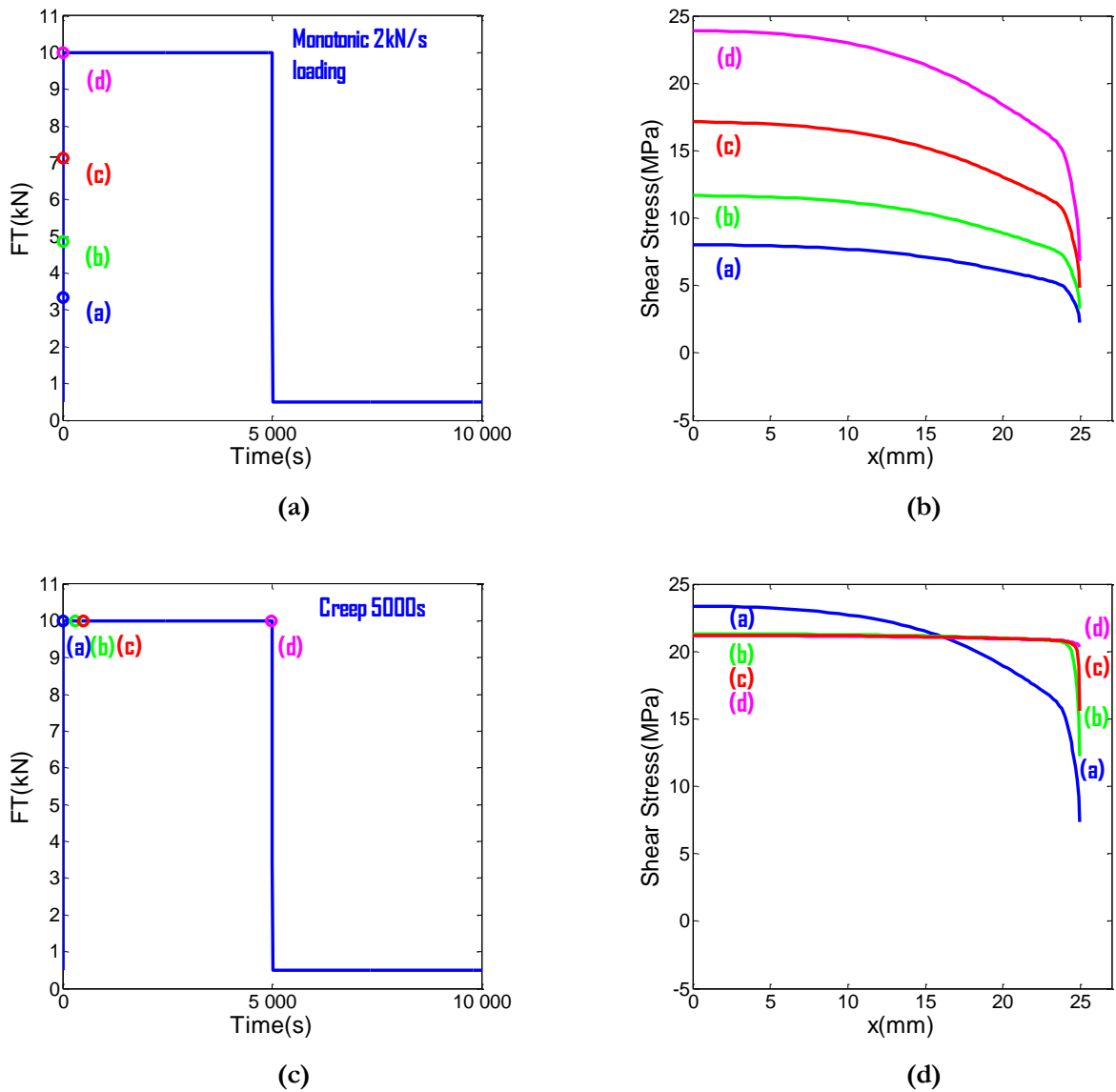


Figure III.1-6: Stress distribution under creep conditions: loading history (a) and stress distribution along the adhesive joint (b).

III.1.4. Numerical and experimental comparison

The set of material constitutive parameters for the viscous mechanical response of the adhesive joint were all identified using a cyclic creep/recovery test. The identification process was divided into several steps considering the reversible mechanical response obtained during the first creep levels separately. Once this identification step was achieved, the entire creep/recovery response was used to identify the plastic behavior. In the following part, with the set of material parameters identified so far, comparison between experimental and numerical response under cyclic and monotonic loadings was carried out. For cyclic loadings, each cycle was computed in the FE analyses.

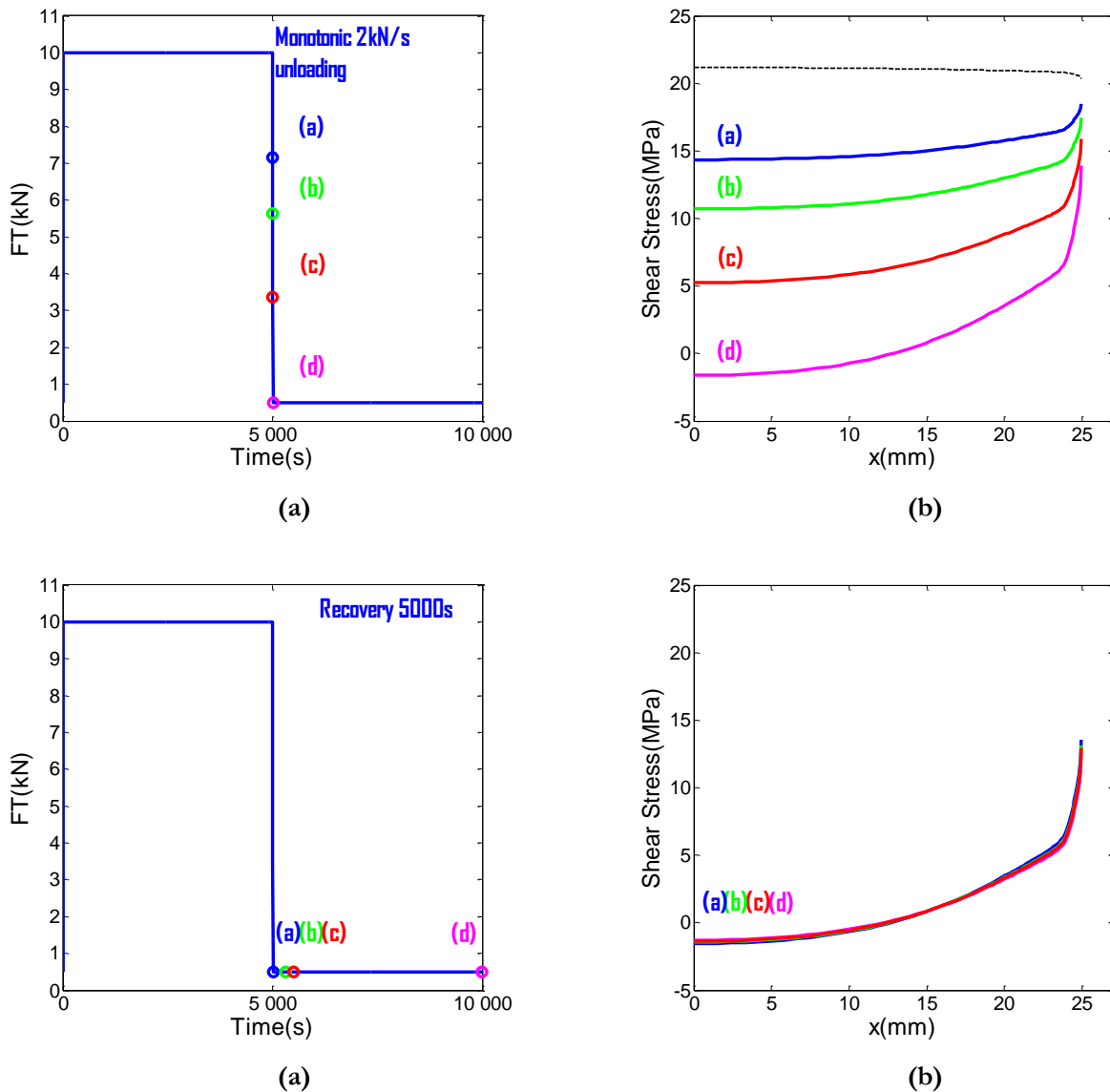


Figure III.1-7: Stress distribution under recovering conditions: loading history (a) and stress distribution along the adhesive joint (b).

a. Cyclic shear loading

Cyclic shear creep/recovery tests with several successive loading levels were the only experimental data chosen in the identification. The experimental response for these tests includes both visco-elastic and visco-plastic parts. It can be assumed that, cyclic creep/recovery may be necessary and enough for the identification work. For comparisons between experimental and numerical responses under shear cyclic loading, presented in Figure III.1-8, the influences of FT_a and FT_m were investigated with the multi-level tests. In these tests and for each level, 150 cycles are performed.

This kind of tests is generally hard to correlate because scattering of each level cumulates. However, they are more comprehensive and more efficient than single level cyclic tests insofar as the influence of the load ratio is observed. For load amplitude FT_a from 1 to 6kN, when the loading increases and plasticity develops, some differences are observed between the numerical and experimental results. Quantitatively, the numerical response overestimates the tangential displacement along cycles for the

three last loading cases. Nevertheless, the simulation qualitatively follows the trend observed experimentally. Concerning the influence of the mean load FT_m , from 2 to 12kN, the comparison involves a lower scatter. The overestimation exists for $FT_m = 10kN$ but the last level ($FT_m = 12kN$) the correlation is much better.

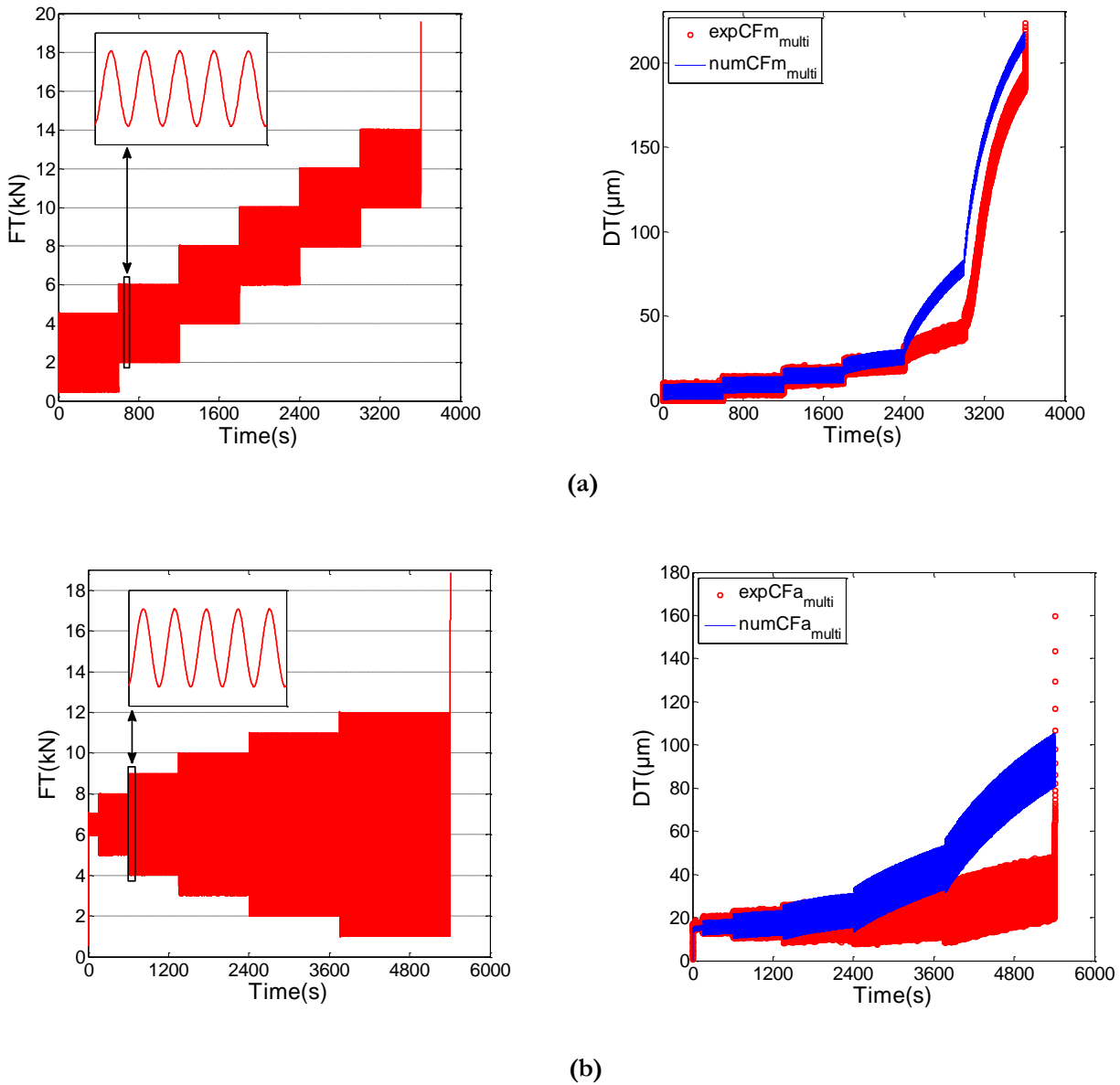


Figure III.1-8: Experimental/numerical comparison of a cyclic test: mean load influence (a) and load amplitude influence (b).

b. Monotonic shear loading

Figure III.1-9 shows comparison between numerical and experimental results under monotonic loadings for three different loading rates. The results show a good correlation in the first part of the curves for loading values under the threshold σ_s . Quantitatively, the measurement and the numerical response are reasonably close in the plastic part for the slowest loading case (0.02kN/s). There is however much more difference in the slopes of the plastic part responses for higher loading rates.

The experimental campaign proposed chapter II was developed in order to investigate every aspects of the viscous behavior of the adhesive: creep/recovery response, loading rate dependency and cyclic behavior. In this section, the inverse identification was developed using Abaqus™ FE analyses of the modified Arcan samples on cyclic creep/recovery tests, with several loading levels.

Results of the optimization were used in another FEA to correlate the loading rate influence on monotonic tests and the cyclic experimental results for multi-level tests, including 150 cycles for each loading. In a general point of view, the numerical response correlates the experimental trend. For cyclic tests, qualitatively it correlates the viscous behavior of the bonded structure, but an overestimation of the cyclic behavior occurs in the investigation of the load amplitude when FT_a becomes higher. However, this first conclusion is performed applying constant loading blocks (150 cycles). In the next chapter, comparisons with fatigue tests with a higher number of cycles were conducted.

However, in a first time, the 1D model developed in this section on the shear mechanical behavior of the adhesive joint will be developed in 3D approach in order to investigate the response under multi-axial loadings.

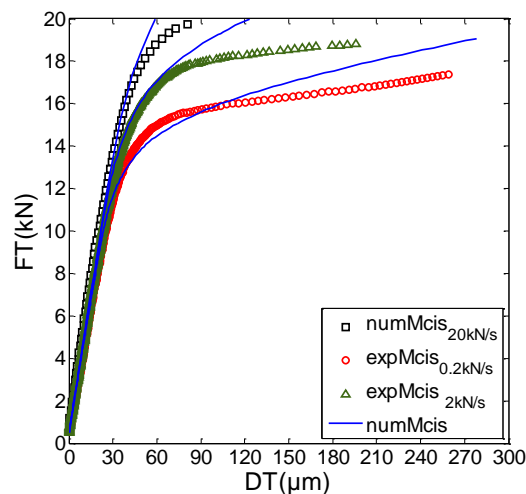


Figure III.1-9 : Experimental/numerical FT vs. DT results under monotonic loading.

III.2. 3D constitutive behavior

The section III.1 permitted to define the necessary elements for the model to describe the viscous behavior of the adhesive for a uni-axial shear test. In this section, we are concerned by the implementation of the model under multi-axial loadings. In regard with the experimental results and considering the previous studies made on the mechanical behavior of structural adhesives, two important aspects will be considered in the implementation:

- The plastic behavior of the structural adhesive is sensitive to the hydrostatic stress component. The model chosen will so include a yield and flow function depending on the hydrostatic stress;
- Non-associated formalism is classically encountered for the structural adhesives model. The possibility to introduce two different functions for the yield surface and the flow rule will be allowed in the implementation.

This section thus presents the 3D implementation of the constitutive viscous equations, the associated identification procedure illustrated with the results obtained in composed traction-shear loading for the SikaForce®7817 L60MR adhesive. Overall results obtained in tension will be showed for the validation.

III.2.1. Constitutive equations

For the 3D definition of the material behavior a strain rate definition is used. In following, the additive strain rate decomposition is assumed:

$$\underline{\dot{\varepsilon}} = \underline{\dot{\varepsilon}}_{el} + \underline{\dot{\varepsilon}}_{v1} + \underline{\dot{\varepsilon}}_{v2} + \underline{\dot{\varepsilon}}_{vp} \quad (\text{Eq 1.44})$$

The Hooke law permits to define the stress state:

$$\underline{\dot{\sigma}} = \underline{C}_e : \underline{\dot{\varepsilon}}_{el} \quad (\text{Eq 1.45})$$

For the visco-elasticity, the stress state is calculated with the following equations:

$$\underline{\dot{\varepsilon}}_{v1} = \frac{1}{\tau_1} (\underline{S}_{v1} : \underline{\sigma} - \underline{\varepsilon}_{v1}) \quad (\text{Eq 1.46})$$

$$\underline{\dot{\varepsilon}}_{v2} = \frac{1}{\tau_2} (\underline{S}_{v2} : \underline{\sigma} - \underline{\varepsilon}_{v2}) \quad (\text{Eq 1.47})$$

where \underline{S}_{v1} and \underline{S}_{v2} are the isotropic compliance tensors for the visco-elasticity and τ_1, τ_2 defines the characteristic creep time for $\underline{\varepsilon}_{v1}$ and $\underline{\varepsilon}_{v2}$.

a. Yield function

As a first approach, the yield surface for the visco-plasticity is based on a linear Drucker-Prager formulation. The yield function is defined with the following equation:

$$f(\sigma, p) = 2J + bI_1 - R_F(p) \quad (\text{Eq 1.48})$$

with,

$$\begin{cases} J = \sqrt{3J_2} \\ J_2 = 1/2 (\underline{S} : \underline{S}) \\ \underline{S} = \underline{\sigma} - (1/3)Tr(\underline{\sigma})\mathbf{Id} \\ I_1 = Tr(\underline{\sigma}) \end{cases}$$

where b is a material constants, J is the equivalent von Mises stress, I_1 is the hydrostatic pressure and the function R_F defines the hardening rule.

b. Hardening and flow rule

For the hardening rule a linear isotropic definition is used, such as the function R_F is written:

$$R_F(p) = R_0 + Qp \quad (\text{Eq 1.49})$$

where R_0 is the initial yield stress and Q a material parameter defining the linear hardening and p is the plastic multiplier. When the yield criterion is reached, the irreversible strain rate defined by $\underline{\dot{\varepsilon}}_{vp}$ occurs and is generated by the following equation:

$$\begin{aligned}\dot{\underline{\epsilon}}_{vp} &= \left\langle \frac{f}{K_{vp}} \right\rangle^m \underline{n} \\ &= \dot{p} \underline{n}\end{aligned}\tag{Eq 1.50}$$

where (K_{vp}, m) are material constants. \underline{n} represents the direction for the visco-plastic flow and depends on the flow function g .

$$\underline{n} = \frac{dg}{d\sigma}\tag{Eq 1.51}$$

$$\text{with, } g(\sigma, p) = J + a_2 I_1^2 - R(p)\tag{Eq 1.52}$$

Thus, the expression of \underline{n} :

$$\underline{n} = 3/2 \frac{S}{J} + 2a_2 I_1 \underline{Id}\tag{Eq 1.53}$$

Therefore, the equations developed in this 3D definition of a visco-elastic visco-plastic model are grounded on 14 material constants:

- The Young modulus E and the Poisson's ratio ν permit to define the linear elastic stiffness $\underline{\underline{C}}_e$;
- (E_1, ν_1) and (E_2, ν_2) are introduced for the compliances $\underline{\underline{S}}_{\nu 1}$ and $\underline{\underline{S}}_{\nu 2}$. Added to τ_1 and τ_2 which are the characteristic creep times, they constitute the necessary parameters to define the visco-elastic behavior;
- Finally, K_{vp}, m, R_0 and Q associated to b and a_2 are the material constants driving the visco-plastic flow and the flow direction.

III.2.2. Computational algorithm

In order to reduce the computation time necessary for the FE analysis performed and to define an efficient computational algorithm, two different implementations of the constitutive equations were performed. Furthermore the convergence of these two implementations to a same numerical response can ensure a certain quality of the implemented algorithms. Therefore, the present chapter presents the following implementations:

- A generic implicit method, presented by Besson et al. (Besson, et al., 2004) in the context of implementation applied to FE code application with the example of local approach to fracture;
- A second one, developed by Simo et al. (Simo, et al., 1998) gives another interesting mean to solve the conventional plasticity and visco-plasticity equations. This method was shown to be efficient on coupled visco-elastic visco-plastic modeling (Miled, et al., 2011).

Both of these methods are implicit iterative procedures developed to obtain the solution over a time increment. For a rate formulation of the constitutive equations, the set of differential equations is performed over a finite time increment $[t_0, t_1]$ with $\Delta t = t_1 - t_0$. All the variables are known at t_0 and the incrementation is then performed to obtain stresses and the state variables at the end of the increment t_1 .

Another quantity is required by FE codes: the consistent tangent matrix $\underline{\underline{L}}$. A good approximation of the consistent tangent matrix evaluated at every Gauss point is used to compute the elementary stiffness matrix.

a. Generic implicit method

A method is called implicit as the unknowns of the problem appear on both hand-sides of the equation of the problem. For any q function, using an implicit iterative procedure, it is assumed that,

$$\begin{aligned}\dot{q} &= \frac{q^{t+\Delta t} - q^t}{\Delta t} \\ &= \frac{\Delta q}{\Delta t}\end{aligned}\tag{Eq 1.54}$$

The constitutive equations of the visco-elastic visco-plastic model form a set of differential equations. The set of constitutive equations of the material behavior is the following:

$$\left\{ \begin{array}{l} \Delta \underline{\underline{\varepsilon}}_{el} = \Delta \underline{\underline{\varepsilon}} - \Delta \underline{\underline{\varepsilon}}_{v1} - \Delta \underline{\underline{\varepsilon}}_{v2} - \Delta \underline{\underline{\varepsilon}}_{vp} \\ \Delta \underline{\underline{\varepsilon}}_{v1} = \frac{\Delta t}{\Delta t + \tau_1} (\underline{\underline{S}}_{v1} : \underline{\underline{\sigma}}^{t+\Delta t} - \underline{\underline{\varepsilon}}_{v1}^t) \\ \Delta \underline{\underline{\varepsilon}}_{v2} = \frac{\Delta t}{\Delta t + \tau_2} (\underline{\underline{S}}_{v2} : \underline{\underline{\sigma}}^{t+\Delta t} - \underline{\underline{\varepsilon}}_{v2}^t) \\ \Delta p = \Delta t \left\langle \frac{f(\underline{\underline{\sigma}}^{t+\Delta t}, p^{t+\Delta t})}{K_{vp}} \right\rangle^m \\ p^{t+\Delta t} = p^t + \Delta p \\ \Delta \underline{\underline{\varepsilon}}_{vp} = \Delta p n^{t+\Delta t} \\ \underline{\underline{\sigma}}^{t+\Delta t} = \underline{\underline{\sigma}}^t + \Delta \underline{\underline{\sigma}} = \underline{\underline{\sigma}}^t + \underline{\underline{C}}_e : \Delta \underline{\underline{\varepsilon}}_{el} \end{array} \right.\tag{Eq 1.55}$$

The material state is described by a set of internal variables which can be represented as a vector $\underline{\underline{A}}$. One of the state variables is assumed to be the elastic strain tensor $\underline{\underline{\varepsilon}}_{el}$ and p is the state variable chosen to represent the irreversible phenomena such as visco-plasticity. Thus the vector $\underline{\underline{A}}$ is defined by:

$$\underline{\underline{A}} = (\underline{\underline{\varepsilon}}_{el}, p)\tag{Eq 1.56}$$

The residual vector $\underline{\underline{R}}$ is defined as

$$\underline{\underline{R}} = (\underline{\underline{R}}_e, R_p)\tag{Eq 1.57}$$

Therefore, the unknowns of the problem (as the components of $\Delta \underline{\underline{A}}$) are $\Delta \underline{\underline{\varepsilon}}_{el}$ and Δp . The system to solve is thus:

$$\left\{ \begin{array}{l} \underline{\underline{R}}_e(\Delta \underline{\underline{\varepsilon}}_{el}, \Delta p) = \Delta \underline{\underline{\varepsilon}}_{el} - \Delta \underline{\underline{\varepsilon}} + \Delta \underline{\underline{\varepsilon}}_{v1} + \Delta \underline{\underline{\varepsilon}}_{v2} + \Delta \underline{\underline{\varepsilon}}_{vp} \\ R_p(\Delta \underline{\underline{\varepsilon}}_{el}, \Delta p) = \Delta p - \Delta t \left\langle \frac{f(\underline{\underline{\sigma}}^{t+\Delta t}, p^{t+\Delta t})}{K_{vp}} \right\rangle^m \end{array} \right.\tag{Eq 1.58}$$

Following a Newton method, the search for the solution of $\underline{\underline{R}} = \begin{pmatrix} 0 \\ 0 \end{pmatrix}$ requires the calculation of the Jacobian matrix $\underline{\underline{J}}$ defined by:

$$\begin{bmatrix} \Delta \underline{\varepsilon}_{el} \\ \Delta p \end{bmatrix}_{i+1} = \begin{bmatrix} \Delta \underline{\varepsilon}_{el} \\ \Delta p \end{bmatrix}_i - \underline{J}^{-1} \begin{bmatrix} \underline{R}_e \\ \underline{R}_p \end{bmatrix}_i \quad (\text{Eq 1.59})$$

with,

$$\underline{J} = \frac{\partial \underline{R}}{\partial \Delta \underline{A}} = \begin{bmatrix} \frac{\partial \underline{R}_e}{\partial \Delta \underline{\varepsilon}_{el}} & \frac{\partial \underline{R}_e}{\partial \Delta p} \\ \frac{\partial \underline{R}_p}{\partial \Delta \underline{\varepsilon}_{el}} & \frac{\partial \underline{R}_p}{\partial \Delta p} \end{bmatrix}_i$$

The components of the Jacobian matrix are:

$$\frac{\partial \underline{R}_e}{\partial \Delta \underline{\varepsilon}_{el}} = \underline{\underline{Id}} + \Delta p \underline{\underline{C}}_e \cdot \left(\frac{3\underline{\underline{P}}J_2 - 3/2 \underline{\underline{S}} \otimes \underline{\underline{S}}}{2J_2 J} + 2a_2 \underline{\underline{Id}} \otimes \underline{\underline{Id}} \right) + \frac{\Delta t}{\Delta t + \tau_1} \underline{\underline{S}}_{v1} \cdot \underline{\underline{C}}_e + \frac{\Delta t}{\Delta t + \tau_2} \underline{\underline{S}}_{v2} \cdot \underline{\underline{C}}_e \quad (\text{Eq 1.60})$$

$$\frac{\partial \underline{R}_e}{\partial \Delta p} = \underline{\underline{n}} \quad (\text{Eq 1.61})$$

$$\frac{\partial \underline{R}_p}{\partial \Delta \underline{\varepsilon}_{el}} = -\frac{m\Delta t}{K_{vp}} \left\langle \frac{f}{K_{vp}} \right\rangle^{m-1} \underline{\underline{C}}_e : \left(\frac{3\underline{\underline{S}}}{J} + b \underline{\underline{Id}} \right) \quad (\text{Eq 1.62})$$

$$\frac{\partial \underline{R}_p}{\partial \Delta p} = 1 + \frac{mQ\Delta t}{K_{vp}} \left\langle \frac{f}{K_{vp}} \right\rangle^{m-1} \quad (\text{Eq 1.63})$$

An advantage of the method is to allow the direct computation of the consistent tangent matrix \underline{L} . After the convergence of the Newton iterations (Eq 1.21) one gets: $\underline{R} \approx \begin{pmatrix} 0 \\ 0 \end{pmatrix}$. The residual vector \underline{R} can be written as:

$$\underline{R} = \underline{R}^* - \begin{pmatrix} \Delta \underline{\varepsilon} \\ 0 \end{pmatrix} \quad (\text{Eq 1.64})$$

with,

$$\underline{R}^* = \begin{pmatrix} \Delta \underline{\varepsilon}_{el} - \Delta \underline{\varepsilon} + \Delta \underline{\varepsilon}_{v1} + \Delta \underline{\varepsilon}_{v2} + \Delta \underline{\varepsilon}_{vp} \\ \underline{R}_p \end{pmatrix}$$

Assuming then an infinitesimal perturbation of $\Delta \underline{\varepsilon}$ causes an infinitesimal perturbation of the state variables vector \underline{A} :

$$\begin{aligned} \delta \underline{R} &= \delta \underline{R}^* - \begin{pmatrix} \delta \Delta \underline{\varepsilon} \\ 0 \end{pmatrix} \\ &= \underline{J} \cdot \delta \Delta \underline{A} - \begin{pmatrix} \delta \Delta \underline{\varepsilon} \\ 0 \end{pmatrix} = 0 \end{aligned} \quad (\text{Eq 1.65})$$

And the perturbation of the state variable can be obtained as:

$$\delta \Delta \underline{A} = \underline{\underline{J}}^{-1} \begin{pmatrix} \delta \Delta \underline{\varepsilon} \\ 0 \end{pmatrix} \quad (\text{Eq 1.66})$$

with,

$$\underline{J}^{-1} = \underline{J}^* = \begin{bmatrix} \underline{\underline{J}}_{ee}^* & \underline{\underline{J}}_{ea}^* \\ \underline{\underline{J}}_{ae}^* & \underline{\underline{J}}_{aa}^* \end{bmatrix}$$

As the inverse of the Jacobian can be expressed as a block matrix, we can write the relation,

$$\delta\Delta\underline{\varepsilon}_{el} = \underline{\underline{J}}_{ee}^* : \delta\Delta\underline{\varepsilon} \quad (\text{Eq 1.67})$$

using the Hooke's law,

$$\delta\Delta\underline{\sigma} = \underline{\underline{C}}_e : \delta\Delta\underline{\varepsilon}_{el} \quad (\text{Eq 1.68})$$

the consistent tangent matrix can finally be computed:

$$\underline{\underline{L}} = \frac{\partial\Delta\underline{\varepsilon}}{\partial\Delta\underline{\sigma}} = \underline{\underline{C}}_e : \underline{\underline{J}}_{ee}^* \quad (\text{Eq 1.69})$$

The implicit method for the integration of the constitutive equations is based on the Newton algorithm which leads to an approximate solution.

b. Return-mapping algorithm for a visco-plastic correction

The return mapping algorithm is one of the most popular mean for the implementation of plasticity constitutive equations (Simo, et al., 1998) (Brannon, 2002). For this algorithm, the first step is to tentatively assume elastic behavior for a given time step:

$$\begin{aligned} \Delta\underline{\varepsilon}_{el}^{trial} &= \Delta\underline{\varepsilon} - \Delta\underline{\varepsilon}_{v1} + \Delta\underline{\varepsilon}_{v2} \\ &= \Delta\underline{\varepsilon} - \frac{\Delta t}{\Delta t + \tau_1} \left(\underline{\underline{S}}_{v1} : \underline{\underline{\sigma}}^t + \underline{\underline{S}}_{v1} \cdot \underline{\underline{C}}_e : \underline{\varepsilon}_{el}^{trial} - \underline{\varepsilon}_{v1}^t \right) \\ &\quad - \frac{\Delta t}{\Delta t + \tau_2} \left(\underline{\underline{S}}_{v2} : \underline{\underline{\sigma}}^t + \underline{\underline{S}}_{v2} \cdot \underline{\underline{C}}_e : \underline{\varepsilon}_{el}^{trial} - \underline{\varepsilon}_{v2}^t \right) \\ &= \underline{\underline{M}}^{-1} \left(\Delta\underline{\varepsilon} - \frac{\Delta t}{\Delta t + \tau_1} \left(\underline{\underline{S}}_{v1} : \underline{\underline{\sigma}}^t + -\underline{\varepsilon}_{v1}^t \right) - \frac{\Delta t}{\Delta t + \tau_2} \left(\underline{\underline{S}}_{v2} : \underline{\underline{\sigma}}^t - \underline{\varepsilon}_{v2}^t \right) \right) \end{aligned} \quad (\text{Eq 1.70})$$

with,

$$\underline{\underline{M}} = \underline{\underline{Id}} - \frac{\Delta t}{\Delta t + \tau_1} \underline{\underline{S}}_{v1} \cdot \underline{\underline{C}}_e - \frac{\Delta t}{\Delta t + \tau_2} \underline{\underline{S}}_{v2} \cdot \underline{\underline{C}}_e$$

the result is a “*trial*” value of the unknown $\Delta\underline{\varepsilon}_{el}$. Using the Hooke's law, a “*trial*” stress, $\underline{\underline{\sigma}}^{trial}$ can thus be defined:

$$\underline{\underline{\sigma}}^{trial} = \underline{\underline{\sigma}}^t + \underline{\underline{C}}_e : \Delta\underline{\varepsilon}_{el}^{trial} \quad (\text{Eq 1.71})$$

If the yield criterion for $\underline{\underline{\sigma}}^{trial}$ and p^t is respected:

$$f(\underline{\underline{\sigma}}^{trial} + p^t) \leq 0 \quad (\text{Eq 1.72})$$

Consequently, we can assume that,

$$\begin{cases} \Delta \underline{\varepsilon}_{el} = \Delta \underline{\varepsilon}_{el}^{trial} \\ \underline{\sigma}^{t+\Delta t} = \underline{\sigma}^{trial} \end{cases} \quad (\text{Eq 1.73})$$

and we are thus able to express the consistent tangent matrix for the reversible strains:

$$\underline{\underline{L}}_{rev} = \frac{\partial \Delta \underline{\varepsilon}}{\partial \Delta \underline{\sigma}} = \underline{\underline{C}}_e \cdot \underline{\underline{M}}^{-1} \quad (\text{Eq 1.74})$$

In the case of the trial stress $\underline{\sigma}^{trial}$ violates the yield criterion, the tentative assumption of elastic and visco-elastic strain is rejected and it is necessary to define the plastic correction. Even, when it is found to violate the yield criterion, the trial stress is nevertheless useful because it can then be projected back to the plastic yield surface to give the updated stress $\underline{\sigma}^{t+\Delta t}$:

$$\underline{\sigma}^{t+\Delta t} = \underline{\sigma}^{trial} - \underline{\underline{C}}_e \underline{\underline{M}}^{-1} : \Delta \underline{\varepsilon}_{vp} = \underline{\sigma}^{trial} - \Delta p \underline{\underline{C}}_e \underline{\underline{M}}^{-1} : \underline{n} \quad (\text{Eq 1.75})$$

The tangent matrix is decomposed as it:

$$\underline{\underline{C}}_e \underline{\underline{M}}^{-1} = 2\mu_{rev} \underline{\underline{Id}} + \lambda_{rev} \underline{\underline{Id}} \otimes \underline{\underline{Id}} \quad (\text{Eq 1.76})$$

So that, the relation in (Eq 1.37) is expressed in a deviatoric and a spherical part:

$$\begin{cases} \underline{\underline{S}}^{t+\Delta t} = \underline{\underline{S}}^{trial} - \Delta p \frac{2\mu_{rev}}{2} \frac{3 \underline{\underline{S}}^{t+\Delta t}}{j^{t+\Delta t}} \\ I_1^{t+\Delta t} = P_h^{t+\Delta t} = P_h^{trial} - 3(3\lambda_{rev} + 2\mu_{rev}) \Delta p (2a_2 P_h^{t+\Delta t}) \end{cases} \quad (\text{Eq 1.77})$$

It can be noticed in the first relation in (Eq 1.39) that $\underline{\underline{S}}^{t+\Delta t}$ and $\underline{\underline{S}}^{trial}$ are proportional. We can thus assume the following relation:

$$\frac{\underline{\underline{S}}^{t+\Delta t}}{j^{t+\Delta t}} = \frac{\underline{\underline{S}}^{trial}}{j^{trial}} \quad (\text{Eq 1.78})$$

And (Eq 1.39) can be developed as

$$\begin{cases} \underline{\underline{S}}^{t+\Delta t} = \underline{\underline{S}}^{trial} \left(1 - \mu_{rev} \frac{3\Delta p}{j^{trial}} \right) \\ P_h^{t+\Delta t} = \frac{P_h^{trial}}{1 + (18\lambda_{rev} + 12\mu_{rev}) \Delta p a_2} \end{cases}$$

The determination of $\underline{\sigma}^{t+\Delta t}$ is now linked to the unknown Δp . So, the actualization of the stress depends on the resolution of the following scalar equation:

$$R_p(\Delta p) = \Delta p - \Delta t \left(\frac{f(\underline{\sigma}^{t+\Delta t}, p^{t+\Delta t})}{K_{vp}} \right)^m = 0 \quad (\text{Eq 1.79})$$

Using the Newton resolution:

$$\Delta p_{i+1} = \Delta p_i - \frac{R_p}{R_p'} \Big|_i \quad (\text{Eq 1.80})$$

So the calculation of R_p' is performed:

$$R'_p = 1 - \frac{m\Delta t}{K_{vp}} \left(\frac{f}{K_{vp}} \right)^{m-1} \left(\left[\frac{3\underline{S}^{trial}}{J^{trial}} + b\underline{\mathbf{Id}} \right] : \left[- \left(3\mu_{rev} \frac{\underline{S}^{trial}}{J^{trial}} + \frac{1}{3} \frac{\partial P_h^{t+\Delta t}}{\partial \Delta p} \underline{\mathbf{Id}} \right) \right] - Q \right)$$

with,

$$\frac{\partial P_h^{t+\Delta t}}{\partial \Delta p} = \frac{P_h^{trial} (18\lambda_{rev} + 12\mu_{rev}) a_2}{(1 + (18\lambda_{rev} + 12\mu_{rev}) \Delta p a_2)^2}$$

With the return mapping algorithms, the visco-plastic correction is performed with the resolution of a single scalar equation, contrary to the generic implicit method in which the Newton resolution leads to the definition of a residual vector. For this second implicit method, assuming the convergence of (Eq 1.41) the tangent matrix defined in (Eq 1.31) is conserved, as the calculation was already done.

In order to evaluate the efficiency of the implementation methods developed, simulations were performed on a single element for a tensile-shear cyclic creep loading. Displacement of the loading node is shown in Figure III.2-1. The methods developed gave a similar response for the implemented equations. These results enabled, without worrying of the numerical integration problem, the use of the return-mapping implementation which implied lower computational times.

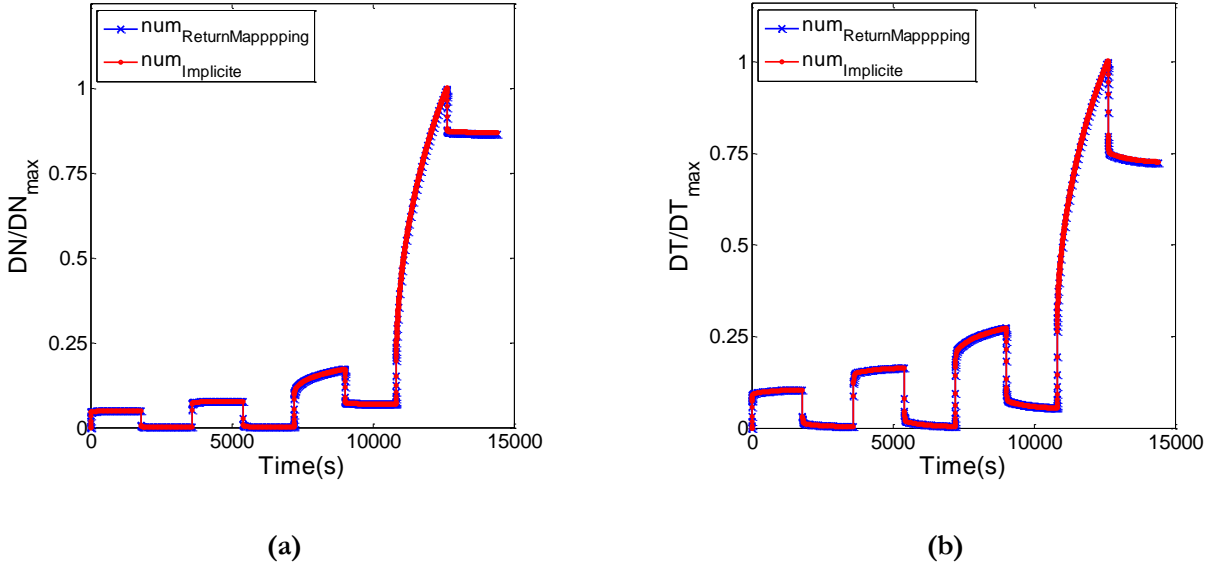


Figure III.2-1 : Response of the two numerical implementations for one element under creep/recovery traction-shear loading ($\gamma = 45^\circ$): tangential displacement (a) and normal displacement (b).

III.2.3. Inverse identification

As described in section III.1, the choice of a step-by-step identification is necessary in order to reduce the computational time for the convergence to the solution. The partition of the material constants to identify for each step is the following:

- Step 1, concerns the identification of the elastic behavior: the parameters of the $\underline{\underline{C}}_e$ tensor are defined using a linear FE analysis of the monotonic shear behavior (Arcan modified tests with $\gamma = 90^\circ$) and in tensile behavior ($\gamma = 0^\circ$);

- Step 2, concerns the identification of the visco-elastic behavior: the same method as the one described in section III.1 is used. Two optimization loops are used on the shear creep results for the $4kN$ and $6kN$ load levels. The first optimization is run to define the characteristic creep times (τ_1 and τ_2) on the normalized value of the equivalent visco-elastic displacement ($DT_{VE_{norm}}$). Then the second optimization is made on the visco-elastic displacement measured (DT_{VE}) for these two loading levels in order to determine $\underline{\underline{S}}_{v1} = \underline{\underline{C}}_{v1}^{-1}$ and $\underline{\underline{S}}_{v2} = \underline{\underline{C}}_{v2}^{-1}$. Concerning the reversible strains ($\underline{\underline{\epsilon}}_{rev} = \underline{\underline{\epsilon}}_{el} + \underline{\underline{\epsilon}}_{v1} + \underline{\underline{\epsilon}}_{v2}$) an assumption of isotropic behavior is made. In this study, the Poisson's ratios for the elastic strain ($\underline{\underline{\epsilon}}_{el}$) and visco-elastic strains ($\underline{\underline{\epsilon}}_{v1}$ and $\underline{\underline{\epsilon}}_{v2}$) are considered to be the same. Hence no results under tension are needed to complete this step;
- Step 3, concerns the identification of the visco-plastic behavior in the shear direction. With the experimental response under shear cyclic creep, the following material constants are defined: the initial yield function stress R_0 , the hardening parameter Q and the parameter of the plastic flow intensity K_{vp} and m . As the modified Arcan test with the $\gamma = 90^\circ$ configuration gives a quasi pure shear stress state the other parameters of the yield function will not have an important influence. Indeed, FE analysis shows that the hydrostatic stress component is negligible within the bonded layer in a shear configuration. Considering the definition of the flow function defined previously, this leads to a behavior independent of b and a_2 ;
- Step 4, concerns the identification of the hydrostatic stress influence. Therefore, experimental results with ratios including tension ($\gamma = 0^\circ$ or $\gamma = 45^\circ$) are needed. The remaining yield function parameter b and flow rule parameter a_2 are determined using an inverse identification based on the cyclic creep/recovery test under tensile-shear loading ($\gamma = 45^\circ$).

A list of the material constants, associated to the test proposed for their identification is given at the end of this section in Table III.2-1.

a. *Finite Element Analysis*

The results presented in section III.1 permitted to evaluate abilities of the visco-elastic visco-plastic equations with a 1D model of the modified Arcan test. With the 3D model developed, a FE analysis including all the particular geometric specificities of the modified Arcan test can now be used for the identification of the material parameters. However, taking the width of the specimen into account will lead to a multiplication of the elements within the model and inescapably a growth in the computational time. Therefore, the convergence of the numerical tangential and normal responses ($\gamma = 45^\circ$) was investigated for two FE models:

- A first 3D model of the Arcan specimen includes the particular shape of the corners and the geometrical widthwise specificities and a meshing refinement was performed in the concerned areas. Nevertheless, the symmetries in the model permitted to divide by two the number of elements;
- A second 3D model was created with a single element in the width (following the \vec{y} direction) assuming the assumption of a low influence of the geometry widthwise.

For a given set of material constants, the simulations were performed using linear brick elements with reduced integration (C3D8R). The loading was applied to driving points cinematically coupled to the

upper surfaces of the substrates and the loading value was adapted to the bonded surface represented on each model. As shown in Figure III.2-2, the numerical response of a monotonic loading gave similar results for these two models. Therefore, in order to reduce the computational time, the 3D model of the modified Arcan bonded specimen with a unique element in the width will be adopted for the rest of this study.

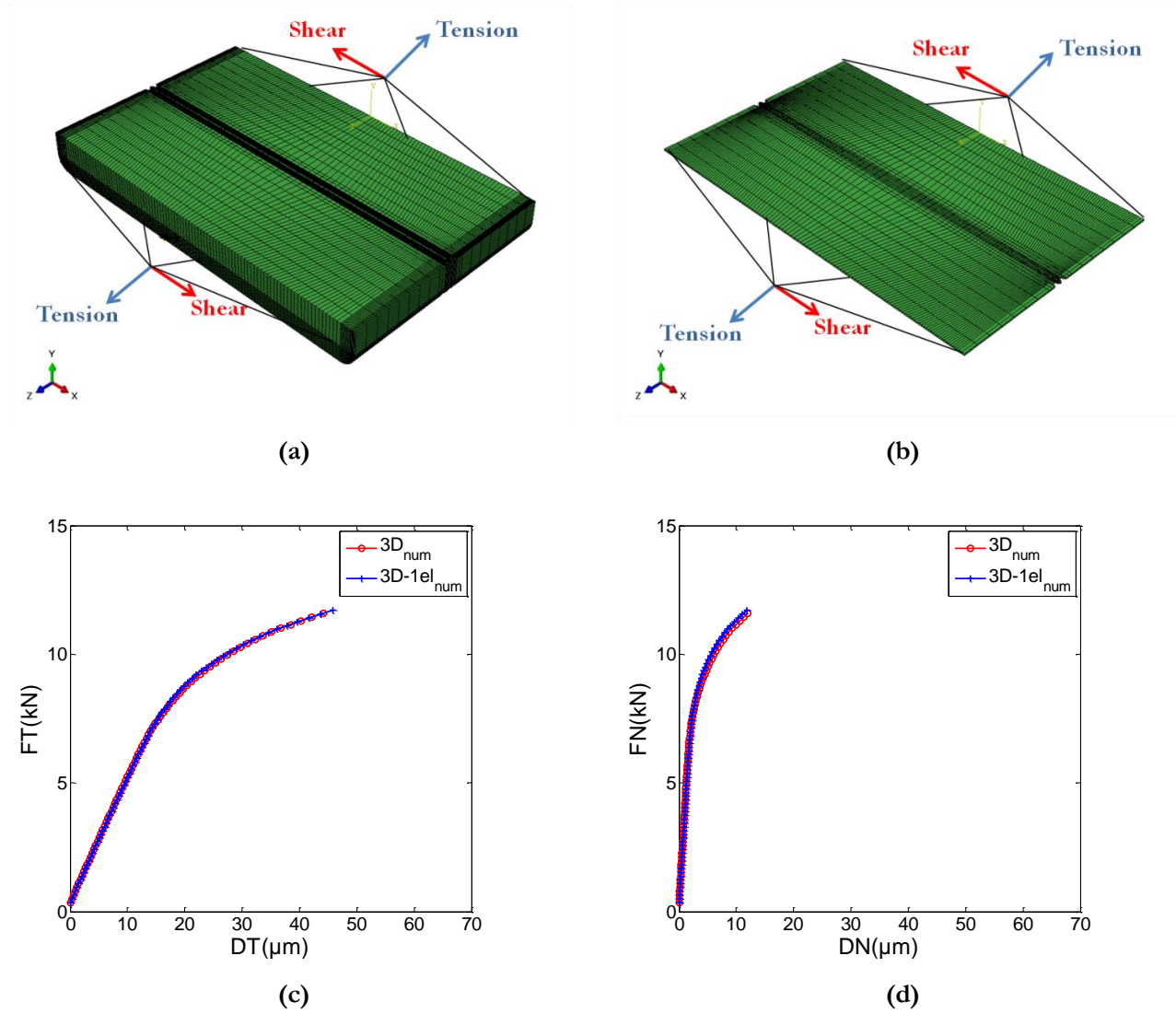


Figure III.2-2 : Comparison between the numerical response of a 3D complete model (a) and a model with a single element in the width (b): monotonic tangential (c) and normal (d) response to a modified Arcan test ($\gamma = 45^\circ$).

b. Step 1, Step 2 and Step 3: from the shear behavior

Concerning the elastic and visco-elastic behavior, the 2D numerical simulations under shear loading have shown good results for the definition of the stiffness (E_0, E_1 and E_2) and the visco-elastic characteristic creep times (τ_1 and τ_2). For visco-elasticity an isotropic behavior is assumed and the assumption of an equivalent Poisson's ratio for elasticity and visco-elasticity is made: $\nu = \nu_1 = \nu_2$.

Concerning visco-plasticity, due to a negligible hydrostatic stress component for the modified Arcan under shear loading ($\gamma = 90^\circ$), the parameters identified with the 2D FE analysis ($K_{vp}^*, m^*, \sigma_s, E_{vp}$) can thus be adapted to define the hardening and flow parameters (K_{vp}, m, R_0, Q) of the 3D

constitutive equations. Indeed the (a_2, b) yield and flow parameters do not influence the shear behavior. Therefore, the parameters resulting from the step 2 (identification of the visco-elastic parameters) and step 3 (identification of the visco-plastic parameters) in our identification strategy were here defined regarding the results presented in section III.1.

c. Identification of parameters (a_2, b)

Until this point, only results in the shear direction were used to define the mechanical behavior. Since the influence of the hydrostatic pressure is considered in our implementation, and given the fact that Arcan pure shear leads to a negligible hydrostatic stress component, identification on experimental data under tensile loading component is necessary. However, the experimental response of SikaForce®7817 L60MR adhesive under tensile loading ($\gamma = 0^\circ$) does not show important non-linear strains. The identification of the remaining parameters was thus made on the tensile-shear behavior ($\gamma = 45^\circ$). The response in both shear and normal direction is regarded. The more important displacement values registered permit to avoid the effect of acquisition noise and the scattering in the experimental results. The results of this identification step are shown in Figure III.2-3.

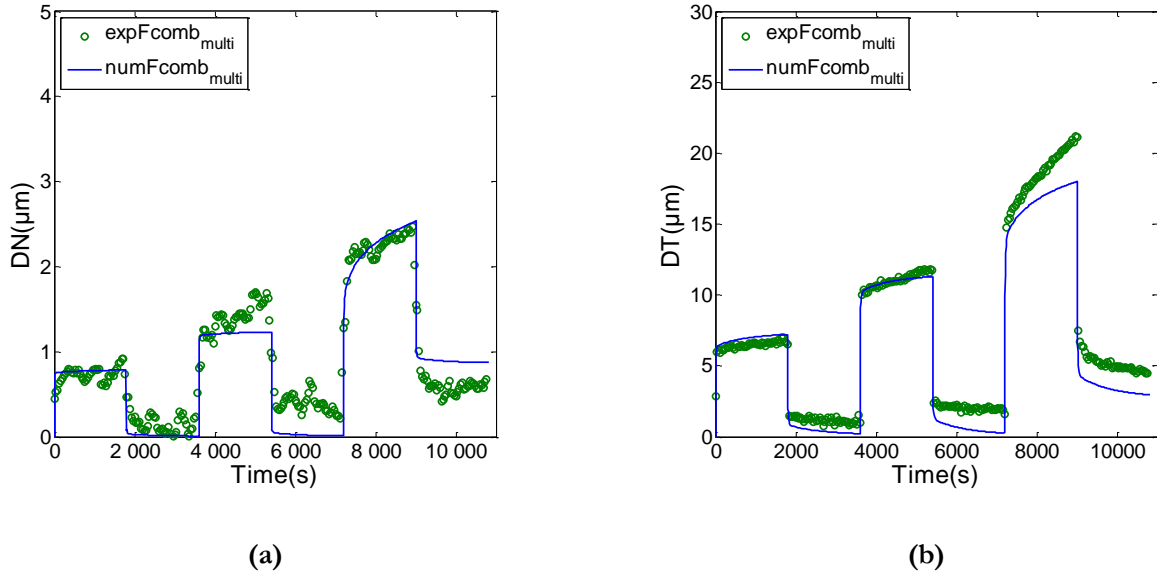


Figure III.2-3 : Identification of the parameters a_2 and b on a cyclic creep tensile-shear test ($\gamma = 45^\circ$): normal (a) and tangential displacement (b).

Furthermore, an identification of these parameters only on the normal behavior $\gamma = 0^\circ$ could lead to a confusion on the flow direction driven by a_2 and on the visco-plastic intensity influenced by the yield function parameter b . Therefore, the identification of the flow rule, performed under composed tensile-shear loading, permits to consider the value of a_2 and b regarding both tangential and normal behavior. For this optimization step, the cost function h (Eq 1.5) is defined as the sum of the discrepancies in normal and tangential directions:

$$h = (DT_{num}(i) - DT_{exp}(i))^2 + (DN_{num}(i) - DN_{exp}(i))^2 \quad (\text{Eq 1.82})$$

d. Numerical and experimental comparison

At the end of the identification strategy, “optimal” parameters are obtained for the SikaForce®7817 L60MR. The list of the identified parameters and their associated values are given in Table III.2-1. The results showed in Figure III.2-3 and Figure III.2-4 show the abilities of the constitutive visco-elastic visco-plastic equations with a non-associated and hydrostatic stress dependent model on cyclic creep tests. The numerical response for loading and unloading with the parameters identified provides interesting results for shear, tensile-shear and tensile loadings.

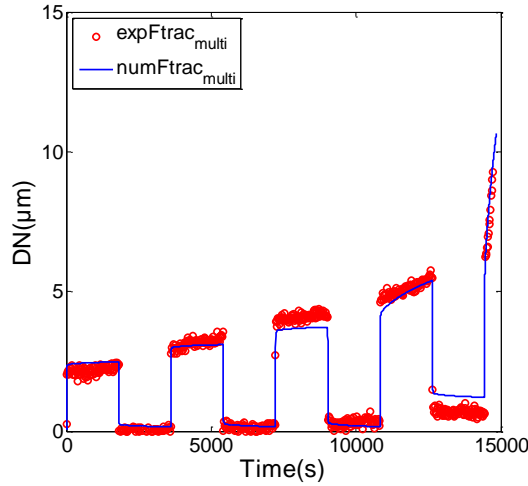


Figure III.2-4 : Cyclic creep tensile test ($\gamma = 0^\circ$): normal displacement.

The interest of the model definition proposed (non-associated formalism, taking into account the hydrostatic stress influence) is justified in Figure III.2-5 regarding the response to the ($\gamma = 45^\circ$). The definition of a new parameter set considering $a_2 = b = 0$ permits to neglect the effect of the hydrostatic stress. If the hydrostatic pressure effect is neglected, the visco-plasticity is considerably underestimated since the loading levels did not validate the von Mises yield criterion.

Associated formalism permits to use only the yield function in the flow definition. The response of an associated formalism is thus investigated by removing the g function in the model definition and replacing it by the yield function f in (Eq 1.12):

$$\dot{\underline{\epsilon}}_{vp} = \dot{p} \frac{df}{d\sigma} \quad (\text{Eq 1.83})$$

A comparison between an associated and non-associated formalism is thus possible. Concerning the plotted results (Figure III.2-5), parameters were not modified from the identification performed with the non-associated formalism. With this parameter set, the numerical response of an associated formalism clearly overestimates the plastic behavior in the tangential direction. On the contrary, the plastic flow in the normal direction was close to zero. Therefore, the uses of a non-associate formalism with the definition of a different flow function permit to reduce the discrepancy observed in the plastic flow in both normal and tangential directions.

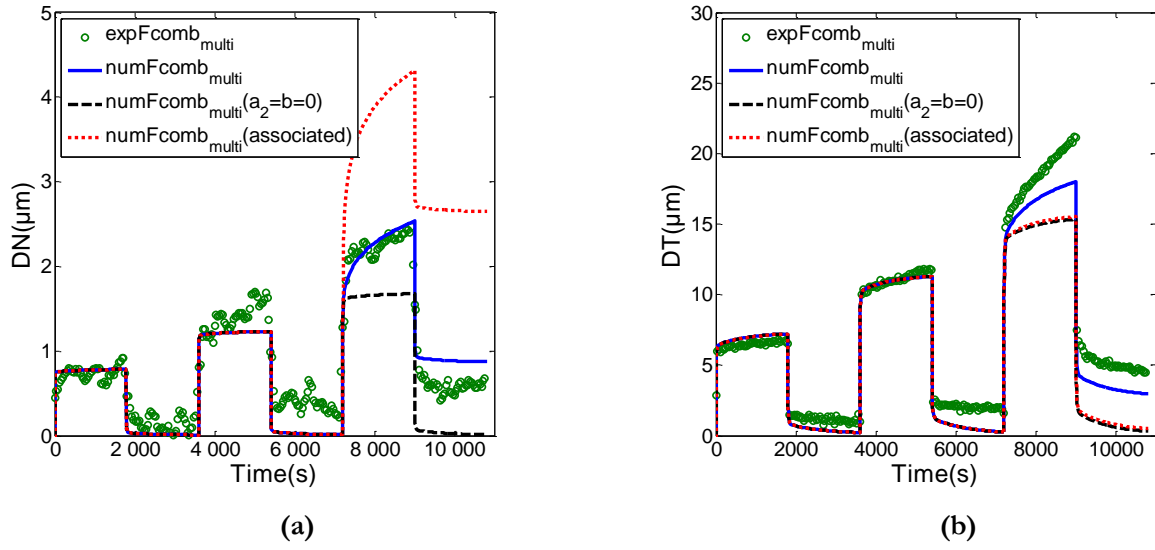


Figure III.2-5 : Interest of a non-associated formalism with influence of the hydrostatic stress: normal response (a) and tangential response (b) to a cyclic creep tensile-shear test ($\gamma = 45^\circ$).

Since all the identification process has been made with creep/recovery experimental data it is interesting to have a view on the model response to monotonic loadings. For a 2kN/s loading rate, under tensile-shear loading ($\gamma = 45^\circ$), the numerical response presented in Figure III.2-6a and Figure III.2-6b, shows satisfactory results in both tangential and normal direction. Furthermore, the slight plastic flow in tensile test is well described with the parameters identified (Figure III.2-6c).

Mechanical feature	Model parameter symbol		Unit	Value	Test for identification
Elasticity	Elastic Young Modulus	E_0	MPa	$1.17 \cdot 10^3$	Tensile and shear monotonic tests
	Poisson's ratio	ν	-	0.47	
Visco-elasticity	Viscous Elastic shear moduli	E_1	MPa	$2.16 \cdot 10^3$	Shear cyclic creep test
		E_2		$3.99 \cdot 10^3$	
	Poisson's ratios	ν_1	-	0.47	
		ν_2		0.47	
Characteristic creep time	τ_1	s	$1.34 \cdot 10^1$		
	τ_2		$8.08 \cdot 10^2$		
Visco-plasticity	Hardening parameter	Q	MPa	$3.10 \cdot 10^1$	Tensile-shear cyclic-creep test
	Plastic threshold	R_0		$5.60 \cdot 10^1$	
	Viscous parameter	K_{vp}	MPa.s	$1.17 \cdot 10^2$	
	Exponent	m	-	5	
	Flow function parameter	b	-	$7.40 \cdot 10^{-1}$	
	Flow direction	a_2		$2.25 \cdot 10^{-3}$	

Table III.2-1 : Material parameters involved in the constitutive model and numerical values calibrated with the identification strategy proposed.

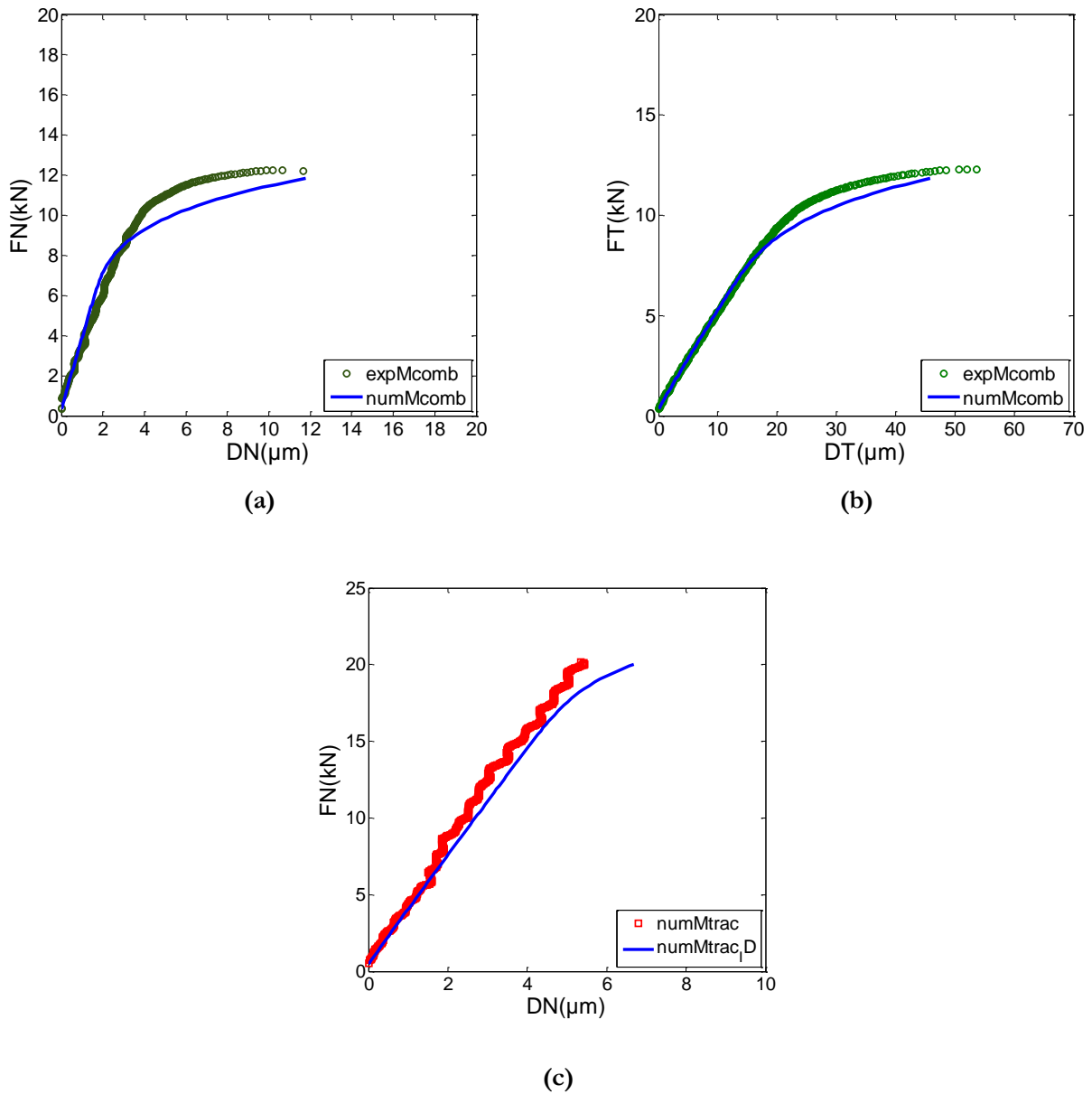


Figure III.2-6 : Numerical response under monotonic loadings for: tensile-shear test ($\gamma = 45^\circ$) (a) and (b) and tensile test ($\gamma = 0^\circ$) (c).

III.3. Conclusion

In a first step, using a visco-elastic visco-plastic definition, the mechanical behavior of a bonded structure with low edge effects was modeled for shear loadings. In this direction, the 1D model developed is able to describe the response of a modified Arcan specimen for creep test, monotonic test with different loading rate and cyclic tests. Then, a non-associated formalism with dependence on the hydrostatic stress component was proposed in order to define the 3D mechanical behavior of this same specimen. The numerical implementation of the constitutive model for FE applications was proposed following two different methods.

The constitutive numerical equations of the visco-elastic visco-plastic model proposed exhibited 14 material constants. Assumptions made on the visco-elastic Poisson's ratios ($\nu = \nu_1 = \nu_2$) permitted to reduce this number to 12. In order to limit the number of parameters to be defined in a same optimization process, a sequential inverse approach for the identification was developed and applied. The abilities of the model to describe shear, tensile and tensile-shear behavior with the identification process proposed were presented in this chapter. However, the uniqueness of the "optimized" solution for the parameter set remains open to discussion. Indeed, the numerical response for the mechanical behavior could be obtained using different parameters. Furthermore, the solution may depend on the optimization algorithm used.

The mechanical behavior modeled can be used to describe the evolution of the cumulative strain of the adhesive joint under cyclic loading will be used to investigate for fatigue life prediction of adhesively bonded structures. A comparison between the numerical predictions and the cyclic experimental results were done to conclude on the validity of the approach proposed and results are presented in Chapter V.

Chapter IV:

Cyclic behavior of a bonded specimen with low edge effects

Introduction:

The approach proposed for cyclic behavior of bonded joints was based on the observations made by Thevenet et al. (Thevenet, et al., 2013) on the modified Arcan experimental results for an epoxy based structural adhesive. In this study, performed on specimen with low edge effects, the mechanical response in terms of deformations was recorded and signs of creep-fatigue coupling were exhibited. These results revealed an important role played by the viscous phenomena.

In the previous section, a model of the SikaForce®-7817 L60MR was proposed for bonded specimen with the same geometries. This visco-elastic visco-plastic model has been characterized using creep/recovery tests. The aim of this chapter was first to study the abilities of the structural adhesive to bear cyclic loadings and then to investigate the reliability of the numerical response of the cyclic behavior using the constitutive model developed. The following section thus proposes a SikaForce®-7817 L60MR fatigue behavior characterization for adhesive joints with a 0.2mm thickness. In the particular case of shear loading, a failure criterion will be proposed in order to perform a fatigue lifetime prediction.

Contents:

<u>IV.1.</u>	<u>Experimental results under shear loading</u>	97
IV.1.1.	Reproducibility	98
IV.1.2.	Mean load influence.....	98
IV.1.3.	Influence of the load amplitude.....	99
IV.1.4.	Influence of the loading rate	100
IV.1.5.	Joint stiffness	101
IV.1.6.	Failure scenarii.....	102
<u>IV.2.</u>	<u>Numerical prediction</u>	103
IV.2.1.	Failure criterion	103
IV.2.2.	Prediction of the cumulative displacement	106
IV.2.3.	Influence of the mean load on the ratcheting effect.....	107
IV.2.4.	Influence of the load amplitude on the ratcheting effect.....	108
IV.2.5.	Influence of the loading rate on the ratcheting effect	108
IV.2.6.	Fatigue life prediction.....	109
<u>IV.3.</u>	<u>Results under tensile-shear loading</u>	110
IV.3.1.	Reproducibility	110
IV.3.2.	Mean load influence.....	110
IV.3.3.	Load amplitude influence	111
IV.3.4.	Joint stiffness	112
IV.3.5.	Fatigue life.....	112
IV.3.6.	Numerical prediction.....	113
<u>IV.4.</u>	<u>Results under tensile loading</u>	116
IV.4.1.	Ratcheting effect	116
IV.4.2.	Joint stiffness	116
IV.4.3.	Fatigue lifetime	116
<u>IV.5.</u>	<u>Conclusion</u>	118

IV.1. Experimental results under shear loading

The experimental data base for fatigue studies were performed with the modified Arcan device (device described in Chapter II). The method of measurement for the substrates relative displacement was the same, using an optical non-contact extensometer. Looking at the results obtained on the SikaForce®-7817 L60MR structural adhesive and described previously, concerning the anisotropy of the viscoplastic behavior, the bonded joints were loaded following three loading cases: shear ($\gamma = 90^\circ$), tensile-shear ($\gamma = 45^\circ$) and tensile test ($\gamma = 0^\circ$). Tests were performed under load control with a constant loading rate, as described in Figure IV.1-1, and the loading was divided in two parts:

- A static loading step at $2kN/s$ in order to reach the mean load F_m of the cyclic loading;
- A cyclic step generated with a sinusoidal waveform loading with a mean load defined by F_m and a load amplitude defined by F_a . The load frequency f of the cyclic loading was led by a mean loading rate of $2kN/s$. In this campaign, the load frequency was not increased as it is commonly done in laboratory experiments to accelerate the fatigue test programs. Hence, for example, a load amplitude $F_a = 2kN$, will lead to a frequency fixed at 0.25Hz and for a load amplitude $F_a = 5kN$ the frequency will be 0.1Hz. This frequency range is typical of modern wind-turbines speed of revolution.

This testing method was previously developed to analyze the cyclic behavior of a ductile epoxy adhesive (Thevenet, et al., 2013). In this study, the experimental results in the different configurations of the Arcan device, underline that the crack initiation phase can be very long especially in shear. Furthermore, in this direction, the cyclic results led to reproducible cyclic results.

The configuration of the modified Arcan device did not allow transitions from compression loading to tensile loading. Therefore, in this chapter, only load ratios $R = F_{min}/F_{max} > 0$ were applied. The cyclic tests were carried with important maximum load levels, in order to cause “plastic” strains within the adhesive joint. Only the low-cycle fatigue domain was thus investigated, that is to say, for number of cycles to failure under a value of 10^5 cycles.

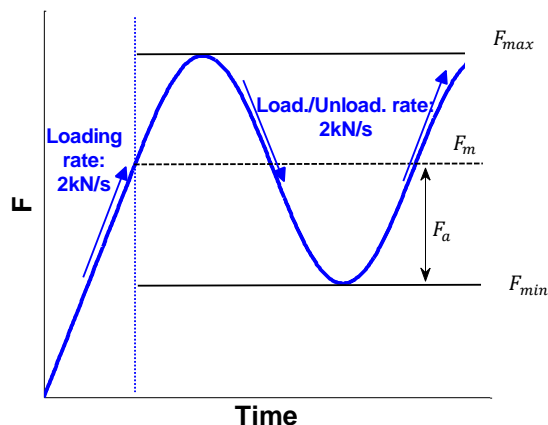


Figure IV.1-1 : Stress controlled, sinusoidal form, constant amplitude loading.

For the tests presented in this section, the acquisition frequency was adapted in order to have at least 80 points per cycle. This rate permitted to have a good description of the relative displacement of the

substrates along the cycle. Therefore, the ratcheting effect was investigated with the mean value of the displacement along a cycle, and for a given number of cycles n , the ratcheting effect is defined with the evolution of the following function:

$$D_r(n) = \frac{D_{max}(n) + D_{min}(n)}{2} \quad (\text{Eq 1.84})$$

where, D_{max} defines the maximum value along the cycle and D_{min} the minimum and D_r represents the “ratcheting” displacement. In the following DT_r will represent the tangential part and DN_r the normal part of this displacement.

IV.1.1. Reproducibility

The reproducibility of the experimental results under static and creep loadings were confirmed in Chapter II. Thus, two cyclic tests were performed with the same tangential loading ratio: $FT_a = 5kN$ and $FT_m = 7kN$. The experimental results presented in Figure II.3-2a showed that the behavior of bonded joints was globally reproducible on a $FT-DT$ diagram. For the ten first cycles, the tangential displacements measured were very reproducible until a 100s test time (Figure II.3-2b). Nevertheless, after this time, the displacement measured in the bonded joint for these tests even for the long-term behavior is increasing with a same trend.

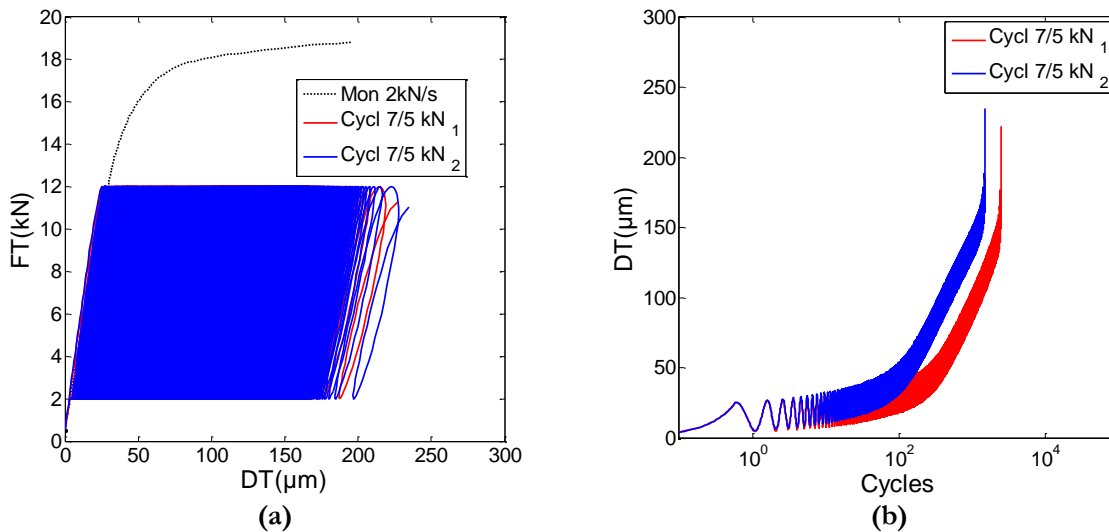


Figure IV.1-2: Cyclic behavior under shear loading: mechanical behavior in the tangential direction under monotonic and cyclic loadings (a), tangential displacement vs. number of cycles (b).

IV.1.2. Mean load influence

Especially at high stress level, creep can have a significant effect on the fatigue lifetime (Dean, 2007). Thus, the influence of the mean load has to be analyzed. This second step concerned the investigation on the mean load effect on the cumulative tangential displacement during the cyclic tests. Therefore, tests were performed with different mean loads $FT_m = 8, 9$ and $10kN$ with a constant load amplitude $FT_a = 2kN$. The cyclic response is presented in Figure IV.1-3a in a $FT-DT$ plane and Figure IV.1-3b concerns the tangential ratcheting displacement DTr (Eq 1.1). It evolves quickly in the first cycles due to the elastic and the short-term viscous behavior. Then, after a hundred of cycles, the fatigue behavior

evolves to a steady-state dominated by the long-term mechanical components with a low rate evolution of the tangential ratcheting displacement. In Figure IV.1-3b, both short-term and long-term behaviors are illustrated by the evolution of DTr . The influence of the mean load in the first part of the fatigue behavior is underlined by the evolution of the ratcheting displacement and the time needed to reach a steady-state. The long-term behavior seems to be ruled by the same mechanical components as the evolution of the ratcheting displacement revealed a same shape for each curve in a logarithmic diagram (Figure IV.1-3b).

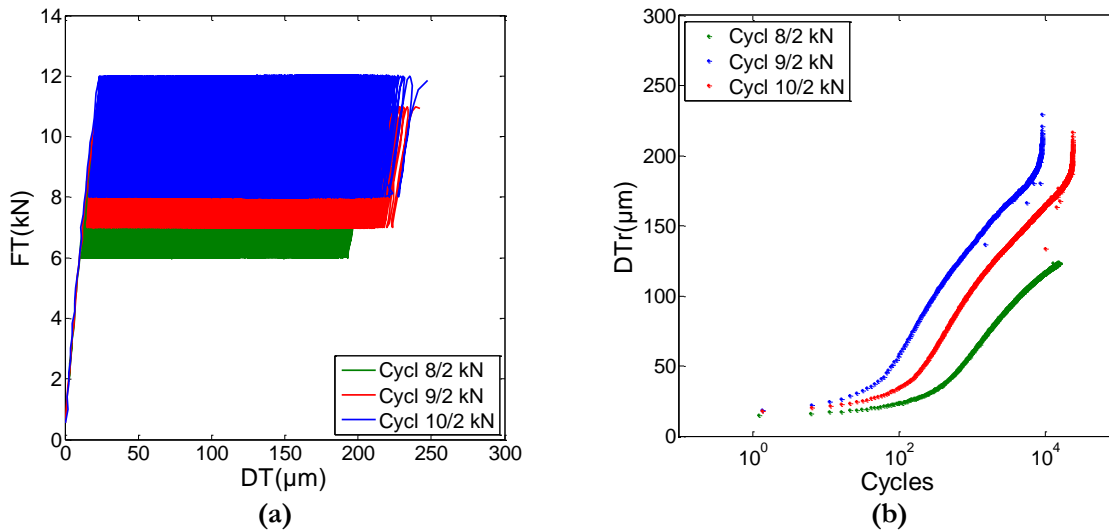


Figure IV.1-3: Mean load influence on cyclic behavior (shear test): mechanical behavior in the tangential direction (a), tangential ratcheting displacement (DTr) vs. number of cycles until failure (b).

IV.1.3. Influence of the load amplitude

Tests were performed to analyze the influence of the load amplitude FT_a keeping a constant maximum load $FT_{max} = 12kN$. The results for two different load amplitudes $FT_a = 2kN$ and $5kN$ are shown in Figure IV.1-4. In order to keep the same loading rate for these two tests, the frequency was so adapted from 0.25 to $0.1Hz$. For both loading cases, the evolution of the cumulative strain which is an indicator of the cumulated visco-plasticity, reaches an asymptotic limit for 500 cycles (Figure IV.1-4).

In a short-term evolution, the ratcheting effect under these two loadings keeping a same maximum load, showed two curves with a slightly different shape. Furthermore, on the long-term behavior, these two different load amplitudes seem to reach a same tendency as a same steady-state. Hence, the important growth in the ratcheting displacement, recorded with the increase of the load amplitude, is not as clear.

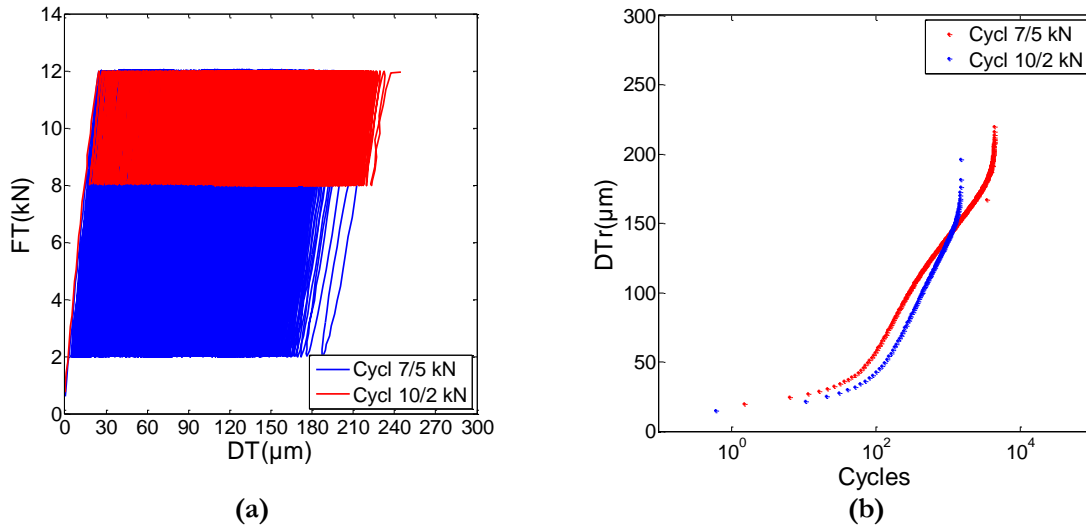


Figure IV.1-4: Load amplitude influence on the cyclic behavior (shear test): mechanical behavior in the tangential direction (a), DT_r vs. number of cycles until failure (b).

IV.1.4. Influence of the loading rate

In order to analyze the loading rate influence, the load amplitude and the mean load were kept constant ($FT_a = 5kN$ and $FT_m = 7kN$) and different frequencies were applied: 0.001, 0.1 and 1Hz. Figure IV.1-5 presents the evolution of the cumulative tangential displacement for these three loading cases. For the lower loading rate, the increase of this cumulative displacement per cycle was exponential as a result of the creep effect. Hence, the failure occurred for the test performed for $0.02kN/s$ ($f = 0.001Hz$) for only a few numbers of cycles.

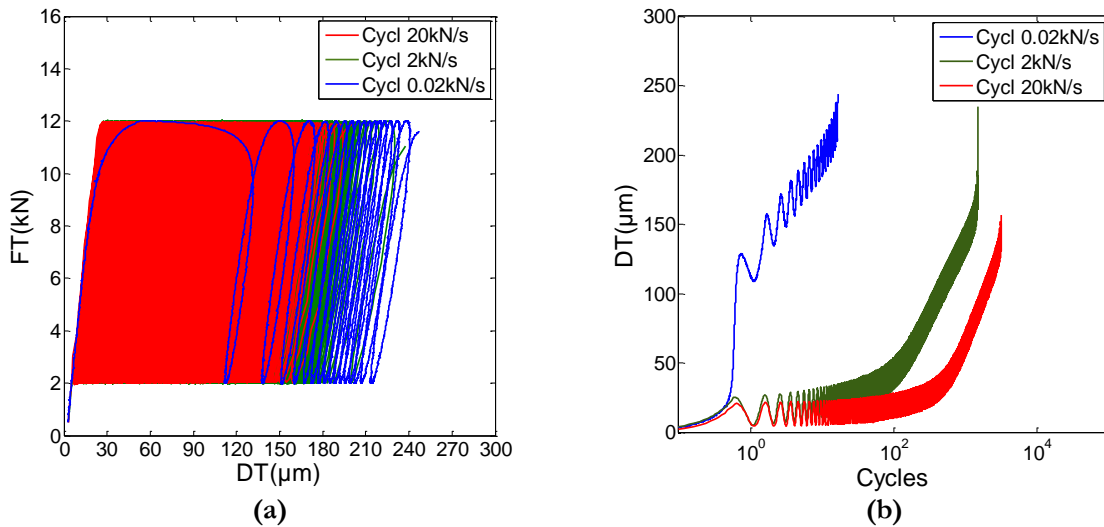


Figure IV.1-5: Loading rate influence on cyclic behavior (shear test): mechanical behavior in the tangential direction (a), tangential displacement vs. number of cycles (b).

The ratcheting effect, presented in Figure IV.1-6a, showed the mean displacement per cycle (ratcheting displacement) was highly dependent on the loading rate and may be attributed mainly to the creep-fatigue coupling. Considering the low number of cycles until failure, the tests performed for $0.02kN/s$ can not be judged as a real fatigue test. However, the data registered and plotted in Figure IV.1-6b, as a function of time, revealed that the ratcheting effect had a similar shape. This result was very interesting

as it underlined the importance of the time dependency of the tangential displacement evolution (creep effect), and it can be assumed to be an evidence of the creep-fatigue coupling.

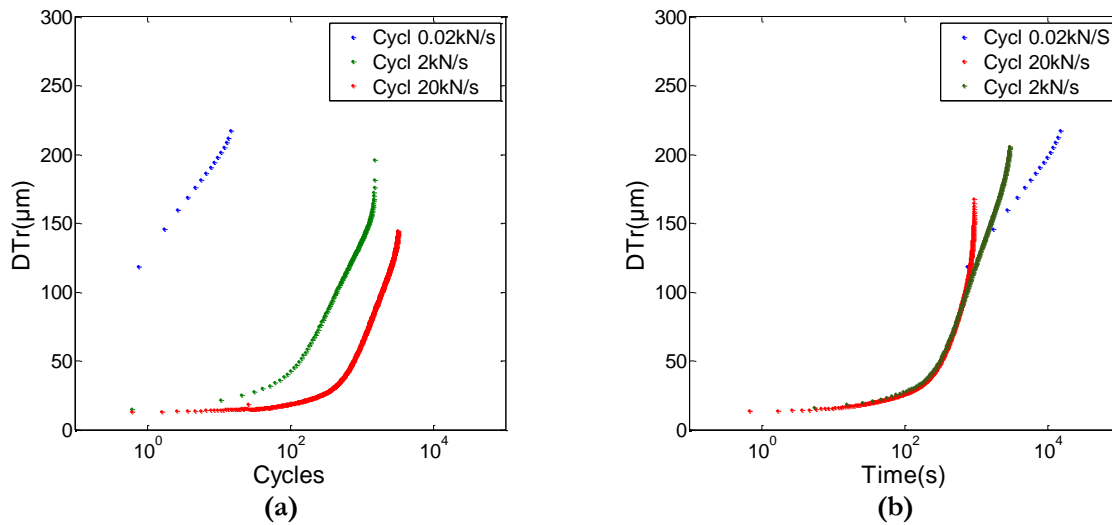


Figure IV.1-6: Loading rate influence on cyclic behavior (shear test): DT_r vs. number of cycles (a) and DT_r vs. Time (b).

IV.1.5. Joint stiffness

In order to estimate the occurrence of damage during shear tests, evolution of the joint stiffness was measured. The joint stiffness was calculated at the beginning of each loading step: a linear regression was made on the ten first points of each cycle. The normalized stiffness (relative to the initial Young modulus E_0) was computed and the more relevant data from the maximum load amplitude tests ($FT_a = 5\text{ kN}$ and $FT_m = 7\text{ kN}$) tests are plotted in Figure IV.1-7. As a constant loading rate was applied on each cycle (2 kN/s), the plotted value was independent of the visco-elastic mechanisms. Figure IV.1-7a shows the stiffness measured in the bonded joint with respect to the number of cycles. This mechanical property seemed to be quite constant during all tests, except under the last cycles leading to failure. This result was quite reproducible for each test when plotted as a function of the tangential displacement (Figure IV.1-7b).

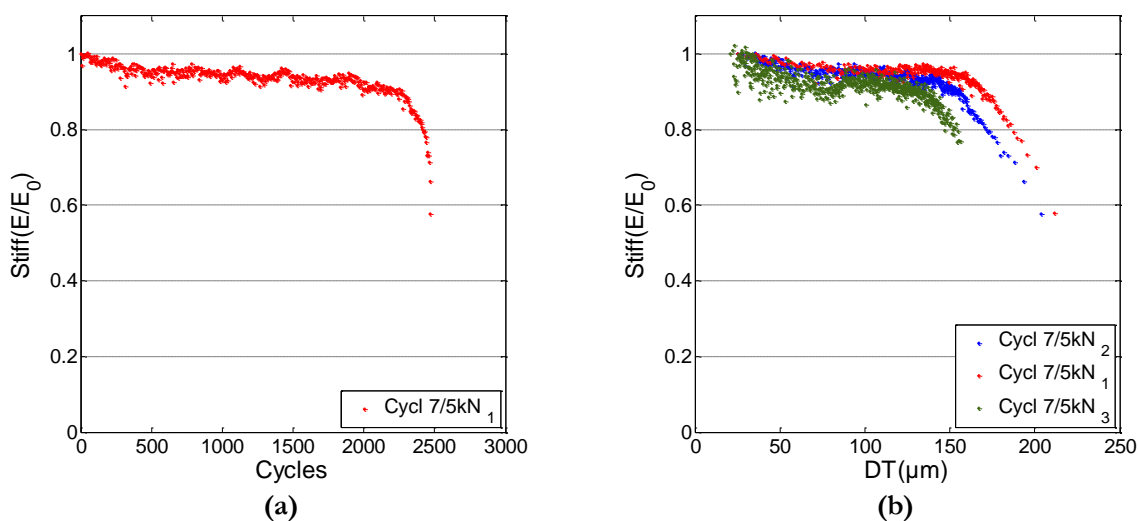


Figure IV.1-7: Joint stiffness in the tangential direction for shear tests: normalized joint stiffness (E/E_0) vs. number of cycles (a) and normalized joint stiffness (E/E_0) vs. tangential displacement (b).

The shape of the hysteretic loops curves (Figure IV.1-8a and Figure IV.1-8b), which did not evolve until the last cycles, was consistent with this observation. The measurement of a constant apparent stiffness for the main part of the fatigue behavior tended to confirm the importance of the visco-plastic mechanical components to explain the ratcheting effect: damage seemed to occur for shear loading at the very end of the test.

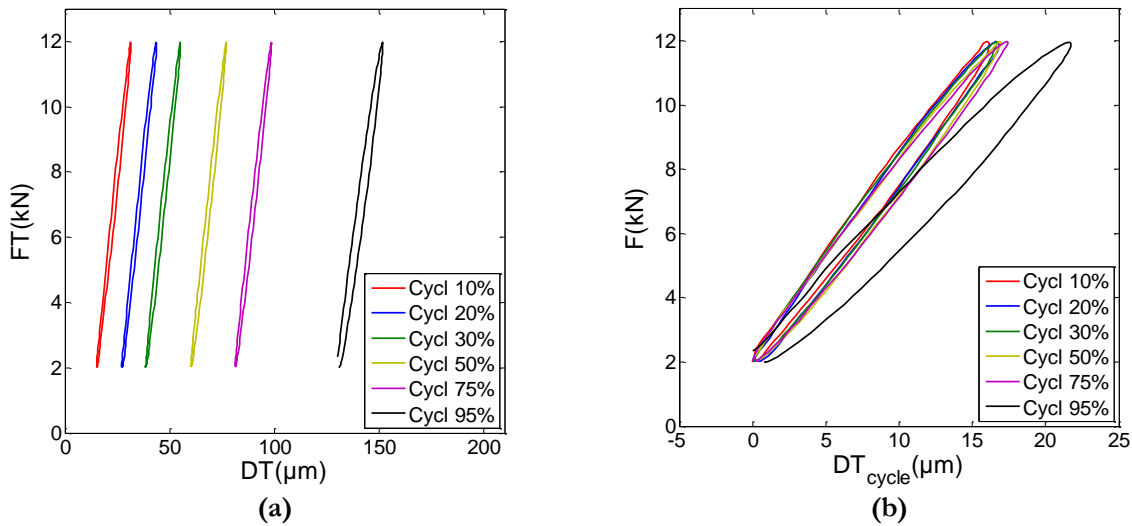


Figure IV.1-8: Evolution of the mechanical response under cyclic loadings (relative to the fatigue life): mechanical behavior in the range of the total tangential displacement (DT) (a) and in the range of the tangential displacement during cycles (DT_{cycle}) (b).

IV.1.6. Failure scenarii

The experimental results in terms of fatigue lives were examined, and experimental values are detailed in Table II.1-2. For all the tests under shear loadings with a $2kN/s$ loading rate, the failure of the bonded joint is systematically observed for a tangential displacement at failure close to the thickness of the adhesive joint. Furthermore, these results did not depend on the load amplitude or the mean load.

Load		Sample N°	Failure	
Frequency	Ratio F_a/F_m		DT (μm)	N_f (cycles)
0.25Hz	2/9kN	1	232	23,119
		2	234	8,893
		3	200	82,215
	2/10kN	4	231	888
		5	229	1,663
		6	236	4,321
	2/8kN	7	158 ^s	100,000 ^s
		8	150 ^s	100,000 ^s
		9	221	21,003
0.1Hz	5/7kN	10	192	1,52
		11	199	2,471
		12	170	1,081
		13	248	517
		14	250	303
		15	290	10
0.01Hz		16	242	18
10Hz		17	160	3,147
		18	185	925

Table IV.1-1 : List of cyclic tests under shear loadings (^s = stopped).

As an important result of this experimental campaign, this observation seemed to constitute a reliable failure criterion. Nevertheless, this observation revealed some limits with a loading rate dependency: the cumulative tangential displacement reached at failure seemed to increase with the low loading rates. Despite the apparent reproducibility of the mechanical behavior and failure criteria brought out, results in terms of fatigue lives were more dispersive than the previous results. Nevertheless, the experimental method permitted to obtain a rather low scatter. Although the results were insufficient in number to confirm the trend observed, fatigue life results in terms of maximum load were plotted in Figure IV.1-9a. The analysis of the influence of the loading rate on the fatigue lifetime was performed. Therefore, in Figure IV.1-9b the number of cycles to failure measured was plotted in function of the loading rate.

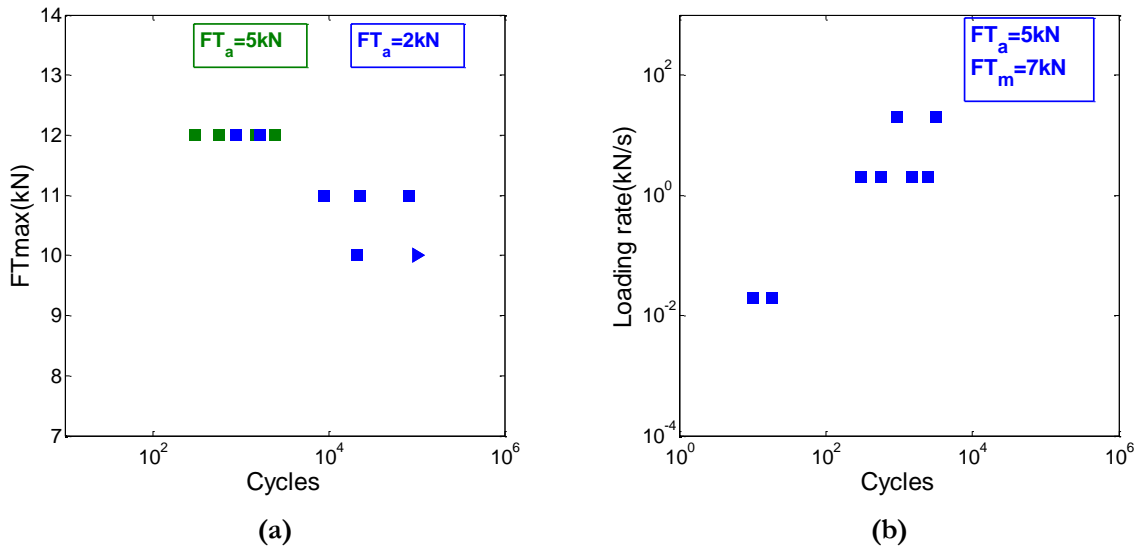


Figure IV.1-9: Fatigue lifetime in FT_{max} scale (a) and influence of the loading rate for a given loading case ($FT_a = 5kN, FT_m = 7kN$) (b) (▶ = stopped).

IV.2. Numerical prediction

The experimental monotonic results were well described using a visco-elastic visco-plastic constitutive model. This model made it possible to retrieve the creep behavior under different load levels. In this section, the cyclic loading cases were applied in Abaqus® FE analysis of the modified Arcan test. Details of the FE analysis were described in Chapter III.

Using a modified Arcan device, under shear loading, the displacement at failure from the comprehensive experimental database underlined a value close to the adhesive joint thickness. This result was acceptable for both monotonic and cyclic tests for a loading rate of $2kN/s$. Therefore, assuming this observation, a failure strain based criterion will be developed.

IV.2.1. Failure criterion

In order to introduce a failure criterion, a User Output Variable ($UVARM$) called C , was created in the user material subroutine. This variable was calculated at each increment of the FE analysis and was defined by:

$$C = \left(\frac{\varepsilon_{eq}}{\varepsilon_{f_{eq}}} \right)^2 + \left(\frac{\varepsilon_H}{\varepsilon_{f_H}} \right)^2 \quad (\text{Eq 1.85})$$

with,

$$\begin{cases} \varepsilon_{eq} = \sqrt{2/3 (\underline{D}:\underline{D})} \\ \underline{D} = \underline{\varepsilon} - (1/3) Tr(\underline{\varepsilon})\mathbf{Id} \\ \varepsilon_H = 1/3 Tr(\underline{\varepsilon}) \end{cases}$$

where $\varepsilon_{f_{eq}}$, ε_{f_H} defined the equivalent and hydrostatic failure strains computed with the total strain tensor $\underline{\varepsilon}$. A failure within the adhesive is considered as soon as the variable C has raised a value above or equal to 1. Then, the criterion is considered to be reached and the numerical simulation is stopped by the subroutine.

The modified Arcan device under shear loading ($\gamma = 90^\circ$), for thin adhesive joints, is associated to a pure shear stress state with no stress concentrations (Cr  ac'hcadec, 2008). Therefore, using the system of axis given in Figure IV.2-2, the out-of-plane strains ε_{12} , ε_{23} , ε_{22} and the ε_{11} , ε_{33} strain tensor components were neglected. In shear, the equivalent and hydrostatic strains were thus computed with the total strain tensor $\underline{\varepsilon}$ of the following form:

$$\underline{\varepsilon} = \begin{pmatrix} 0 & 0 & \varepsilon_{13} \\ 0 & 0 & 0 \\ \varepsilon_{13} & 0 & 0 \end{pmatrix} \quad (\text{Eq 1.86})$$

For bonded specimen under shear loading, the following assumption is thus made:

$$\begin{cases} \varepsilon_{eq} = \left(\frac{2}{\sqrt{3}} \right) \varepsilon_{13} \\ \varepsilon_H = 0 \end{cases} \quad (\text{Eq 1.87})$$

Following the previous assumptions, the failure criterion (Eq 1.2) may thus be expressed as follow:

$$C = \left(\frac{\varepsilon_{eq}}{\varepsilon_{f_{eq}}} \right)^2 \quad (\text{Eq 1.88})$$

In Chapter II, concerning results under shear loading, a dependency on the loading rate of the measured displacement at failure was observed on the monotonic behavior as well as the cyclic behavior. In order to investigate the influence of different factors on the fracture characteristics of metals, Johnson et al. (Johnson, et al., 1985) proposed a failure criterion based on the experimental results of samples subjected to various temperatures, pressures and loading rate. The criterion was based on the definition of the strain to fracture as a function of the strain rate, the temperature within the material and the stress value. Concerning composite materials (Aubry, 2013) and epoxy adhesives (Morin, et al., 2010) applications, failure criteria based on an equivalent failure strain which evolves with the strain rate, were adapted from the work of Johnson et al. From these works, the components depending on the temperature can be removed. Indeed, the assumption that with the relatively low loading rates applied, no evolution of temperature within the material occurred.

Therefore, a definition of the equivalent failure strain suitable this application case could be expressed as follow:

$$\varepsilon_{f_{VM}} = D_1(1 - D_2 \ln(\dot{\sigma}^*)) \quad (\text{Eq 1.89})$$

with,

$$\dot{\sigma}^* = \frac{\dot{\sigma}_{VM}}{\dot{\sigma}_{VM_{2kN/s}}}$$

where, D_1 and D_2 are material constants to be identified, $\dot{\sigma}_{VM}$ is the equivalent von Mises stress rate and $\dot{\sigma}_{VM_{2kN/s}}$ the mean equivalent von Mises stress rate within the adhesive joint of a Arcan specimen under a $2kN/s$ loading rate. Based on the works of Cowper et al. (Cowper, et al., 1957), performed in order to represent the strain rate effects for dynamic loadings, another expression of $\varepsilon_{f_{VM}}$ may be developed:

$$\varepsilon_{f_{VM}} = D_1^*(1 - D_2^*(\dot{\sigma}^*)^{1/D_3^*}) \quad (\text{Eq 1.90})$$

In this last expression a set of three material parameters are needed: D_1^* , D_2^* and D_3^* . As the values of the failure strain were equivalent in cyclic and monotonic tests the identification of the material parameters can be done on both.

For these two expressions, the first parameter, D_1^* or D_1 , could be seen as an initial mean value for the strain to failure $\varepsilon_{f_{VM}}$. Therefore, these parameters were defined equal to the mean equivalent failure strain measured for a $2kN/s$ shear test. The remaining parameters, (D_2^* , D_3^*) or D_2 were defined using the failure data of a second loading rate. The parameter identification was performed considering a mean value in the adhesive joint strain. In order to develop a more accurate definition of the parameters, an inverse-identification should be developed.

Figure IV.2-1a presents the results in a logarithmic diagram of the Cowper et al.(Eq 1.7) and the Johnson et al. (Eq 1.6) failure criteria. Parameters were identified with the failure recorded on monotonic tests for the higher loading rates $20kN/s$ and $2kN/s$ (Figure IV.2-1b). The two parameter sets identified are listed in Table III.2-1. The Cowper et al. criterion seemed to have a better description for the $0.2kN/s$ loading rate. Furthermore, this second criterion reached an asymptotic evolution for the lower loading rates in the logarithmic diagram which can be considered more physically admissible. As fatigue behavior is associated to low rate evolutions, it was important to define this asymptotic value with the decrease of the loading rates. Therefore, the criterion developed by Cowper et al. was chosen to characterize the loading rate dependency observed for the failure.

Failure criterion	Material constants	Value	Test for identification
Johnson et al.	D_1	1.16	Strain to failure for monotonic shear tests under different loading rates ($20kN/s$ and $2kN/s$)
	D_2	$1.02 \cdot 10^{-1}$	
Cowper et al.	D_1^*	1.50	
	D_2^*	$2.04 \cdot 10^{-1}$	
	D_3^*	2.08	

Table IV.2-1 : Material parameters involved in the constitutive model and numerical values defined with the identification strategy proposed.

The variable C was computed at each integration points of the adhesive bond-line elements (FE model used in the parameters identification described in Chapter III). Numerically, under monotonic shear loadings, the criterion was reached in the middle of the overlap (Figure IV.2-2). This result was consistent with the previous studies performed on the failure prediction based on a modified Arcan device (Carrère, et al., 2013).

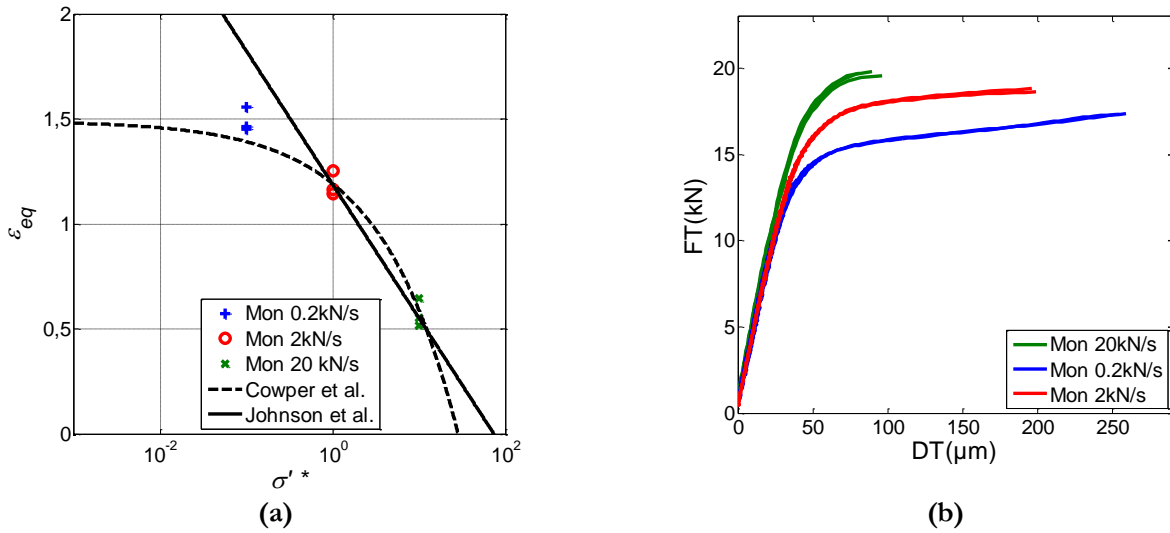


Figure IV.2-1: Identification of the Cowper et al. and Johnson et al. criteria material parameters (a) based on failures observed under monotonic shear loadings (b).

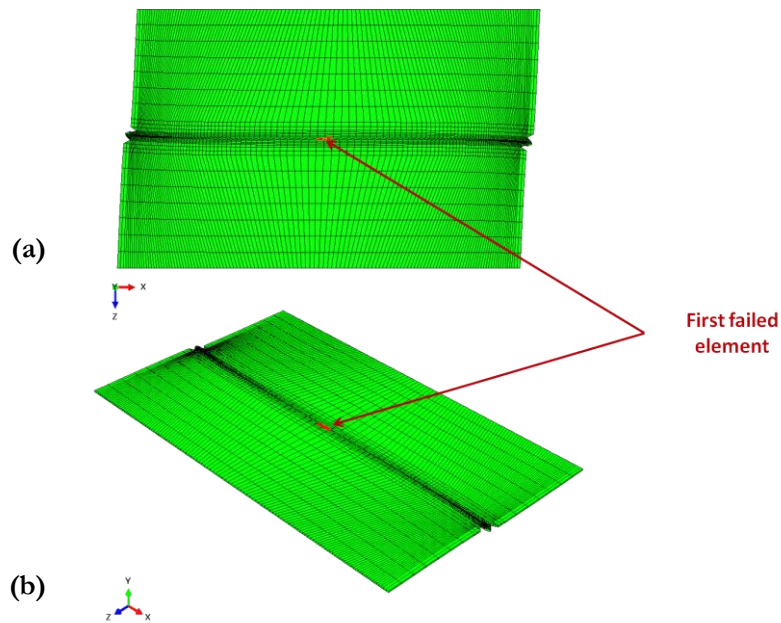


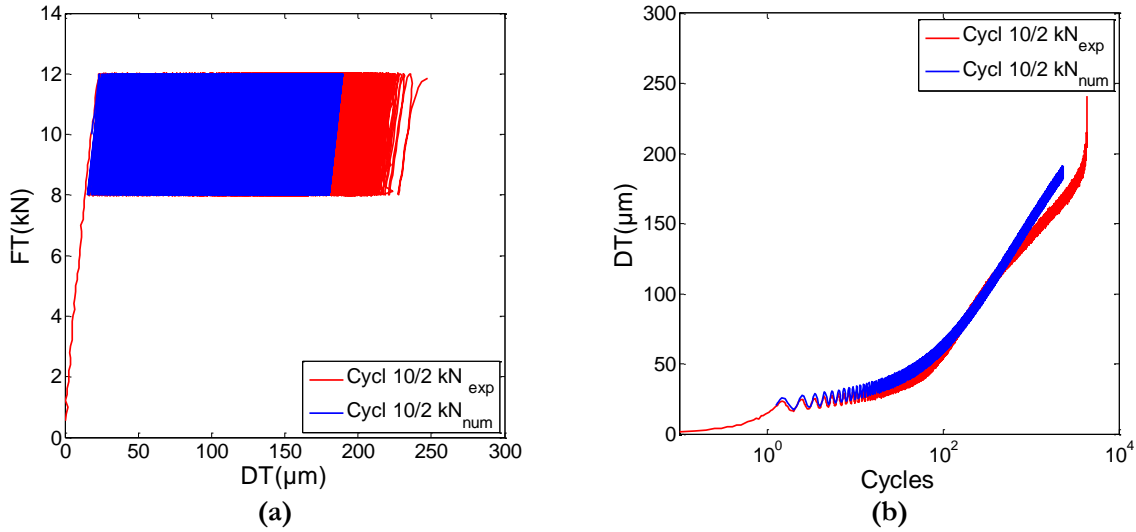
Figure IV.2-2: 3D FEM of the modified Arcan sample in the deformed configuration: 3D isometric view (a) and 2D view in the (z,x) plane (b).

IV.2.2. Prediction of the cumulative displacement

The material parameters, introduced in the cyclic FE analyses, were given using only two types of tests:

- The parameter set used for the material viscous behavior, resulting from the identification process developed in Chapter III, is taken from creep/recovery tests (on five load levels);

- The material three constants necessary to the development of the failure criterion were defined using monotonic tests using two different loading rates and validated using a third one.



- **Figure IV.2-3: Experimental/numerical comparison under cyclic shear loading ($FT_a = 2kN / FT_m = 10kN$): mechanical behavior in the tangential direction (a) and tangential displacement vs. number of cycles (b).**

Abilities of the model to describe the cumulative displacement are presented in Figure IV.2-3 for the following loading case: $1Hz$, $FT_a = 2kN$ and $FT_m = 10kN$. The model was able to describe accurately the cyclic behavior with the material constants identified on creep/recovery tests. Presented in Figure IV.2-3b, in a logarithmic evolution, the numerical response defines a cumulative displacement with a low discrepancy with the experimental results all along the fatigue life. The computation of the numerical response was stopped by the strain based failure criterion for a tangential displacement value close to the adhesive joint thickness. This result is consistent with the observations made on the fatigue experimental campaign.

IV.2.3. Influence of the mean load on the ratcheting effect

The abilities of the model to take into account the influence of the mean load are presented in Figure IV.2-4a with the ratcheting displacement plotted as a function of the number of cycles. The trend, observed on the experimental campaign, seems to be well transcribed by the model. On the 500 first cycles, even if the description of the mean behavior is well described for the higher mean load ($FT_m = 10kN$) the effects of a decreasing loading are slightly overestimated. Nevertheless, the abilities shown by the simulation on the description of the long-term behavior permit to give a good evaluation of the cumulative displacement. Hence, a fatigue life evaluation can be determined.

The numerical simulation, performed with the lower load level ($FT_m = 8kN$), was manually stopped “before” reaching the failure criterion as the computation time was considered as heavy. Even if, for this loading case, both simulation and experimental tests did not achieve by failure, a first estimation on the abilities of the numerical response can be developed. Indeed, the strong assumptions made on a fatigue behavior neglecting the damage mechanics and the environmental aspect seems to show their limits on low load levels.

IV.2.4. Influence of the load amplitude on the ratcheting effect

Figure IV.2-4b presents a comparison between the simulation and the experimental results for two loading cases: $FT_a = 5kN / FT_m = 7kN$ and $FT_a = 2kN / FT_m = 10kN$. The FE analysis slightly overestimated the mean tangential displacement (DTr) for high load amplitudes in the short-term fatigue behavior. However, the trend of a low discrepancy observed in the experimental response between two tests with the same maximum load ($FT_{max} = 12kN$) was defined by the numerical simulations. Hence, the numerical results on the effect of the load amplitude permitted to retrieve the low influence observed for this parameter on the cumulative displacement.

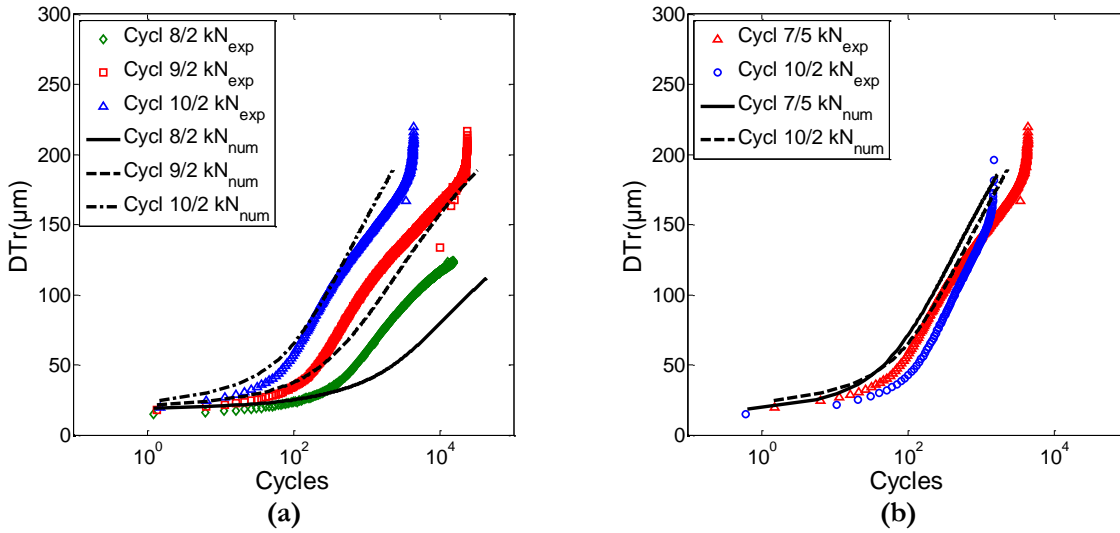


Figure IV.2-4: Experimental/numerical comparison of DTr until failure: influence of the mean load (a) and influence of the load amplitude (b).

IV.2.5. Influence of the loading rate on the ratcheting effect

The description of the loading rate influence by the numerical model is presented in Figure IV.2-5.

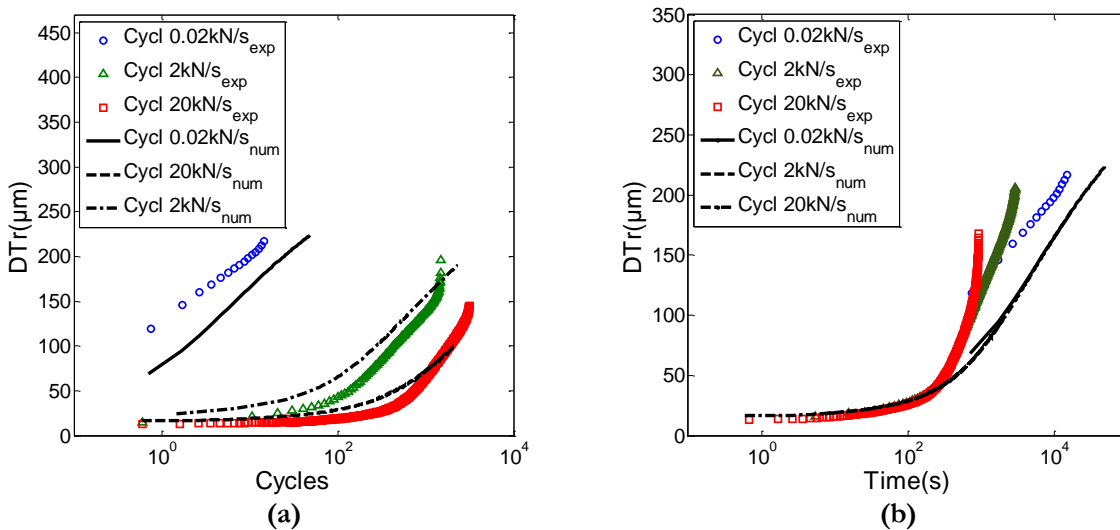


Figure IV.2-5: Experimental/numerical comparison under shear cyclic loading ($FT_a = 5kN / FT_m = 7kN$): influence of the loading rate - DTr vs. number of cycles (a) and DTr vs. Time (b).

Plotted as a function of time (Figure IV.2-5b), for the three different loading rates tested, the numerical model gave a similar response for the three different loading rates. Therefore, time seems to be the main factor of influence in the numerical ratcheting effect. This result was consistent with the observations made on the importance of the creep-fatigue coupling.

IV.2.6. Fatigue life prediction

The FE analysis ensured a satisfying description of the ratcheting displacement (DTr) under fatigue loading for the underlined factors of influence: mean load, load amplitude, loading rate. Therefore, a numerical prediction of the fatigue life of modified Arcan specimens under shear loading was thus possible. As the load amplitude FT_a did not involve substantial differences in the experimental and numerical fatigue lives, the results are plotted as a function of FT_{max} in Figure IV.2-6a.

Figure IV.2-6b presents the results of a numerical/experimental comparison concerning the influence of the loading rate on the number of cycles to failure. As observed in the previous section, the mean cumulative displacement, highlighted with DTr plotted in function of time, showed the same evolution for the different loading rates tested. Therefore, with this observation in mind, in order to model the loading rate influence (or frequency) on DTr a linear relation can be developed: increasing the loading rate, the number of cycles to failure will grow proportionally. Nevertheless, the criterion developed and identified from monotonic tests was loading rate dependent and this criterion predicted lower displacements for the higher loading rates. Hence, concerning the influence of the loading rate, for the loading case ($FT_a = 5kN / FT_m = 7kN$), the number of cycles until failure was also related to the cumulative tangential displacement at failure predicted by the Cowper et al. criterion. The numerical response on DTr using the constitutive model, coupled with the criterion developed, permitted to perform a good prediction of the influence of the loading rate with a non-linear evolution.

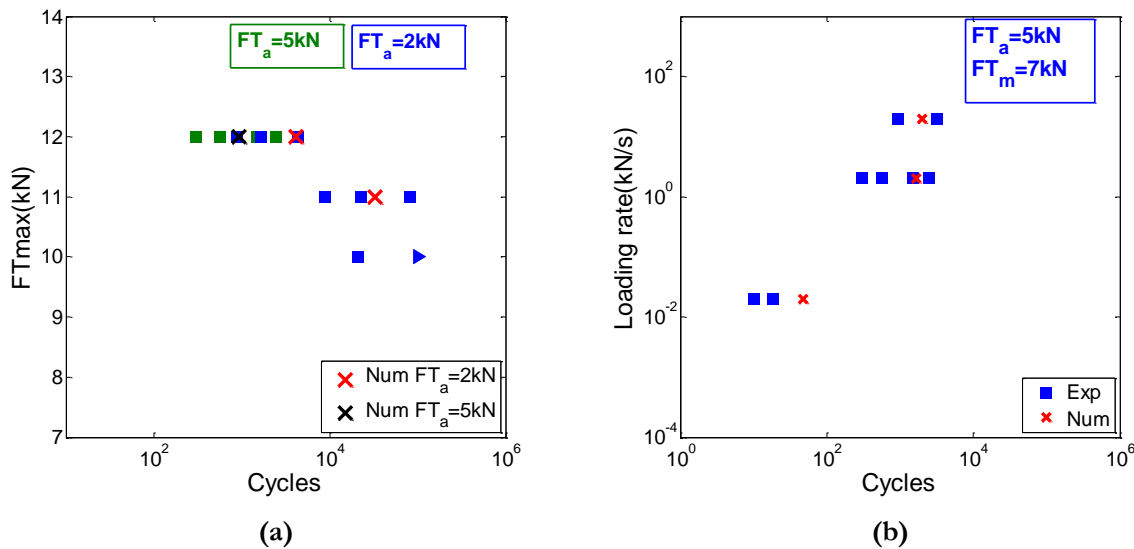


Figure IV.2-6: Experimental/numerical comparison of fatigue lifetime in FT_{max} scale (a) and influence of the loading rate for a given loading case ($FT_a = 5kN, FT_m = 7kN$) (b) (▶ = stopped).

IV.3. Results under tensile-shear loading

For combined tensile-shear loadings ($\gamma = 45^\circ$), the inelastic curve in the monotonic behavior for a $2kN/s$ loading rate was reached for lower load levels. Evolution of the cumulative displacement was pointed out as an interesting factor. The load levels have thus been reduced in order to observe the fatigue behavior for an equivalent number of cycles to failure. In the following section, all the tests were performed using a $2kN/s$ loading rate.

IV.3.1. Reproducibility

Analyze of the reproducibility for cyclic tensile-shear tests was performed on the following loading ratio: $FT_a = 1.4kN$ and $FT_m = 7.1kN$. Results in the tangential direction, presented in Figure IV.3-1a, showed that the ratcheting effect of bonded joints, plotted as the evolution of DTr in function of the number of cycle, is globally reproducible. In the normal direction, concerning the ratcheting displacements measured (DNr) results are plotted in Figure IV.3-1b. In these three tests, the experimental DNr values were relatively low, and the experimental response presented a higher discrepancy.

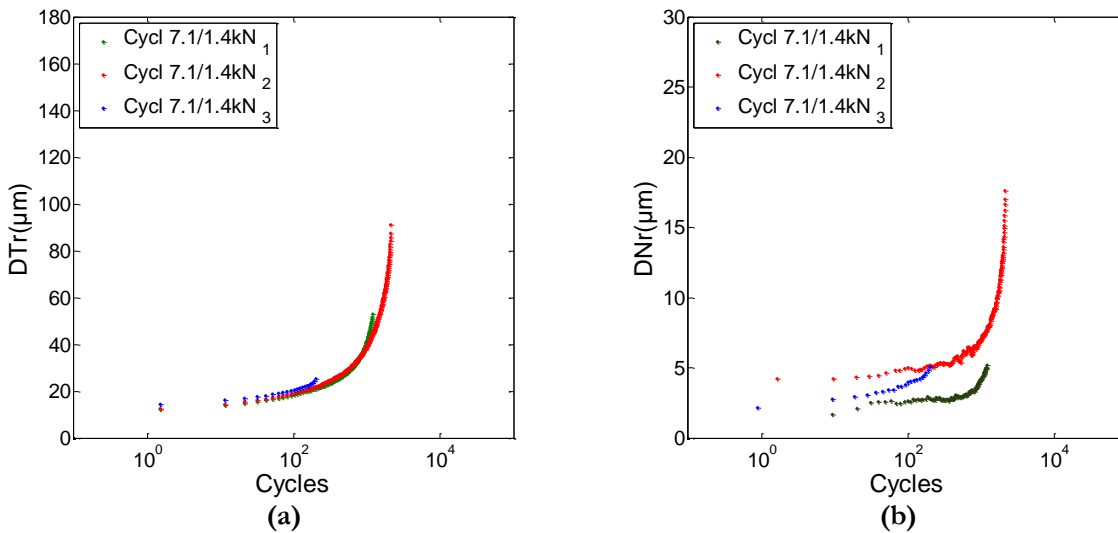


Figure IV.3-1: Ratcheting effect under cyclic tensile-shear loading: tangential ratcheting displacement (DTr) vs. number of cycles (a) and normal ratcheting displacement (DNr) vs. number of cycles (b).

IV.3.2. Mean load influence

The influence of the mean load was observed on two different loading cases with same load amplitude ($FT_a = FN_a = 1.4kN$): $FT_m = FN_m = 7.1kN$ and $FT_m = FN_m = 6.4kN$. The mechanical response presented in Figure IV.3-2 in terms of ratcheting displacement in the tangential direction (DTr), illustrates the acceleration in the ratcheting effect for the higher mean loads. In this direction, in a hundred cycles two different steady-states are reached for these two loading cases (Figure IV.3-2a). In the normal direction component, the same trend can be observed in the mechanical behavior (Figure IV.3-2b). Nevertheless, the lower values measured in the normal displacements did not lead to clear observations, especially in the short term behavior.

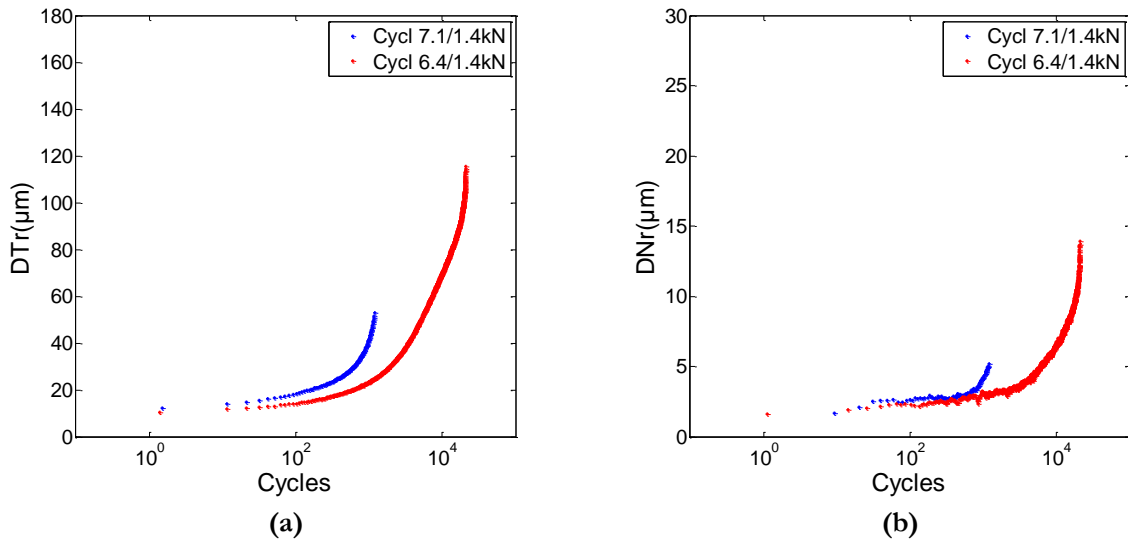


Figure IV.3-2: Mean load influence on cyclic behavior (tensile-shear test): tangential ratcheting displacement (DTr) vs. number of cycles (a) and normal ratcheting displacement (DNr) vs. number of cycles (b).

IV.3.3. Load amplitude influence

With the same approach as in the shear behavior influence of load amplitude was observed on two different loading cases with a same maximum load: $FT_{max} = FN_{max} = 8.5\text{kN}$. Experimental results in both normal and tangential directions presented in Figure IV.3-3, illustrated the low effect of the load amplitude on the ratcheting displacement. The tendency of a mechanical behavior driven by the mean loads and maximum loads parameters observed on the shear tests seems to be confirmed on the tensile-shear behavior.

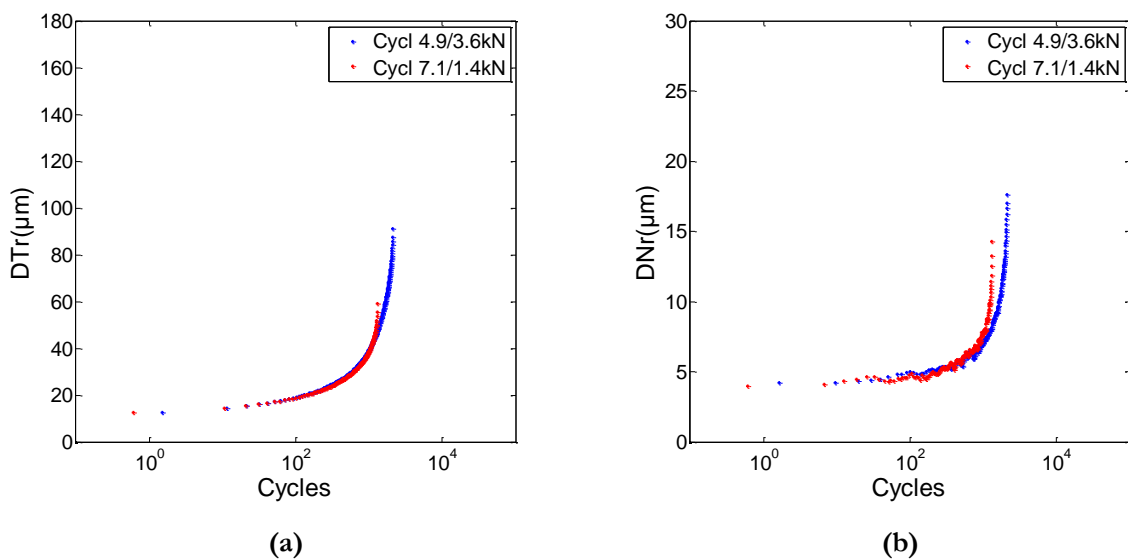


Figure IV.3-3: Load amplitude influence on cyclic behavior (tensile-shear test): tangential ratcheting displacement (DTr) vs. number of cycles (a) and normal ratcheting displacement (DNr) vs. number of cycles (b).

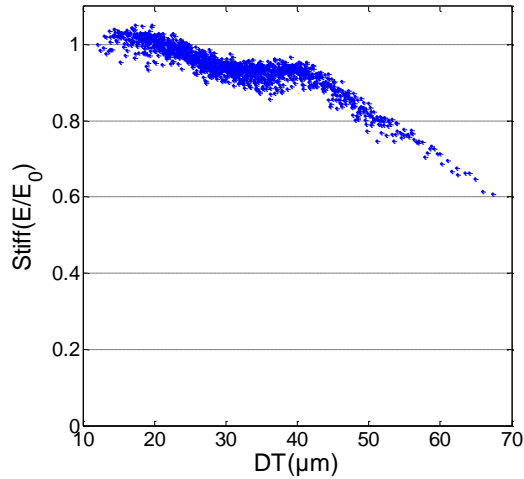


Figure IV.3-4: Joint stiffness in the tangential direction for tensile-shear test: normalized joint stiffness (E/E_0) vs. tangential displacement.

IV.3.4. Joint stiffness

Under tensile-shear cyclic loading, the stiffness of the joint in the tangential direction is plotted in Figure IV.3-4 for a $FT_a = 3.6kN / FT_m = 4.9kN$. The results indicated that damage occurs earlier than in the shear test as a decrease in the stiffness value seems to be constant along the test.

IV.3.5. Fatigue life

From the cyclic tests summarized in Table IV.3-1, the influence of the maximum load on the fatigue life is shown in Figure IV.3-5. In this study, the influence of two different mean loads and two different load amplitudes were investigated. The number of samples tested is not large enough to perform conclusions. Nevertheless, concerning the influence of the maximum load, the conclusions based on the shear behavior could be brought to the results under tensile-shear loading.

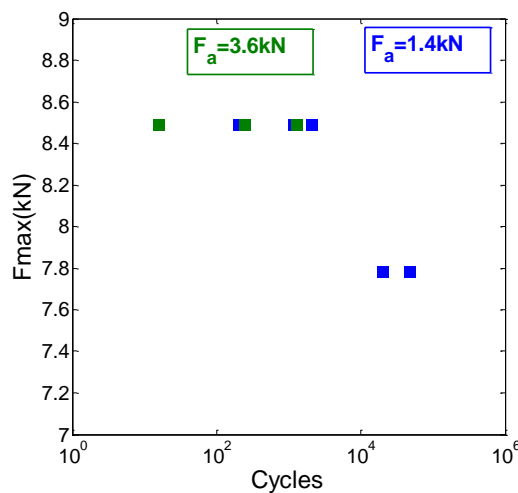


Figure IV.3-5: Fatigue lifetime for tensile-shear loadings in F_{max} scale.

Under shear loading, the tangential displacement measured at failure was shown to be close to the adhesive thickness. Under tensile-shear loading, the experimental displacements measured in both tangential and normal direction take values with a more important discrepancy.

Load		Sample	Failure		
Frequency	Ratio F_a/F_m	N°	DT (μm)	DN (μm)	N_f (cycles)
0.25Hz	1.4/6.4kN	1	115	14	20,709
		2	116	15	48,210
	1.4/7.1kN	3	25	5	200
		4	87	17	2,103
		5	91	18	2,113
		6	53	5	1,187
0.1Hz	3.6/4.9kN	7	13	4	16
		8	24	5	250
		9	53	13	1,314

Table IV.3-1 : List of cyclic tests under tensile-shear loadings.

IV.3.6. Numerical prediction

a. Failure criterion

The failure criterion presented in Eq 1.2, developed for the modified Arcan test under shear loadings, permitted (under particular assumptions) to define the equivalent failure strain $\varepsilon_{f_{eq}}$. As the effect of the loading rate on $\varepsilon_{f_{eq}}$ was visible under both monotonic and cyclic loadings, a Cowper et al. criterion was used. Nevertheless, the hydrostatic strain component ε_{f_H} was not determined under shear loading as this component can be neglected in a modified Arcan specimen (Créac'hcadec, 2008).

Concerning the modified Arcan device under tensile-shear loading ($\gamma = 45^\circ$), the out-of-plane strains ε_{12} , ε_{23} , ε_{22} were neglected. Therefore, the equivalent and hydrostatic strains were computed with the strain tensor $\underline{\varepsilon}$ of the following form:

$$\underline{\varepsilon} = \begin{pmatrix} 0 & 0 & \varepsilon_{13} \\ 0 & 0 & 0 \\ \varepsilon_{13} & 0 & \varepsilon_{33} \end{pmatrix} \quad (\text{Eq 1.91})$$

For bonded specimen under tensile-shear loading, the following assumption was thus made:

$$\begin{cases} \varepsilon_{eq} = \frac{2}{3} \sqrt{(3\varepsilon_{13}^2 + \varepsilon_{33}^2)} \\ \varepsilon_H = \frac{1}{3} \varepsilon_{33} \end{cases} \quad (\text{Eq 1.92})$$

Under monotonic tensile loading, experimental results presented in Chapter II, did not reveal a dependency on the loading rate. Moreover, these monotonic tests performed under two loading rates ($2kN/s$ and $0.2kN/s$) did not show an evolution of the displacement at failure. Therefore, for the determination of the hydrostatic failure strain ε_{f_H} the Cowper et al. criterion was not used.

Hence, in order to define the last constant ε_{f_H} of the criterion (Eq 1.2), experimental data of a single loading rate ($2kN/s$) was taken. The identification was performed on the displacement at failure recorded in monotonic tests under tensile shear loadings. Considering an equivalent mean strain in the adhesive joint, the identified value was:

$$\varepsilon_{f_H} = 0.0165 \quad (\text{Eq 1.93})$$

In Figure IV.3-6a, is plotted the failure criterion for two different loading rates ($2kN/s$ and $0.2kN/s$) in an equivalent strain (ε_{eq}) - hydrostatic strain (ε_H) plane. As experimental failure points under

monotonic shear loading ($\gamma = 90^\circ$) and tensile-shear loadings ($\gamma = 45^\circ$) were used to the identification, predictions of their failure coordinates were well predicted using the criterion developed. Further experimental results under tensile-shear loading using a $0.2kN/s$ loading rate should be done to confirm the results.

The criterion developed did not lead to a prediction of failure under tensile loading (plotted along the horizontal axis). Indeed, in the normal direction, the displacement at failure measured under tensile loading was lower than those measured under tensile-shear loading, and the criterion developed did permit to retrieve this trend. Therefore, in order to investigate failure under tensile loading the criterion should be coupled to another one (damage-based criterion for example).

Concerning the fatigue loading, results are plotted in Figure IV.3-6b and compared to the failure criterion obtained for a $2kN/s$ loading rate. As developed in the previous section, the failure criterion could prove a good predictive tool for fatigue behavior under shear loading. Nevertheless, the discrepancy obtained under tensile-shear loading in the displacements to failure did not permit to validate its suitability for this loading.

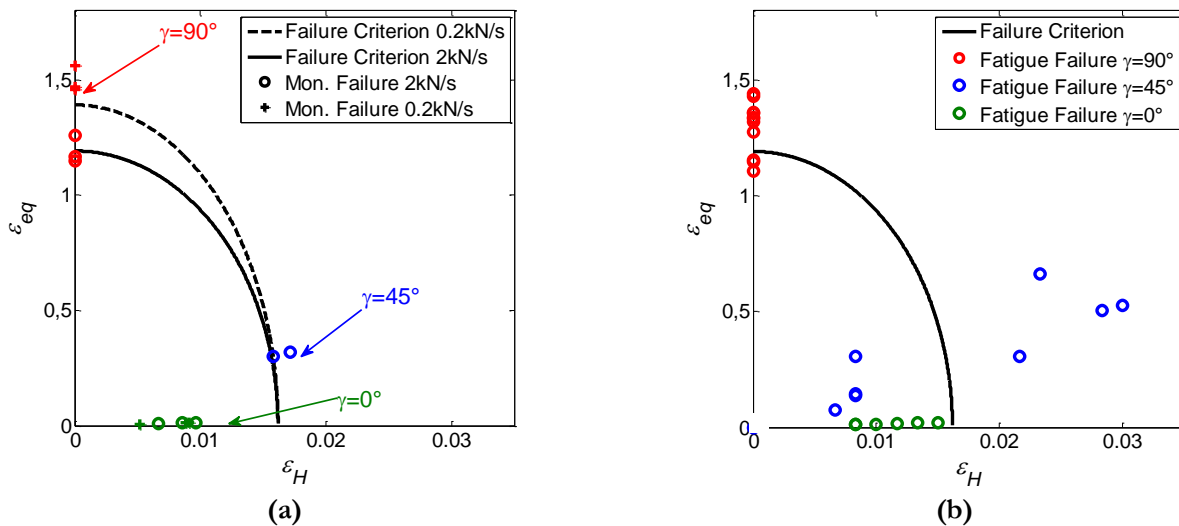


Figure IV.3-6: Comparison between numerical predictions and experimental results: monotonic loadings (a) and cyclic loadings (b).

b. Prediction of the ratcheting effect

Even if the displacements at failure measured under tensile-shear loadings, did not show a repetitive value, regarding the experimental results presented in the previous section, the ratcheting effects seemed to be reproducible (especially in the tangential direction). As the model was developed to predict the mechanical behavior under multi-axial loadings, numerical results are presented for a tensile-shear loading case.

The numerical results under tensile-shear loadings using the visco-elastic visco-plastic model are presented in Figure IV.3-7a, for the tangential displacement and Figure IV.3-7b, for the normal direction. In both tangential and normal directions, numerical prediction was less convincing than the results obtained under shear loading (previous section). Indeed, the FE analysis performed, even if they permit to draw an interesting trend, generally overestimated the ratcheting effect. In order to understand the differences observed several hypotheses could be advanced.

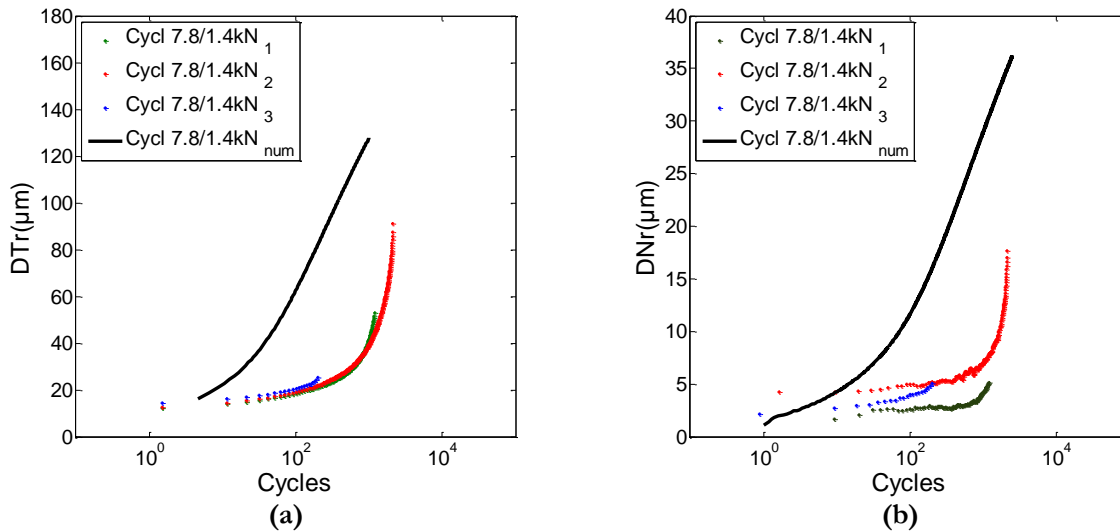


Figure IV.3-7: Experimental/numerical comparison under tensile-shear loading: DTr vs. number of cycles (a) and DNr vs. number of cycles (b).

A first explanation may be performed, developing a criticism of the identification strategy developed. As the mechanical behavior of the adhesive introducing tensile loading components revealed a brittle behavior, the shear direction was chosen to be used for the characterization of the viscous-plastic behavior (Chapter III). Therefore, of the six material constants required for the definition of viscoplasticity, four were defined on the experimental results under shear loading. “Only” the two last parameters (associated to the hydrostatic stress dependency of the yield and flow functions) necessary for the 3D definition of the model were identified using experimental results under tensile-shear loading. A “more” ductile behavior under tensile-shear (or tensile) loading could permit a different identification strategy using the non-linear behavior in the normal direction more efficiently. However, as presented in Chapter III, the experimental/numerical comparison performed under monotonic and creep/recovery loadings permitted to show interesting results from the model. But, under cyclic loadings, the numerical predictions results only fit to the experimental database for the direction in which the viscous flow was defined (behavior under shear loading). The two parameters introduced to take into account the hydrostatic stress dependency of the SikaForce®-7817 L60MR adhesive may not be enough to describe the cyclic behavior under tensile-shear loading.

For reasons of availability of the testing machines all the experimental campaign could not be performed at once. Therefore, a second explanation could be based upon the fact that the tests performed under cyclic tensile and cyclic tensile-shear loadings were performed three to four months after the test campaign performed under shear loading. As the two components of SikaForce®-7817 L60MR revealed an important ageing effect; even if precautions were taken the adhesive behavior may have changed. These phenomena were shown for more important time scales in Chapter III. Hence, in advance of each test campaign, in order to ensure the reliability of the results to come, a similar test should have been performed in order to make a comparison.

IV.4. Results under tensile loading

IV.4.1. Ratcheting effect

Experimental results of the characterization campaign revealed really low values concerning the cumulative displacement measured. Thus, the ratcheting displacement (DNr), presented in Figure IV.4-1a as the evolution of the mean normal displacement for a $FN_m = 6kN / FN_a = 5kN$ loading case, did not show a clear trend: the displacement measured increased slowly until a certain value and start to decrease for the last cycles. These results were compared to a $FN_m = 7kN / FN_a = 5kN$ loading case in order to investigate the influence of the mean load (Figure IV.4-1b). For the second loading case, the trend observed was completely different as the displacement measured increases exponentially. The difference may be explained by the appearance of an early crack within the second adhesive joint tested.

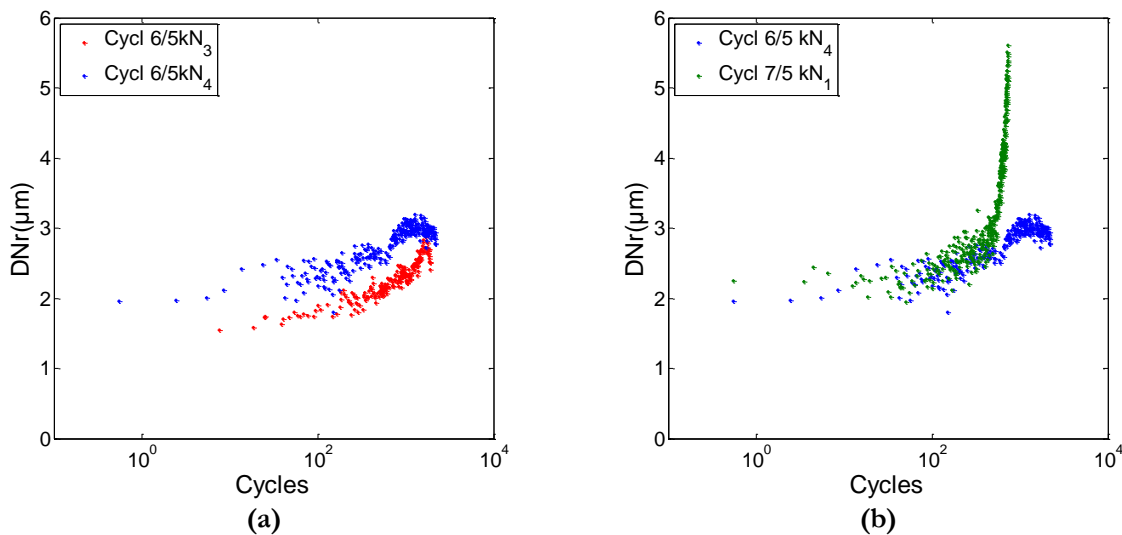


Figure IV.4-1: Mechanical behavior under cyclic tensile loading: reproducibility of the ratcheting displacement (DNr) (a) and influence of the mean load (b).

IV.4.2. Joint stiffness

The evolution of the joint stiffness for the two last loading cases was compared in Figure IV.4-2. Although the higher mean load tested involved an important and quick decrease in the stiffness, its value did not show any evolution for the second and lower mean load. Therefore, under tensile loading the joint stiffness measured seem to strongly depend on the loading case. Nevertheless, as the measured displacement values were really low, precautions must be taken on this conclusion. Further experimental results are needed to perform hypothesis on the evolution of the joint stiffness with the increase of the loading case.

IV.4.3. Fatigue lifetime

The cyclic tests performed under tensile loadings are listed in Table IV.4-1. As in the previous sections, the influence of the maximum load on the fatigue life is shown in Figure IV.4-3. The experimental scattering was clearly higher than for the fatigue tests performed under shear and tensile-shear loadings. However, the study of the influence of three different mean loads was investigated. The conclusions

developed on the shear behavior and tensile-shear behavior could be extended to the results under tensile loading as despite early failure for two tests, the influence of the maximum load can be observed. Nevertheless, further experimental results are needed to confirm the trend observed.

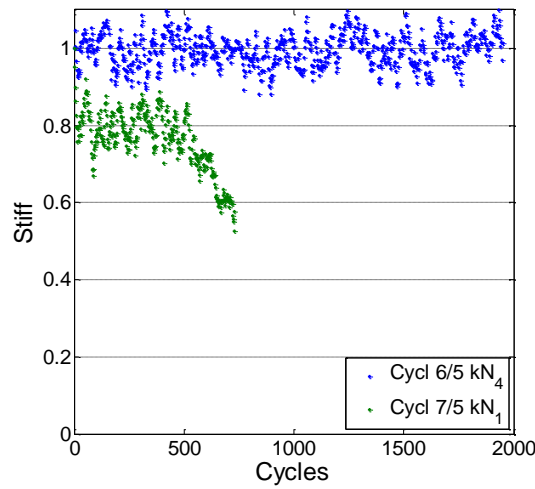


Figure IV.4-2: Evolution of the joint stiffness under cyclic tensile loading: normalized joint stiffness (E/E_0) vs. number of cycles.

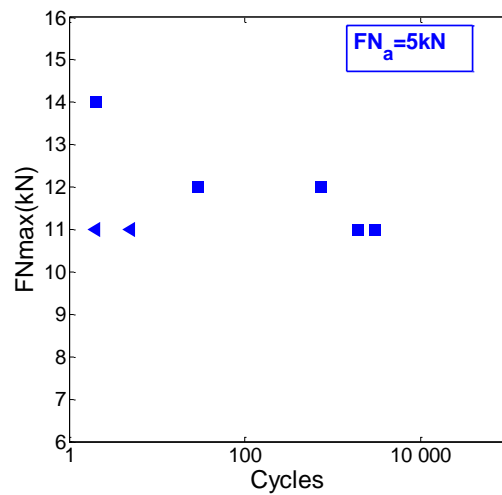


Figure IV.4-3: Fatigue lifetime under tensile loadings in FN_{max} scale, (\blacktriangleleft = premature failure).

Load		Failure	
Frequency	Ratio F_a/F_m	DN (μm)	N_f (cycles)
0.1Hz	5/8kN	8	2
	5/7kN	9	731
		5	30
	5/6kN	7	5
		8	8
		5	2,115
		5	2,029

Table IV.4-1 : List of cyclic tests under tensile loadings.

IV.5. Conclusion

The approach of the adhesive joint mechanical behavior proposed in this thesis was extended to the prediction of the cyclic behavior of 0.2mm modified Arcan specimens. Experimental and numerical investigations were performed in order to take into account the influences of the mean stress and the stress amplitude and the effect of the frequency (loading rate) in the characterization of the fatigue behavior. To achieve this goal, the approach outlined in this project was to model the viscous behavior for the adhesive joint and to investigate the numerical response in term of cumulative displacement. Under cyclic shear loading, the mean cumulative displacement (DTr) numerical response correlated the experimental response measured. For a given loading rate, experimental results under shear loading revealed that the displacement measured at failure was reproducible for each FT_a/FT_m couples tested. Taking into account this interesting experimental observation, a strain based criterion was developed. Numerical prediction of the fatigue lifetime was thus perform for loading cases involving number of cycle to failure below 10^5 . Under shear loading and for the tested loading cases, experimental/numerical comparisons in terms of fatigue lifetime allowed us, to show the relevancy of such approach.

Nevertheless, the method applied under shear loading did not seem to be applicable in its entirety under tensile-shear loading. Indeed, the value of the displacement at failure measured showed a more important scattering. Furthermore, the results of the comparison of the numerical cyclic response with the experimental data showed an important discrepancy. The 3D model was developed to take into account the influence of the hydrostatic stress. The formalism, proposed in the Chapter III, described efficiently the creep mechanical behavior under shear, tensile-shear and tensile loadings. FE analyses performed under cyclic tensile-shear and tensile loadings did not give the same quality in the experimental/numerical results comparison. Under tensile loading, since the cumulative normal displacement measured gave low values, and no reproducible evolutions under cyclic loadings, the criterion based on strain at failure was not applied.

This chapter presented the case study of bonded specimens presenting low edge effects. Concerning the use of the modified Arcan device this means that the study implied thin adhesive joints. In order to converge to an industrial approach using composite bonded specimens with thick joints, the next chapter will present results obtained using different samples and structures: evolution of the adhesive joint thickness and the nature of the adherend.

Chapter V:

Toward cyclic behavior of windmill structures: case studies

Introduction

In this last chapter, the aim was to investigate the applicability of the approach developed on Arcan specimen with low edge effects, on cases converging step-by-step to the industrial application. Therefore, in a first step, using the modified Arcan device, the case of thicker adhesive joints (2mm) will be investigated experimentally and numerically under shear and tensile loadings. Then, in a second section, the study of “hybrid” Arcan samples introducing composite blades in the middle plane of the 2mm adhesive bond-line was proposed in order to evaluate the adhesive/composite interface.

The last section of this chapter aims to study the case of a typical composite bonded joint developed in wind-blade structures. Experimentally, a bending device was developed in order to apply a specific loading to composite samples with a 2mm adhesive bond-line. A first step was to define the best specimen geometry and to validate this geometry and the loading device under monotonic loading. Then, cyclic loadings were applied to the structure and the ratcheting effect of the structure was investigated. Numerically, a FE analysis using elastic assumptions for the composite substrates and the visco-elastic visco-plastic model developed for the adhesive joint were performed in order to compare the numerical and experimental cyclic responses.

Contents

<u>V.1. Arcan specimen with thick adhesive joint.....</u>	<u>121</u>
V.1.1. Bonded specimen.....	121
V.1.2. Monotonic results	121
V.1.1. Identification of parameters for thick adhesive.....	126
V.1.2. Stress distribution under creep conditions.....	129
V.1.3. Cyclic results	131
V.1.4. Numerical simulation of cyclic tests.....	135
<u>V.2. Arcan specimen with composite blade.....</u>	<u>136</u>
V.2.1. Composite material.....	136
V.2.2. Bonded specimen.....	138
V.2.3. Monotonic results	139
V.2.4. Cyclic results	141
<u>V.3. Case study.....</u>	<u>144</u>
V.3.1. Wind blade structure	144
V.3.2. Testing wind blade structures.....	145
V.3.3. Development of a coupon-size experimental method	147
V.3.4. Experimental results	152
V.3.5. Toward a fatigue lifetime prediction: numerical investigations.....	157
<u>V.4. Conclusions.....</u>	<u>160</u>

V.1. Arcan specimen with thick adhesive joint

V.1.1. Bonded specimen

The geometry of the typical bonded specimen used for a 0.2mm adhesive joint was used to evaluate the mechanical behavior of a 2mm adhesive joint. No evolutions were brought to the bonded substrates, except the spacer's length. The positioning on the substrates of the two markers used for the measurement of DT and DN was not changed. Figure V.1-1 shows pictures of the specimen tested for 0.2 and 2mm thick adhesive.

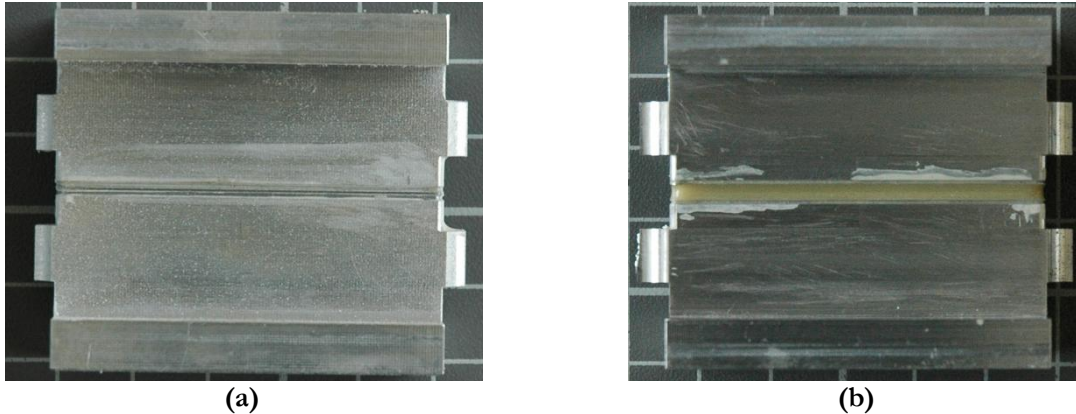


Figure V.1-1: Pictures of 0.2mm and 2mm Arcan specimens.

V.1.2. Monotonic results

Influence of the adhesive thickness was investigated on different loading cases. The cure cycle for all samples was the same as the one used for the 0.2mm bond lines thicknesses: 24h at room temperature, followed by 72h at 60°C and 48h at room temperature.

The first experimental campaign was carried out on the monotonic behavior of SikaForce®-7817 L60MR. The effect of the adhesive bond line thickness was clearly seen since important differences were observed in the mechanical behavior. Figure V.1-2 presents the mechanical response of 2kN/s monotonic shear and tensile tests for a displacement value normalized in relation with the adhesive thickness. As a first observation the mechanical behavior of the 2mm bond line specimen seems to be completely changed. For the two cases examined, the bond line thickness influences the strength of the bonded specimen, with a larger influence for tensile tests. It is clear that, depending on the load case chosen, a tendency for measured failure load to decrease with increasing bond line thickness was revealed. A similar observation can be done on the value of the displacement at failure.

Figure V.1-3a and Figure V.1-3b present the fracture surfaces obtained under shear and tensile loadings. Under shear loading, shear bands appeared clearly in the transversal view Figure V.1-4. For 0.2mm bond lines under shear loading, the failure was “cohesive” and occurred in the middle of the thickness. Concerning the 2mm thick adhesive joints, failures under shear loading were observed at the interface (close to the substrates) and could be “adhesive” in some cases at some locations on the substrate. Nevertheless, under tensile loading, the “cohesive” failure observed was conserved with the new bonded specimen geometry.

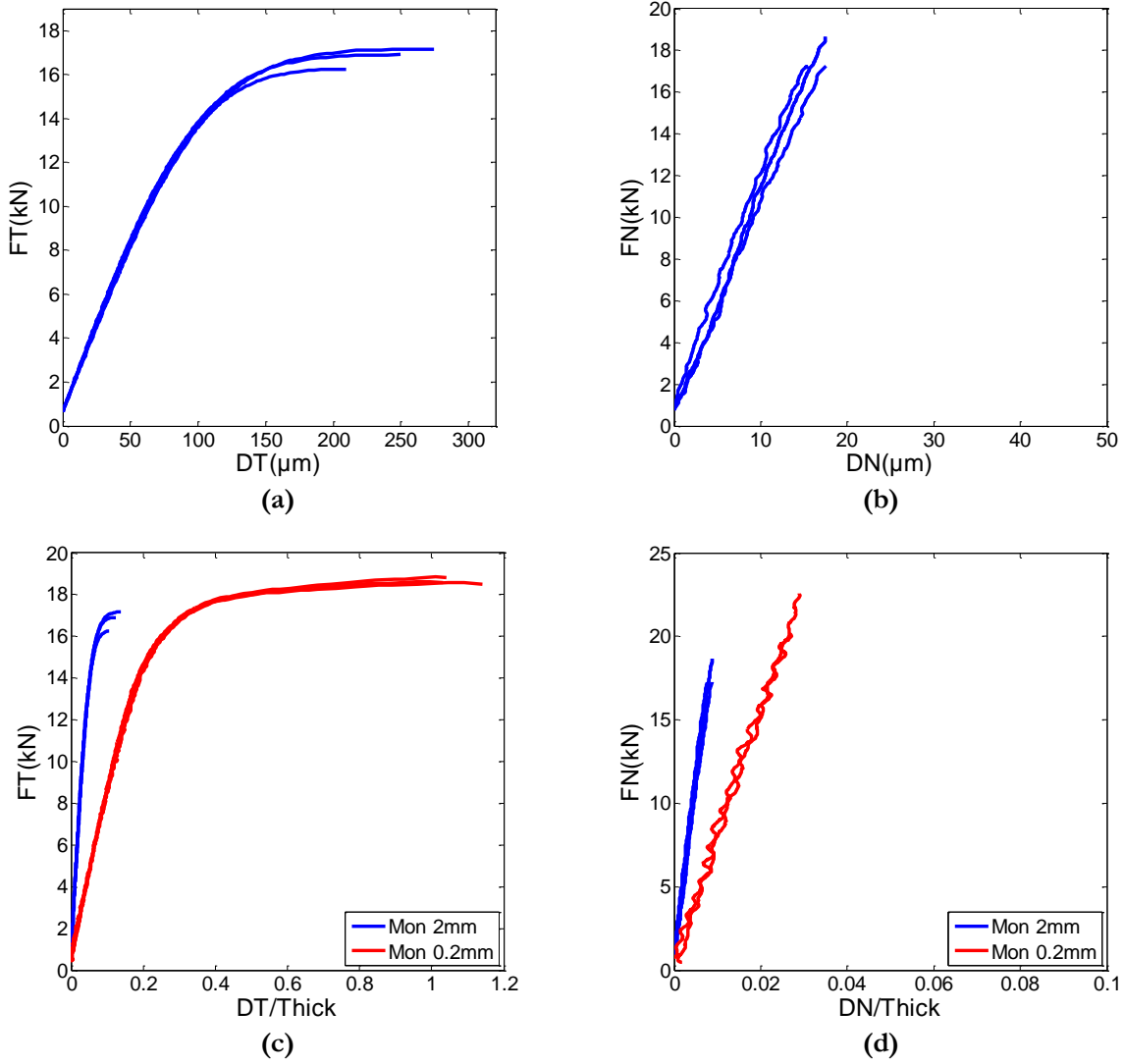


Figure V.1-2: Experimental results under monotonic shear (a) and tensile loadings (b) and comparison with results for 0.2mm thick adhesive joints (c) (d).



Figure V.1-3: Fracture surfaces: monotonic test under shear loading (a) and tensile loading (b).

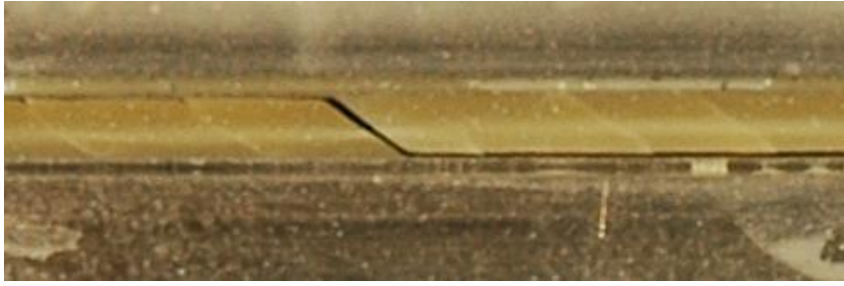


Figure V.1-4: Fracture surface under shear loading in the transversal view: appearance of shear bands in the bond-line.

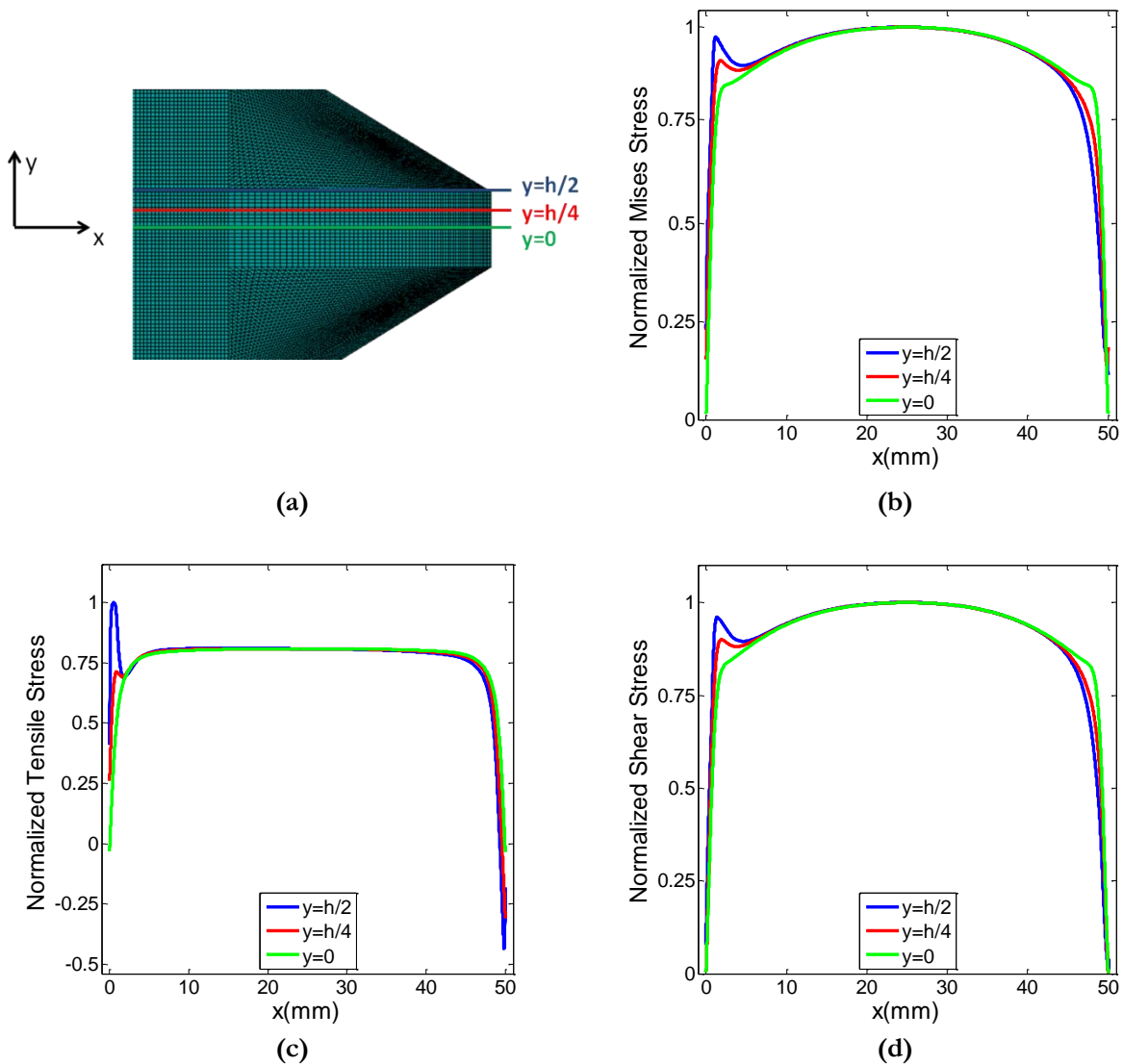


Figure V.1-5: Stress states within a 2mm bonded layer under tension-shear loading: equivalent von Mises stress (b), tensile stress (c) and shear stress (d) normalized values along the overlap length (under elastic assumptions).

A whole array of studies have already investigated the influence of the substrates local geometries on the stress concentrations for bonded joints under elastic assumptions for the adhesive (Leguillon, et al., 1987) (Kotousov, 2007) (Wang, et al., 2006) (Créac'hacdec, 2008). As it had been shown by Cognard et al. (Cognard, et al., 2010) using a modified TAST fixture including similar beak geometry, an increase in the adhesive thickness, increases the risk of crack initiation near the free edges of the adhesive.

Therefore, the analysis of the stress distribution throughout the thickness has to be performed in order to observe the strains within the adhesive joint.

With the same assumptions as the 0.2mm thickness, Figure V.1-5 shows the results of the 2D FE analysis performed with a 2mm adhesive joint. The element dimensions are conserved and 200 elements are thus used through the thickness. The simulation was performed for a ($\gamma = 45^\circ$) modified Arcan test as it permits to include both tensile and shear loading under elastic assumptions.

For this thicker bonded joint and for each component, the stress states show a dependency on the thickness level of the path considered. For a similar loading and under similar hypotheses, numerical results for thin adhesive layers (0.2 mm) showed the stress states did not evolved throughout the joint thickness. However, for 2mm specimen geometry, a thickness dependency appeared. Getting close to the substrates, a maximum value in shear stress and tensile stress is growing under the beaks.

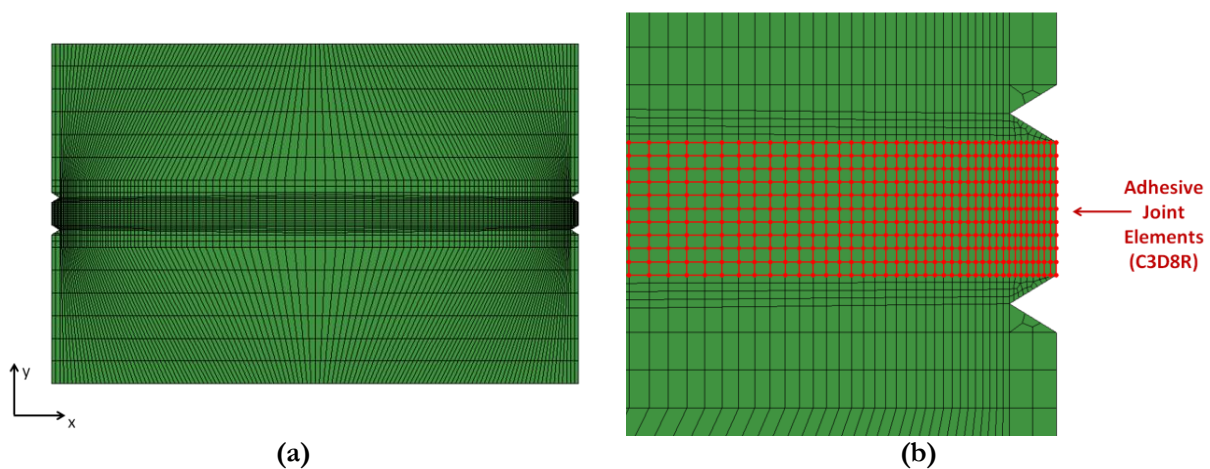


Figure V.1-6: FE mesh of the model (a) with a focus on the elements of the adhesive layer (b).

As a conclusion, increasing the thickness to 2mm, the beaks influence on the stress distribution for 0.2mm bond line was thus partially lost.

The change in specimen geometry, with increasing the bond line thickness, modified the stress state within the joint so that tests on specimens with different thicknesses are not measuring same local properties of the adhesive material. In order to evaluate the effect involved by a 2mm thick adhesive on the non-linear visco-elastic visco-plastic response, a FE simulation was performed with the constitutive equations implemented for the adhesive material behavior.

The 3D FEM used in this simulation is based on the model developed to identify the material parameters. Figure V.1-6a and Figure V.1-6b present the meshing used in the FE simulation. The element size was conserved from the 0.2mm thick specimen FEM. Only one element was taken in the thickness for the previous geometry, so that 10 elements were used in the thickness for the 2mm model. For a monotonic shear test, Figure V.1-7a shows the numerical results performed with the material constants identified. For 0.2mm under monotonic loading, the parameters were validated for shear, tensile-shear and tensile tests. However, as presented on Figure V.1-7a and Figure V.1-7b, it was clear that the material constants was not adapted to this thicker adhesive bond line and the FEM driven, to take into account the new stress profiles in the 2mm specimen model did not permit to retrieve the experimentally recorded behavior. These results were thus an evidence of changes in the adhesive material itself.

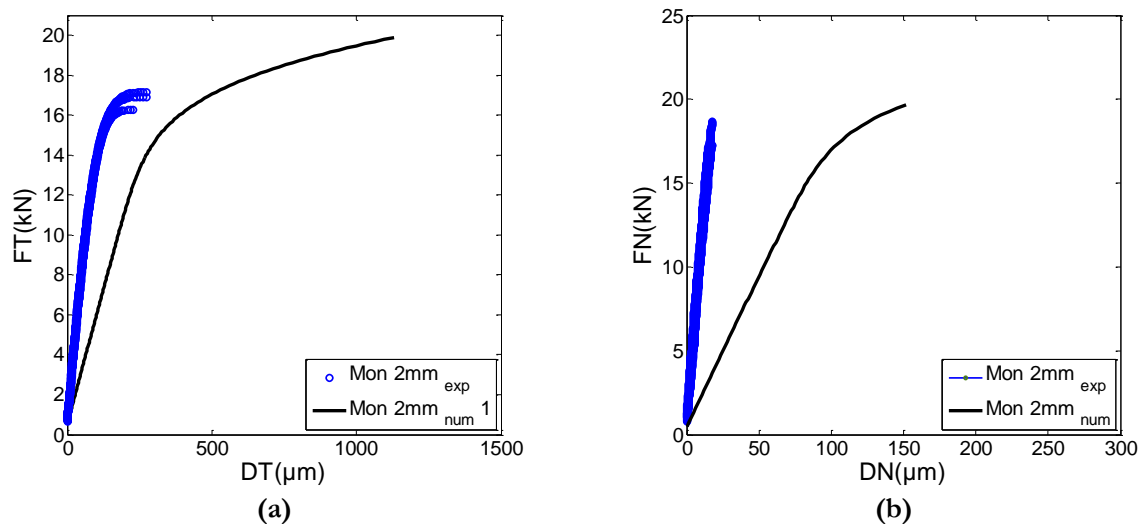


Figure V.1-7: Numerical response of the 2mm specimen for a parameter set identified on the 0.2mm thickness specimens: under monotonic shear loading (a) and under monotonic tensile loading (b).

Hence, other factors may intervene to modify the mechanical properties of the bonded specimen. Evolutions in the experimental response may be justified through modifications within the adhesive polymeric material. Davies et al. (Davies, et al., 2009), listed the factors of influence in these studies:

- The first one is linked to the defects within the adhesive joints which may vary in dimensions and in number for thicker adhesive joints. The use of a high speed mixing of the two components permit to avoid these heterogeneities and the bubbles in the bond line;
- The bonding process including a high temperature curing may cause differences in the cure conditions with the increasing of the adhesive bond-line thickness. This second factor is linked to the heterogeneous thermal behavior of the assembly and will depend on the conductivity and the proximity of the substrates. The thermal curing used in this work is sufficiently long (3 days) to consider that the temperature is harmonized in the specimen during this process;
- A third factor is considered as the effects of residual stresses (Guo, et al., 2006). The adhesive/substrates interface properties may be modified as thickness increases due to internal stresses developing during the bonding process;
- The migration of species from the environment or the substrates into the adhesive may lead to changes of stoichiometry within the adhesive near the edges and the adherend. Previous studies (Davies, et al., 2009) shown with nano-indentation and mechanical testing that for an epoxy adhesive that these phenomena could be neglected.

For polyurethane adhesives, isocyanate groups react with NH- or OH functional groups and build a cross-link network. For two component adhesive as the SikaForce®-7817 L60MR, the components were put different cans and mix before use. The curing speed depends on the reactivity of the reaction partners. The catalyst amount can be adjusted to the required production speed.

Based on the same reaction, the one component polyurethane adhesives are, for the most part, moisture curing, which means they react with water as the second component. Formulating one component moisture curing adhesives requires detailed chemistry. This chemistry is based on the fact that Polyurethane adhesives exhibit a high permeation, and migration of moisture from the environment is thus possible. Hence, curing occurs through diffusion of moisture into the adhesive and

the process may be controlled through the speed of water diffusion. Environmental conditions like temperature and humidity significantly influence the curing speed.

A drawback of moisture curing systems is the release of CO₂ when curing. An evidence of this curing process is thus the appearance of bubbles within the adhesive joint. Despite the fact that the SikaForce®-7817 L60MR in its two components formulation is not defined as a moisture curing adhesive, bubbles could appear during the curing process. Therefore, moisture in the environment may have an important role in the curing of this adhesive.

With the assumption made that moisture exchange with the air plays an important role in the curing process, a 2mm adhesive bond line have a 10 time greater surface exchange area with the ambient humidity. Hence in the following section, even if the same bonding process was performed, two different materials may be considered for the 0.2mm and 2mm adhesive bond lines thicknesses.

One of the other main aspects previously listed is the influence of the stress state involved by the use of different thicknesses. In some studies (Guo, et al., 2006), this “residual” stresses was shown to be influent on the mechanical behavior of the bonded specimen. The identification of the parameter set was made with a 0.2mm thick adhesive joint geometry, for which the particular internal stress state involved by the bonding process was not taken into account. The complex stress distribution due to these phenomena and their effects on the mechanical behavior may thus change with a modification of the bond line geometry such as the increase of the thickness. The FE analysis neglected this internal stresses, and may thus explain some differences in the mechanical behavior between the two tested geometries.

Previous studies (Davies, et al., 2009) showed, with nano-indentation and mechanical testing for an epoxy adhesive, the two phenomena putted forward could be neglected. The observations made on epoxy adhesives showing that the chemical phenomena due to the migration of species from the substrates or the environment and the “residual” stresses were negligible may not be applied on the SikaForce®-7817 L60MR adhesive. Further studies on the adhesive bond line, in the micro-scale, need to be conducted to make conclusion on this experimental phenomenon.

V.1.1. Identification of parameters for thick adhesive

Considering a new material for this thicker bond line, an inverse identification work had to be done on the 2mm experimental database. Cyclic creep tests were performed under shear loading and under tensile loading for four load levels: 4, 6, 8 and 10kN (Figure V.1-8). With the growth of the adhesive thickness, the discrepancy in the experimental results was increased. Nevertheless, as in the 0.2mm configuration, the different load values applied allow a splitting of the viscous phenomena in a reversible and a non-reversible part. Following the assumptions made in the previous sections, the time-dependent residual displacement was considered as a sign of plasticity.

The cyclic creep test was used to perform the material constants identification. Following the steps defined previously, identification of the visco-elastic parameters was performed on the lower creep level (4kN).

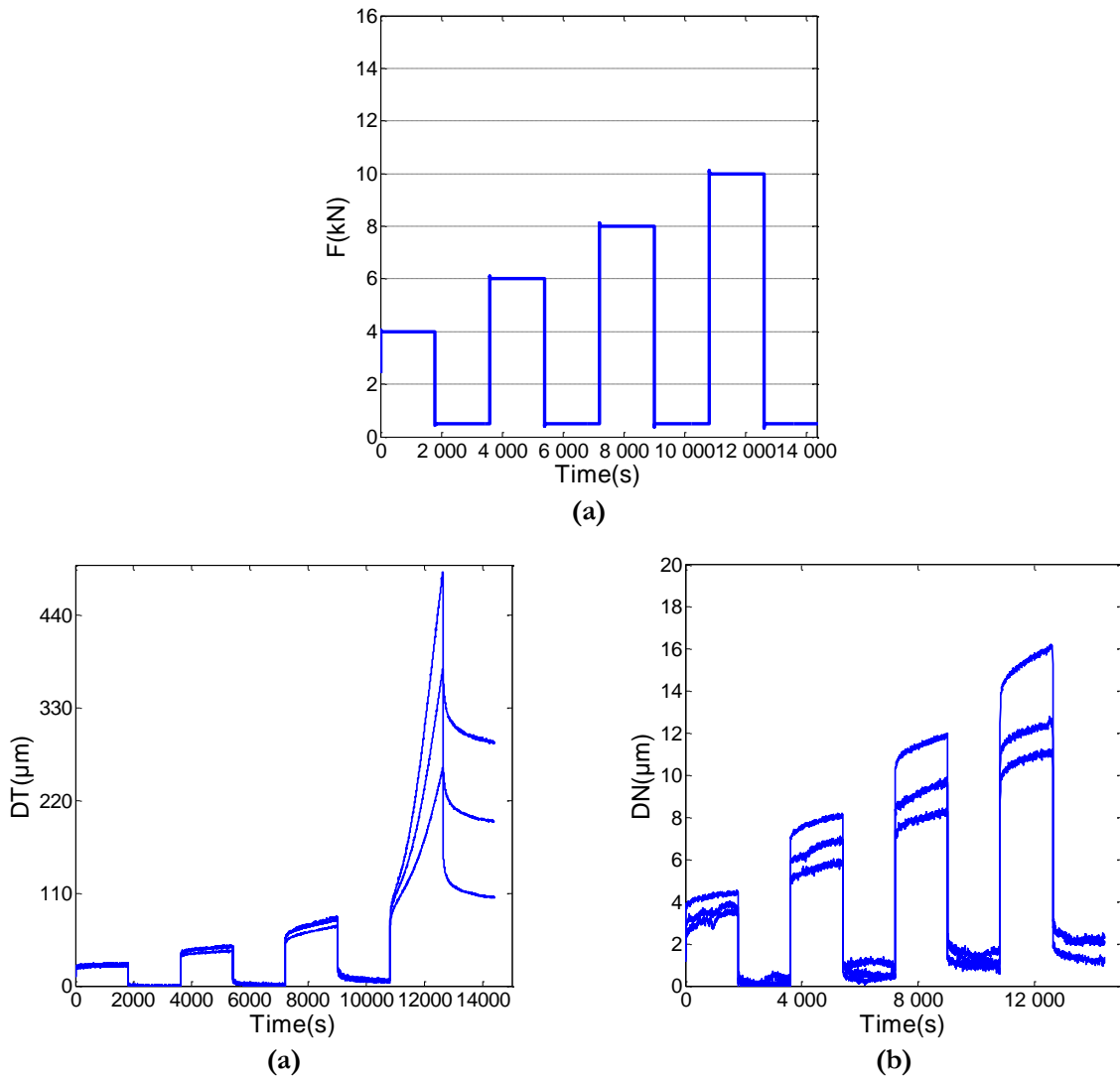
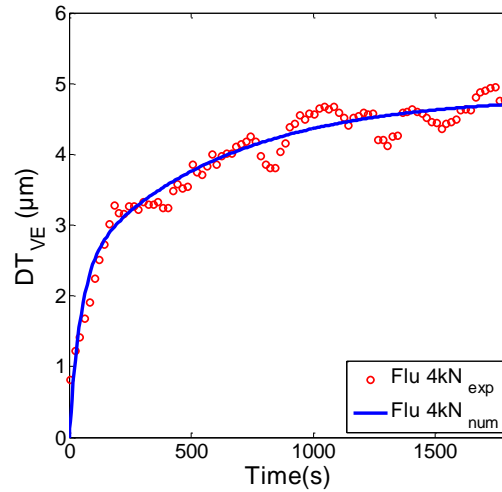


Figure V.1-8: Cyclic creep/recovery test: loading applied (a) DT vs. Time under shear loading (a) and DN vs. Time under tensile loading (b).

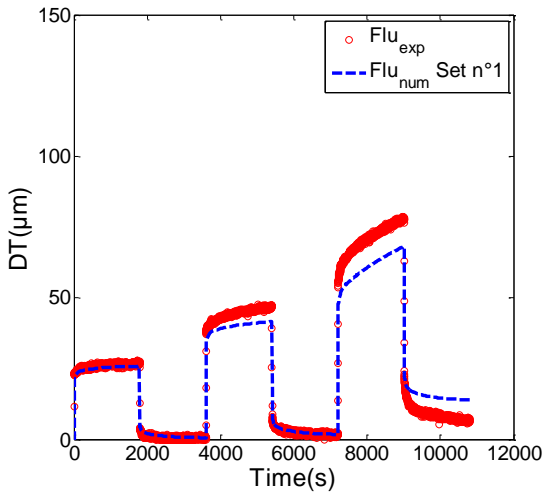
In the second step, the identification of the viscous flow function is performed on the cyclic creep test including the higher load levels. As the discrepancy is increased on the last load level, two identifications were performed:

- A first one presented in Figure V.1-9a, is performed on the experimental results without the last load level (10kN);
- A second one is performed on the experimental test showing the lowest tangential displacement. This experimental test is chosen for this second identification considering that the model do not have the necessary components to describe the highest displacements as damage is not consider in the model definition.

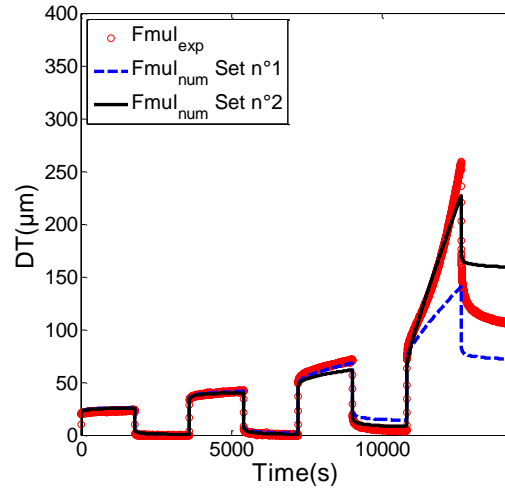
Regarding the normal behavior (Figure V.1-8b), the assumptions made on the 0.2mm adhesive joint thickness to build a visco-elastic visco-plastic model seems to be not further adapted to this new material. In the normal behavior, the plastic strains seemed to occur on each load level with a really low rate. Therefore, the flow function identified on the shear behavior may not be adapted to the normal behavior with the non associated model developed.



(a)



(b)



(c)

- **Figure V.1-9: Identification of the viscous behavior: definition of the visco-elastic parameter set (a) and definition of a first visco-plastic parameter set on 4, 6 and 8kN creep levels (b) and a second one on 4, 6, 8 and 10kN creep levels (c).**

Furthermore, the important discrepancy recorded in the cyclic-creep response did not permit to evaluate easily the mechanical response in this direction. Hence, the material parameters defining the influence of the hydrostatic stress were conserved from the previous identification work. The new parameter sets defined are listed in Table III.2-1.

Mechanical feature	Model parameter symbol		Unit	0.2mm thickness	2mm thickness	
					1 st ID strategy	2 nd ID strategy
Elasticity	Elastic Young modulus	E	MPa	$1.17 \cdot 10^3$	$2.44 \cdot 10^3$	$2.44 \cdot 10^3$
	Poisson's ratio	ν	-	0.47	0.48	0.48
Visco-elasticity	Viscous elastic shear moduli	E_1	MPa	$2.16 \cdot 10^3$	$2.03 \cdot 10^4$	$2.03 \cdot 10^4$
		E_2		$3.99 \cdot 10^3$	$2.09 \cdot 10^4$	$2.09 \cdot 10^4$
	Poisson's ratios	ν_1	-	0.47	0.48	0.48
		ν_2		0.47	0.48	0.48
	Characteristic creep time	τ_1	s	$1.34 \cdot 10^1$	$4.20 \cdot 10^1$	$4.20 \cdot 10^1$
τ_2		$8.08 \cdot 10^2$		$5.95 \cdot 10^2$	$5.95 \cdot 10^2$	
Visco-plasticity	Hardening parameter	Q	MPa	$3.10 \cdot 10^1$	$2.20 \cdot 10^1$	7.01
	Plastic threshold	R_0		$5.60 \cdot 10^1$	$5.45 \cdot 10^1$	$4.30 \cdot 10^1$
	Viscous parameter	K_{vp}	MPa.s	$1.17 \cdot 10^2$	$5.22 \cdot 10^2$	$2.43 \cdot 10^2$
	Exponent	m	-	5	5	5
	Flow function parameter	b	-	$7.40 \cdot 10^{-1}$	$7.40 \cdot 10^{-1}$	$7.40 \cdot 10^{-1}$
	Flow direction parameter	a_2	-	$2.25 \cdot 10^{-3}$	$2.25 \cdot 10^{-3}$	$2.25 \cdot 10^{-3}$

Table V.1-1 : Material parameters for a 2mm adhesive bond line defined with the two identification strategies proposed.

V.1.2. Stress distribution under creep conditions

The increase of the adhesive thickness of the Arcan sample involves that the beaks influence is partially lost. Indeed, with elastic assumptions, for a tensile shear loading case, in getting closer to the adhesive/substrate interface, FE analyses revealed growing values in the stress field under the beaks. Furthermore, considering a visco-elastic visco-plastic material for the adhesive, evolutions of the stress state happening in the bond line during the applied loading were underlined during a creep loading (Chapter III).

Therefore, using the FEM developed for the 2mm bond line specimen geometry, simulations were conducted in order to investigate the evolution of the stress distribution in the adhesive joint under creep conditions for shear loading. The constitutive model developed was implemented to model the adhesive joint behavior. This analysis on the stress distribution was performed on the closest layer of element to the substrate. Figure V.1-10 shows the numerical results concerning the evolution of the stress distribution for a $FT = 10\text{kN}$ loading at four different creep times. All the stress values were taken at the integration point of the C3D8R elements. The material constants used in this simulation are those defined by the previous identification performed on 2mm adhesive joint thickness.

The monotonic loading step led to an increase of the stresses in the entire adhesive joint with a characteristic concave profile. The blue curve named (a) in Figure V.1-10b, Figure V.1-10c and Figure V.1-10d presents the stress state for different stress components at the end of the monotonic loading step. At this step of the test, the maximum value for the von Mises stress was measured in the middle of the overlap ($x = 0$). For (b), (c) and (d) representing different creep time, a stress concentration began to appear at the edge with an exponential evolution of the tensile stress at the edge of the overlap.

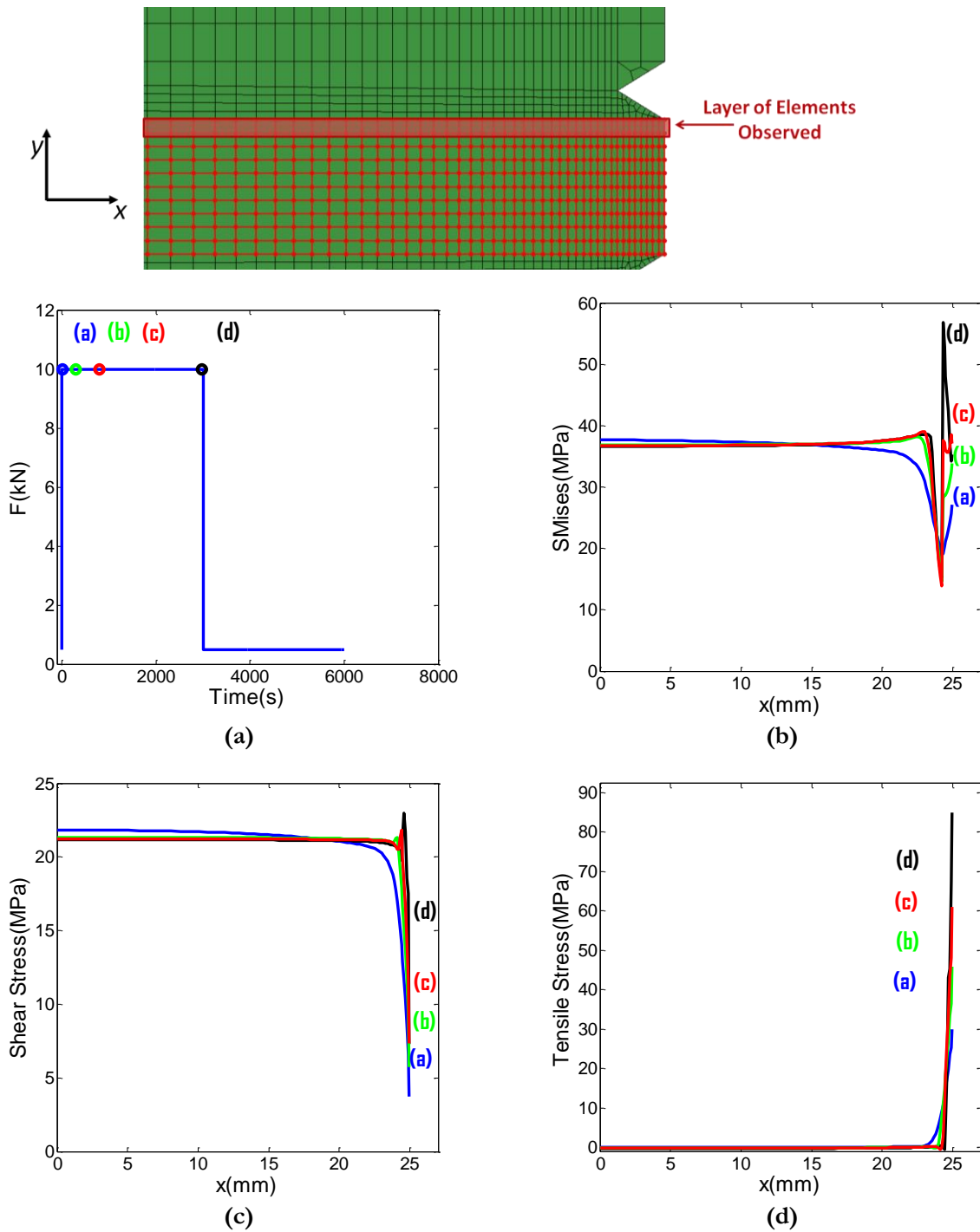


Figure V.1-10: Stress states under creep shear test (10kN) within the layer of elements closest to the substrate for a 2mm bond line: loading (F) vs *Time* (a), von Mises stress(b), shear stress (c) and tensile stress (d) along the overlap length.

Indeed, under creep loading, the stress distribution quickly evolved from the profile (a) to a stress field (b) (after 500s) which revealed for each stress component, a maximum values close to the edge of the bonded specimen. During the creep step, the stress field continued to evolve with the same trend to the state (d) in which the von Mises stress values showed a critical exponential growth in the last elements of the overlap. This concentration in the equivalent von Mises stress values seemed to be greatly driven by the increase of the tensile stress during the loading in this area.

Under constant shear loading, the viscous behavior of the adhesive material led to stress profiles evolving in time and these results underlined important edge effects within viscous adhesive materials for thicker bond lines. Indeed, at the adhesive/substrate interface, the evolutions seemed to introduce stress concentration areas at the end of the overlap growing in function of time.

The stress concentration is observed as the distribution of the von Mises stress in this layer of elements showed at the state (d) an important value close to the edge. This growth was strongly linked to the tensile stress value. Indeed, at this particular edge point, the tensile stress distribution increased all along the creep loading reaching values considerably greater than the shear stress.

As shown in Figure V.1-11, under a similar creep loading, the load and the displacement at failure measured for a 2mm adhesive joint was significantly lower than the one measured with 0.2mm adhesive joint. Therefore, as a constant load (10kN) led to increasing values over time, the tensile stresses seem to drive the failure scenarii in creep.

These stress distribution with important local values may explain the discrepancy in the experimental results under creep shear loadings. Indeed, de-cohesion issues may occur in the stress concentration areas happening at different time for different samples. Then, fracture mechanics may strongly contribute in the bonded specimen mechanical behavior.

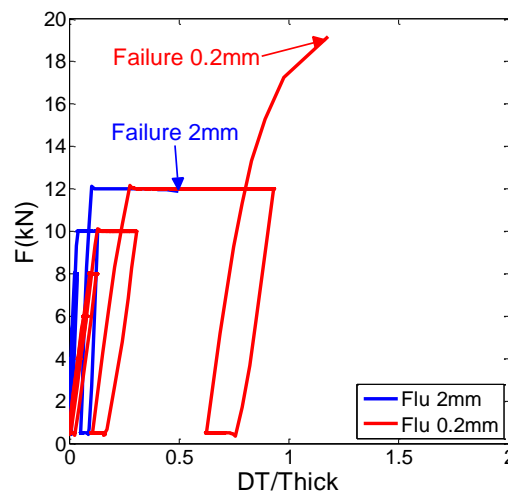


Figure V.1-11: Comparison of the mechanical behavior under cyclic-creep shear tests performed on 0.2mm and 2mm thick specimens.

V.1.3. Cyclic results

a. *Experimental results*

For the 2mm bond-lines specimen, reproducibility of the cyclic results in shear direction was tested on $FT_a = 2kN$ and $FT_m = 9kN$ loading ratio and with a $2 kN/s$ loading rate. Globally, under shear loadings, the recorded cumulative displacement presented in Figure V.1-12a in its mean value per cycle DT_r , was reproducible. The displacement at failure, recorded during these tests, was also reproducible and close to a value of $DT_f = 1mm$. In the normal direction, the mean cumulative normal displacement is plotted in Figure V.1-12b for $FN_a = 2kN$ and $FN_m = 10kN$ loading case. The mechanical behavior in this direction seems to be reproducible until a displacement value of $DN =$

30 μm which continued to evolve with a different shape, while the second one already failed. As for the 0.2mm test campaign the introduction of tensile loading seems to increase the discrepancy in the displacement and the number of cycles to failure.

A mean load influence is clearly visible on the shear direction as the ratcheting displacement accelerated with the increase of the loading case (Figure V.1-13a). Concerning the normal direction, the influence of the load amplitude was investigated in order to maximize the normal displacement and to evaluate the importance of the damage behavior (Figure V.1-13b). The two tests were performed under a similar mean load. For the lower load amplitude, the cumulative displacement was lower in the first 100 cycles but it grows rapidly in the last cycles until failure. Furthermore, for this loading case, failure occurred for a lower mean cumulative displacement (DN_r). Therefore, the load amplitude seems to influence the mechanical behavior under tensile loading.

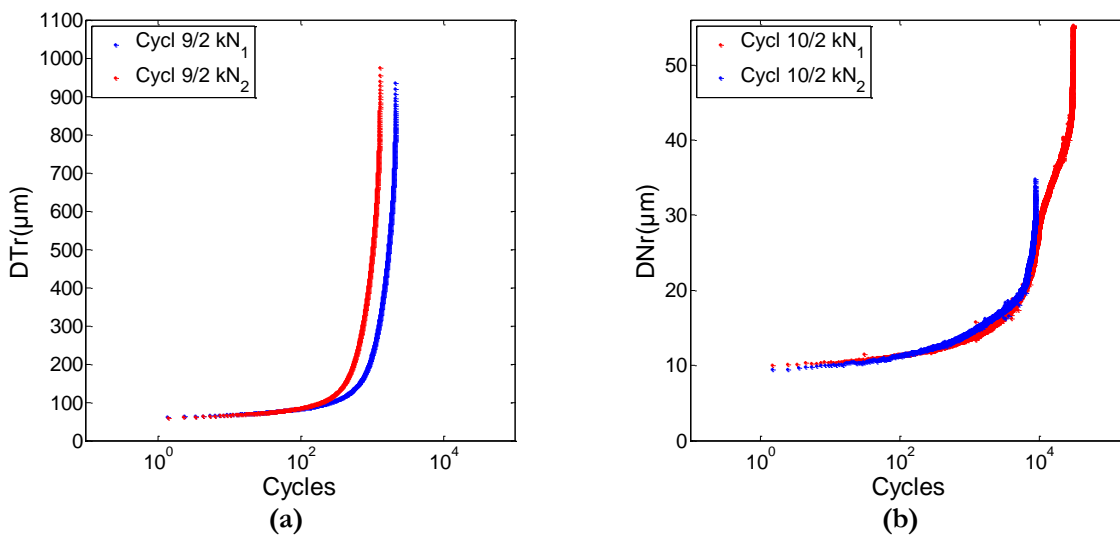


Figure V.1-12: Ratcheting effects under cyclic shear loading (DTr vs number of cycles) (a) and under tensile loading (DNr vs. number of cycles) (b).

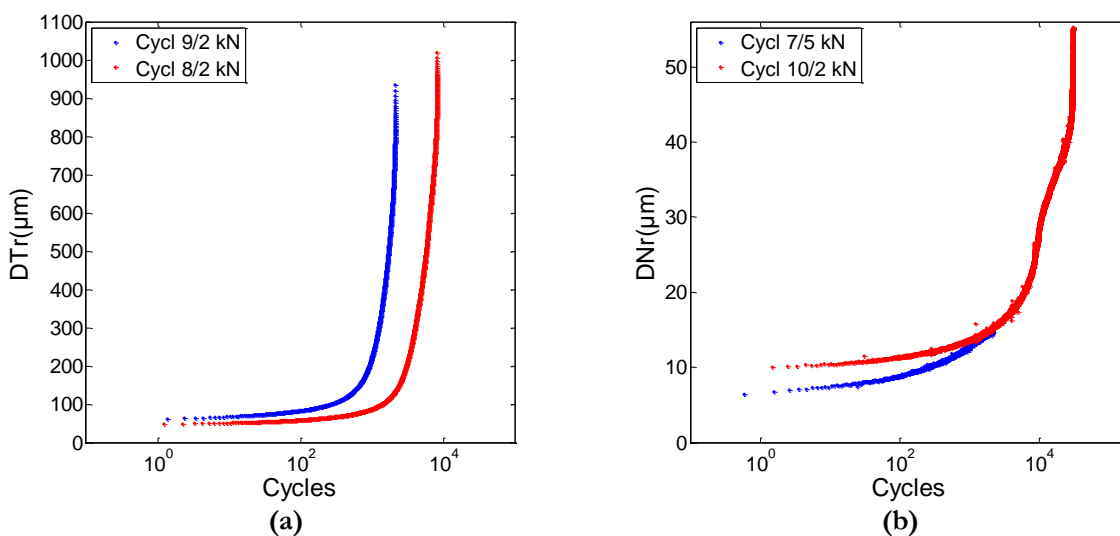


Figure V.1-13: Influence of the loading case on the cyclic behavior: tangential ratcheting (DTr) under shear loading ($\gamma = 90^\circ$) (a) and normal ratcheting (DNr) under tensile loading ($\gamma = 0^\circ$) (b).

b. Joint stiffness

The bonded specimen stiffness is taken to estimate the occurrence of damage within the adhesive bond-line or at the substrate/adhesive interface. Figure V.1-14 presents the evolution of this damage behavior marker for $FT_a = 2kN$ and $FT_m = 9kN$ (shear loading case), and with $FN_a = 5kN$ and $FN_m = 7kN$ for a tensile test (tensile loading case). These values plotted as a function of the cumulative displacement revealed appearance of damage behavior in both loading case. Although, for shear tests, damage behavior was almost not recorded in 0.2mm joints the increase in the adhesive bond-line introduced greater tensile stress component and may explain this greater evolution in thicker joints. For the tensile cyclic loadings the influence of the damage behavior was more clearly visible as the decrease of the joint stiffness was almost constant along the test.

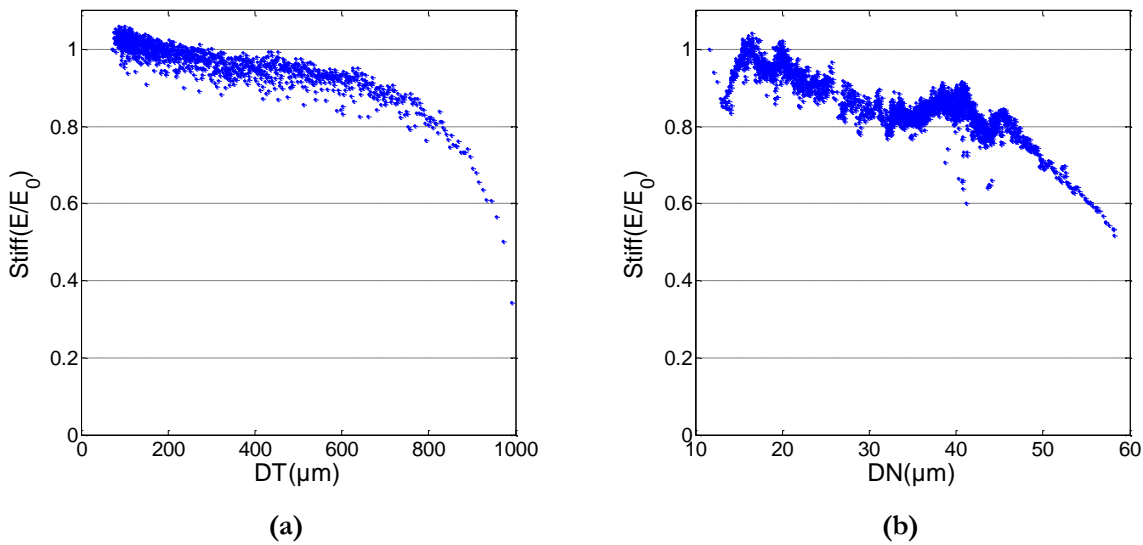


Figure V.1-14: Joint stiffness evolution: under shear loading ((E/E_0) vs. tangential displacement) (a) and under tensile loading ((E/E_0) vs. normal displacement) (b).

c. Fatigue lifetime

Results concerning the fatigue campaign proposed for thick adhesive joints are presented in Table V.1-2 for the tests performed under shear loadings and Table V.1-3 for those performed under tensile loadings. Results, for thick adhesive joints under shear loading, presented a similar cumulative displacement to failure (approximately $1000\mu m$), such as for the lower adhesive joint thickness ($0.2mm$). Under tensile loading, the cumulative displacement at failure evolved with the loading case: a growth in the load amplitude seemed to increase the value of DN at failure.

Load		Sample	Failure	
Frequency	Ratio F_a/F_m	N°	DT (μm)	N_f (cycles)
0.25Hz	2/9kN	1	1,092	2,094
		2	1,152	1,268
		3	833	2,758
	2/8kN	4	1,131	5,675
		5	1,084	9,442
		6	1,110	8,019

Table V.1-2 : List of cyclic tests under shear loadings.

Load		Sample	Failure	
Frequency	Ratio F_a/F_m	N°	DN (μm)	N_f (cycles)
0.25Hz	5/7kN	1	38	8,871
		2	58	30,527
		3	55	22,650
	2/10kN	4	21	2,147
		5	15	4,942
		6	21	5,084

Table V.1-3 : List of cyclic tests under tensile loadings.

Despite a seemingly adhesive material evolution with the two different bond line thicknesses, a comparison is performed in terms of fatigue lifetime to investigate the influence of the bond line thickness on the fatigue behavior. Figure V.1-15a shows the fatigue life as a function of a maximum tangential load FT_{max} under cyclic shear loading. For all the tests plotted in this figure, constant load amplitude ($FT_a = 2\text{kN}$) was applied. Even if the number of loading cases was not sufficient to confirm it, a first observation is clear in the trend of a decreasing fatigue lifetime with a growth of the adhesive bond line for shear loading.

In the normal direction, the results in terms of fatigue life plotted in Figure V.1-15b shows that the discrepancy is clearly reduced for thicker adhesive bond lines. Furthermore, for the single loading case, applied to three bonded specimens, the fatigue lifetime seems to increase with the thickness of the adhesive joints. Nevertheless, further experimental results have to be done in order to bring clearer conclusions on these aspects.

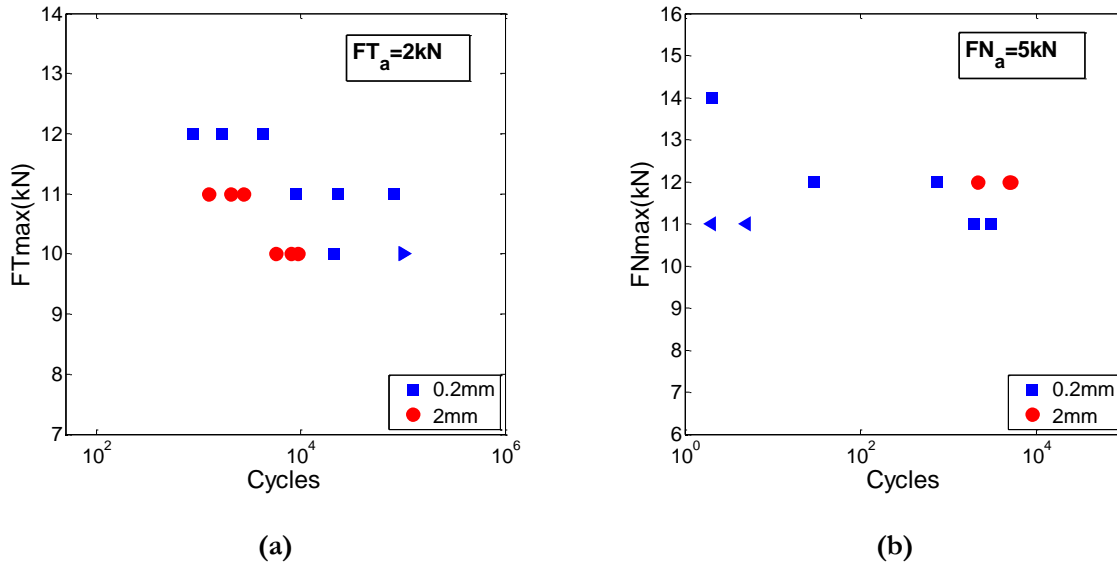


Figure V.1-15: Fatigue lifetime in F_{max} scale under: shear loading ($\gamma = 90^\circ$) (a) and tensile loading ($\gamma = 0^\circ$) (b) (\blacktriangleright = stopped, \blacktriangleleft = premature failure).

The principal weakness of the 2mm geometry is the appearance of edge effects which may lead to the early failure in the monotonic tests performed, in terms of displacement and load at failure. Appearance of stress concentration areas in the bond line may also be characterized by earlier failure in the shear fatigue behavior. A second observation is the stiffness decrease, on both tensile and shear behaviors, which may be induced by the introduction of significant defects. Evidences of defects varying in size can be observed in the fracture surfaces.

However, the increase of the adhesive thickness also led to clear modification in the adhesive material parameters. Therefore, these observations seem to confirm the fact that two materials were tested with the two different adhesive bond-line thicknesses. Results in the tensile behavior thus led to important variations in terms of fatigue lifetime as 2mm adhesive joint are more reproducible and had a more important fatigue lifetime.

As a first conclusion, the adhesive joint seems to need a minimal exchange surface area with the ambient air to complete the material polymerization.

V.1.4. Numerical simulation of cyclic tests

A numerical simulation of the cyclic shear behavior was performed for two loading cases with different mean loads. The simulations were performed for the two parameter sets defined with the two different identification strategies. The first parameter (Figure V.1-16a) set identified from the three first load levels of the cyclic creep curve clearly underestimated the cumulative displacement under cyclic shear loading. The second parameter set (Figure V.1-16b) permitted to retrieve a better mechanical behavior even if the transition to the steady state was not greatly defined. Therefore, even if more scattering was observed in the experimental results, the 10kN creep level seems to be necessary to retrieve the cyclic behavior. The three first load levels (4, 6 and 8kN) were not enough for the identification of the parameter sets. This observation was consistent with the fact that the maximum value under cyclic loading FT_{max} drives the fatigue behavior. Indeed, a parameter set identified on experimental tests without data on high loading creep levels (Set n°1) were not efficient.

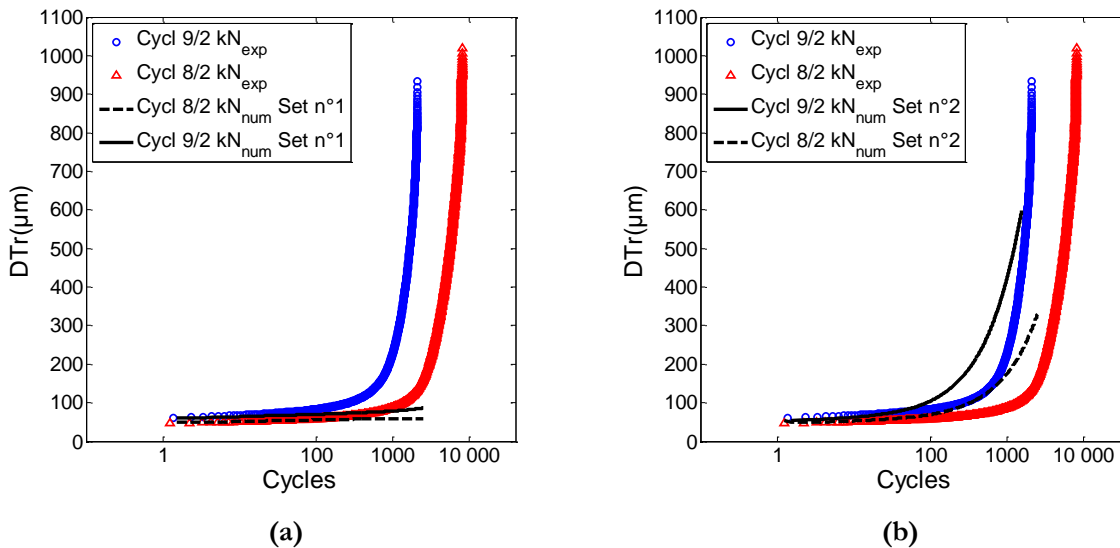


Figure V.1-16: Experimental/numerical comparison of the cyclic behavior with two parameter sets: material constants defined with the 4, 6 and 8kN creep levels (a) and material constants defined with the 4, 6, 8 and 10kN creep levels (b).

V.2. Arcan specimen with composite blade

V.2.1. Composite material

The composite material used was a glass fiber reinforced composite material from ITA. In this study, a linear assumption is made for the composite material ($\underline{\epsilon}_{ve} = \underline{\epsilon}_{vp} = \mathbf{0}$). Unidirectional composite materials with long fibers composites “UD” represent the basic element in modeling all laminates. They are considered as transversely isotropic materials composed of two phases: the reinforcement phase and the matrix phase. Therefore, considering a unidirectional layer (Figure V.2-1a), the relation between the stress tensor $\underline{\sigma}$ and the strain tensor $\underline{\epsilon}$ may be written as:

$$\underline{\epsilon} = \underline{\underline{S}} : \underline{\sigma} \quad (\text{Eq 1.94})$$

where $\underline{\underline{S}}$ defines the compliance of a transversally isotropic material. Noting that the direction 1 is along the fiber, the compliance is given as follow:

$$\underline{\underline{S}} = \begin{bmatrix} 1/E_1 & -\nu_{12}/E_1 & -\nu_{12}/E_1 & 0 & 0 & 0 \\ -\nu_{21}/E_1 & 1/E_2 & -\nu_{23}/E_2 & 0 & 0 & 0 \\ -\nu_{21}/E_1 & -\nu_{23}/E_2 & 1/E_2 & 0 & 0 & 0 \\ 0 & 0 & 0 & \frac{2(1+\nu_{23})}{E_2} & 0 & 0 \\ 0 & 0 & 0 & 0 & 1/G_{12} & 0 \\ 0 & 0 & 0 & 0 & 0 & 1/G_{12} \end{bmatrix} \quad (\text{Eq 1.95})$$

The effective stiffness and compliance matrices are thus defined in the elastic regime by five independent engineering constants: longitudinal and transversal Young moduli E_1 and E_2 , longitudinal and transversal shear moduli G_{12} and $G_{23} = \frac{E_2}{2(1+\nu_{23})}$ and the major Poisson's ratio $\nu_{12} = \nu_{21}$. The engineering constants of the glass/epoxy composite material used were identified following the ISO 527-4 and ISO 527-5 standards (ASTM). Therefore, the identification of the five parameters was made on three unidirectional tensile tests on three different laminated composite materials. During these tests, gauges permitted (Figure V.2-1b) to follow the strains in the transversal and longitudinal directions. Table V.2-1 details the material constants identified on each test.

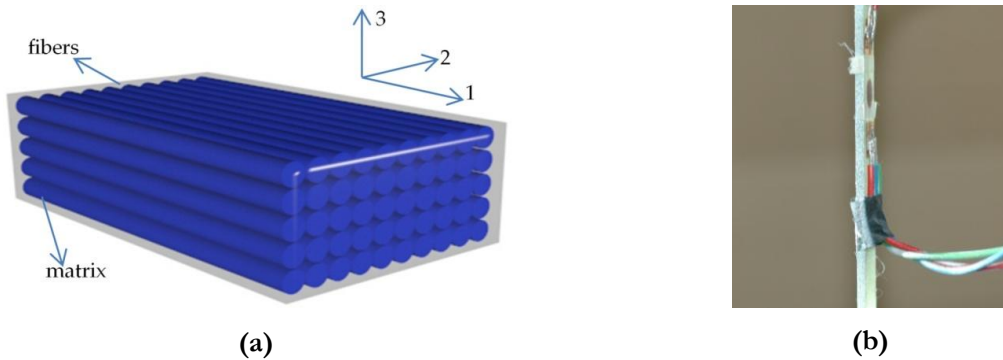


Figure V.2-1: Description of a unidirectional layer of glass fiber reinforced composite (a) and strain measurement with gauges on a standard tensile test (b).

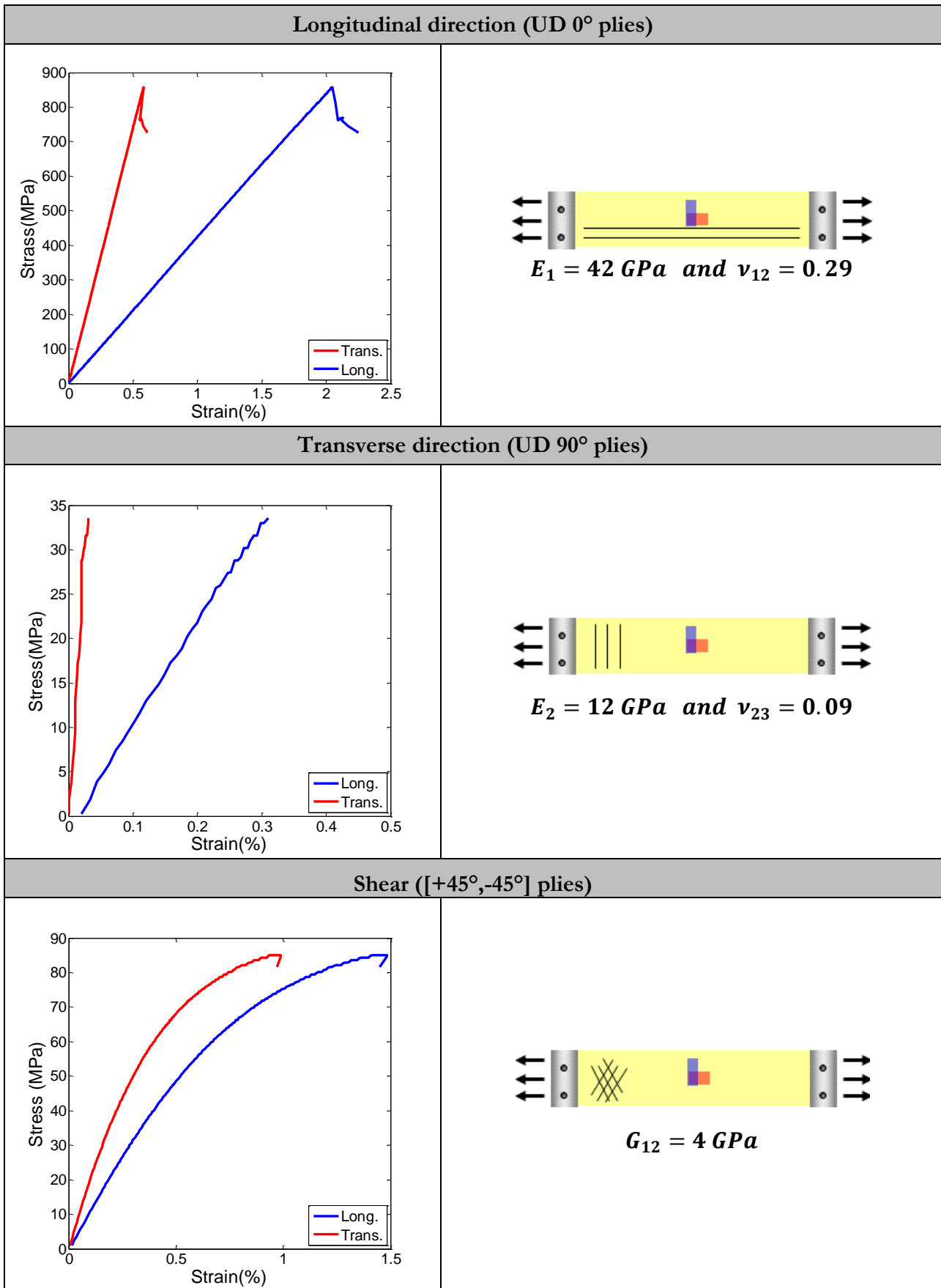


Table V.2-1 : Table of the characterization tests defined by the ISO 527-4 and ISO 527-5 standards with the engineering constants identified values.

V.2.2. Bonded specimen

The mechanisms of adhesion are strongly linked to the substrates used. In order to evaluate the abilities of a structural adhesive for composite material bonding a characterization test was implemented. The test method was proposed by (Cognard, et al., 2010) for composite bonding optimization through a modification of the Arcan test. As shown in Figure V.2-2, specimens were adapted to a hybrid assembly aluminum-adhesive-composite-adhesive-aluminum. During the bonding process, a 2mm thick composite blade ($95 \times 14 \text{mm}^2$) is placed between the two substrates with an adhesive layer (of 1mm each) on both sides. These hybrid bonded mini-structures permit to keep the same Arcan device for the testing method.

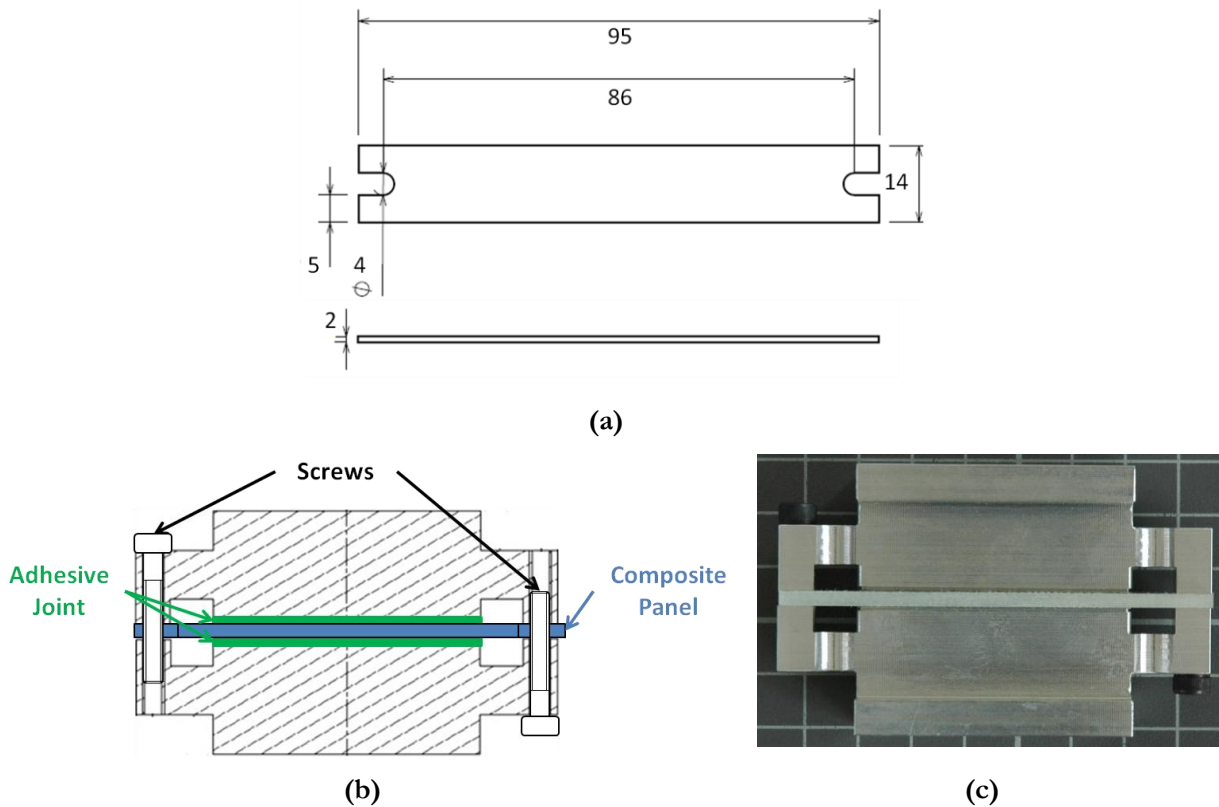


Figure V.2-2: Presentation of the hybrid bonding process: composite blade main dimensions (in mm) (a), drawing (b) and image (c) of the bonding assembly.

For the previous experimental tests, the edge effects were limited at the aluminum-adhesive interface, using a machining of beaks on the substrates. Therefore, following the same assumptions, linear numerical studies are performed to investigate the stress states within the adhesive bond line. Normalized stress profiles, under tensile-shear loading, are shown in Figure V.2-3 following six paths (z positions). FE analyses are performed on a 1mm bonded joint on each side of the composite blade. As no local geometry is defined for the adhesive-composite interface ($y = -h/4$), the equivalent von Mises stress shows a high value at the edge of the overlap. Indeed, for the bond line thickness considered the right local value becomes much higher for the tensile stress and the same phenomenon appears in the shear stress. The specific beaks, developed for thin adhesive joints to avoid stress concentration in the overlap using beaks, were not efficient for this hybrid bonded joint and the edge effects are important at the composite-adhesive interface.

In his thesis, Créac'hcadec (Créac'hcadec, 2008) analyzed the effects of the cleaning of the adhesive bond line and the shape of the edges for these hybrid assemblies. The importance of the free edges geometry was underlined and the machining of specific geometries may permit to limit these edge effects. However, due to its material properties, the machining of a long fiber composite blade reducing could not be considered in this study as it may degrade its mechanical behavior.

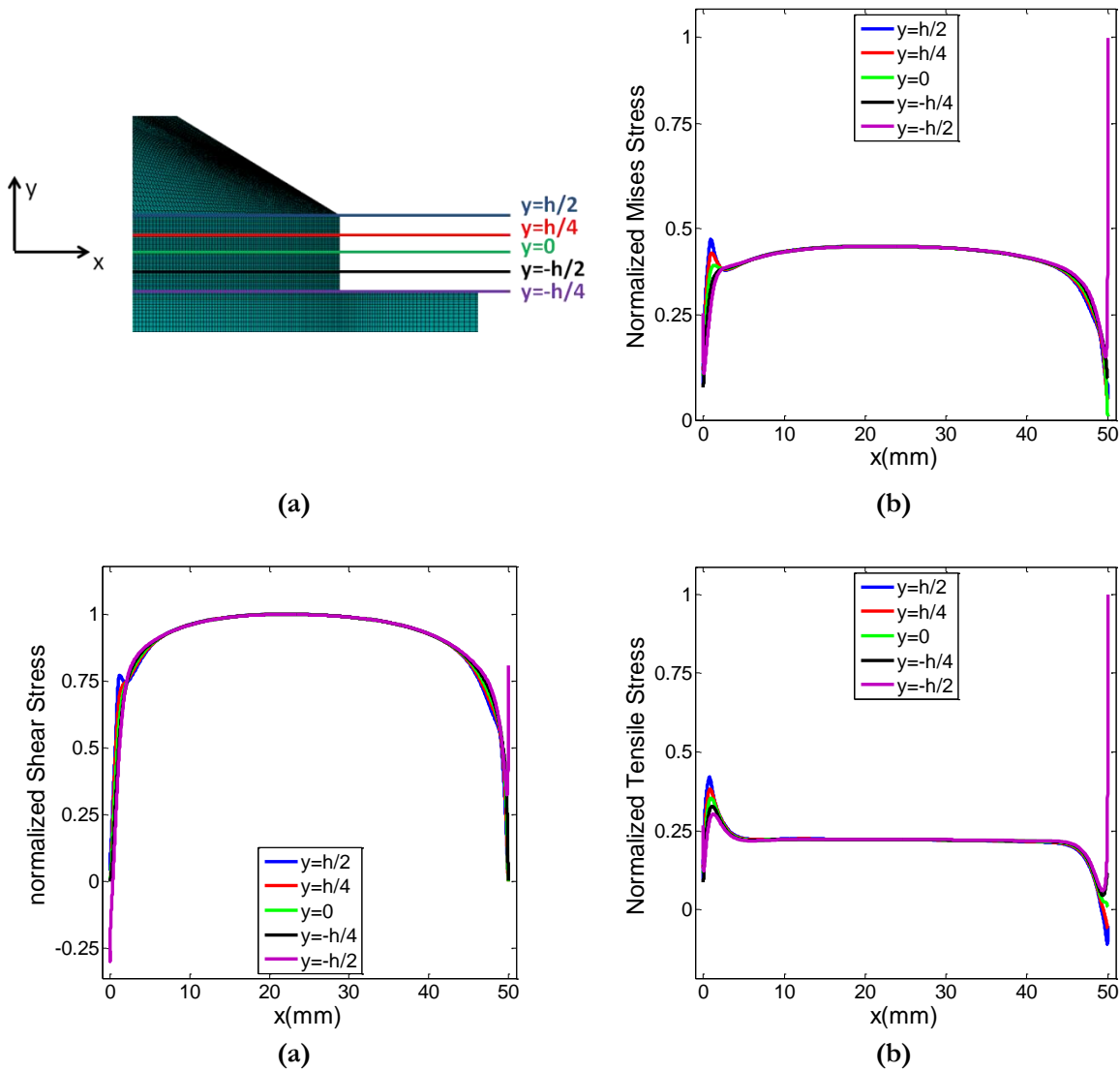


Figure V.2-3: Stress states within 1mm bonded layer and composite blade under tension-shear loading: tensile (a) and shear stress (b) normalized values along the overlap length (elastic assumptions).

V.2.3. Monotonic results

The experimental process presented in the previous chapters was conserved. The relative displacement is measured on the aluminum substrates for the same markers as defined for the simple specimen. Figure V.2-4 shows the view of the 3D real time sensor for a bonded specimen with the two markers.

Figure V.2-5 presents the experimental response of the hybrid specimen under monotonic tensile and shear loadings. In these diagrams are plotted the results for a simple 2mm bonded joint and a specimen including a UD 0° 2mm composite blade between two adhesive bond lines. As the response of two bond lines was considered in the measurements performed on the hybrid specimen, the adhesive joint

thickness was divided by two. The curves from both tested assemblies revealed a similar shape except a slight variation in the linear part for tensile and shear loadings. Figure V.2-6 presents some fracture surfaces for these both loadings on composite assemblies. As no damage was clearly visible in the composite failure, the adhesive mechanical behavior joint seems to drive the failure of the hybrid specimen. The adhesive mode of failure systematically appeared at the composite/adhesive interfaces or at the aluminum/adhesive surfaces. As these interfaces were revealed to be the critical areas for appearance of stress concentrations, edge effects seem to be responsible of the specimen failure. Therefore, as a first observation, the linear assumptions made on the composite material seem to be sufficient in order to explain the recorded differences in the mechanical behaviors.

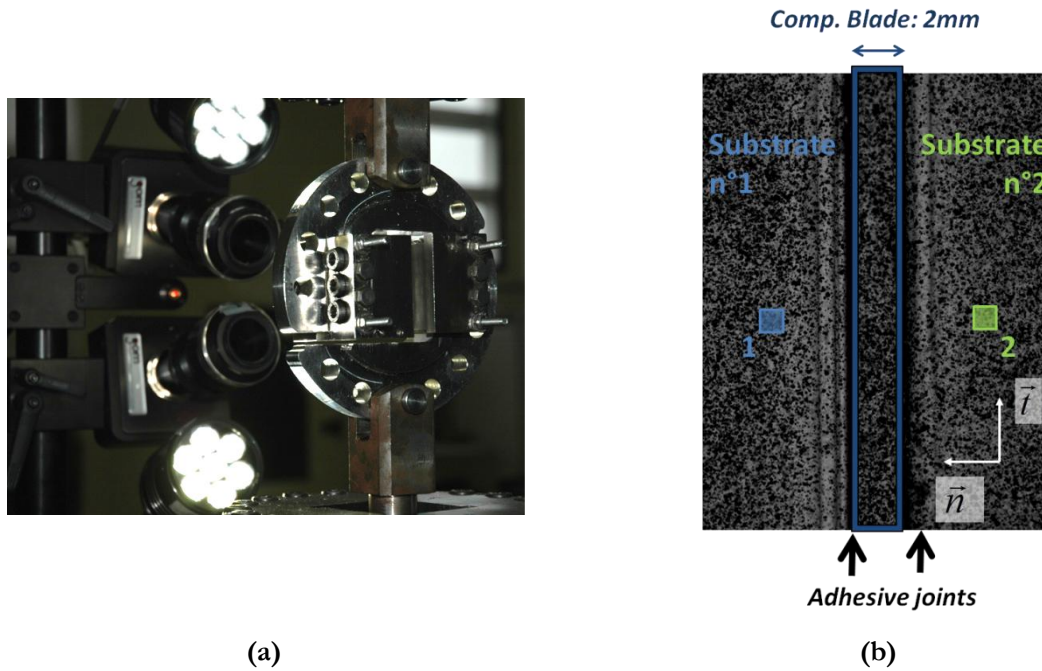


Figure V.2-4: Modified Arcan device under shear loading with 3D real time sensor GOM device (a) 3D real time sensor view of the bonded specimens using markers (1 & 2) to measure the relative displacement of the substrates in the shear (\vec{t}) and tensile directions (\vec{n}) (b).

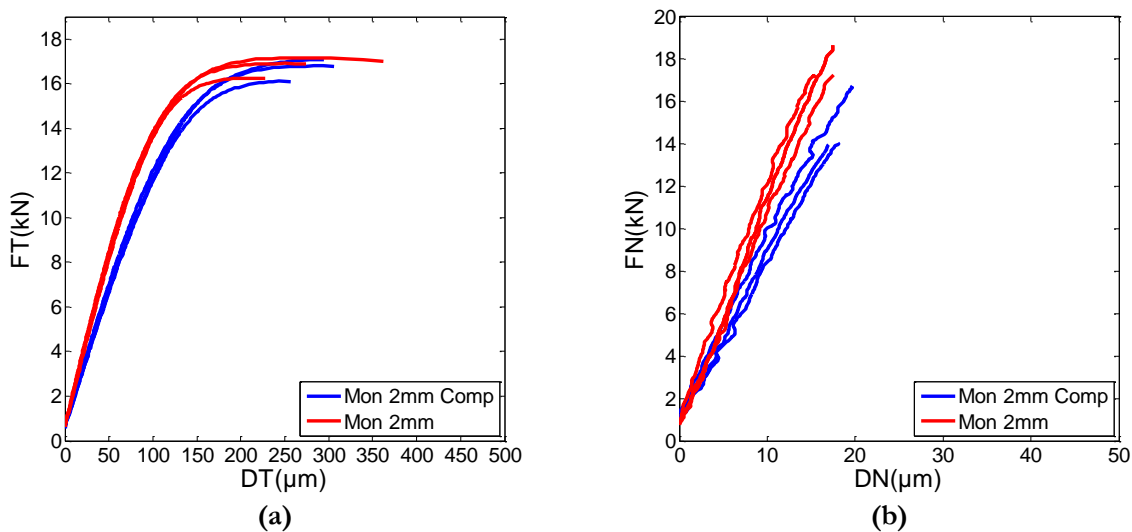


Figure V.2-5: Monotonic tensile-shear tests results (compared to 2mm adhesive joint without composite blade): FT vs. DT (a) and FN vs. DN (b).

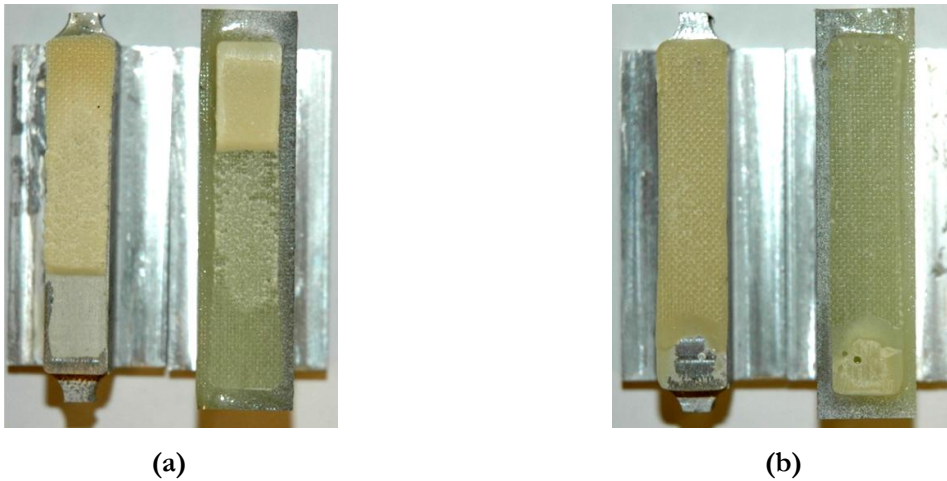


Figure V.2-6: Fracture surfaces: under monotonic shear loading (a) and tensile loading (b).

V.2.4. Cyclic results

In Figure V.2-7 are plotted the experimental results of the hybrid assemblies under cyclic shear and tensile loadings. In terms of ratcheting effect, both mean tangential and normal displacements seem to define a same fatigue behavior as observed with the 2mm simple specimen. Nevertheless, a difference in the instantaneous mechanical behavior may be observed from the beginning of the plotted curves with an increase of the displacement value.

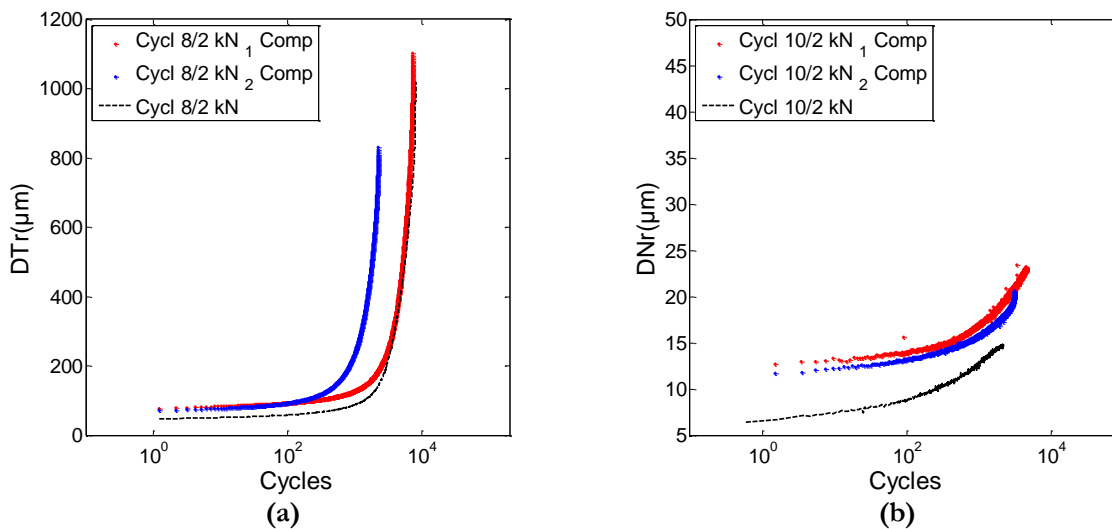


Figure V.2-7: Ratcheting effects under cyclic shear loading (DTr vs. number of cycles) (a) and under tensile shear loading (DNr vs. number of cycles) (b).

The effect of mean load on the bonded joint in the hybrid assembly seems to be conserved. Indeed, as presented on Figure V.2-8, for equivalent load amplitude the cumulative displacement accelerated with the increase of the mean load. These phenomena were clearly visible in the tangential direction for a shear loading (Figure V.2-8a) as the displacement were more important, but the same conclusions could be brought in the normal direction (Figure V.2-8b).

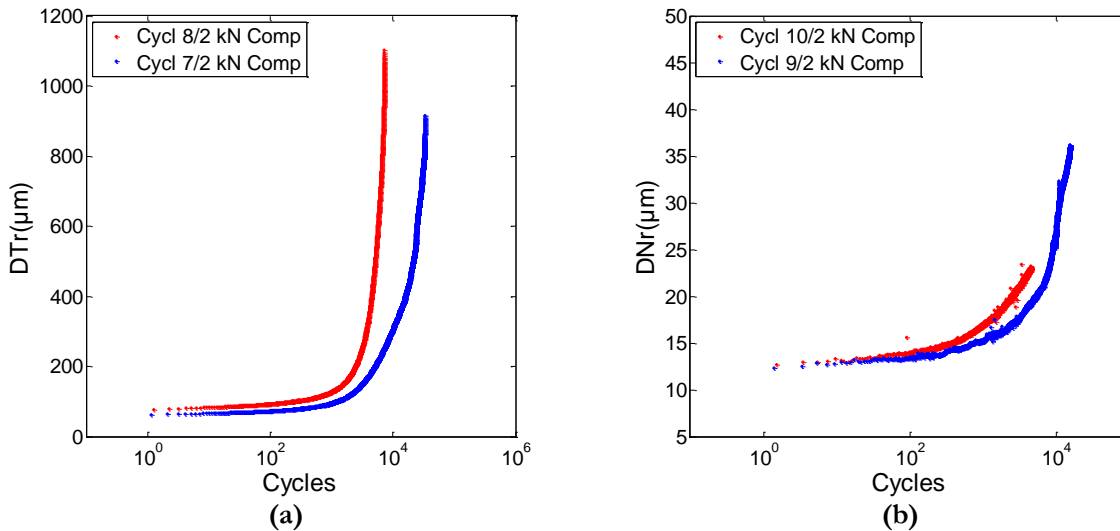


Figure V.2-8: Mean load influence on the ratcheting effect: under shear loading (DTr vs. number of cycles) (a) and under tensile loading (DNr vs. number of cycles).

a. Numerical prediction

3D FE simulations were performed in order to investigate the mechanical behavior of the bonded specimen with composite blade. The FEM was based on the previous numerical model developed for the modified Arcan specimens: reduced integration elements C3D8R were used in this model, size of elements and the refinement performed close to the beaks area in the bond lines were conserved and meshing of the substrates was similar. The composite blade was meshed with ten elements in the thickness. Figure V.2-9a presents the meshing of the hybrid assembly. The material constants, used for the mechanical behavior of the two 1mm bond lines, were those identified on the 2mm bonded samples with the second identification strategy.

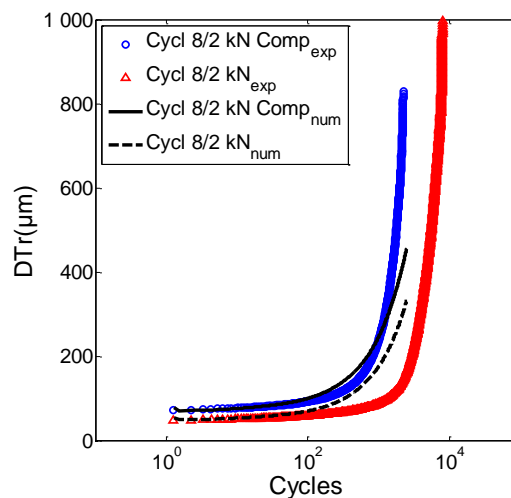


Figure V.2-9: Experimental/numerical comparison of the influence of the composite blade: tangential ratcheting displacement (DTr) vs. number of cycles (b).

As shown in Figure V.2-9b, the second parameter set permitted to retrieve the mechanical behavior under cyclic loading observed experimentally. The difference in terms of ratcheting effect, due to the introduction of the composite blade, was well described under the elastic assumptions made for the glass fiber composite.

b. *Fatigue lifetime*

The results in term of number of cycles at failure are listed in Table V.2-2 and Table V.2-3. Concerning the cumulative displacement, the same conclusions as those made on the thick adhesive joints without composite blade may be underlined. Despite a more important discrepancy, the cumulative displacement at failure seemed to give quite reproducible values.

In order to evaluate the influence of the maximum load, these results are plotted for specimen under shear loading in Figure V.2-10a and tensile loading in Figure V.2-10b.

Load		Sample	Failure	
Frequency	Ratio F_a/F_m	N°	DT (μm)	N_f (cycles)
0.25Hz	2/9kN	1	655	3
		2	1,158	7,275
	2/7kN	3	894	2,240
		4	1,074	30,749
		5	1,098	22,241
		6	966	32,957

Table V.2-2 : List of cyclic tests under shear loadings

Load		Sample	Failure	
Frequency	Ratio F_a/F_m	N°	DN (μm)	N_f (cycles)
0.25Hz	2/10kN	1	42	41,007
		2	26	4,480
		3	23	3,091
	2/9kN	4	27	5,676
		5	28	30,159
		6	39	15,115

Table V.2-3 : List of cyclic tests under tensile loadings

The conclusions made on the experimental results obtained with the Arcan specimen with a 2mm bond line may be extended to the results obtained with the introduction of a composite blade as the fatigue lifetime observed were quite similar. Nevertheless, the hybrid specimen introduced a more important discrepancy in fatigue life measured for both normal and tangential directions.

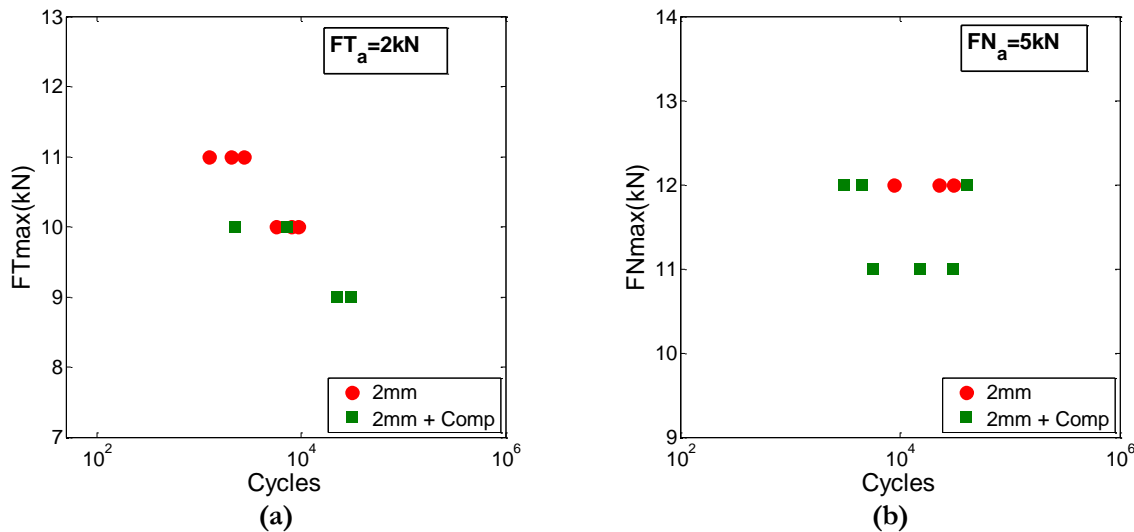


Figure V.2-10: Fatigue lifetime in F_{max} scale under: shear (a) and tensile loadings (b).

V.3. Case study

The previous cases allowed the investigation of the viscous phenomena on different Arcan specimens. In this section, the study of composite bonded specimens with thick adhesive joints will be performed.

V.3.1. Wind blade structure

Generally a wind turbine should work for 20-25 years without repair and with minimum maintenance. Therefore, durability was pointed out as an essential aspect for wind turbine designs (Jensen, et al., 2006) (Mishnaevsky). One of the main work of the wind blades in the case of durability means:

- The blade deformations should remain very small in order to sustain the aerodynamic properties and to avoid hitting other parts of the wind turbine;
- The effects of materials damaging due to cyclic loading from the rotation and the wind loads are negligible.

The high reliability of modern wind blades became especially important as the increase of the dimensions made the maintenance and the repairs on wind turbines extremely difficult and expensive.

Among all the parts of wind turbines, composite materials are mostly used in blades. Wind blade is the key-component of an efficient wind turbine, whose properties should determine performances and lifetime of the turbine. Therefore increasing the lifetime and the abilities to bear cyclic loadings for these products, is an important problem for the designers.

The different wind blade parts and their functions are detailed in Figure V.3-1 and Table V.3-1. The blade skin is and the shear webs are often produced with $\pm 45^\circ$ laminates, whereas, in the root area, tri-axial materials are utilized $\pm 45^\circ/90^\circ$ (Ustunel, 2006).

Part	Function	Materials used
Blade shell	Maintaining the blade shape, resisting the wind and gravitation forces	String and lightweight composites
Integral web, spars or beam	Resisting the shell buckling / shear stresses due to flap wise bending	Biaxial lay-ups at $\pm 45^\circ$
Adhesive layers between composite plies, and web and the blade shell	Ensuring the out-of plane strength and stiffness of the blade	Strong and highly adhesive matrix

Table V.3-1: Description of the functions associated with the mechanical features of a wind blade.

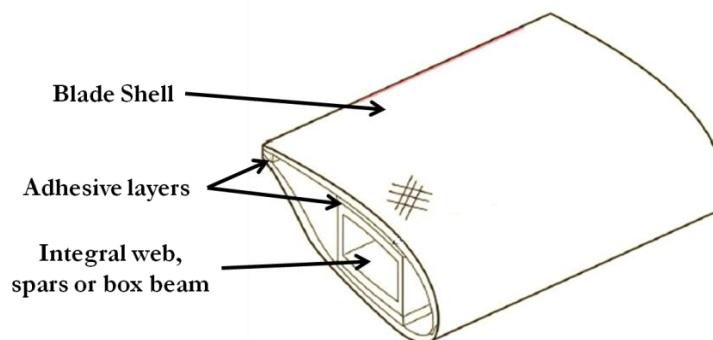


Figure V.3-1: Scheme of the section of a wind blade.

V.3.2. Testing wind blade structures

Testing wind blade is a critical factor in maintaining high levels of reliability and evaluating the latest technological developments in materials and airfoils. Therefore, the research of an adequate testing is needed by wind energy in order to be more competitive.

a. *Full-scale tests*

Recently large blade testing centers have been developed to offer blade testing in full scales (Maine) (Massachusset). Generally, as shown in (Figure V.3-2), in these tests design, the blade is pulled in the horizontal or vertical axis, flap-wise or edgewise, in order to measure the deflection of the blade and strains within the different components. These latest facilities permit to perform static tests for wind blade length up to 90 meters with horizontal displacement up to 32 meters, horizontal displacement up to 21 meters and with a maximum bending moment of 84 MN.m. Fatigue testing may be performed using hydraulic inertial resonance excitation generating 20 years of cyclic field loads in a matter of months. Testing wind blade in full scale permit to simulate what a blade goes through in its lifetime on a wind turbine and to evaluate its capacities to bear cyclic loadings. Furthermore, these tests permit to investigate what are the failure scenarii involved in the full structure (Figure V.3-3), and the weaker components. Nevertheless, the major part of the testing facilities only permits to generate uni-axial fatigue loadings on a single point of the structure. Until further developments, the testing devices can not accurately simulate the real loading endured by the wind blade during its service life.



(a)



(b)

Figure V.3-2: Large blade testing centers: monotonic tests performed flap-wise (a) and edge-wise (b).



(a)



(b)

Figure V.3-3: Failure scenarii in full-scale tests: failure appearing in the blade shell (a) and in the adhesive bond line between the blade shell and the box beam (b).

b. Sub-structural tests

Full scale tests remains so expensive and time consuming that they are performed as a final validation of a prototype or as a certification test of the wind turbine. Furthermore, a disadvantage of full-scale tests is that the full-structure fails locally. Therefore, full-scale tests on wind turbine blades frequently showed static and fatigue failures at stresses and strains well below the values to be anticipated from materials tests (Mandell, et al., 1998). This implies that either the materials perform less well in structures than they do in small laboratory material testing, or that structural problems are leading to premature failure. The main objective of testing sub-structural elements is to develop, in an intermediate-scale, structural elements representative of wind turbine blades and develop methods used to predict blade structural performance. Therefore, testing structural details of the blade can help the designer focus on the specific failure mode.

Concerning investigations on the wind blade substructures, the major part of the studies rely on testing adhesively bonded samples that represents assemblies of blade shell and the integral web, spar or beam. These tests permit to examine the mechanical behavior of the shear web material of a beam structure. In wind turbine blades design, two main types of structures are revealed. These main types of design are shown in Figure V.3-4a and Figure V.3-4b: I-beam design (Mandell, et al., 1998) (Potter, et al., 2001) (Sharp, et al., 2013) and Box-beam design (Belingardi, et al., 2004) (Zarouchas, et al., 2012).

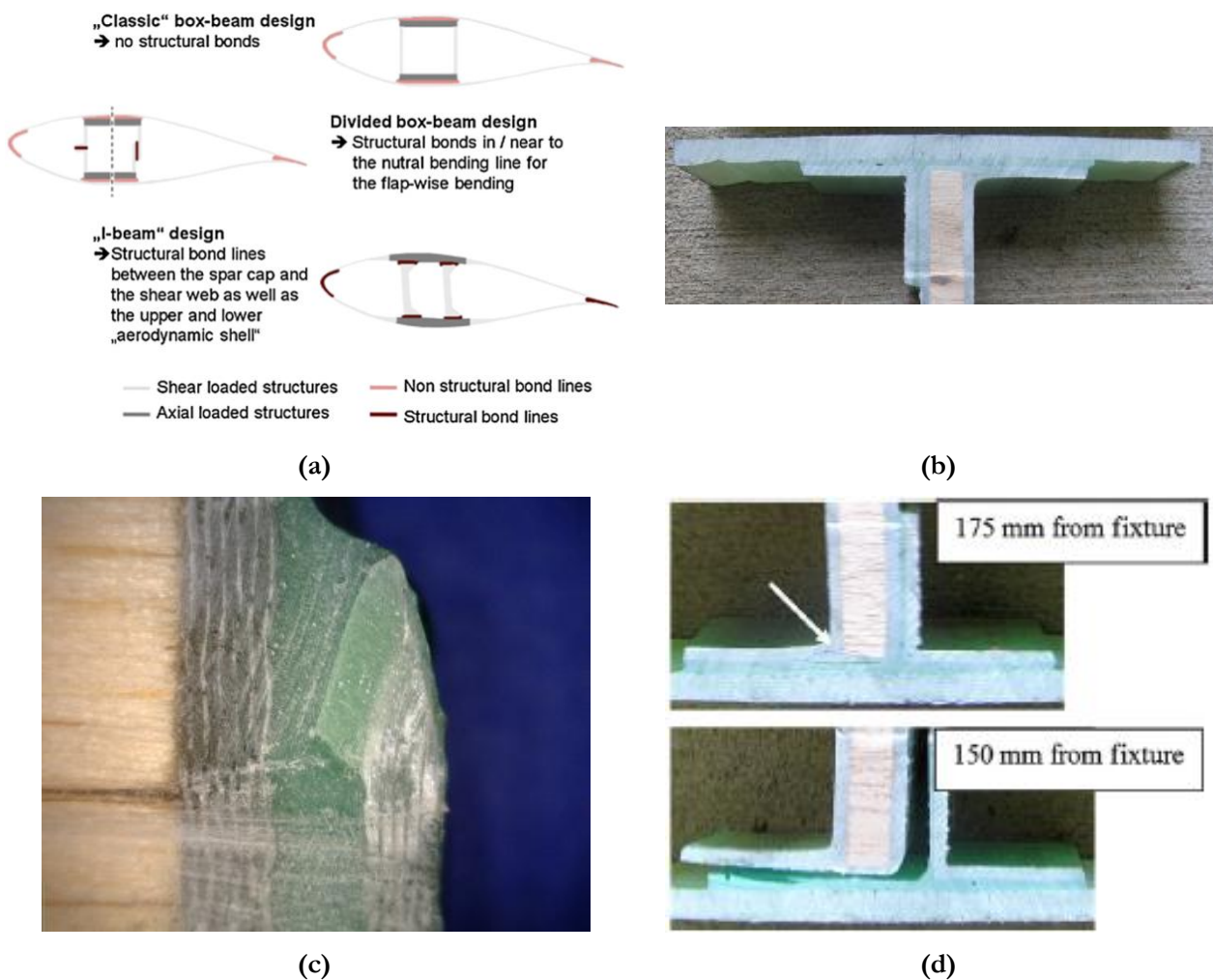


Figure V.3-4: Sub-structural tests: designs in wind-blade structures (a), case study of a T-joint (b) with evolution from crack initiation (c) to failure of the sample (d).

In the major part of these studies, three and four point bending tests were performed in order to develop a confidence in the ability to design and analyze such a structure by determining the quality of the bond-lines and identify the site of failure (Figure V.3-4c and Figure V.3-4d). Generally, the outcome was a list of recommendations regarding the design the modeling and the testing of subcomponents.

c. Coupon-size samples

Experimentally, for the several configurations tested, substructures enable the identification of a crack-onset occurring in the spew fillets (Zarouchas, et al., 2012) (Sharp, et al., 2013). The influence of the bond-line geometric parameters are thus of a main importance in the strength of the assembly, as they lead to stress concentrations and early cracks apparitions. The numerical approaches linked to these experimental observations are in the main part related to fracture mechanics (Ji, et al., 2014) (Kalkhoran, et al., 2013).

Nevertheless, damages such as crack initiations in assemblies may be considered as critical for a bonded structure. Therefore, the aim of the approach developed remains the investigation of the initiation phenomena. Following this philosophy, the coupon-size samples developed should serve as a reliable test bed to validate the mechanical behavior of the materials identified with the use of characterization tests (modified Arcan test for the adhesive).

Experimental studies performed in a coupon level could be seen as the first basic step in the design process of wind turbine blades. Indeed, as the size of the specimen decreases, experimental campaigns using coupon-size samples can easily be performed for a high number of samples (Samborsky, et al., 2009). Therefore, coupons could be a necessary step to validate the mechanical behavior of the bonded assembly. This basis of validation will then permit to take the next level with the development of failure scenarii on sub-structural tests and later to determine a fatigue lifetime of wind-blade full structures.

V.3.3. Development of a coupon-size experimental method

Experiments at structure and substructure scales revealed that endurance of the bonded assemblies between the blade shells and the structural beam are key points in the fatigue behavior of wind blades. The following section, will thus present a study of bonded materials and an adhesive joint issued from typical composite blade assemblies in a coupon size.

a. Bonded samples

For the tested specimens, the laminates were composite material commonly used in the design of offshore wind turbines blade shells: a glass/epoxy with a $[45; -45]_s$ stacking. The bonded assemblies were nominally 11mm thick: two 4.5mm composite blades bonded with a 2mm adhesive joint. The composite blades on each side of the adhesive joint were positioned in order to have a 45° ply on the top of the sample and a -45° ply at the bottom. Before bonding, the peel-ply was removed on the composite adherend bonded faces with no further surface preparations. As shown on Figure V.3-5, the adhesive thickness was controlled using spacers at the corners of the plate. The curing process performed was the same as the one used for the Arcan modified characterization samples: 24h at room temperature after the bonding procedure then 72h at 60°C and finally 48h at room temperature. From the bonded assembly performed, the coupons geometry is extracted using a high pressure water jet. The results were samples with flat edges without spew fillets (Figure V.3-5).

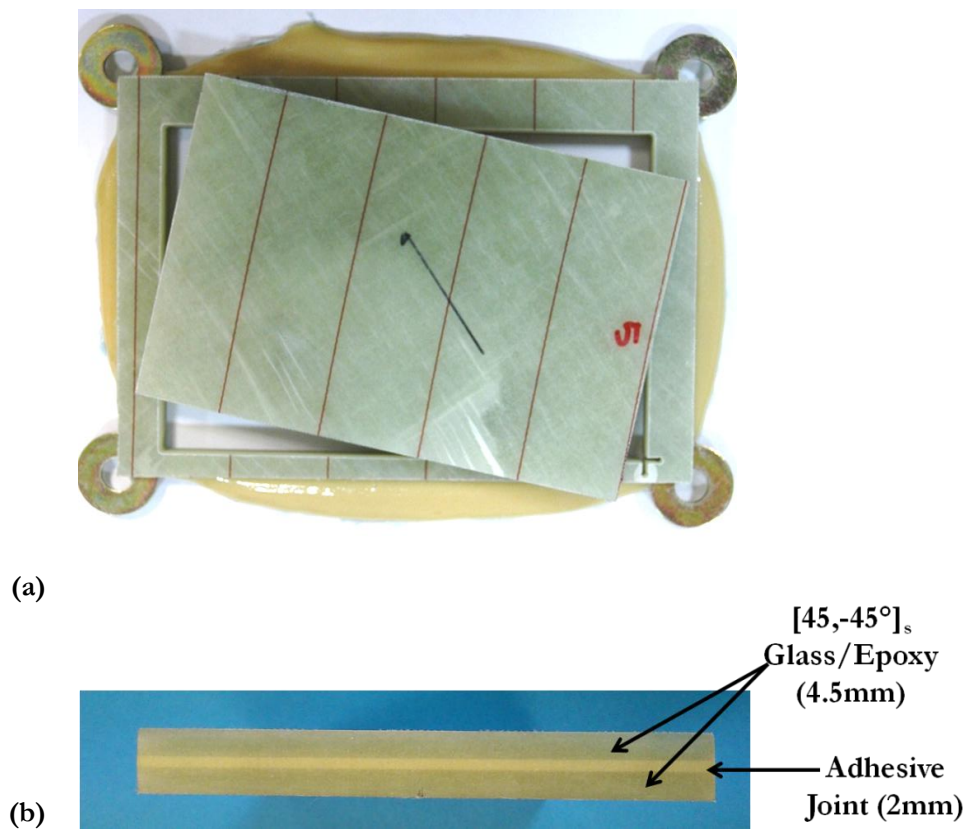


Figure V.3-5: Presentation of the bonded sample: cut-out in the bonded composite specimen (a) and view of the adhesively bonded joint (b).

b. Testing device

A particular bending mode test was developed, in order to characterize the bonded assembly. Issued from a mode III characterization test developed for fracture of composite materials (de Morais, et al., 2009) (Ratcliffe, 2004), the Edge Crack Torsion (ECT) test permits to generate, with a four-point bending, important shear stresses between composite layers of a rectangular sample. The testing device developed for this study, presented in Figure V.3-6, was designed and based on two parallel plates. Ensured by four cylindrical joints, the only degree of freedom conserved between these two plates was the translation following the normal direction of their parallelism plane (\vec{z}). These two rigid frames permitted to support the guide-pins and the loading fixtures. In the ECT tests, the loading was applied at the corners of the sample. Loading pins were placed on the same face of the sample on a straight diagonal line. The loading fixtures were made up of truncated spheres in order to limit indentation effects on the external composite plies. In order to avoid displacement of the sample during the loadings three guide-pins are conserved during the tests as shown on Figure V.3-6.

With a fixed position of the loading pins, the dimensions of the testing device developed permit to test three sample geometries: two square samples and one rectangular specimen. Stress states within the adhesive layer for each specimen were studied in 3D FE analyses, simulating the ECT test, under linear assumptions for the material behaviors. The models were built using 8-node elements. Each ply of the composite material was modeled with a C3D8 element layer. For these layers, the transversally isotropic properties were respected and the material constants were defined with the previously identified parameters. In the FEM, the adhesive layer was set-up with two C3D8 element layers. The models

included two upper loading and two lower support rigid spheres. Contact surfaces were defined at the faces of the elements. A mesh refinement was performed on the areas under influence of the spheres indentation by the spheres was not modeled. Rigid body motions were prevented by constraining lengthwise and widthwise displacements of different nodes. It was verified in previous studies on the ECT model that those constraints did not influence the results (Ratcliffe, 2004). However, these boundary conditions were removed after an initial loading step corresponding to the “indentation”. After this step, forces developed by contact with the spheres prevented rigid body motions. The typical deformed configuration of an ECT specimen is presented in Figure V.3-7. FE analyses were performed for a 4mm displacement of the loading points.

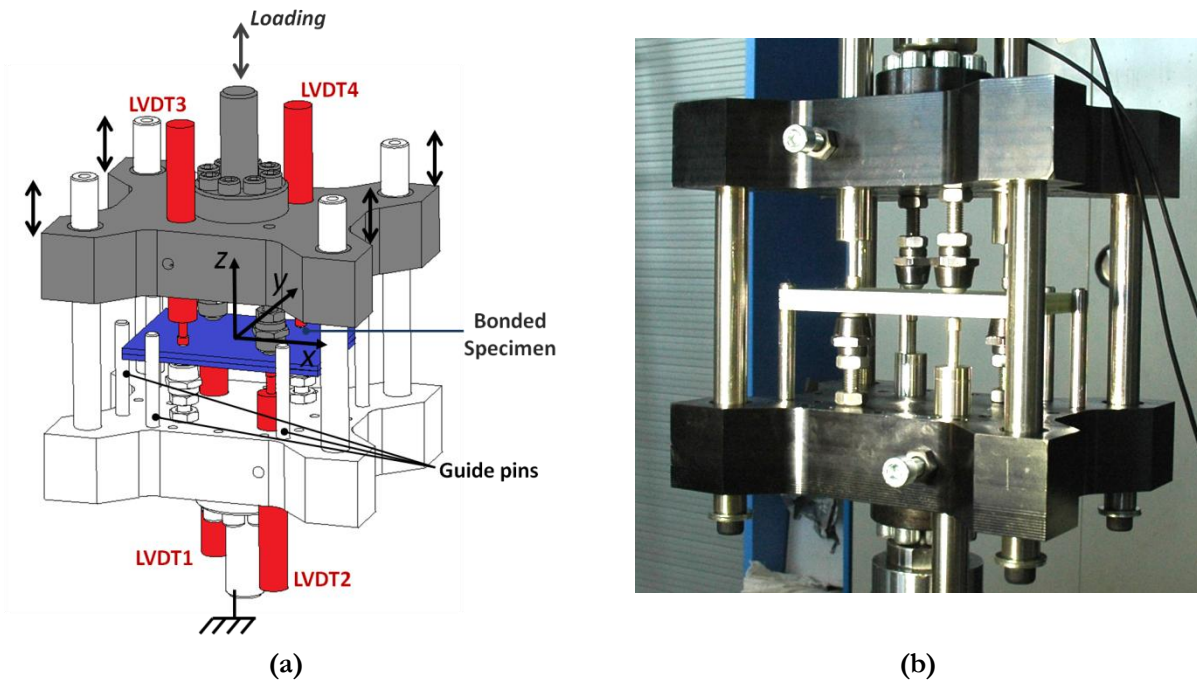


Figure V.3-6: Presentation of the ECT testing device developed: scheme of the testing device (a) and picture of the device with the bonded assembly before loading (b)

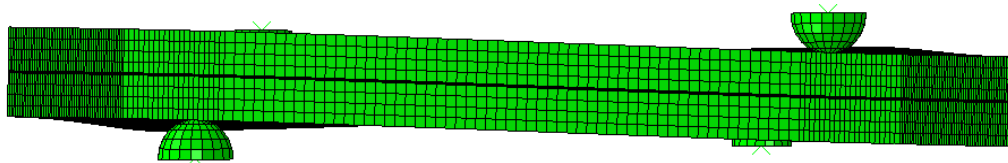


Figure V.3-7: Abaqus® FE simulation results: deformed configuration

The results concerning the von Mises stress and in-plane shear stresses, in the adhesive mid plane, are shown for the three following different geometries:

- In Figure V.3-8, the case of a 150x150mm² square sample leads to important values of the von Mises equivalent stress concentrated in areas characteristics of the effect of the loading points. However, stress concentrations appeared on the edges of the sample due to shear stresses S13 and S23 shear stresses;
- In Figure V.3-9, the case of a 100x100mm² square sample permits to have the loading points closer to the edges. Therefore, the von Mises stress showed increasing values at the edges of the

sample and effects of the indentation of the spherical contacts was smoothed. S13 and S23 shear stresses seem to drive this phenomenon;

- In order to facilitate the observation of the failure phenomena shear stresses may be concentrated on only two edges using an intermediate rectangular geometry. In Figure V.3-10, the case of 150x100mm² shows S13 shear stress on the edges of lengthwise dimension twice as much as S23 shear stress on the two other edges;

This last geometry will be studied through monotonic and cyclic loadings in the following section.

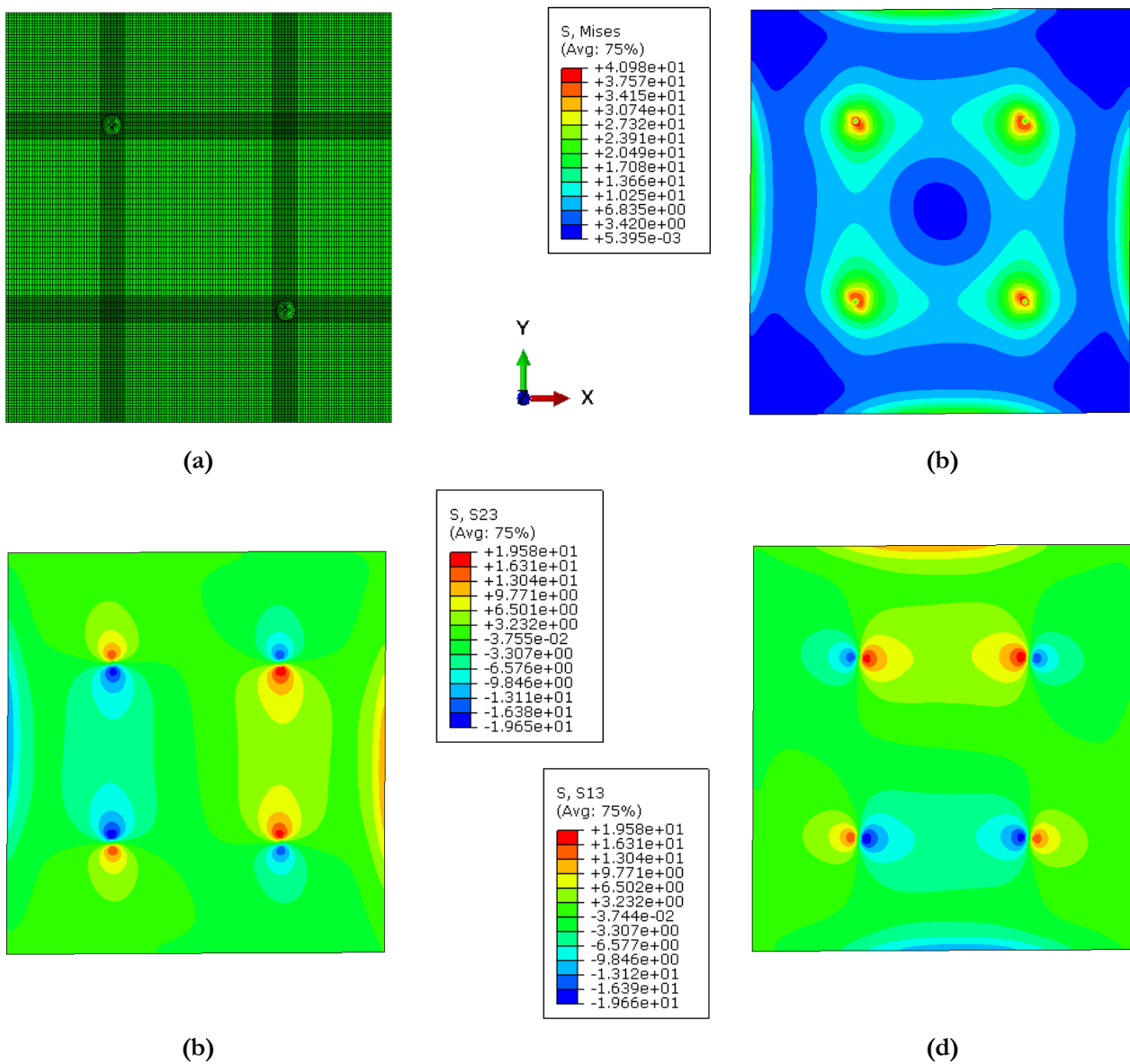
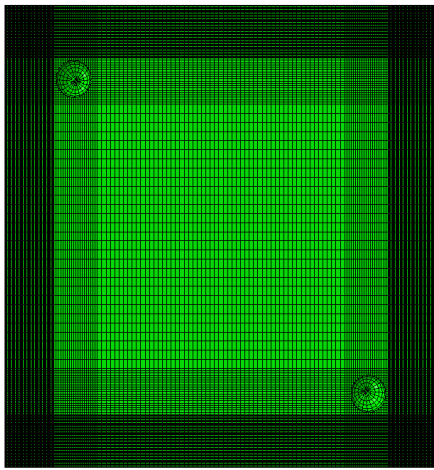
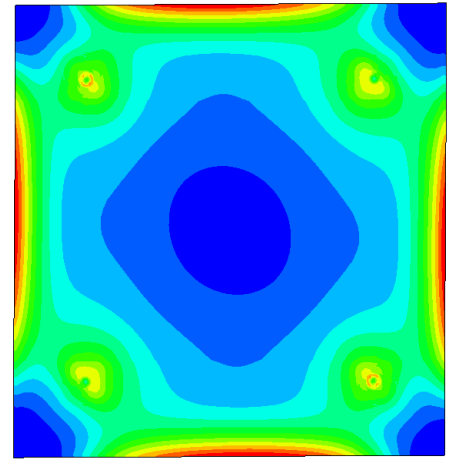
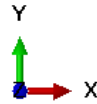
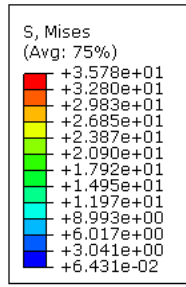


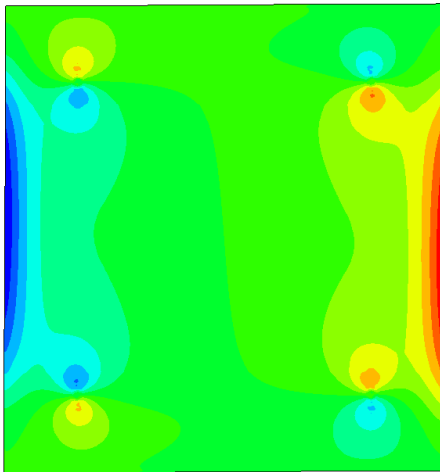
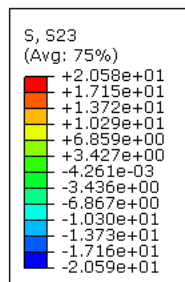
Figure V.3-8: Stress distribution within the adhesive joint for a 150x150mm² specimen: FE mesh (a), equivalent von Mises stress (b), S23 shear stress (c) and S13 shear stress (d).



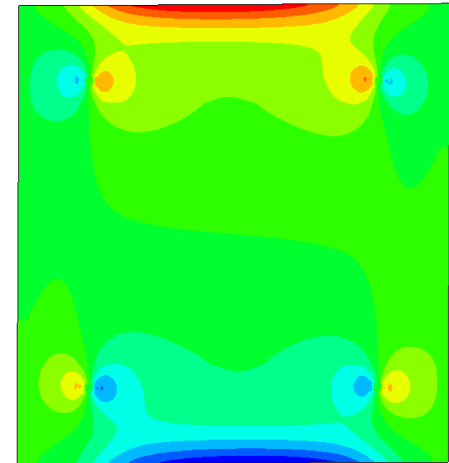
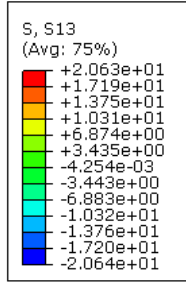
(a)



(b)



(c)



(d)

Figure V.3-9: Stress distribution within the adhesive joint for a 100x100mm² specimen: FE mesh (a), equivalent von Mises stress (b), S23 shear stress (c) and S13 shear stress (d).

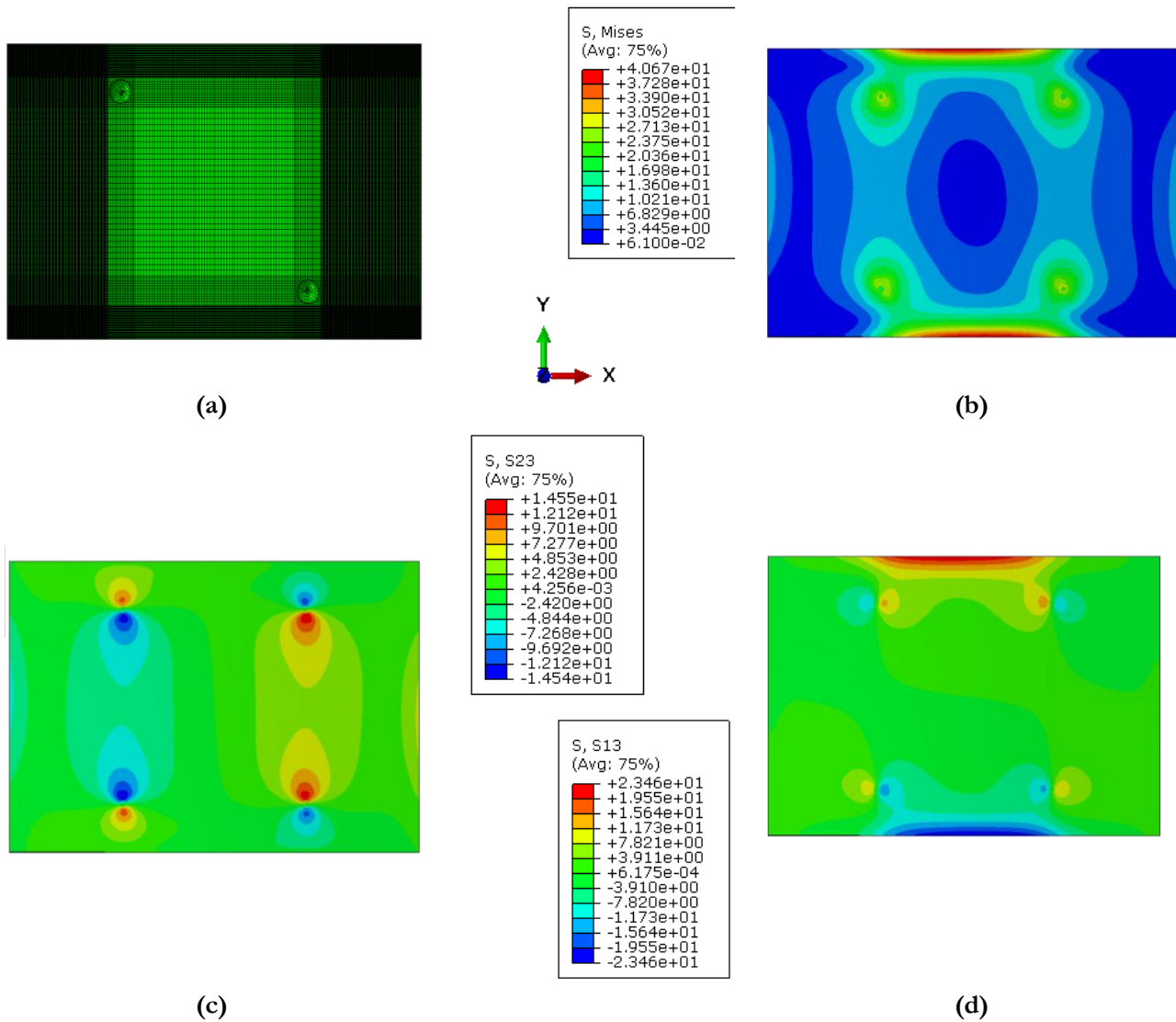


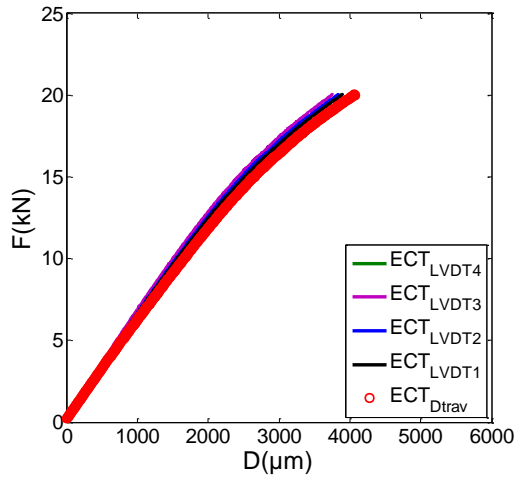
Figure V.3-10: Stress distribution within the adhesive joint for a 150x100mm² specimen: FE mesh (a), equivalent von Mises stress (b), S23 shear stress (c) and S13 shear stress (d).

V.3.4. Experimental results

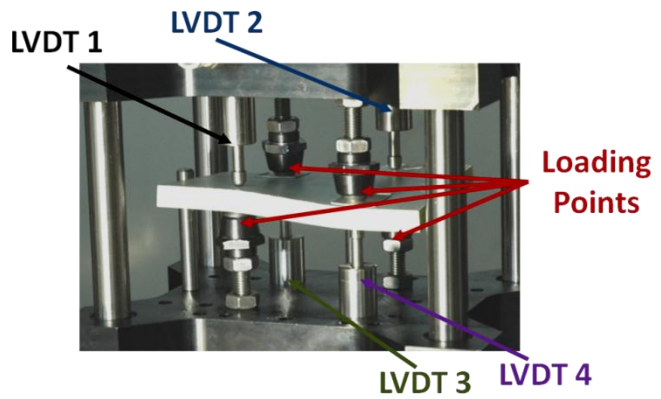
a. *Monotonic loading*

In order to verify the validity of the applied loading, quasi-static displacement ($0.5\text{mm}\cdot\text{min}^{-1}$) was applied to the $150\times 100\times 11\text{mm}^3$ samples. As a first step, the displacement of the loading fixture is verified using four LVDT sensors placed on the loading points (x,y) coordinates, measuring the vertical amplitude of the deformations of the sample. Figure V.3-11a shows that the values measured by each sensor were similar to the displacement given by the testing machine (crosshead). This result enabled to validate different aspects:

- First, the deformed shape (Figure V.3-11b) imposed to the sample was validated. As the four local measurements gave similar values, the symmetries in the loading were conserved and no rotations happened during the loading of the sample;
- Secondly, the stiffness of the testing device. As the displacement measured by the machine displacement sensor showed a low discrepancy with the local measurements performed on the sample, deformations of the loading device may be neglected.



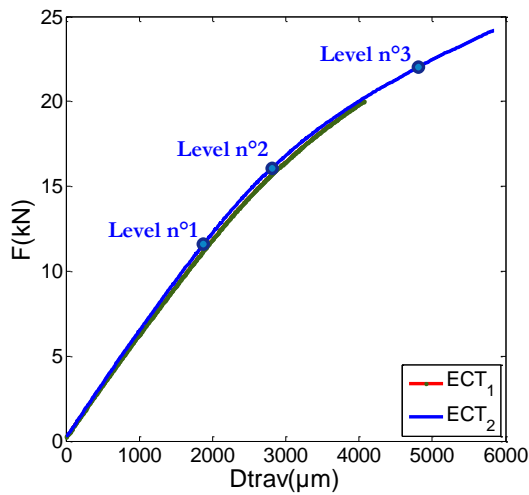
(a)



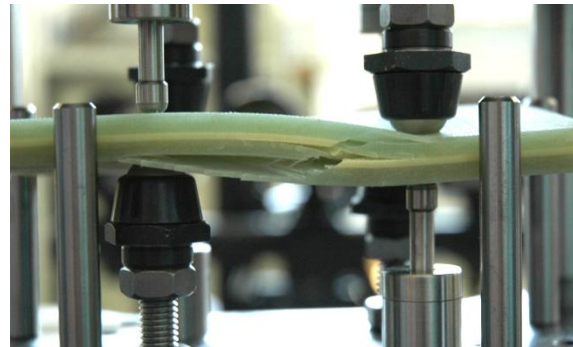
(b)

Figure V.3-11: Monotonic test using ECT device: experimental results (a) and deformed shape picture (under a 4mm loading) (b).

Following the same testing procedure, the reproducibility of this test was evaluated. The responses of two bonded samples are plotted on Figure V.3-12a. The monotonic tests, performed on these samples, showed a repetitive mechanical response until failure. The experimental tests were stopped when clear signs of failure appeared in the samples. For each sample tested, a characteristic failure mode, as presented on Figure V.3-12b, occurred in both adhesive and composite adherends. Failure was systematically observed on the lengthwise edges of the sample, which was consistent with the stress state revealed by previous numerical simulations (Figure V.3-10).



(a)



(b)

Figure V.3-12: Reproducibility of the monotonic tests using: experimental results (a) and picture taken at failure (for ECT₁ sample) (b).

In the previous chapters, the GOM device permitted to measure the 3D relative displacements of the substrates in real time. This same device may be used as a 3D Digital Image Correlation (DIC) system with the same accuracy. In order to enable the surface strain field to be computed, DIC systems allow observations to be performed on one side of the sample, and thus to indicate the strain concentrations. Therefore, the GOM device was placed to observe one of the *X-Z* faces.

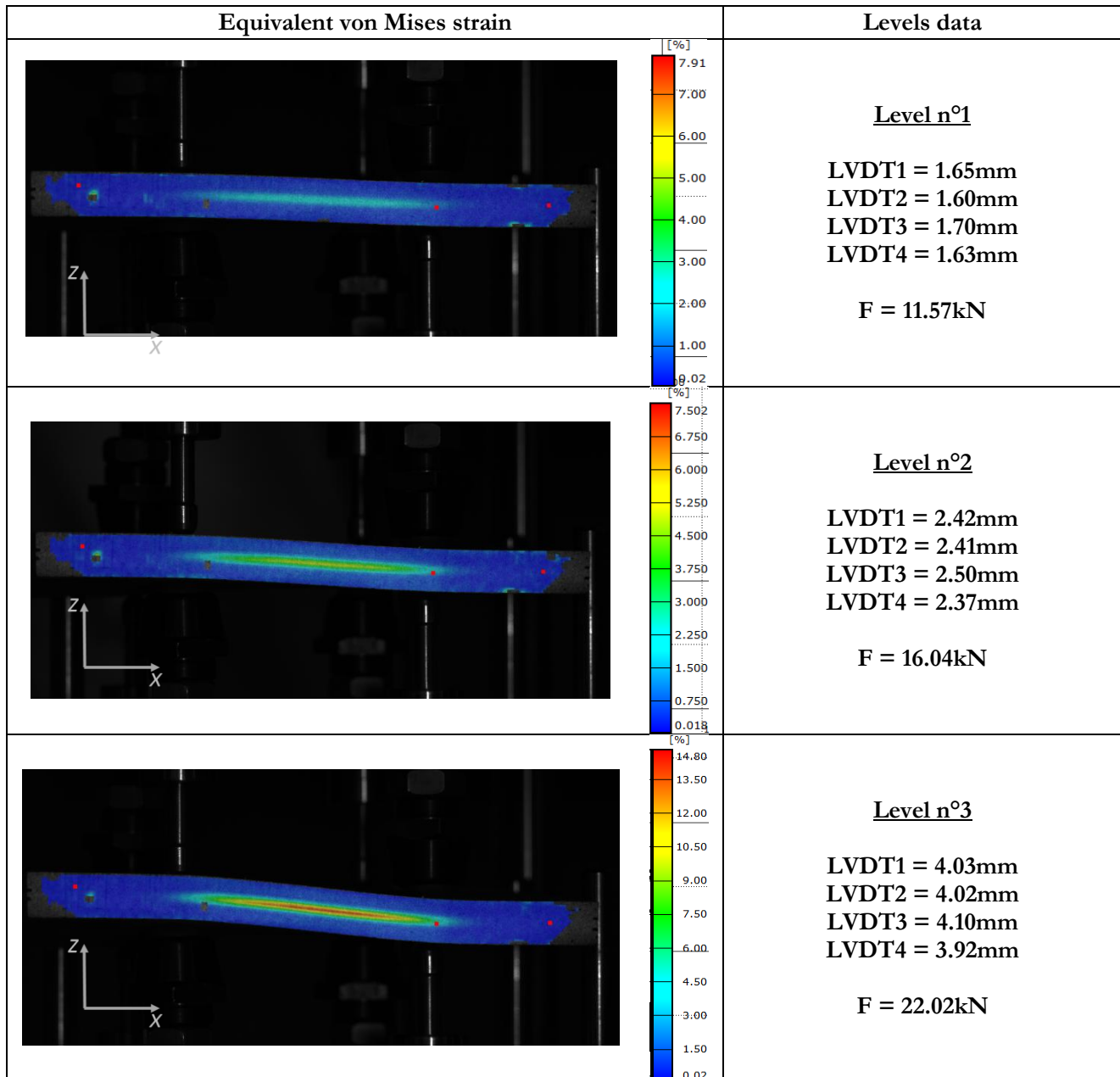


Figure V.3-13: Equivalent von Mises strain under monotonic loading (experimental)

In Figure V.3-13 are plotted the equivalent von Mises strain measured for three different load levels during a monotonic test (Figure V.3-12a). The maximum values within these strain fields were measured in the middle plane of the sample, in an area corresponding to the adhesive layer. Furthermore, the location of the strain concentrations was consistent with the failure mode observed: the peak in the measured strain correlates with the identified areas of failure (Figure V.3-12b).

Based on observations made on the X-Z faces, the experimental method using an ECT device seemed to locate of the maximum strain in the adhesive layer. Thus, the device seems to be an interesting tool in order to characterize the adhesive mechanical behavior. Nevertheless, questions remain about the stress concentrations under the loading points. If local damage appears in these areas, the assumption is made that it will not influence the adhesive joint mechanical behavior. Further studies (acoustic emission) are needed to conclude. In the next section, cyclic loadings were thus applied to specimens with the same geometry in order to evaluate the mechanical behavior of the adhesive material.

b. Cyclic loading

The cyclic loadings were performed under load control, using a sinusoidal signal with a constant loading rate equal to 5 kN/s ($f = 0.25\text{Hz}$). The mechanical response of an ECT tests for a $F_a = 5\text{kN}/F_m = 10\text{kN}$ is presented in Figure V.3-14.

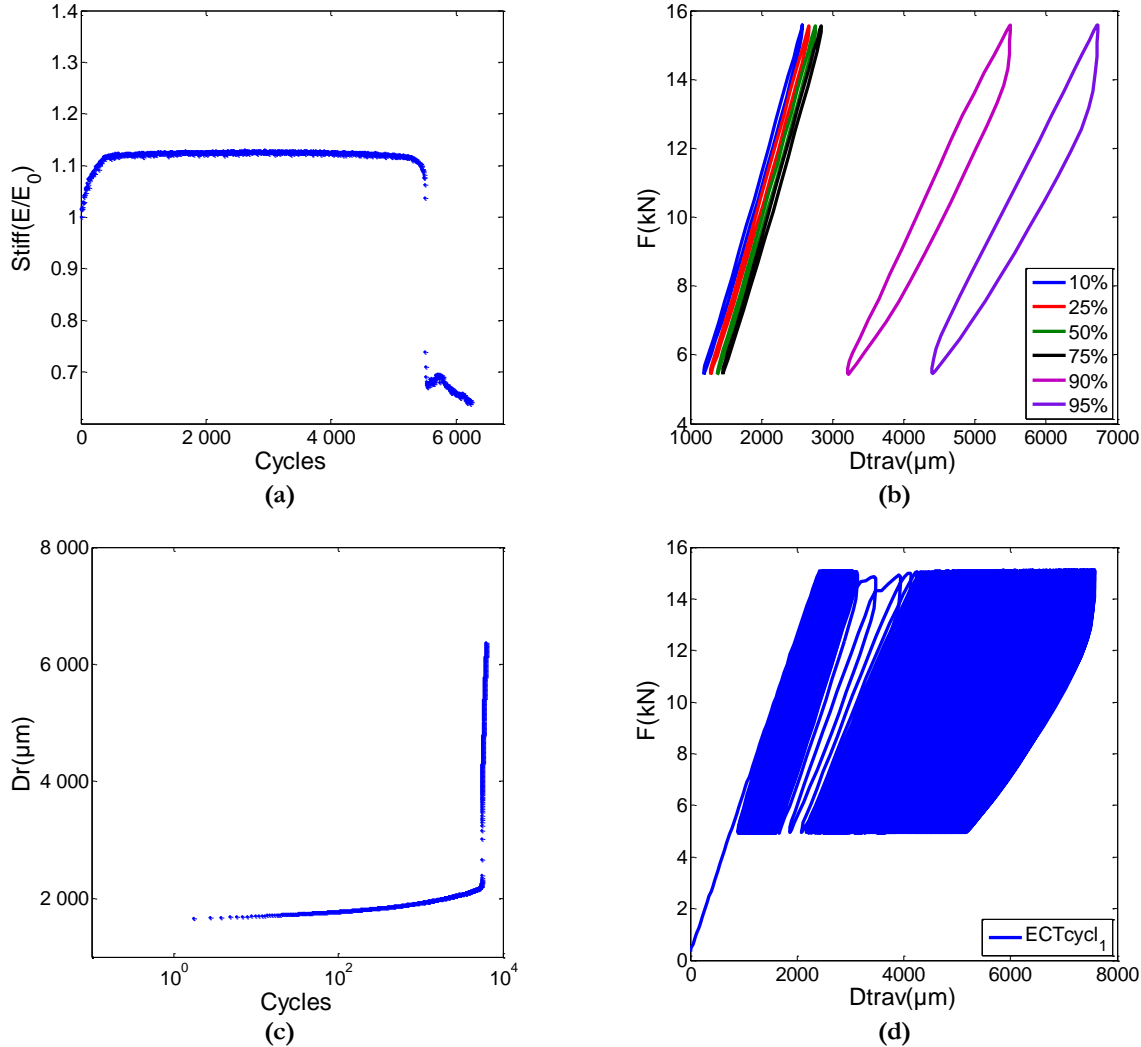


Figure V.3-14: Cyclic results ($F_a = 5\text{kN}/F_m = 10\text{kN}$) using ECT device: evolution of the stiffness (a), the hysteretic loops (b) and ratcheting effect along the cycles (c) and mechanical behavior (d)

The experimental results permit to divide the mechanical response of the sample in 2 parts:

- Until 5,000 cycles, the stiffness plotted in Figure V.3-14a, presented no evolutions with a E/E_0 ratio stabilized at a value slightly greater than initially measured. Hysteretic loops presented in force/displacement diagrams for Figure V.3-14b and Figure V.3-14d, revealed a stabilized shape for more than 75% of the test time. In terms of ratcheting during this period, the mean displacement evolves slowly to an approximate value of 2.2mm;
- After this period, the displacement increased exponentially (Figure V.3-14c), hardly driven by an important lost of stiffness. This sudden change in the mechanical properties, characterized by the evolution of the E/E_0 and the shape of the hysteretic loops was observed for each tested sample and may be taken as a sign of failure initiation. Furthermore, the damaging phenomenon observed was correlated with clear in-situ observations of fractures in both adhesive bond-line and composite material.

For the following cyclic testing campaign, the mechanical response of the bonded specimen will be considered only on the period preceding these clear failure evidences.

As shown in Figure V.3-15, the mechanical response recorded with the testing machine displacement shows low discrepancy in the results and a repetitive ratcheting effect may be observed. Furthermore, a trend concerning the mean load effect on the mean displacement (Dr) evolution may also be seen with the two loading cases evaluated.

For all the cyclic testing campaign, experimental results are summarized in Table II.1-2. In order to evaluate the influence of the loading cases, results are plotted in a F_{max} scale (Figure V.3-16). The low number of samples tested cannot permit to draw clear trends. Nevertheless, it was interesting to notice that failure (as defined previously) occurred for a repetitive value of displacement.

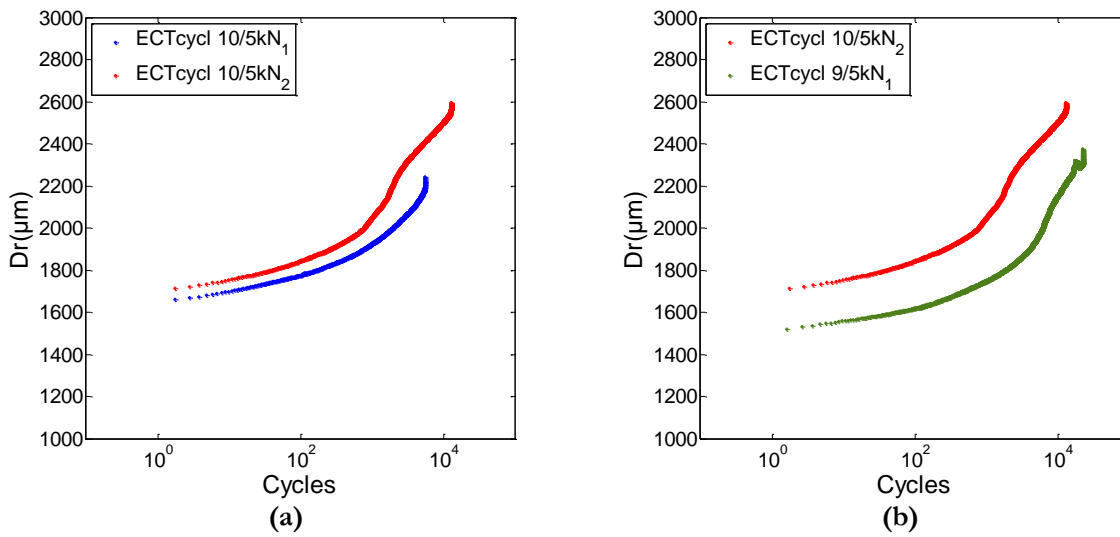


Figure V.3-15: Ratcheting effect under cyclic loading (Dr vs number of cycles): reproducibility (a) and mean load influence (b).

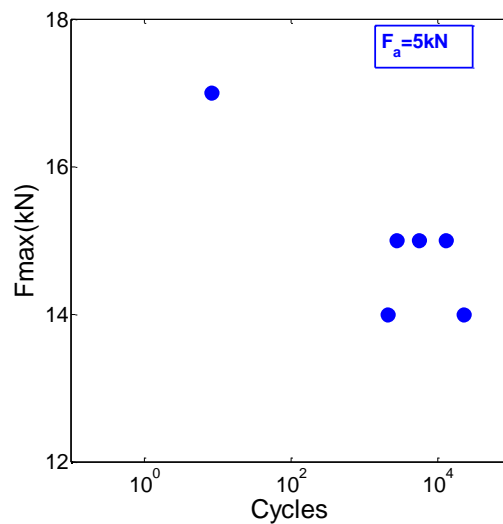


Figure V.3-16: Fatigue life of composite assemblies using the ECT device in F_{max} scale.

Load		Failure	
Frequency	Ratio F_a/F_m	Displacement (μm)	N_f (cycles)
0.25Hz	5/12kN	2,857 μm	8
		2,953 μm	5,395
	5/10kN	3,303 μm	12,750
		2,722 μm	2,676
	5/9kN	3,101 μm	22,157
		2,554 μm	2,060

Table V.3-2 : List of cyclic tests performed using the ECT device

V.3.5. Toward a fatigue lifetime prediction: numerical investigations

a. *Ratcheting effect in the adhesive joint*

In order to evaluate the ratcheting effect within the adhesive joint, a simplified FE model was developed in order to obtain reasonable computation times. As no symmetry planes may be defined, a complete geometry was necessary to be meshed. For the mesh, 3D elements were used (C3D8). The contact surfaces were not defined and the indentation was not modeled the spheres was not modeled, because this would require high levels of local mesh refinement and create unnecessary numerical convergence difficulties. The kinematic boundary conditions were imposed on nodes of the elements under the action of the sphere. Therefore, the loading was imposed, directly driving these nodes.

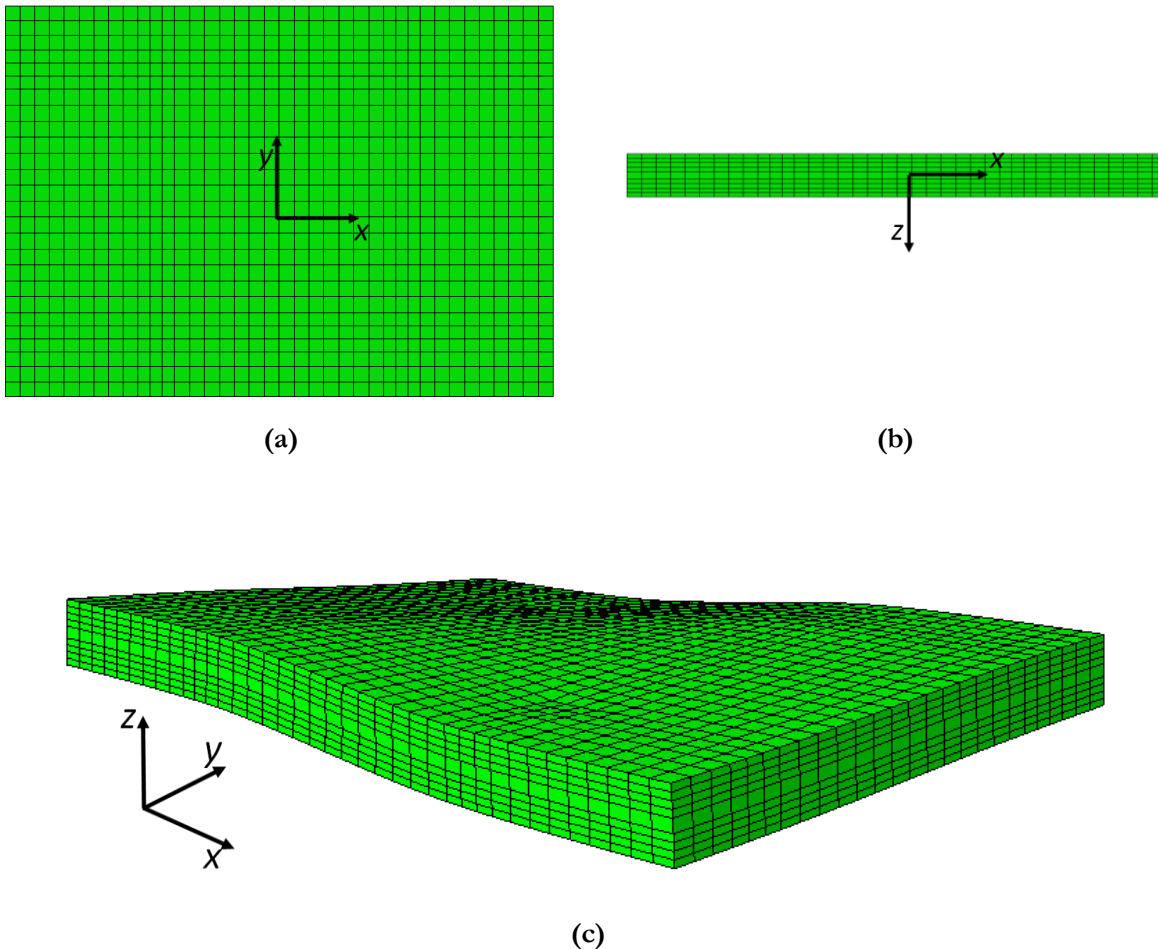


Figure V.3-17: FE element mesh of a simplified for cyclic loading application: view in a X - Y plane (a), Z - X plane (b) and shape of the deformed configuration (c)

The stacking of the composite blade was represented by orthotropic material properties for each layer. The computations were performed using the model developed for the adhesive material behavior. The FE mesh is presented in Figure V.3-17. In the sample thickness, a single element was used to each layer: 1 element for the 2mm thick adhesive joint, 8 elements for the 8 layers of the stacking ($2 \times [45^\circ; -45^\circ]$). The numerical investigation on the ratcheting effect of the adhesive joint was performed with two parameter sets: the first defined with the 0.2mm thick adhesion joint (Chapter III) and the second parameter set defined with the 2mm thick adhesion joint. Under elastic assumptions for the composite material, the numerical response underestimates the experimental cumulative displacement for the first cycles. However, concerning the long-term behavior, the numerical response seems to follow the trend observed experimentally for the two loading cases: $F_a = 5kN/F_m = 9kN$ (Figure V.3-15a) and $F_a = 5kN/F_m = 10kN$ (Figure V.3-15b). The parameter set defined using 0.2mm modified Arcan specimens presents a better response concerning the ECT experimental/numerical comparison. The effects of the confined adhesive joint are not enough understood to perform hypotheses at this stage. Obviously, the thickness of the adhesive was not the only parameter.

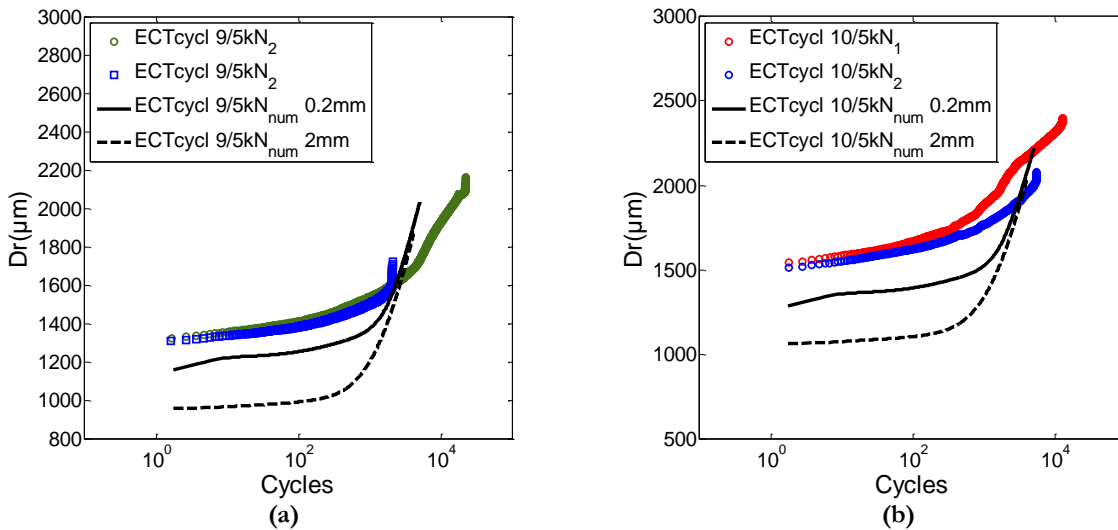


Figure V.3-18: Numerical simulation of the ratcheting effect in the adhesive joint: comparison to experimental response of the bonded structure for $F_a = 5kN/F_m = 9kN$ (a) and $F_a = 5kN/F_m = 10kN$ loading cases (b)

b. Evolution of the criterion

As cumulative displacements were observed along the cycles (ratcheting effect), in the experimental and numerical responses, a strain-based criterion may be relevant. For a $F_a = 5kN/F_m = 9kN$ loading case, the evolution of the equivalent strain ϵ_{eq} within the adhesive joint, was plotted after the first cycle (Figure V.3-19a) and after 500 cycles (Figure V.3-19b). These ϵ_{eq} values were calculated at each integration point at a (14kN) load level. The equivalent strain state showed a maximum value at the edges of the sample, with strain concentrations consistent with the observations performed with DIC in Figure V.3-13. The equivalent strain ϵ_{eq} , plotted in Figure V.3-19d in function of the y coordinate, for a same load level, showed that the strain increased in these areas along the cycles. Therefore, relying on a strain based criterion, the identified areas may be taken as responsible of a possible crack initiation within the adhesive. The numerical model developed may thus permits a fatigue life estimation for this kind of structure. Nevertheless, as the definition of the fatigue life will be based on numerical investigations of local values in concentration areas further studies are needed.

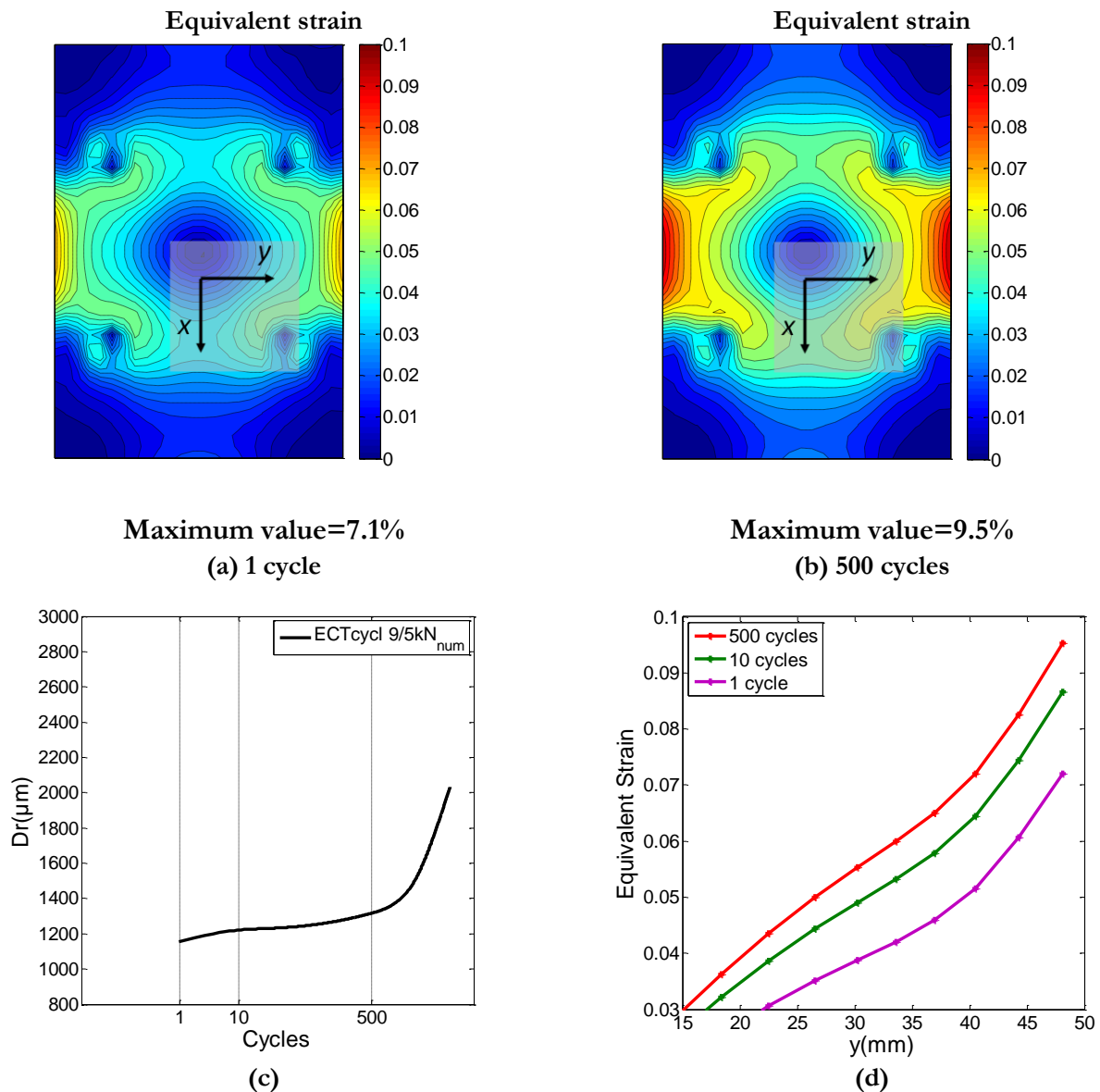


Figure V.3-19: Evolution of the equivalent strain within the adhesive joint after 1 cycle (a) and after 500 cycles (b) in the X - Y plane, numerical displacement in the structure (c) and evolution of ϵ_{eq} in the stress concentration area ($x = 0$) along the \vec{y} direction (d)

c. Prospects

In the numerical study of bonded joints with low edge effects, such as modified Arcan specimen with a 0.2mm bond-line, a strain-based criterion could be applied without worrying of the stress concentrations area issues. However, for the case studies performed, numerical investigations in stress concentration areas are strongly linked to the mesh refinement of the FE model (Bjorkman, et al., 2008). Indeed, in these areas, the mesh refinement has a significant effect on the maximum plastic strain response. Therefore, a “standard” mesh needs to be clearly defined and applied to the entire approach (identification/FE analysis). From this point, an accurate evaluation of the failure criterion may be performed.

Then, a “point stress” approach (Nuismer, et al., 1975) (Whitworth, et al., 2008) applied to the failure criterion proposed in this work may be developed. The “point stress” failure criterion assumes that failure will occur when a stress or strain based variable, at a fixed distance d ahead of the edge of the

singularity, first reached a certain value. Using this failure criterion, further tests have to be defined in order to identify this distance parameter d . In the case of the SikaForce®-7817 L60MR, the variable C , developed in Chapter IV (Eq 1.2), can be used. Further numerical investigations are also necessary in order to evaluate the role of the composite mechanical behavior in the numerical response. Therefore, viscous phenomena occurring within the composite matrix may have to be taken into account in order to have a more accurate simulation.

Concerning the experimental approach, in order to observe more precisely the adhesive joint behavior, 3D real-time local measurements of two points were applied on the cyclic tests. Such as the measurements performed for the modified Arcan test, two markers were located on the substrates on both side of the adhesive joint. But, the real-time signal obtained did not permit to evaluate easily the local adhesive joint behavior because the “noise”, due to the macroscopic displacement of the specimen, was too heavy.

Nevertheless, in order to have some pictures of the strain state, at different steps of the cyclic test, DIC may be performed. Therefore, a correlation may be obtained between the experimental macroscopic strain field and deformed shape developed by the FE analysis.

V.4. Conclusion

Presented in this chapter, different experimental studies were performed in order to validate the abilities of the approach developed along this work:

- The case of a 2mm adhesive joint permitted to point out the influence of the “joint thickness” parameter into the mechanical response of the adhesive bond-line. Physic-chemicals aspects of the polymerization seemed to play an important role, as different viscous behaviors were obtained with an evolution of the adhesive joint confinement. Therefore, a new parameter set was identified for the polymeric material obtained in 2mm adhesive joints. Furthermore, in a structural aspect, the new adhesive joint geometry led to stress concentration areas in the adhesive/substrate interface revealed at the edges of the overlap. In these regions, the stress distribution was ruled by important tensile stresses that increased with the test time. A fatigue test campaign was also performed under both tensile and shears loadings. The trend observed brought some interesting observations: fatigue lifetime of the adhesive joint decreased in the shear direction due to stress concentration, but the new adhesive joint obtained permits to have a more reproducible fatigue lifetime concerning the tensile fatigue behavior;
- Another issue investigated was the adhesion on composite. Therefore, following the approach proposed by Cognard, et al. (Cognard, et al., 2005), modified Arcan specimens including composite blades were studied. The behavior of the bonded hybrid samples were modeled using elastic assumptions for the composite behavior. Using FE analysis, important stress concentrations areas were revealed in the adhesive/composite interface;

Chapter VI: In the last section of this chapter, the study of a particular four-point bending test, as an application to an industrial case was proposed. Based on studies performed on ECT tests, a device was developed in order to test adhesively bonded composite blades. The non-linear behavior of the specimen was observed under monotonic loading and the ratcheting effect was evaluated under cyclic loadings. As displacement at failure measured gave reproducible values, a method based on a strain criterion was proposed in order to evaluate the fatigue life.

Conclusions & prospects

In order to reduce fossil fuel dependency, the renewable energy production, in particular, wind energy generation, must be drastically increased. This can be realized by the development and expansion of off-shore wind-parks built with large wind turbines. The size of wind-turbine blades is thus expected to considerably increase in the future, demanding a better understanding of the structural behavior on a different scale. Due to the high costs of repair and maintenance of off-shore located large wind-turbines, the reliability of the wind-blades should be increase to ensure an efficient work for decades. The durability of these structures can be ensured, among others, if the materials used and their assembly has high fatigue and environmental strengths. Adhesive bonding is an interesting way for the joining of wind-blade structures introducing composites, polymeric or dissimilar materials assembly.

Different parts of a wind-blade are thus bonded with structural adhesives such as the SikaForce®-7817 L60MR product. For example the “box beam” inside the blade is adhesively joined to the shell. Such an adhesive joint is subject to cyclic loadings due to edge-wise and flap-wise bending moments applied to the wind-blade. It is thus of the utmost importance to understand and to predict the fatigue behavior of this structural adhesive bond-lines in order to evaluate the wind-blade durability.

∞

The first chapter of this work was dedicated to the establishment of the framework. An overview of the studies concerning the fatigue behavior of bonded structures is done. Then, an analysis of the experimental methods and numerical tools available in the literature permitted to identify a process was performed, giving us the keys to observe and model the mechanical phenomena occurring within an adhesive bond-line under cyclic loadings. This preliminary work thus led us to define the approach developed in this thesis: based on an investigation of the viscous behavior of the adhesive in an assembly, the aim is to study the role of such mechanical phenomena occurring within the bond-line in order to model the cyclic behavior and evaluate a fatigue lifetime for a low number of cycles (below 10^5 cycles).

∞

In the second chapter, a characterization of the viscous mechanisms was thus done. The experimental method used was based on an approach previously developed for the characterization of 3D elastic-plastic (Maurice, 2012) and 2D elastic-visco-plastic behaviors (Créac'hcadec, 2008). This approach was grounded on an experimental campaign performed with a modified Arcan fixture including a unique type of bonded assembly. Indeed, previous studies have shown that, the specific geometry of the samples used permits to reduce the edge effects for thin adhesive joints (0.2mm), from which most of the standard tests available suffers. This method was shown to lead to low scatter in the experimental

results under monotonic loadings. However, the characterization of the viscous behavior needs to reach this result for tests under creep loadings in a long-timescale. Therefore, the definition of an accurate bonding process including, among others, a precise thermal cure and an accurate control in the testing schedule, permitted to avoid ageing and polymerization effects on the experimental response. Then, using the modified Arcan device, effects of viscosity have thus been underlined, through the loading rate influence under monotonic and cyclic loadings, and the mechanical response under creep loadings. As a conclusion of this chapter, a useful database has been created for the characterization of the viscous behavior relying on cyclic creep/recovery tests with a range of loading covering tension to shear.

In this chapter importance was given to the bonding process to obtain reproducibility in the results. If precautionary principles are not followed in the experimental process, potential scattering is obtained in the experimental response due to chemical or physical mechanisms. The sensitivity of the viscous mechanisms to the physicochemical phenomena may be handled through two different aspects: ageing and polymerization. Therefore, in order to understand these phenomena and their link with the macroscopic experimental response, further studies are needed on the role of ageing (Bordes, et al., 2009) (Arnaud, 2014) and on the polymerization mechanisms (Devaux, 2014).

∞

In the third chapter, in order to model the mechanical joint behavior, the numerical approach proposed was based on the use of a non-linear visco-elastic visco-plastic model. In a first step, to reach this purpose, a work based on the cyclic creep/recovery tests under shear loading has been performed to define the constitutive equations for the viscous mechanisms. Therefore, the numerical response of a 1D model was investigated to describe the experimental modified Arcan database under shear loadings.

Then, in the same chapter but in a second step, a non-associated formalism with dependence on the hydrostatic stress component was proposed in order to define the 3D mechanical behavior. In their expressions, the constitutive numerical equations proposed exhibit 12 material constants. A sequential inverse approach was thus developed and applied for the identification of the parameter set necessary to the 3D mechanical behavior modeling. In the identification strategy proposed, modified Arcan tests under tensile-shear cyclic creep/recovery, formed with the results under shear the necessary experimental database. The parameter set identification done, abilities of the model were then validated on the description of tensile cyclic creep/recovery and shear, tensile-shear and tensile monotonic tests.

In the approach proposed, the experimental displacement was considered to be due to a visco-plastic flow occurring above a certain stress value. Existing models with other approaches (Laurin, 2005) (Launay, et al., 2011) (Nguyen, 2013) can explain with different mechanisms the cumulative strain over time under creep or along cycles under stress controlled cyclic loading. In this area, a wide field of research remains open and the study of the numerical response of different inelastic models could also be studied.

∞

The fourth chapter was built to validate the approach adopted on the case of modified Arcan specimen with a thin adhesive joint, under fatigue loadings. The model was developed in order to evaluate the

evolution of the cumulative strain in the adhesive joint under cyclic loading. A comparison between the numerical predictions and the experimental results were thus done on the displacement:

- Under shear loading, the cumulative displacement numerically defined correlated the ones effect the experimentally measured. Furthermore, the development of a loading rate dependent strain-based failure criterion (identified on 0.2 thick adhesive joints under monotonic loadings) permitted to develop an efficient numerical prediction of the fatigue life. The numerical prediction was able to describe the mean load influence as well as the frequency. Nevertheless, this predictive tool was not built to be conservative. A modification in the material constants defining the failure criterion could easily be performed with this purpose;
- Nevertheless, the method applied under shear loading did not seem to be applicable in its entirety under tensile-shear and tensile loading. Indeed, the value of the experimental displacement at failure showed here a more important scattering. Furthermore, the comparison between the numerical and experimental responses concerning the cumulative displacement showed an important discrepancy.

As the approach proposed permitted a reliable prediction of the fatigue behavior only under shear loadings, the first prospects may thus be to develop a more accurate description of the adhesive mechanical behavior under loading including tension. Under tensile loading, the decrease of the stiffness value became more obvious than under shear loading. Therefore, damaging occurring along the cycles may play an important role in the fatigue behavior. Further investigations on the damage behavior are thus needed. Following this approach, observation and analysis in the micro-scale of the mechanisms involved may form an important step (Joannes, 2007).

The fatigue tests performed remain in the low number of cycles framework. An interesting perspective to the observations developed on cyclic test below 10^5 cycles would be the analysis of experimental results with an increasing number of cycles. At this step, the framework of the study only concerned specimens with low edge effects.

∞

Therefore, after the case study of bonded specimens implying thin adhesive joints (0.2mm), the fifth chapter of this thesis was built to converge toward an industrial approach using composite bonded specimens with thicker joints. Considering this objective, three steps were used:

- The first step considered the application of thicker adhesive bond-lines (2mm) on the modified Arcan specimen. A first clear observation made was that the bond-line thickness played an important role on the mechanical behavior of the adhesive material itself. Hypothesis was performed in order to explain the evolution of the mechanical properties based on an increase of the chemical exchanges. However, as no evidences are shown, further investigations are needed. Despite the “new” material properties, the adhesive joint geometry also led to stress concentration areas in the adhesive/substrate interface revealed at the edges of the overlap, ruled by important tensile stresses. This observation may be brought as an explanation in the decrease of the fatigue life under shear loading. Nevertheless, the new material obtained in the thick adhesive joint geometry led to more reproducible fatigue lives concerning the tensile fatigue behavior. Concerning the numerical aspect, the material obtained with the 2mm bond-line was submitted to a new identification and a new parameter set was defined. These

parameters were then used to model the ratcheting effect under shear loading and a good agreement was found with the experimental results.

- The second step permitted to investigate the adhesion properties of the SikaForce®-7817 L60MR on composite substrates. The approach was based again on the use of modified Arcan specimens in which a composite panel was introduced. Compared to results obtained with a same bond line thickness, the composite “hybrid” specimens revealed that a same trend can be drawn in the results under both shear and tensile loadings, even if a certain growth in the discrepancy was obtained. Under elastic orthotropic assumptions for the composite panel mechanical behavior, the 3D model implemented for the adhesive bond-line behavior showed a good agreement between the numerical and experimental cumulative displacement. As the parameter set used was not modified between the 2mm thick adhesive joint and the hybrid specimen, the composite/adhesive interfaces did not seem to play an important role on the non-linear mechanical properties of the adhesive material.
- Finally, after an overview of the different testing methods developed in the characterization of wind-blade bonded structures, a coupon size experimental method was proposed based on studies performed on ECT tests. A loading device was thus developed in order to test adhesively bonded composite panels. The experimental process permitted to observe the non-linear behavior of composite bonded specimen under monotonic and cyclic loadings. As a cumulative displacement was measured along the cycles, the ratcheting effect of such a structure was also evaluated. FE analyses permitted to describe the cumulative strains within the adhesive bond-line and to highlight critical areas. Furthermore, the experimental displacement at failure gave reproducible values, and the failure scenarii were consistent with the critical areas numerically highlighted. Therefore, a fatigue life prediction, based on a strain-based criterion seems to be interesting to apply. However, further experimental results are needed in order to clearly define the crack-onset and to generate a link with an experimental local measurement.

Furthermore, as no fatigue life prediction was brought in the case of these assemblies, the field of research remains wide open. However, the reproducible values obtained for displacements at failure under cyclic shear loading were promising signs for the abilities of strain-based criteria. Development of such crack initiation criteria may thus be the missing link between the numerical cumulative displacement obtained and the experimental fatigue lives.

Concerning the approaches made on structures including important stress/strain concentration areas, the choice of a level of description in terms of mesh refinement is a necessary preliminary step.

References

- (Adams, 1989) Adams, R. D., 1989. Strength predictions for lap joints, especially for composite adherends: a review. *Journal of Adhesion*, Issue 30, pp. 219-42.
- (Adams, 2005) Adams, R. D., 2005. *Adhesive bonding: science technology and applications*. Bristol: Woodhead Publishing.
- (Adams, et al., 1977) Adams, R. D. & Coppendale, J., 1977. The elastic moduli of structural adhesives. In: *Adhesion Vol.1 Applied Science*. London: s.n., pp. 1-17.
- (Adams, et al., 1992) Adams, R. D. & Mallick, V., 1992. A method for the stress analysis of lap joints. *Journal of Adhesives*, Issue 38, pp. 199-217.
- (Adams, et al., 1997) Adams, R. D., Comyn, J. & Wake, W. C., 1997. *Structural adhesive joints in engineering, 2nd Ed.*. London: Chapman et Hall.
- (AFNOR, 2005) AFNOR, N. E. 5.-1., 2005. Aluminium et alliages d'aluminium - Composition chimique et forme des produits corroyés - Partie 1 : système de désignation numérique.
- (AFNOR, 2008) AFNOR, N. E. 9., 2008. *Adhésifs-Terms et définitions*. s.l.
- (AFNOR, 2012) AFNOR, N. E. I. 5., 2012. *Plastiques-Détermination des propriétés en traction*. s.l.
- (AFNOR, 1981) AFNOR, N. T. 5.-1., 1981. *Plastiques-Détermination des propriétés en compression*. s.l.
- (Albouy, 2013) Albouy, W., 2013. *De la contribution de la visco-elasto-plasticité au comportement en fatigue de composites à matrice thermoplastique et thermodurcissable*. Normandie Université.
- (Al-Ghamdi, et al., 2003) Al-Ghamdi, A. H., Ashcroft, I. A., Crocombe, A. D. & Abdel Wahab, M. M., 2003. Crack growth in adhesively bonded joints subjected to variable frequency fatigue loading. *Journal of Adhesion*, Issue 79, pp. 1161-82.
- (Almeida, et al., 1999) Almeida, J. R. M. & Monteiro, S. N., 1999. The Iosipescu test method as a method to evaluate tensile strength of brittle materials. *Polymer Testing*, Issue 18.
- (Arcan, et al., 1978) Arcan, M., Hashin, Z. & Voloshin, A., 1978. A method to produce uniform plane stress states with applications to fiber reinforced materials. *Experimental Mechanics*, Issue 18, p. 141.

- (Arcan, et al., 1987) Arcan, L., Arcan, M. & Daniel, L., 1987. SEM Fractography of pure mixed Mode interlaminar fracture in Graphite/Epoxy composites. *ASTM Tech. Publ. ASTM*, Issue 948, pp. 41-67.
- (Arnaud, et al., 2014) Arnaud, N., Créac'hcadec, R. & Cognard, J. Y., 2014. A tension/compression-torsion test suited to analyze the mechanical behaviour of adhesives under non proportional loadings. *International Journal of Adhesion and Adhesives*.
- (Arnaud, 2014) Arnaud, N., 2014. *Analyse de l'effet du vieillissement en milieu humide sur le comportement mécanique d'adhésifs en assemblages sous sollicitations multiaxiales*. Université de Bretagne Occidentale.
- (Ashcroft, et al., 2002) Ashcroft, I. A. & Shaw, S. J., 2002. Mode I fracture of epoxy bonded composite joints, Part 2: Fatigue Loading. *International Journal of Adhesion and Adhesives*, Issue 22, pp. 151-67.
- (ASTM Int., 2003) ASTM Int., E., 2003. *Standard test method for shear strength and shear modulus of structural adhesive*. s.l.
- (ASTM Int., 2006a) ASTM Int., D., 2006. Standard test method for apparent shear strength of single-lap-joint adhesively bonded metal specimens by tension loading (Metal-to-Metal).
- (ASTM Int., 2006b) ASTM Int., D., 2006. *Standard test method for measuring strength and shear modulus of nonrigid adhesives by the thick-adherend tensile-lap specimen*. s.l.
- (ASTM Int., 2006c) ASTM Int., D., 2006. *Standard test method for tensile properties of adhesive bonds*. s.l.
- (ASTM Int., 2008) ASTM Int., D., 2008. *Standard test method for tensile strength of adhesives by means of bar and rode specimen*. s.l.
- (ASTM Int., 2010) ASTM Int., D., 2010. *Standard test method for compressive properties of rigid plastics*. s.l.
- (ASTM Int., 2012) ASTM Int., D.-9., 2012. *Standard test method for fatigue properties of adhesives in shear by tension loading (metal/metal)*. s.l.
- (Aubry, 2013) Aubry, J., 2013. *Etude expérimentale et numérique d'impacts sur structures : application aux pâles d'hélicoptères*. s.l.:Université de Toulouse.
- (Belingardi, et al., 2004) Belingardi, G. & Chiandussi, G., 2004. Stress flow in thin walled box beams obtained by adhesive bonding joining technology. *International Journal of Adhesion and Adhesives*, pp. 423-39.
- (Berthier, 2009) Berthier, J., 2009. Polyuréthane PUR (Matières thermodurcissables:monographie - Plastiques et composites - Matériaux) am3425. *Techniques de l'ingénieur*.

- (Besson, et al., 2001) Besson, J., Cailletaud, G., Chaboche, J. & Forest, S., 2001. *Mécanique non linéaire des matériaux*. Paris: Hermes.
- (Besson, et al., 2004) Besson, J. & Desmorat, R., 2004. Numerical implementation of constitutive models. In: *Local approach to fracture*. Paris: Les presses de l'écoles des mines de Paris.
- (Bidaud, et al., 2012) Bidaud, P., Créac'hcadec, R., Thévenet, D. & Cognard, J., 2012. Analysis of the cyclic behavior of an adhesive in an assembly under tensile-shear loading. *Proceedings of the 9th European adhesion conference, Friedrichshafen*.
- (Bjorkman, et al., 2008) Bjorkman, G.S. & Piotter, J.M., 2008. Finite element mesh considerations for reduced integration elements. in proceedings of ASME Pressure Vessels and Piping Conference.
- (Bodner, et al., 2010) Bodner, S. R. & Partom, Y., 2010. Constitutive equations for elastic-viscoplastic strain-hardening materials. *Journal of Applied Mechanics*, Issue 42, pp. 385-89.
- (Bordes, et al., 2009) Bordes, M., Davies, P. & J.Y., C., 2009. Prediction of long term strength of adhesively bonded joints in sea water. *International journal of adhesion and adhesives*, Issue 29, pp. 595-608.
- (Bouvet, 2013) Bouvet, G., 2013. Fluorescence spectroscopy applied to study cyclic creep behavior and internal stresses of semi-crystalline high density polyethylene. *Journal of Applied Physics*, pp. 50-62.
- (Brannon, 2002) Brannon, R. M., 2002. Geometrical insight into return mapping plasticity algorithms.
- (Brosh, et al., 1996) Brosh, T., Pilo, R. & Arcan, M., 1996. Shear modulus -Measurement methodology with application to light cured resin composites. *Dental Materials*, Issue 12, pp. 52-57.
- (Burchardt, 2010) Burchardt, B., 2010. Advances in polyurethane structural adhesives. In: *Advances in structural adhesive bonding*. Oxford, Cambridge, New Dehli: Woodhead Publishing in Materials, pp. 35-65.
- (Carrère, et al., 2013) Carrère, N., Badulescu, C. & Cognard, J., 2013. Determination of the failure envelop on an adhesive using a modified arcan tests device - Role of the plasticity and of the residual stresses. *Proceedings of the second international conference on structural adhesive bonding (AB2013)*.
- (Cernocky, 1982) Cernocky, E. P., 1982. Comparison of the unloading and reversed loading behavior of three viscoplastic constitutive theories. *International Journal of Non-Linear Mechanics*, pp. 255-65.
- (Chen, et al., 2011) Chen, Z., Adams, R. D. & daSilva, L. F. M., 2011. Fracture toughness of bulk adhesives in mode I and mode III and curing effect. *International Journal of Fracture*, Issue 167(2), p. 221.

- (Chiu, et al., 1995) Chiu, W. K. & Jones, R., 1995. Unified constitutive model for thermoset adhesive, FM73. *International Journal of Adhesion and Adhesives*, Issue 15, pp. 131-136.
- (Cognard, 2008) Cognard, JY., 2008. Numerical analysis of edge effects in adhesively-bonded assemblies application to the determination of the adhesive behavior. *Computers and Structures*, Issue 86.
- (Cognard, et al., 2005) Cognard, JY., Davies, P., Gineste, B. & Sohier, L., 2005. Development of an improved adhesive test method for composite assembly design. *Composite Science and Technology*, p. 359.
- (Cognard, et al., 2008) Cognard, JY., Créac'hcadec, R., Sohier, L. & Davies, P., 2008. Analysis of the non linear behavior of adhesive in bonded assemblies, comparison of TAST and Arcan test. *International Journal of Adhesion and Adhesives*, Issue 28, pp. 393-404.
- (Cognard, et al., 2010a) Cognard, JY., Créac'hcadec, R., Sohier, L. & Leguillon, D., 2010. Influence of the thickness on the behavior of bonded assemblies under shear loadings using a modified TAST fixture. *International Journal of Adhesion and Adhesives*, Issue 30, pp. 257-66.
- (Cognard, et al., 2010b) Cognard, JY., Davies, P. & Sohier, L., 2010. Advances in testing adhesively bonded composites. In: *Advances in structural adhesive bonding*. Oxford, Cambridge, New Dehli: Woodhead Publishing in Materials.
- (Cognard, et al., 2011a) Cognard, JY. et al., 2011. Experimental analysis of the influence of hydrostatic stress on the behavior of an adhesive using a pressure vessel. *Journal of Adhesion*, pp. 804-25.
- (Cognard, et al., 2011b) Cognard, JY., Créac'hcadec, R. & Sohier, L., 2011. Strategies for the analysis of the behavior of a adhesive in bonded assemblies. *J. of Eng. Mat.-Transaction of the ASME*, pp. 1-9.
- (Cowper, et al., 1957) Cowper, G. R. & Symonds, P. S., 1957. *Strain-hardening and strain rate effects in the impact of cantilever beams*, Providence: Brown University Division of Applied Mathematics.
- (Créac'hcadec, 2008) Créac'hcadec, R., 2008. *Analyse et modélisation du comportement non linéaire d'assemblages collés pour application marine*. s.l.:Université de Bretagne Occidentale.
- (Crocombe, 1995) Crocombe, A. D., 1995. Modelling and predicting the effects of test speed on the strength of joints made with FM73 adhesive. *International Journal of Adhesion and Adhesives*, Issue 15, pp. 21-27.
- (Crocombe, et al., 1999) Crocombe, A. D. & Richardson, G., 1999. Assessing stress state and mean load effects on the fatigue response of adhesively bonded joints. *International Journal of Adhesion and Adhesives*, Issue 19, pp. 19-27.

- (da Silva, et al., 2011) da Silva, L., Öchsner, A. & Adams, R. D., 2011. *Handbook of Adhesion Technology*. Berlin: Springer.
- (Davies, et al., 2009) Davies, P. et al., 2009. Influence of the adhesive bondline thickness on joint strength. *International Journal of Adhesion and Adhesives*, pp. 724-36.
- (de Morais, et al., 2009) de Morais, A. B., Pereira, A. B., de Moura, M. F. S. F. & Magalhães, A. G., 2009. Mode III interlaminar fracture of carbon/epoxy laminates using the Edge Crack Torsion (ECT) test. *Composite Science and Technology*, pp. 670-76.
- (de Moura, et al., 2008) de Moura, M. F. S. F., Fernandez, M. V. C., de Morais, A. B. & Campilho, R. D. S. G., 2008. Numerical analysis of the Edge Crack Torsion test for mode III interlaminar fracture of composite laminates. *Composite Science and Technology*.
- (Dean, 2006) Dean, G., 2006. Modeling non-linear creep behaviour of an epoxy adhesive. *International Journal of Adhesion and Adhesive*, pp. 636-46.
- (Dean, 2007) Dean, G., 2007. Modeling non-linear creep behaviour of an epoxy adhesive. *International Journal of Adhesion and Adhesives*, Issue 27, pp. 636-46.
- (Dean, et al., 2004) Dean, G., Crocker, L., Read, B. & Wright, L., 2004. Prediction of deformation and failure of rubber toughened adhesive joints. *International journal of adhesion and adhesives*, pp. 295-306.
- (Deb, et al., 2007) Deb, A., Malvade, I., Biswas, P. & Schroeder, J., 2007. An experimental and analytical study of the mechanical behaviour of bonded joints for variable extension rates and temperatures. *International Journal of Adhesion and Adhesives*, Issue 28, pp. 1-15.
- (Deryagin, et al., 1957) Deryagin, B. et al., 1957. *In Proceedings of the Second International Congress on Surface activity*.
- (Dessureault, et al., 1997) Dessureault, M. & Spelt, J. K., 1997. Observation of fatigue crack initiation and propagation in an epoxy adhesive. *International Journal of Adhesion and Adhesives*, Issue 17, pp. 183-95.
- (Deveaux, et al., 2014) Deveaux, O. et al., 2014. FE simulation of the curing behavior of the epoxy adhesive Hysol EA-9321. *International Journal of Adhesion and Adhesives*.
- (Dillard, et al., 1985) Dillard, D. A. & Hiel, C., 1985. *Proceedings of the 1985 SEM spring conference on experimental mechanics*, p. 142.
- (Erpolat, et al., 2004) Erpolat, S., Ashcroft, I. A., Crocombe, A. D. & Abdel-Wahab, M. M., 2004. A study of adhesively bonded joints subjected to constant variable amplitude fatigue. *International Journal of Fatigue*, Issue 26, pp. 1189-96.
- (Fichaux, et al., 2011) Fichaux, N., Beurkens, J., Jensen, P. H. & Wilkes, J., 2011. *Upwind project*, s.l.: European Wind Energy Association.

- (Gay, et al., 2007) Gay, D. & Hoa, S. V., 2007. *Composite Materials: Design and Applications (second edition)*. s.l.:CRC Press.
- (Gegner, et al., 2004) Gegner, J. & Öchsner, A., 2004. Destructive testing of adhesively bonded joints under static tensile loading. *Symposium proceedings swiss bonding 04*, p. Swibotech.
- (Geiss, 1998) Geiss, P. L., 1998. *Verarbeitungskonzepte und belastungskriterien für Haftklebstoffe. Dissertation*. University of Kaiserslautern ed. Munich: s.n.
- (Geiss, et al., 2007) Geiss, P. L. & Vogt, D., 2007. Durability of pressure sensitive adhesive joints. *Proceedings of 30th Pressure Sensitive Tape Concl Tech. Conference*, pp. 147-54.
- (Gineste, 1993) Gineste, B., 1993. *Assemblages de structures en matériaux composites par stratification d'un élément de liaison: caractérisation de l'endommagement*. s.l.:Ecole Centrale Nantes.
- (Goland, et al., 1944) Goland, M. & Reissner, E., 1944. The stresses in cemented joints. *Journal of Applied Mechanics*, Issue 11, pp. A17-A27.
- (Green, et al., 1960) Green, A. E. & Adkins, J. E., 1960. *Large elastic deformations and non-linear continuum mechanics*. New York: Oxford University Press.
- (Griffith, 1921) Griffith, A. A., 1921. The phenomena of rupture and flow in solids. *Philosophical Transaction of the Royal Society*, Issue 221, pp. 163-98.
- (Guo, et al., 2006) Guo, S., Dillard, D. A. & Naim, J. A., 2006. Effect of residual stress on the energy release rate of wedge and DCB test specimens. *International Journal of Adhesion and Adhesives*, pp. 285-94.
- (Hadaviana, et al., 2003) Hadaviana, H., Kinloch, A. J., Little, M. S. G. & Taylor, A. C., 2003. The prediction of crack growth in bonded joints under cyclic-fatigue loading. *International Journal of Adhesion and Adhesives*, 449-61(23).
- (Harris, et al., 1984) Harris, J. A. & Adams, R. D., 1984. Strength prediction of bonded single lap joints by non linear finite element methods. *International Journal of Adhesion and Adhesives*.
- (Hart-Smith, 2002) Hart-Smith, L., 2002. Adhesive-bonding of composite structures: progress to date and some remaining challenges. *NASA Langley Research Center*, Issue 24, pp. 133-51.
- (Hencky, 1924) Hencky, H. Z., 1924. *Math. Mech.*, Issue 4, p. 323.
- (Hiel, et al., 1983) Hiel, C., Cardon, A. H. & Brinson, H. F., 1983. The non-linear visco-elastic response of resin matrix composite laminates. *Virginia Polytechnic Institute and State University Report*, Issue VPI-E-83-6.

- (Imanka, et al., 2003) Imanka, M., Hamano, T., Ashino, R. & Kimoto, M., 2003. Fatigue damage evaluation of adhesively bonded butt joints with rubber modified epoxy adhesive. *Journal of Adhesion Science and Technology*, Issue 17(7), pp. 981-94.
- (Irwin) Irwin, G. R., n.d. Fracture. In: F. S, ed. *Handbuch der physics VI.* s.l.:s.n., pp. 551-590.
- (Ishii, et al., 1999) Ishii, K., Imanakab, M., Nakavamak, H. & Kadamad, H., 1999. Evaluation of the fatigue strength of adhesively bonded CFRP/metal single and double joints. *Composite science and technology*, pp. 1675-83.
- (Jeandrau, 2011) Jeandrau, J., 2011. Environmental adn fatigue durability of structural adhesive-joints. *Proceedings of RC International Conference on Structural Adhesive Bonding*.
- (Jensen, et al., 2006) Jensen, F. M., Falzon, B. G., Ankersen, J. & Stang, H., 2006. Structural testing and numerical simulation of a 34 m composite wind turbine. *Composite structures*, Issue 76, pp. 52-61.
- (Ji, et al., 2014) Ji, Y. M. & Han, K. S., 2014. Fracture mechanics approach for failure of adhesive joints in wind turbine blades. *Renewable Energy*, pp. 22-28.
- (Joannes, 2007) Joannes, S., 2007. *Caractérisation mécanique et outil d'aide au dimensionnement des collages structuraux*. s.l.:Mines Paris ParisTech.
- (Johnson, et al., 1985) Johnson, G. R. & Cook, W. H., 1985. Fracture characteristics of three metals subjected to various strains, strain rates, temperature and pressures. *Engineering Fracture Mechanics*, Issue 21, pp. 31-48.
- (Jousset, 2008) Jousset, P., 2008. *Constitutive modelling of structural adhesives, experimental and numerical aspects*. s.l.:Université de Technologie de Compiègne.
- (Kalkhoran, et al., 2013) Kalkhoran, A., Salimi-majd, D. & Mohammadi, B., 2013. Fatigue life prediction for adhesively bonded root joint of composite wind turbine blade using cohesive zone approach. In: *Recent Advances in Composite Materials for Wind Turbine Blades* . s.l.:The World Academic Publishing Co. Ltd., pp. 221-32.
- (Khoramishad, et al., 2010) Khoramishad, H., Crocombe, A. D., Katnam, K. B. & Ashcroft, I. A., 2010. Predicting fatigue damage in adhesively bonded joints using a cohesively zone model. *International Journal of Fatigue*, Issue 32, pp. 1146-58.
- (Kinloch, 1987) Kinloch, A. J., 1987. *Adhesion and Adhesives*. s.l.:Chapman and Hall.
- (Kinloch, et al., 1993) Kinloch, A. J. & Osiyemi, S. O., 1993. Predicting fatigue life of adhesively-bonded joints. *Journal of Adhesion*, pp. 79-90.
- (Kotousov, 2007) Kotousov, A., 2007. Effectadhesive layer of a thin plastic adhesive layer on the stress singularity in a bi-material wedge. *International Journal of Adhesion and Adhesives*, pp. 647-57.

- (Krieger, 1988) Krieger, R. B., 1988. Stress analysis concepts for adhesive bonding of aircraft primary structure. In: *Adhesive bonded joints: testing , analysis and design*. Philadelphia: American Society for Testing and Materials, pp. 264-275.
- (Landes, et al., 1976) Landes, J. D. & Begley, J. A., 1976. *Mechanics of crack growth (ASTM STP 590)*. Philadelphia: American Society for Testing and Materials.
- (Launay, et al., 2011) Launay, A. et al., 2011. cyclic behavior of short glass fiber reinforced polyamid: Experimental study and constitutive equations. *International Journal of Plasticity*, Issue 27, pp. 1267-93.
- (Laurin, 2005) Laurin, F., 2005. *Approche multiechelle des mécanismes de ruine progressive des matériaux stratifiés et analyse de la tenue de structures composites*. s.l.:Université de Franche-Conté.
- (Leguillon, et al., 1987) Leguillon, D. & Sanchez-Palancia, E., 1987. *Computation of singular solutions in elliptic problems and elasticity*. Paris: Editions Masson.
- (Lemaître, et al., 2000) Lemaître, J. & Chaboche, J., 2000. *Mechanics of Solid Materials*. s.l.:Cambridge University Press.
- (Lilleheden, 1994) Lilleheden, L., 1994. Mechanical properties of adhesives in situ and in bulk. *International Journal of Adhesion and Adhesives*, Issue 14, pp. 31-37.
- (Mahnken, et al., 2005) Mahnken, R. & Scklimmer, M., 2005. Simulation of strength difference in elasto-plasticity for adhesive materials. *International Journal for Numerical Methods in Enginnering*, pp. 1461-1477.
- (Maire, 1992) Maire, JF., 1992. *Etude théorique et expérimentale du comportementde matériaux composites en contraintes planes*. s.l.:Université de Franche-Conté.
- (Maine) *Advanced structures and composite center - brochure*. s.l.:The University of MAINE.
- (Ma, et al., 2011) Ma, J., Gao, H., Gao, L. & Chen, X., 2011. Uniaxial ratcheting behavior of anisotropic conductive adhesive film at elevated temperature. *Polymer Testing*, pp. 571-77.
- (Malvade, et al., 2009) Malvade, I., Deb, A., Biswas, P. & Kumar, A., 2009. Numerical prediction of load-displacement behaviors of adhesively bonded joints at different extension rates and temperatures. *Computational Material Science*, Issue 44, pp. 1208-1217.
- (Mandell, et al., 1998) Mandell, J. F. et al., 1998. *Fatigue of Composite Material Beam Elements Representative of Wind Turbine Blade Structure*, Bozeman: National Renewable Energy Laboratory.
- (Massachusset) *Wind Technology Testing Center (WITTC) - brochure*. s.l.:Massachusset Clean Energy Center.

- (Maurice, 2012) Maurice, J., 2012. *Characterization and modeling of the 3D elastic-plastic behavior of structural adhesive films for aeronautical applications*. s.l.:Université de Bretagne Occidentale.
- (Mc Bain, et al., 1925) Mc Bain, J. W. & Hopkins, D. G., 1925. Adhesives and adhesive actions. *Journal of Physical Chemistry*, Issue 29(2), pp. 215-233.
- (Miled, et al., 2011) Miled, B., Doghri, I. & Delannay, L., 2011. Coupled viscoelastic-viscoplastic of homogeneous and isotropic polymers: numerical algorithm and analytical solutions. *Computational Methods in Applied Mechanics and Engineering*, Issue 200.
- (Mishnaevsky) Mishnaevsky, L. J., n.d. Thermal to Mechanical Energy Conversion Engines and Requirements: Composite materials in wind energy technology. In: *Encyclopedia of Life Support Systems*. s.l.:s.n.
- (Morin, et al., 2010) Morin, D., Haugou, G., Bennani, B. & Lauro, F., 2010. Identification of a new failure criterion for toughened epoxy adhesive. *Engineering Fracture Mechanics*, pp. 3481-00.
- (Moroni, et al., 2009) Moroni, F. & Pirondi, A., 2009. An investigation of fatigue failure prediction of adhesively bonded metal/metal joints. *International Journal of Adhesion and Adhesives*, Issue 29, pp. 796-805.
- (Moussa, et al., 2012) Moussa, O., Vassilopoulos, A. & Keller, T., 2012. Effect of low temperature curing on physical behavior of cold curing epoxy adhesives in bridge construction. *International Journal of Adhesion and Adhesives*, Issue 32, pp. 15-22.
- (Mubashar, et al., 2009) Mubashar, A., Ashcroft, I. A., Critchlow, G. & Crocombe, A. D., 2009. Modeling cyclic moisture uptake in an epoxy adhesive. *Journal of adhesion (85)*, pp. 711-35.
- (Nadai, 1931) Nadai, A., 1931. *Plasticity: a mechanics of the plastic state of matter*. New York: McGraw-Hill.
- (Nguyen, 2013) Nguyen, S. T. T., 2013. *Caractérisation expérimentale et modélisation thermomécanique de l'accommodation cyclique du polyéthylène*. s.l.:ISAE - ENSMA.
- (Nuismer, et al., 1975) Nuismer, R.J. & Whitney, J.M., 1975. Uniaxial failure of composite laminates containing stress concentration (ASTM STP 593). pp.117-42.
- (Pan, et al., 2010) Pan, D., Kang, G., Zhu, Z. & Liu, Y., 2010. Experimental study on uniaxial time-dependant ratcheting of a polyetherimide polymer. *Journal of Zhejiang University of Science*, pp. 804-10.
- (Paris, et al., 1961) Paris, P. C., Gomez, M. P. & Anderson, W. E., 1961. *Trend Engineering*. Issue 13, p. 9.

- (Petermann, et al., 2002) Petermann, J. & Schulte, K., 2002. The effects of creep and fatigue stress ratio on the long-term behaviour of angle-ply CFRP. *Composite Structures*, Issue 57, pp. 205-10.
- (Petipas, 2000) Petipas, C., 2000. *Analyse et prévision du comportement à long terme des composites fibres de carbone / matrice organique*. s.l.:Universté de Franche-Conté.
- (Potter, et al., 2001) Potter, K. D. et al., 2001. Heavily loaded bonded composite structure: design, manufacture and test of 'I' beam specimens. *Composite Structures*, pp. 389-99.
- (Python, 2014) Python, S., 2014. <https://www.python.org/>. [Online].
- (Quaresimin, et al., 2006) Quaresimin, M. & Ricotta, M., 2006. Fatigue behavior and damage evolution of single lap bonded joints in composite material. *Composite science and technology*, pp. 176-87.
- (Ratcliffe, 2004) Ratcliffe, J. G., 2004. Characterization of the Edge Crack Torsion test for mode III fracture toughness measurement of laminated composites. *NASA/TM-2004-213269*.
- (Ravi-Chandar, et al., 1984) Ravi-Chandar, K. & Knauss, W. G., 1984. *International Journal of Fracture*, Issue 25, p. 247.
- (Renieri, et al., 1976) Renieri, M. P., Herakovich, C. T. & Brinson, H. F., 1976. Rate and time dependant behavior of structural adhesives. *Polytechnic Institute and State University*, Issue VPI-E-76-7.
- (Rhagava, et al., 1973) Rhagava, R. S. & Cadell, R. M., 1973. The macroscopic behavior of polymers. *Journal of Material Science*, Issue 8, pp. 225-32.
- (Rice, 1968) Rice, J. R., 1968. A path independent integral and the approximate analysis of train concentration by notches and cracks. *Journal of Applied Mechanics*, Issue 35, pp. 379-86.
- (Rochefert, et al., 1983) Rochefert, M. A. & Brinson, H. F., 1983. Nonlinear viscoelastic characterization of structural adhesives. *Virginia Polytechnic Institute and State University Report*, Issue VPI-E-83-26.
- (Rolfes, 2008) Rolfes, R., 2008. Strength of textile composites in Multiscale simulation. In: *Trends In Computational Structures Technology*. Stirlingshire: Saxe-Coburg Publications, pp. 151-171.
- (Samborsky, et al., 2009) Samborsky, D. D., Sears, A. T. & Mandell, J. F., 2009. Static and fatigue testing of thick adhesive joints for wind turbine blades. *ASME Wind Energy Symposium*.
- (Sancaktar, 2011) Sancaktar, E., 2011. Constitutive Adhesive and Sealant Models. In: *Handbook of Adhesion Technology*. Berlin: Springer, pp. 554-95.

- (Sancaktar, et al.) Sancaktar, E. & Brinson, H. F., n.d. The viscoelastic shear behavior of a structural adhesive. *Virginia Polytechnic Institute and State University Report*, Issue VPI-E-83-26.
- (Shanahan, et al., 1991) Shanahan, M. E. R. & Michel, F., 1991. Adhesion and wetting: singularities and differences (physical phenomena). *Rubber world*, Issue 205(1), pp. 28-36.
- (Sharp, et al., 2013) Sharp, K. et al., 2013. Wind blade joints based on non-crimp 3D orthogonal woven Pi shaped performs. *Composites: Part A*, pp. 9-17.
- (Shenoy, et al., 2009) Shenoy, V. et al., 2009. An investigation into the crack initiation and propagation behaviour of bonded single-lap joints using backface strain. *International Journal of Adhesion and Adhesives*, Issue 29, pp. 361-71.
- (Shenoy, et al., 2010) Shenoy, V., Ashcroft, I., Critchlow, G. W. & Crocombe, A., 2010. Unified methodology for the prediction of the fatigue behaviour of adhesively bonded joints. *International Journal of Fatigue*, Issue 32, pp. 1278-88.
- (Sika, 2010) Sika, 2010. *Sika® Aktivator-205 Product data sheet Version1*. s.l.:s.n.
- (Sika, 2011) Sika, 2011. *SikaForce®-7817 L60 MR Product data sheet Version 1*. s.l.:s.n.
- (Simo, et al., 1998) Simo, J. C. & Hughes, T. J. R., 1998. *Computational inelasticity (interdisciplinary applied mathematics)*. Berlin: Springer.
- (Spathis, et al., 2012) Spathis, G. & Kontou, E., 2012. Creep failure time prediction of polymers and polymer composites. *Composite Science and Technology*, Issue 72, pp. 959-64.
- (Tao, et al., 2005) Tao, G. & Xia, Z., 2005. A non-contact real-time strain measurement and control system for multiaxial cycli/fatigue tests of polymer materials by digital image correlation method. *Polymer testing*, Issue 24, pp. 844-55.
- (Tao, et al., 2007) Tao, G. & Xia, Z., 2007. Mean stress/strain effect on fatigue behavior of an epoxy resin. *International Journal of Fatigue*, Issue 29, pp. 2180-90.
- (Thevenet, et al., 2013) Thevenet, D., Créac'hcadec, R., Sohier, L. & Cognard, J., 2013. Experimental analysis of the behavior of adhesively bonded joints under tensile/compression shear cyclic loadings. *International Journal of Adhesion and Adhesives*, Issue 44, pp. 15-25.
- (Ustunel, 2006) Ustunel, U., 2006. Modern multiaxials improve performance. *Reinforced Plastics*, Issue 50, pp. 34-38.
- (Vernet, et al., 2005) Vernet, D., Cluzel, C. & Allix, O., 2005. Modélisation et identification de collages à usage marin: une approche expérimentale dédiée. *JNC14 proceedings*, pp. 259-267.
- (Vinogradov, et al., 2001) Vinogradov, A. M., Jenkins, C. H. M. & Winter, R. M., 2001. Cyclic loading effects on durability of polymer systems. *Long Term Durability of Structural Materials*, pp. 159-70.

- (Volkersen, 1938) Volkersen, O., 1938. Die nietkrafteerteilung in zubeanspruchten nietverbindungen mit onstanten loshonquerschnitten. *Luftfabrtforschung*, Issue 15, p. 41.
- (Voyutskii, et al., 1957) Voyutskii, S. S. & Margolina, Y., 1957. The nature of self-adhesion (tack) of polymers. *Rubber and technology*, Issue 30, pp. 531-43.
- (Wang, et al., 2000) Wang, C. H. & Chalkley, P., 2000. Plastic yielding of a film adhesive under multiaxial stresses. *International Journal of Adhesion and Adhesives*, Issue 20, pp. 155-64.
- (Wang, et al., 2006) Wang, P. & Xu, L. R., 2006. Convex interfacial joints with least stress singularities in dissimilar material. *Mechanics of Materials*, pp. 1001-11.
- (Weissberg, et al., 1988) Weissberg, V. & Arcan, M., 1988. A uniform pure shear testing specimen for adhesive characterisation (ASTM STP 981). In: *Adhesively bonded joints: testing, analysis and design*. Philadelphia: American Society for Testing and Materials , pp. 28-38.
- (Weitsman, 1981) Weitsman, Y., 1981. *Journal of Adhesion*, Issue 11, p. 279.
- (Whitworth, et al., 2008) Whitworth, H.A., Aluko, O. & Tomlinson, N.A., 2008. Application of the point stress criterion to the failure of composite pinned joint. *Engineering Fracture Mechanics*, (75), pp.1829-39.
- (Wisandrakkit, et al., 2003) Wisandrakkit, G. & Gilham, J., 2003. Glass transition temperature as an index of chemical conversion for high-Tg amine epoxy/system: chemical and diffusion controlled reactions kinetics. *Journal of Applied Polymer Science*, Issue 41, pp. 2885-929.
- (Yu, et al., 2001) Yu, X. X., Crocombe, A. D. & Richardson, G., 2001. Material modeling for rate dependant adhesives. *International Journal of Adhesion and Adhesives*, Issue 21, pp. 197-210.
- (Zarouchas, et al., 2012) Zarouchas, D. S. et al., 2012. Investigations on the mechanical behavior of a wind rotor blade subcomponent. *Composites: Part B*, pp. 647-54.
- (Zhang, et al., 2010) Zhang, Z., Chen, X. & Wang, Y., 2010. Uniaxial ratcheting behavior of polytetrafluoroethylene at elevated temperature. *Polymer Testing*, Issue 29, pp. 352-57.
- (Zhao, et al., 2009) Zhao, B. & Lu, Z. H., 2009. A two dimensional approach of single lap adhesive bonded joints. *Mech. Adv. Mater. Struct*, Issue 16, pp. 130-59.

Analysis of the cyclic behaviour of an adhesive in an assembly for offshore windmill applications

Estimating capacities of adhesives to endure repetitive loadings is an essential point to perform fatigue assessments. Nevertheless, few studies have been performed on the cyclic behaviour of adhesively bonded structures. Moreover, fatigue crack initiation is less studied for adhesives than the fatigue crack propagation. Fatigue behaviour is mainly analysed using lap-shear type specimens, which are associated with complex stress states and stress concentrations. The aim of this work is to develop a predictive tool describing the cyclic behaviour of an adhesive in an assembly under fatigue loading using an experimental approach based on modified Arcan tests. Such a device is associated with low edge effects and a maximum stress state in the centre of the adhesive. Accurate experimental results under monotonic, creep and cyclic loading are presented for several load amplitudes, mean loads and loading rates. For a two-component polyurethane SikaForce®-7817 L60 MR adhesive, experimental results led to reproducible behaviour.

These results underline that the evolutions of the non linear strains strongly depend on the loading type. This behaviour is well described using a visco-elastic-visco-plastic model with non-linear viscous parameters. This model, implemented in 3D finite element simulations, allows analysing the influence of viscosity. In order to limit the experimental test time the inverse identification of the model parameters is performed from modified Arcan creep-relaxation tests. The finite element simulations of bonded structures allowing an efficient description of the cyclic behaviour and using an adequate failure criterion based on the viscous strains evolutions, a validation on fatigue life predictions is performed.

This work is dedicated to the study of fatigue of bonded structures in offshore windmills applications. From this strategy a fatigue life estimation of composite structures tests and on an application test is proposed.

Keywords: Adhesive, Creep, Cyclic loadings, Fatigue, Windmills, Experimental, Law Behaviour, Inverse Identification, Finite Element Analysis.

Analyse du comportement cyclique d'un adhésif dans un assemblage dans le cadre d'applications éoliennes offshore

L'une des principales exigences d'utilisation d'un adhésif est son aptitude à conserver sa capacité à supporter des efforts, appliqués de manière répétée, tout au long de sa vie en service. Toutefois, on dénombre peu d'études sur le comportement en fatigue des assemblages collés. De plus, ces études concernent majoritairement la propagation de fissures et non l'amorçage. Le comportement en fatigue d'assemblages collés est généralement caractérisé grâce à des essais simple-recouvrement auxquels sont associés des états de contrainte complexes présentant de fortes concentrations de contrainte.

Le but de ce travail est de développer un outil prédictif du comportement cyclique d'un adhésif dans un assemblage soumis à un chargement de fatigue, en utilisant des essais basés sur l'utilisation d'un montage Arcan modifié. Ce type de montage utilise des éprouvettes générant un état de contrainte avec peu d'effets de bord et un maximum au centre du joint de colle. Une base expérimentale constituée d'essais monotones, cycliques et de fluage pour différents modes de chargement sont présentés. Les résultats expérimentaux concernant un adhésif bi-composant polyuréthane SikaForce®-7817 L60MR permettent de caractériser un comportement reproductible.

Ces résultats soulignent une évolution non-linéaire des déformations et fortement dépendante du type de chargement. Ce comportement peut être décrit par l'utilisation d'un modèle visco-élastique-visco-plastique. Implémenté dans un code de calcul par éléments finis, ce modèle a permis d'analyser l'influence des phénomènes visqueux. Afin de limiter les temps d'essais, une identification inverse des paramètres a été menée à partir d'une campagne d'essais Arcan en fluage/recouvrement. Les simulations par éléments finis ont permis de décrire le comportement cyclique de structures collées et en utilisant un critère de rupture pertinent, d'effectuer un calcul de durée de vie à l'amorçage d'une fissure.

Ce travail a été appliqué à l'étude du comportement en fatigue d'assemblages collés pour applications éoliennes offshore. Aussi, à partir de la stratégie développée, des estimations de la durée de vie de structures composites collées ainsi que d'un cas d'application représentatif ont été réalisées.

Mots-clés : Adhésif, Fluage, Chargement cyclique, Fatigue, Eolienne, Expérimental, Loi de comportement, Identification inverse, Calcul par éléments finis.